Advanced Signal Processing Techniques for Underwater Acoustic Transmission using Steerable Transducer Arrays

Wichian Ooppakaew

PhD

2012

Advanced Signal Processing Techniques for Underwater Acoustic Transmission using Steerable Transducer Arrays

Wichian Ooppakaew

A thesis submitted in partial fulfilment
of the requirements of the
University of Northumbria at Newcastle
for the degree of
Doctor of Philosophy

in Electrical Engineering

Research undertaken in the School of
Computing, Engineering and Information Sciences
and in collaboration with the ACoRNE, UK

October 2012

Abstract

The main objective of this research is to design and implement an eight-hydrophone transmitter array for generating bipolar acoustic pulses mimicking those produced by cosmogenic neutrino interaction in sea water. In addition, the research was conducted as part of the ACoRNE collaboration. The work initially investigated a single hydrophone system. Due to the nature of hydrophone, the acoustic output signal does not precisely follow a given driving voltage input. Hence signal processing techniques and hydrophone modelling were applied. A bipolar acoustic generation module was built using 8-bit PIC microcontrollers for processing and control. A NI USB-6211 National Instruments commercial module was used for validation of results. The modelling was compared to experimental data generated in a water tank, showing excellent agreement.

This single hydrophone instrument was deployed at the Rona array in 2008. Both 10 kHz and 23 kHz pulses were injected, whilst seven hydrophones at Rona site were chosen as the receiver hydrophone array. Signal processing techniques were applied to identify these pulses. The result showed that the triggered pulses can be detected and identified at Rona over a distance of a few hundred metres. A model for an eight-hydrophone transmission linear array system for the ANTARES site was developed. The simulation showed that the eight hydrophones arranged over an eight-metre spacing structure can mimic the anticipated pancake behaviour predicted from neutrino-induced showers as well as generating the acoustic bipolar pulse shape of sufficient amplitude for detection at ANTARES.

An eight-channel arbitrary waveform generator module was designed and built using 16-bit dsPIC microcontrollers. Signal Processing techniques were again applied to calibrate the hydrophone transmitter array. The behaviour of an acoustic transducer array was examined in a laboratory water tank to study the shape and direction of such a signal in water. The results were validated against a PXI-6713 commercial module. Excellent agreement was achieved.

Finally, the system was deployed at the ANTARES site in September 2011. A range of test signals including 23 kHz bipolar pulses, sine signals and orthogonal signals were injected into seawater to simulate neutrino interactions and investigate signal coding. Signal processing techniques were applied to the data deployed in order to recognise the signals emitted. However, the vessel was far away from the position planned (c 1km), hence the signal received was too weak and no signal was detected. However, the deployed data is still very useful in order to study the noise background of seawater and much has been learned for future sea campaigns.

Acknowledgement

I would like to express my sincere gratitude to Prof. Sean Danaher, who is my principal supervisor, for his excellent academic advice. I especially thank my supervision team, Dr. Peter D Minns and Dr. Lee Thompson, for providing me the opportunity to undertake the study under their supervision.

I would like to thank Northumbria University for providing some funding, necessary equipment and the testing laboratory. I would also like to thank Prof. Fary Ghassemlooy and Dr. Krishna Busawon for their good advice and encouragement during this research. My sincere thanks to Dr. Edward Bentley and Dr. David Johnston for proof reading this thesis.

Sincere thank also go to the ACoRNE collaboration, the University of Sheffield and Dr. Omar Veledar who support the research with valuable existing equipment and provided a laboratory for practical work at Sheffield University. My thanks to Maria Saldana, who helped me in testing the hydrophone array at the Northumbria University laboratory.

My special thanks also go to the ECAP collaboration: Dr. Robert Lahman, Dr. Kay Graf, Bjorn Herold, and to Qing Lu who supported and organised facilities and travel for the laboratory experiments at the University of Erlangen (Germany) and the sea campaign at the ANTARES site (France). I wish to thank the sea operation organiser, Dominique Lefever, all collaborators from INSU, France, the crews on vessel (Tethys II), for their support during two days and one night living on the vessel. Without their help and support, my practical work in the field could not have been finished.

I would like to express my deepest gratitude toward the Rajamangala University of Technology Thanyaburi and the Ministry of Science and Technology of Thailand, who give the opportunity and financial support throughout my PhD course.

I wish to express my thank to my parents, who are my inspiration, brothers, sisters for their support and encouragement. Special thanks go to Napasiri Ooppakeaw for her constant support, patience and encouragement throughout the duration of this work. Last but not least, I would like to thank to the United Kingdom to give me a good opportunity of language and culture learning, which are very high valuable knowledge and experience.

Declaration

I declare that the work contained in this thesis has not been submitted for any other award and it is my own work.

Name: Wichian Ooppakaew

Signature:

Date:

Table of Content

List of Figures

List of Tables

Glossary of abbreviations

ACoRNE = Acoustic Cosmic Ray Neutrino Experiment

ADC = Analogue-to-Digital Converter

AMADEUS = ANTARES Modules for the Acoustic Detection Under the Sea

AMANDA = Antarctic Muon And Neutrino Detector Array

ANITA = Antarctic Impulsive Transient Antenna

ANTARES = Astronomy with a Neutrino Telescope and Abyss environment RESearch

AUTEC = Atlantic Undersea Test and Evaluation Centre

B&K = Bruel and Kyaer coperation

CERN = Centre Europeenne pour la Recherché Nucleaire

CPU = Central Processing Unit

DAC = Digital to Analogue Converter

DAQ = Data Acquisition

dB = Decibel

DC = Direct current

dc-to-dc = Direct current to direct current converter

dsPIC = Digital Signal Peripheral Interface Controller

DSP = Digital Signal Processing

E = East

ECAP = Erlangen Centre for Astroparticle Physics

EU = European Union

eV = Electron Volt

FFT = Fast Fourier Transform

FIR = Finite Impulse Response

FT = Fourier Transform

FPGA = Field-programmable gate array

GPS = Global positioning system

GUI = Graphic User Interface

HTI = Hi Tech Inc

IC = Integrated Circuit

I^2C = Inter-Integrated Circuit

IceCube = IceCube Neutrino Observatory

IL = Instruments Line

KM3NET = Cubic Kilometre Neutrino Telescope

kt = Knot (is a unit of speed = 1 Nautical mile = 1.852 km per hour

LabVIEW = Laboratory Virtual Instrumentation Engineering Workbench

LED = Light Emitting Diode

LTI = Linear Time Invariant

MATLAB = Matrix Laboratory

MCU = Microcontroller Unit

N = North

NEMO = Neutrino Mediterranean Observatory

NESTOR = Neutrino Extended Submarine Telescope with Oceanographic Research Project

NI = National Instruments

NM = Nautical Mile = 1.852 km per hour = 1.151 mile per hour

Op-amp = Operation Amplifier

Pa = Pascal

PC = Personal computer

PCB = Printed Circuit Board

PCI = Peripheral Component Interconnect

PIC = Peripheral Interface Controller

PXI = PCI Extensions for Instrumentation

RAM = Random Access Memory

RMS = Root Mean Square

RICE = Radio Ice Cerenkov Experiment

S = South

SAUND = Study of Acoustic Ultra-high energy Neutrino Detection

SCL = Serial Clock

SDA = Serial Data

SMD = Surface Mount Device

SMT = Surface Mount Technology

SNR = Signal to Noise Ratio

UHE = Ultra High Energy

UK = United Kingdom

USB = Universal Serial Bus

UTC = Coordinated Universal Time

VDC = Direct Current Voltage

W = West

WGS84 = World Geodetic System 1984

Glossary of symbol

p	Pressure change from equilibrium
v	Particle velocity
Φ	Velocity potential
ρ	Density
q_s	Time rate of change of small volume
c	Velocity of sound
E	Energy density
t	Time
β	Thermal expansion coefficient
C_p	Specific heat capacity
τ	Thermal time constant
λ	Dummy variable used to evaluate the integral
γ_G	Gruneisen coefficient
t_0	Flight time from the centre of the shower to the observer
X	Colum vectors of the states
$\dot{X}$	Time derivatives of states
R	External series resistor
K	Omni-directional constant
K_1	Piezoelectric constant
K_2	Piezoelectric constant
V_C	Capacitor voltage
v_1, v_2	Velocities of masses
V_{in}	Applied voltage
F_1, F_2	External forces
C	Capacitance
R	Electrical resistance
m_1, m_2	Masses
r_1, r_2	Mechanical resistances

k_1, k_2, k_3	Spring constants
$h(t)$	Impulse response in time domain
$y(t)$	Output response in time domain
$x(t)$	Input signal in time domain
$h(\omega)$	Impulse response in frequency domain
$y(\omega)$	Output response in frequency domain
$x(\omega)$	Input signal in frequency domain
$H(s)$	Transfer function
kS/s	Kilo sample per second
z	Depth
S	Salinity
T	Temperature
pH	Acidity
ω_B	High pass filter for boric acid
ω_{Mg}	High pass filter for magnesium sulphate
a_B	Attenuation for boric acid
a_{Mg}	Attenuation for magnesium sulphate
a_w	Attenuation for frequency of signal
dB/km	Attenuation coefficients
μPa	Micro Pascal
dB	Decibel
mPa	Milli Pascal
V_{ref}	Voltage reference
D	Digital data
I/V	Current to voltage converter

Chapter 1

Introduction

1.1 Introduction

Over the past 30 years, underwater acoustic communication and detection systems have been developed for use in both military and commercial applications, for example, submarine communications, marine species identification, marine monitoring, the offshore oil industry, pollution monitoring in environmental systems, collection of scientific data recorded at ocean-bottom stations and by unmanned underwater vehicles, speech transmission between divers, mapping of the ocean floor for object detection and recovery and so on [1].

In recent years, underwater acoustic detection has been used in many applications. The interest has grown in the detection of ultra-high energy (UHE) cosmic ray neutrinos which offer an unexplored window on the Universe [2].

However, there is still some challenge to detect this type of signal as the probability of neutrino interaction is very small [3]. It can be detected from interaction with dense media, for instance, distilled water, sea water, ice [4]. However, the large scale volume detection of more than 10 km^3 is necessary especially where the fluxes of neutrinos are very low. This leads to the complicated technical design and intensive cost in construction [5]. The detection of neutrinos has been investigating continuously in order to study and understand the universe with different techniques and systems [6]. Optical, air shower, radio, and acoustic techniques have been used for the neutrino detection. More details of acoustic technique research are presented in Chapter 2.

The acoustic technique is utilised in the research as it has advantages over the optical technique. It is based on the effect that cascade, evolving from a neutrino interaction in a medium, generates a sound wave. The two advantages of this method that make the acoustic technique more interesting than the optical detection are following. Firstly, the attenuation length is longer (typically a few km) as opposed to 50-100m for light hence the signal can travel much further. Secondly, the speed of both signals is very different. The speed of acoustic signal is running in m/millisecond whilst the optical signal needs the

process in the m/nanosecond range. As a result, it is much simpler to design and build acoustic sensors and electronic equipment than optical tools. In addition, this technique would allow easily to implement real-time data signal processing which is more important in the data acquisition and monitoring [7], especially when the signal to noise ratio is very low.

Traditionally the analysis of underwater acoustics is carried out exclusively on the amplitude response in the frequency domain. No knowledge of the phase response of the transmitter, receiver or channel is assumed or used. As of a few years ago the only system capable of injecting precise phase controlled acoustic signals into seawater was that developed by Blacknor Technology UK [8], however the implementation detail is vague and subject to commercial secrecy. The traditional technique for injecting acoustic impulses into water is to drop hollow glass spheres which explode when they reach a certain depth [9].

To study the neutrino telescope using an acoustic technique, the calibration of acoustic sensors is essential to generate neutrino-like signals that mimic the neutrino interaction in seawater. Many different techniques for hydrophone calibration have been proposed by various research groups. However, there is challenge because the nature of the hydrophone which could not produce directly an electrical output signal as input signal given.

A study of the reciprocity calibration method for acoustic sensors has been presented by the Institute for Integrated Management of Coastal Areas (IGIC) collaboration [10]. It is a common method to calibrate the sensitivity of acoustic sensors. The advantage of this method is a simple procedure using a calibrated hydrophone with non-calibrated ones. Consequently, it is very convenient to apply in the physics laboratory. In addition, the generation of artificial neutrino signals using transducers has also been presented. The first attempt is to use the known bipolar pulse as a reference. However, the received signal is highly distorted when compared with the emission signal. The second experiment has been done by the inverse method. The transfer function is determined from impulse response. The two equalizations, Flatten spectrum and inverse filter, are applied in order to mimic the neutrino signals. The final result has shown that the inverse filter technique can reproduce the bipolar pulse shape better than the other.

Most recently, the IGIC has developed a calibrator using a parametric acoustic source to generate neutrino-like pulses [11-13]. This method uses two sources for emitting slightly different high frequency signals travelling along the medium, for example water. As a

result of interference, it produces directional low frequency signals. The advantage of this technique is allowing compact calibrator design that is very convenient to deploy in laboratories or in the field.

Hydrophone calibration has been developed by many research groups with different methods[14], however it still remains the challenge of generating neutrino-induced pulse in both directivity and shape. In addition, it is very interesting to design and implement the acoustic transmitters that can generate and control the generation of artificial neutrino-like pulse in sea water.

1.2 Research motivations and justification

In order to study the feasibility of detecting such neutrinos by the acoustic technique, it is necessary to understand the production and detection of the acoustic signal from the shower induced by an interacting neutrino in a medium. Then, an acoustic transmitter is needed to send an artificial acoustic signature emulating UHE neutrino interactions in the sea to study the behaviour of such a signal. It is very important to design and implement an acoustic transmitter that has to be able to imitate the neutrino acoustic pulse, in directivity (pancake) and shape (a short bipolar pulse) as much as possible.

Using a single hydrophone as a transmitter only gives knowledge of the signal shape. Now, the trend of acoustic neutrino detection is moving forward to a hydrophone array detector [15-17].

The commercial acoustic array transmitter system of sufficient standard, particular with respect to phase information, is very expensive and normally only possible in a few national laboratories such as the National Physical Laboratory Wraysbury in the UK [18]. As a result, the design and building of an electronic systems to generate acoustic bipolar pulses with such characteristics are very challenging.

The development of hydrophone array is very useful in order to synchronise signals from each hydrophone getting a high amplitude pulse. It would be very useful for transmission signals in deep sites as acoustic neutrino telescopes are normally sited at large depth, for example, the ANTARES site is about 2475 metres. This advantage cannot be done in a single hydrophone experiment.

As Northumbria University is a member of ACoRNE collaboration, this research has enjoyed the full support of our collaborators which use the acoustic technique to create an

acoustic neutrino telescope. During this work, ACoRNE collaboration has formed excellent relations with the ECAP collaboration who is the organiser and collaborator to deploy a hydrophone array transmitter at the ANTARES site.

1.3 Research objectives

The main interest of this project is to design and implement an eight-hydrophone transmitter array to generate artificial UHE neutrino-induced pulses using digital signal controllers. To achieve this, the research objectives are outlined as follows.

1. Study and simulate the signal processing techniques for artificial acoustic bipolar pulse based on thermo-acoustic theory using single hydrophone modelling.
2. Design and implement a single channel acoustic signal generation module using microcontrollers.
3. Test a single hydrophone calibrator in laboratory water tank using a microcontroller module and a NI commercial module to validate the results.
4. Deploy a single hydrophone transmitter at the Rona (west coast of Scotland) site and analyse the single hydrophone data.
5. Study the signal processing techniques for simulation of acoustic array calibration and generation of artificial UHE neutrino signals using eight hydrophones.
6. Design and implement a high voltage dc-to-dc converter power supply module, eight-channel hydrophone power amplifier module, eight-channel acoustic generation module using digital signal controllers.
7. Experiment an eight-channel acoustic transmitter array in a laboratory water tank using the eight-channel digital signal controller module and the eight-channel NI digital to analogue commercial module to validate the resulting data.
8. Deploy the eight-channel acoustic hydrophone array transmitter system at a site, for the example ANTARES, France or NEMO (Sicily).
9. Analyse the deployed data from a site to draw suitable conclusions and make suitable recommendations for future work.

1.4 Original Contributions

As a result of the study, the author has made the following original contributions to knowledge.

1. A single hydrophone calibration for generation of artificial Ultra High Energy (UHE) neutrino-induced pulses based on a thermo-acoustic model has been presented. A bipolar acoustic generation module has been built using PIC microcontrollers for processing and control. The NI USB-6211 has been used to validate the result with PIC module. The experiments in a laboratory water tank have already been verified the computer simulation showing excellent agreement, see Chapter 3.
2. A single hydrophone transmitter was deployed at the Rona site. The analysis of data from the deployment has been made and presented, see Chapter 4.
3. The simulation of a hydrophone array to emit acoustic pulses that mimic the neutrino interaction in seawater has been investigated and presented, see Chapter 5.
4. The design and implementation of an eight-channel acoustic generation module using 16-bit digital signal controllers, the +12Vdc to ±100Vdc dc-to-dc converter power supply module and the eight-channel hydrophone power amplifier module have already been built and tested at the laboratory water tank. The NI PXI-6713 digital to analogue converter commercial module has been use to verified the results from the simulation and dsPIC module, see Chapter 6.
5. The eight-channel acoustic array transmitter was deployed at the ANTARES site using dsPIC and NI PCI-6713 module for generation of neutrino-like signal, see Chapter 7.
6. The deployed data from ANTARES site was analysed using signal processing techniques to recognise the pulses emitted. The suitable conclusions and recommends for future work has been discussed, see Chapter 7.

1.5 Organization of the thesis

This thesis comprises eight chapters. Chapter 1 begins with an introduction and a brief background of the research. The objectives of this research are also presented in this chapter including the original contribution of the research. The list of publications is finally added in this chapter.

Following the introduction is Chapter 2 that presents an overview of the neutrino telescopes. The formation of a neutrino-like signal based on thermo-acoustic model is also

presented. The Attenuation and noise background for acoustic signal detection in seawater are discussed.

The simulations and experiments for UHE neutrino detection using an acoustic technique from many research groups are presented. The main discussions are focussed on the ACoRNE collaboration, using Rona site for a test bed, and the ANTARES collaboration. This research has used both sites for the sea operation.

Chapter 3 discusses a simple model of an omni-directional hydrophone using a state space equation that can be converted to a transfer function. The calibration of a single hydrophone, for generation of artificial Ultra High Energy (UHE) neutrino-induced pulses, is investigated using signal processing techniques. A bipolar acoustic generation module is built using PIC microcontrollers, the NI USB-6211 module is used for comparison. The experiment has already been done in the laboratory water tank. The results from simulation and experiment are compared showing excellent agreement. This single hydrophone calibrator has been deployed at the Rona site in order to study the behaviour of such signal characteristics.

Chapter 4 starts with the simulation of sound attenuation in sea water using ACoRNE parameterisations to compare the results with other references. The 10 kHz and 23 kHz bipolar pulses are simulated with varying distances from the observer. In addition, the response of the Rona hydrophone is investigated for the response to both 10 kHz and 20 kHz bipolar pulses.

The main section of this chapter discusses the deployment and data collection using a point source hydrophone that deployed at the Rona site in September 2008. An array of hydrophones at the Rona site has been studied. The signal injection and data collection are presented. The identification of such signals using the signal processing techniques is presented.

The simulation of acoustic array calibration and signal processing techniques for UHE neutrino generation is presented in Chapter 5. The simulation of neutrino shower and calculation of sound signal in water using complex attenuation are presented in this chapter. A hydrophone array calibration technique, which applies to eight new TC-4033 hydrophones, is also detailed. The orthogonal pulses for investigation of the possibility of signal coding are presented in the last session of the chapter.

Chapter 6 discusses the design and building of an eight-channel acoustic array transmitter module. Especially, the micro electronic design based on 16-bit digital signal processors is used to generate acoustic bipolar pulse. The eight-channel acoustic transmitter is experimented in the laboratory water tank using a dsPIC module. The NI PXI-6713 Arbitrary waveform generation commercial module is used to validate the results showing excellent agreement.

The most challenging aspect in this research is presented in Chapter 7. The deployment of an eight-channel acoustic array transmitter at the ANTARES site using dsPIC and NI PCI-6713 acoustic generation modules is presented. The setting up of hardware and software and the injection of signals into sea water are illustrated in more detail. Signal processing techniques are applied to investigate the deployed data in order to recognise signals emitted. Finally, the conclusion and future work are presented in Chapter 8.

1.6 List of publications

1.6.1 Journal papers

1. W. Ooppakaew and S. Danaher, "Hydrophone calibration based on microcontrollers for acoustic detection of UHE neutrinos," *Nuclear Instruments and Methods in Physics Research A,* vol. 662, pp. S249-S253, 2012.
2. S. Danaher and W. Ooppakaew, "Acoustic detection of primordial balck holes at the ACoRNE experiment," *Nuclear Instruments and Methods in Physics Research A,* vol. 662, pp. S198-S202, 2012.

1.6.2 Conference papers

1. W. Ooppakaew, S. Danaher, and O. Veledar, "Hydrophone calibration based on microcontrollers for acoustic detection of UHE neutrinos," CSNDSP2010, Newcastle, UK, 21-23 July2010.
2. W. Ooppakaew, M. Saldana, S. Danaher, “Acoustic Array Calibration and Signal Processing for UHE Neutrinos Generation,” The 8th IEEE International Conference on Mobile Ad-hoc and Sensor Systems (MASS 2011), Valencia, Spain, 17-22 October 2011.
3. W. Ooppakaew, S. Danaher, R. Lahmann, and K. Graf, "A Linear Array Hydrophone Transmitter for the calibration of acoustic UHE Neutrino Telescopes " in *ARENA 2012- Acoustic and Radio EeV Neutrino Detection Activities*, Erlangen Castle,Germany, 19-22 June 2012.

1.6.3 Posters

1. W. Ooppakaew, S. Danaher, P. Minns, L. Thompson, C. Rhodes, and O. Veledar, "Advanced signal processing techniques for underwater acoustic transmission using steerable acoustic transducer arrays," in School of CEIS research-teaching forum 2009, Northumbria University, 2009.
2. W. Ooppakaew, S. Danaher, P. Minns, L. Thompson, and O. Veledar, "Signal processing techniques for underwater acoustic detection of UHE neutrinos," in Northumbria University research conference, Northumbria University, UK, 2010.
3. W. Ooppakaew, S. Danaher, P. Minns, L. Thompson, and O. Veledar, "Hydrophone calibration based on microcontrollers for acoustic detection of UHE neutrinos," in School of CEIS research-teaching forum 2010, Northumbria University, 2010.
4. W. Ooppakaew, S. Danaher, P. Minns, L. Thompson, and O. Veledar, "An acoustic hydrophone linear array calibrator for UHE neutrinos," in ARENA2010 June 29, to July 2 2010, Universite de Nantes, France, 2010.

1.6.4 Presentations

1. W. Ooppakaew, "Advanced signal processing techniques for underwater acoustic transmission using steerable acoustic transducer arrays," in CEIS school research seminar, Northumbria University, 24th March 2010.
2. W. Ooppakew,S Danaher, P. Minns, L. Thompson “Advanced signal processing techniques for underwater acoustic transmission using steerable acoustic transducer arrays: Laboratory experimental result” in CEIS school research seminar, Northumbria University, 9th Febuary 2011.

Chapter 2

Introduction to neutrino telescope

2.1 Introduction

Neutrino astronomy is now fairly mature and there has been considerable success at lower neutrino energies. Neutrinos are a family of particles so-called Leptons that consist of three flavours, electron neutrino (v_e), muon neutrino (v_μ) , tau neutrino (v_τ). The three types of anti-neutrino are anti-electron neutrino ($\bar{v}_e$), anti-muon neutrino ($\bar{v}_\mu$) , anti-tau neutrino ($\bar{v}_\tau$).

Much work still needs to be done for the exploration of UHE (E>1EeV) regime with neutrinos in order to study and understand about our universe. Neutrinos at these energy are rare and require detectors of the order of 1 km^3 in order to have sufficient events in reasonable timescales. As mentioned in the previous chapter, the simulations and experiments for neutrino detection have been studying using different techniques. Optical Cerenkov, air shower, radio Cerenkov and acoustic detectors have different ranges of detection. The acoustic technique is very popular as it has two advantages over the optical neutrino telescope. A much increased attenuation length (in the order of km rather than 100m) is the first factor to make this method very interesting. The design and implementation of acoustic sensors and data acquisition system is also simpler than the optical technique and allows for coherent detection, with many associated advantages in terms of sensitivity and signal processing.

This chapter presents a brief history of the neutrino discovery, sources and types of neutrinos. The formation of the acoustic signal is also discussed in more details. The simulations and experiments of neutrino detection from many research groups using various techniques are also presented. The main overview is focused on the acoustic technique as the present research uses this method for neutrino detection. The works of the collaborators and test bed sites are discussed, especially the Rona and the ANTARES sites which we have deployed a single hydrophone transmitter and an eight-hydrophone array transmitter, respectively. More details on the Rona site present in Chapter 4. The sea campaign at the ANTARES site with the Erlangen Centre for Astroparticle Physics (ECAP) collaboration details in Chapter 7.

2.2 Overview of UHE Neutrinos

The traditional study and observation of the Universe have been made via photons and cosmic rays. However, there are some limitations of the observation via these particles [4]. As a result of photon interacts with matter and the cosmic microwave background, some information could not be carried by photons to our Earth. Particularly for large distances (>1Mpc), protons and nuclei are deflected by magnetic fields during their travelling through the Universe, so directional information is lost.

In order to achieve the study and understanding about the Universe, it would be very useful to study the particle with no electrical charge which was generated in astrophysical sources. However, it would have very small chance to interact with other substances. In addition, being uncharged, they will not be affected by electromagnetic fields. So, these particles can travel for a long distances and can keep information from their original source that would be very useful to study of the Universe. From these reasons, the trend of particle study has been moved toward to neutrinos. The current best mass estimation for the neutrino, based on experimental evidence, is about 0.2eV. Figure 2.1 shows different types of particles from astrophysical sources travelling to the Earth.

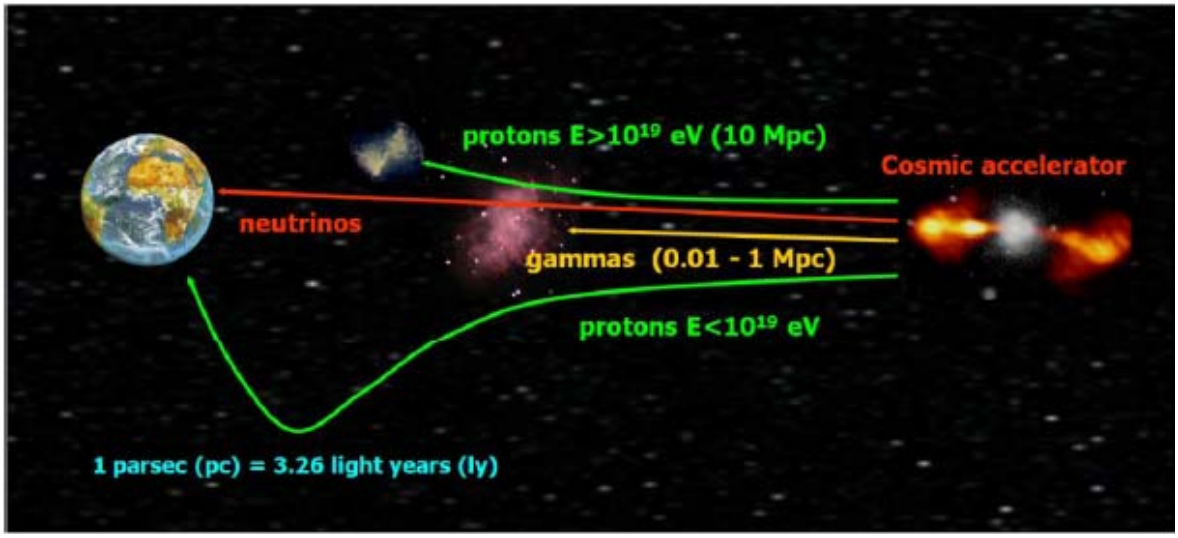

Figure 2.1 Different types of particles travelling to the Earth [4].

Neutrinos are the second most abundant particles in the Universe after cosmological photons. They are uncharged sub-atomic particles without electric charges, which were predicted by Wolfgang Pauli in 1930. Pauli had explained the conservation of energy and linear momentum of β decay. From the Pauli proposal, the neutrinos had a very small diameter and were massless. In 1956, Federick Reines and Clyde Cowan detected

neutrinos from the Hanford nuclear reactor using a delayed-coincidence technique on the reaction [19]. In 1998, the Super-Kaminokande collaboration proved that the neutrino has a very small mass [20].

Neutrinos are produced from many sources, for the example, Active Galactic Nuclei, Gamma Ray Bursts, dark matter, Supernova remnants and so on. There are about three hundred million neutrinos per cubic metre of space and billions of neutrinos pass through our bodies every second [6]. However, our understanding of neutrinos is still not totally satisfactory. Astronomers are very interested to study and detect this particle as it only interacts with the weak nuclear and gravitational forces. It can therefore travel while retaining its energy and directionality far away from the original place. So it can arrive on Earth with original information that would be very useful to study about their original source.

2.3 Formation of the acoustic signal

The production mechanism of the bipolar acoustic pulse is based on the thermo-acoustic model. The standard equations of the thermo-acoustic model have been presented in [21-22]. The simulations of acoustic bipolar pulse based on the thermo-acoustic model have been studied by the ACoRNE collaboration [2]. More details of thermo-acoustic mechanism equations have been derived [19]. The experimental verification of the thermo-acoustic sound generation has been presented by [5].

The thermo-acoustic model is utilised to describe the ultra-high energy neutrino interaction in sea water. When the ultra-high energy neutrino passes through the seawater, it deposits energy along its path, causing heating of the sea water which results in an acoustic wave.The shower induced by neutrino interaction in water deposits most of its energy in a cylindrical volume of few centimeter in widths and about ten meter in lengths. Each point along the path is an acoustic point source. Constructive interference occurs at a distance away from the original neutrino energy deposition.

Along the path of the neutrino energy deposition the temperature increases nearly instantaneous. The corresponding acoustic pulse shape is defined by the derivative (with respect to time) of this temperature profile. The acoustic pulse generated sits in a “pancake” perpendicular to the original neutrino direction. The typical opening angle, theta, is about 5 degrees. This gives rise to a characteristic acoustic signal which is bipolar

in shape and has a typical frequency of 10-30 kHz. The steps of acoustic signal formation from top (left to right) and bottom (left to right) are shown in Figure 2.2 [23].

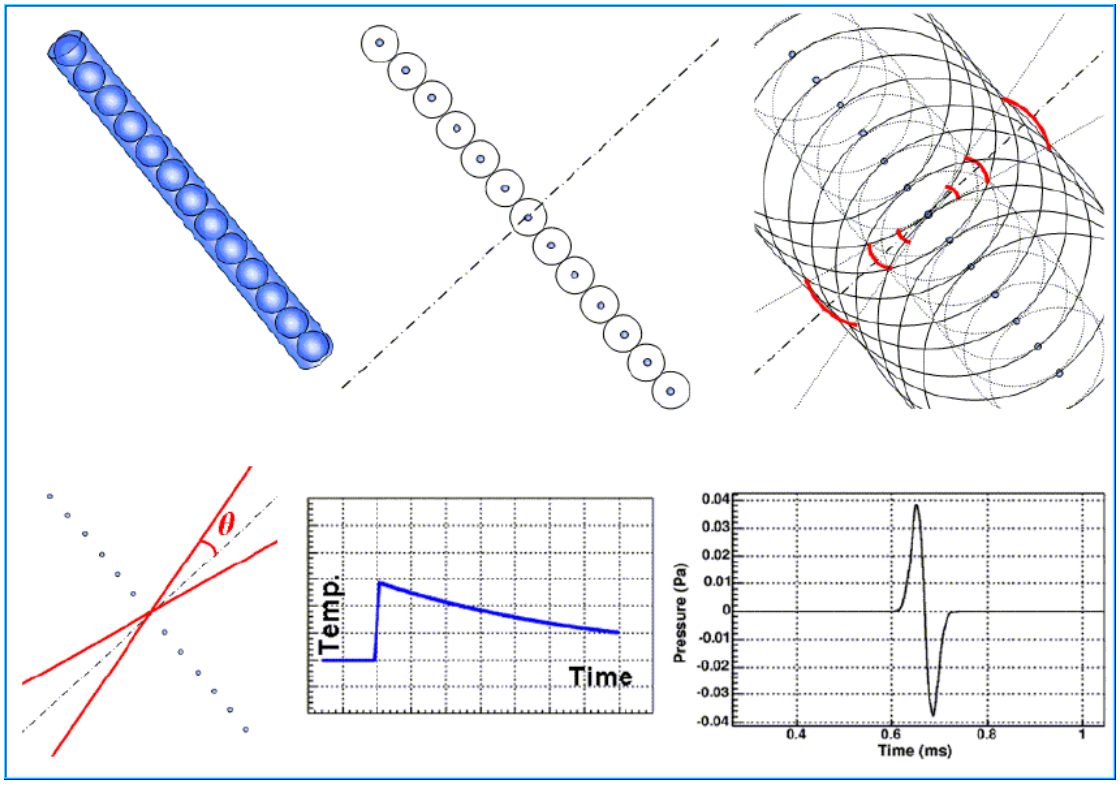

Figure 2.2 The formation of acoustic signal.

The calculation of the pressure pulse for the simulated energy deposition of the cascade has been done by the ACoRNE collaboration [2]. The important variables of acoustic bipolar generation are the pressure change from equilibrium(p), the particle velocity (v), and the velocity potential (Φ). The relations of the three variables when assuming zero curl are express in equation (2.1).

$$v = \nabla\Phi, \qquad p = -\rho\frac{\partial\Phi}{\partial t} \tag{2.1}$$

Where ρ is the density. The velocity potential is a function in acoustics equivalent to the magnetic vector potential in electromagnetism. The wave equation is solved to get the pressure pulse at the location of an observer placed at $|\bar{r}|$. It can be done by integrating all the contributions of infinitesimally small sources at locations $|\bar{r'}|$. A shower event at the point $\bar{r'}$ and an observer at the point$\bar{r}$, are separated by the distance $r = |\bar{r} - \bar{r'}|$.

$$\nabla^2\Phi - \frac{1}{c^2}\ddot{\Phi} = \int q_s(r', t')dt' \tag{2.2}$$

Where q_s is the time rate of change of small volume and the velocity of sound (c). In this case, it is focused in integrating q_s over the cascade volume where this volume change is caused by the injection of an energy density E(in $\mathrm{Jm^{-3}s^{-1}}$) over this cascade volume. For an infinitesimal volume, the volume change starting at time $t = 0$, is given by

$$q_s(\bar{r'}, t) = \frac{\beta}{\rho C_p} E(\bar{r'}, t) - \frac{1}{\tau}\int_0^t q_s(\bar{r'}, t')dt' \tag{2.3}$$

Where β is the thermal expansion coefficient, C_p is the specific heat capacity, ρ is the density and τ is the thermal time constant. The integral term is caused by cooling as the deposited energy, within the volume, conducts or convects away into the surrounding fluid. However, the time constant for this thermal cooling mechanism is of the order of tens of milliseconds. As this research is primarily interested in the case where the energy is injected nearly instantaneously in acoustic terms, the second term in equation (2.3) can be ignored as it is about six orders of magnitude lower than the first term. Then equation (2.3) can be integrated over the entire volume cascade using Green's function [24] and yields for an observer at distance, r, from the source.

$$\Phi(\bar{r}, t) = \iint_V \frac{1}{|\bar{r} - \bar{r'}|} E(\bar{r'}, t')_{(t=t'+|\bar{r}-\bar{r'}|/c} dV dt' \tag{2.4}$$

Where $t - r/c$ is the retarded time, this simply implies that the contribution from each point in the source, in both space and time, travels to the listener with the speed of sound. Then equation (2.4) lends itself to efficient numerical solution. If the energy deposition is modelled using Monte Carlo points with a density proportional to energy, $\Phi(t)$ will be a scaled histogram of the flight times to the observer. The pressure can now be derived from equation (2.1). A further simplification can be made if the energy deposition as a function of time is identical at all points in the volume. The velocity potential can then be calculated from the convolution integral from equation (2.5).

$$\Phi(t) = \frac{\beta}{4\pi C_p \rho} \iint_V \frac{1}{r} E_s(\bar{r'}) dV E_t(t' - \lambda) d\lambda \tag{2.5}$$

Where λ is a dummy variable used to evaluate the integral. This can be simplified further since $E(t)$ can be approximated by $\delta(t)$ for this case. The time dependence on the right-hand side will disappear as the integral of a delta function is equal to one. This formulation of the thermo-acoustic mechanism leads to a solution in the far field which is proportional to the Gruneisen coefficient γ_G[25]. If, after an arbitrary 3D rotation, the observer is, for example, at a distance from the source along the x'-axis much further away than the

dimensions of the source, then with increasing observer distance, x'_0, $E(y')$ and $E(z')$ contribution will more and more closely resemble delta functions as the spread in arrival times caused by their contributions approaches zero. Then equation (2.5) reduces to equation (2.6).

$$\Phi(t) = \frac{\beta}{4\pi C_p \rho} \frac{c}{x'_0 - x'} E(c(t - t_0)) \approx \frac{\beta}{4\pi C_p \rho} \frac{c}{x'_0} E(c(t - t_0)) \tag{2.6}$$

Where t_0 is the flight time from the centre of the shower to the observer. The velocity potential, $\Phi(t)$, is simply a scaled cross-section of the energy deposition and $p(t)$ a projection of $\Phi(t)$.

$$\begin{aligned} p(t - t_0) &= \frac{\beta}{4\pi C_p} \frac{c}{x'_0 - x'} \frac{d}{dt} E(c(t - t_0)) \\ &= \frac{\beta}{4\pi C_p} \frac{c^2}{x'_0 - x} \frac{d}{dx'} E(x') \\ &\approx \frac{\beta}{4\pi C_p} \frac{c^2}{x_0 - x} \frac{d}{dx'} E(x') \end{aligned} \tag{2.7}$$

The term $\frac{\beta C^2}{C_p}$ is the Gruneisen coefficient and gives the relative acoustic pulse heights for different media. A bipolar pulse can determine from a derivative of the Gaussian distribution. Then, a bipolar pulse ($y(t)$) can determine from equation (2.8).

$$y(t) = \frac{d}{dt} e^{-(t-\mu)^2/(2\sigma^2)} \tag{2.8}$$

Where parameter μ is the mean and σ^2 is the variance. In this research defines $\mu = 0$ and $\sigma = 16 \times 10^{-6}$ for 10 kHz and $\sigma = 6.9 \times 10^{-6}$ for 23 kHz bipolar pulses. The simulation of neutrino-like signal will be studied and presented in Chapter 5 for a single hydrophone and Chapter 7 for an array of eight-hydrophones.

2.4 Attenuation and noise background of acoustic signals

One more obstacle for the detection of acoustic radiation in water is the signal attenuation resulting from the properties of the medium which it travels. The high frequency of signals is attenuated by water as it is equivalent to a low pass filter. The comparison of attenuation between seawater and distilled water is presented by Lehtinen [26] and plotted in Figure 2.3. The graph shows the attenuation frequency ranges from about 1 kHz to 1 MHz. The attenuation of seawater is much higher than distilled water at low frequency whereas it is slightly different for the attenuation values of the frequency up to 1 MHz. However, the

frequencies of interest for acoustic detection are in the range from 10 kHz to 100 kHz, the attenuation is quite different for both media.

The noise background is more important to consider in acoustic detection in sea water [27]. The studies of noise made in recent years have vastly improved and extended our knowledge about the characteristics and sources of deep-sea noise. It can be classified into two types; transient noise and ambient noise. Firstly, transient noise is mostly caused by marine life in the water. Human activities such as submarines and ship traffics are other causes for the transient noise. Secondly, ambient noise is usually caused by weather at the surface for frequencies of our interest. Figure 2.4 shows the average deep-water ambient-noise spectra for different conditions of shipping and wind speed, taken from [1]. Seismic noise dominates and rolls off as a power law at frequencies below 10 Hz. Shipping noise can be seen in the range 20-50 kHz in most parts of the ocean, even if vessels are not seen in the vicinity. Between 0.5 kHz and 50 kHz are dominated by wind and waves at the surface of ocean [28].

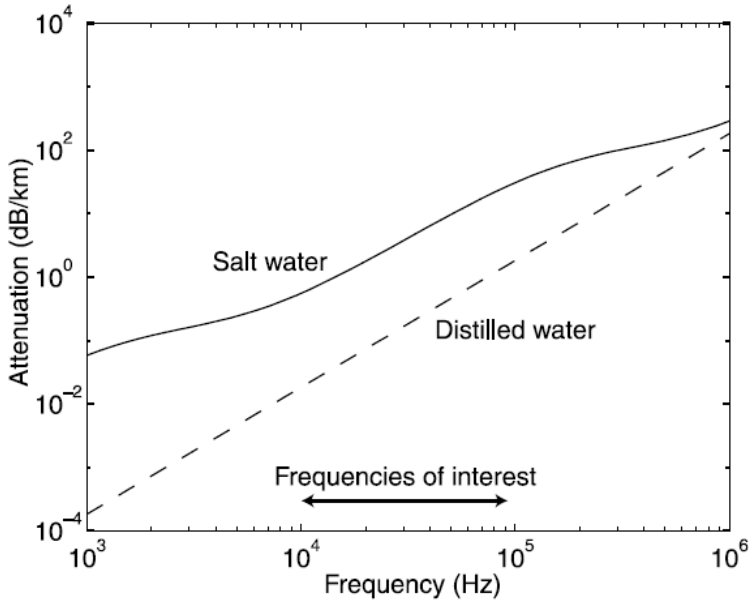

Figure 2.3 Comparison of attenuation in seawater and distilled water

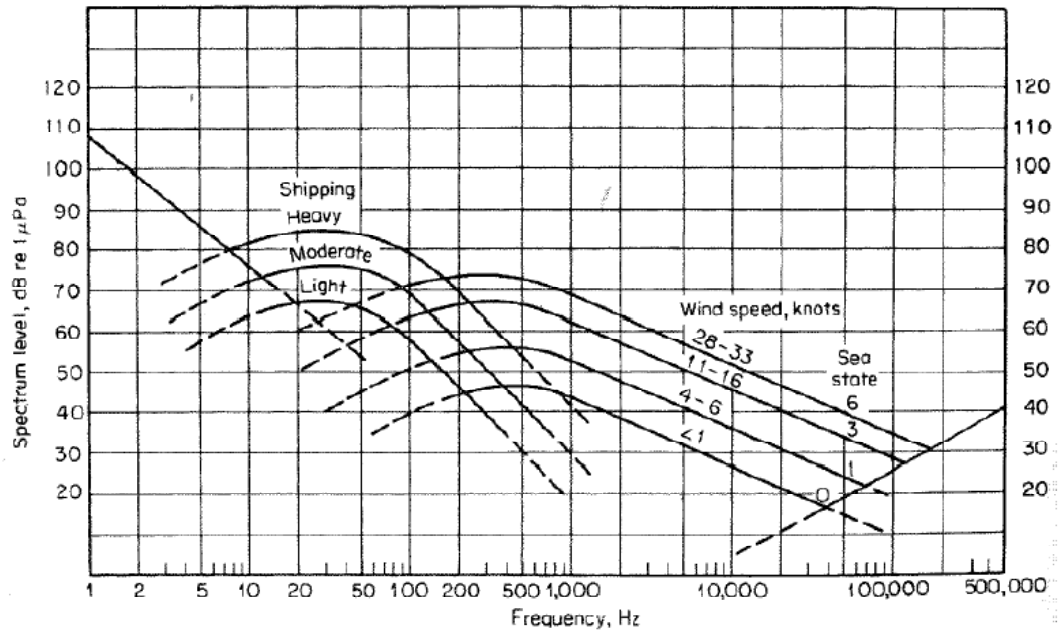

Figure 2.4 Average deep-seawater ambient noise spectra [1].

The noise for acoustic particle detection can be classified into three different ranges of frequency [19].

1. **Below 200 Hz:**

The ambient noise below 200 Hz is not relevant to acoustic particle detection as this frequency range is much lower than the acoustic signal of interest. The noise in this range results from sea current, turbulence whilst transients in this frequency range are produced by ships and marine life.

2. **200 Hz to 50 kHz:**

The maximum interference to acoustic particle signals is in this range. Interference signals depend on the weather conditions, in the main resulting from motion of the sea surface, wind turbulence and interaction of surface waves.

3. **Above 50 kHz:**

In this range, the main contribution to background noise arises from thermal noise. It is caused by the motion of water molecules moving in different direction to hit the sensors.

The ambient noise in the deep-sea results from the wind waves and swell, the relation between the wind speed at a given location and the swell of the sea surface (sea-state) is presented by US Navy and Beaufort Sea-state Codes [5] as shown in Table 2.1.

Table 2.1 Description of the sea-state by the wind speed at the surface.

Sea-State (SS)	Beaufort Number	Wind Speed (knots)	Wind description
0	0	< 1	Calm
0	1	1-3	Light air
1	2	4-6	Light breeze
2	3	7-10	Gentle breeze
3	4	11-16	Moderate breeze
4	5	17-21	Fresh breeze
5	6	22-27	Strong breeze
6	7	28-33	Near gale
7	8	34-40	Gale
8	9	41-47	Strong gale
9	10	48-55	Storm
9	11	56-63	Violent storm
9	12	≥ 64	Hurricane

Studies of the spectral density of the ambient noise at the ANTARES site have been made by ECAP [5]. The HTI and ECAP hydrophones and one AM sensor were used to record the noise levels on Line 12 over several time periods with a combined duration of six months. The noise floor is the lowest for the HTI hydrophones, the difference in the power spectral density to the ECAP hydrophones and AM sensor being 10 to 15 dB. The ANTARES hydrophone sensitivity is around -145dB re 1V/μPa (or 0.0562V/Pa) for the frequency range up to 50 kHz. The mean ambient noise level is about 10 mPa in the frequency range from 10 to 50 kHz and 20 mPa for 1 to 50 kHz that would give an RMS value around 0.5mV and 1mV for the respective frequency ranges.

The calculation and simulation of sea water attenuation using ACoRNE parameters, for Rona site and ANTARES site, are presented in more details in Chapter 4 and Chapter 5, respectively.

2.5 Overview of contemporary neutrino telescope experiments

Many experiments have made advances with new results over recent years in neutrino detection. There are various research groups and collaborations trying to improve the neutrino detection with different techniques. The main purpose of experiments is to study a

suitable technique that should give a good result at a reasonable cost. Traditional neutrino detection experimental techniques are based on optical Cerenkov, Air shower, Radio Cerenkov and acoustic techniques. However, a hybrid technique, with comprising two or three techniques, is now interesting from various research groups.

The optical experiments include AMANDA [29], IceCube [30-32] and ANTARES [33].The Pierre Auger collaboration, using an extended air shower array detector, is searching for upward and almost horizontal showers from neutrino interactions [34]. Radio experiment includes RICE [35], ANITA [36], all have progressed the field and published competitive limits for the neutrino flux. The last technique in the neutrino telescope is the acoustic detection which has been being studied by the SAUND[28], Lake Baikal [37-38], KM3NET[39-40], NEMO [41-42], NESTOR[43-44], SPATS [45],ANTARES[33] and ACoRNE [16] collaborations. However, this latter research is supported by our ACoRNE collaboration which uses the Rona site as a test bed for single source hydrophone emission. Moreover, ACoRNE has collaborated with the ECAP collaboration using the ANTARES site for deployment of eight-channel hydrophone transmitters. Then, the main details will focus on the research at the ACoRNE collaboration for the Rona site field trip and the ANTARES detector in the sea campaign with ECAP.

2.5.1 SAUND collaboration

The Study of Acoustic Ultra-high energy Neutrino Detection (SAUND I) experiments have been done using a seven hydrophone array in July 2001 in the Bahamas [46]. The SAUND uses the US Navy's Atlantic Undersea Test and Evaluation Centre (AUTEC) hydrophone array as a test base. It is a deep-sea with depth of 1-2 km within several miles of shore. The SAUND II project was started in July 2006. Forty-nine hydrophones were built instead of the previous seven hydrophones. Real time data was transmitted to shore via optical fibres which interfaced to seven computers for analysis. The data analysis and the comparison of results between the SAUND I and SAUND II have been published in [47].

2.5.2 Lake Baikal collaboration

The Lake Baikal neutrino telescope is in the south of the Russian region of Siberia. The first NT200 underwater neutrino Cherenkov detector was constructed in 1998 [48]. The recent project is the NT200+ which has been operated since 2005. In this project, a prototype acoustic module which consists of 4 hydrophone acoustic sensors has also been included. As the water in Lake Baikal is fresh water, the attenuation length is much higher

than seawater. For instance, at the frequency 40 kHz, the attenuation length of fresh water is about 10 km whilst it is 4 km for seawater. The acoustic hardware design, noise studies and data analysis from the experiment have been published in [49].

2.5.3 KM3NET consortium

The Cubic KiloMetre NEutrino Telescope (KM3NET) is a consortium of forty institutes or universities from ten countries, Cyprus, France, Germany, Greece, Ireland, Italy, Netherlands, Romania, Spain and United Kingdom. The main purpose of this collaboration is a deep sea research of neutrino telescopes with a volume of several cubic kilometres constructed in the Mediterranean Sea[50]. The KM3NET test bed sites consist of three locations in the Mediterranean Sea, ANTARES, NEMO, NESTOR. The most advanced project is the ANTARES collaboration which is operating at a site off the south coast of France near Toulon. The NEMO is constructing the site at the Sicily (Capo Passero) whereas the NESTOR site is located in the coast of Greece at the depth over 4500 metres. Figure 2.5 shows the map of three sites for KM3NET consortium [51-53].

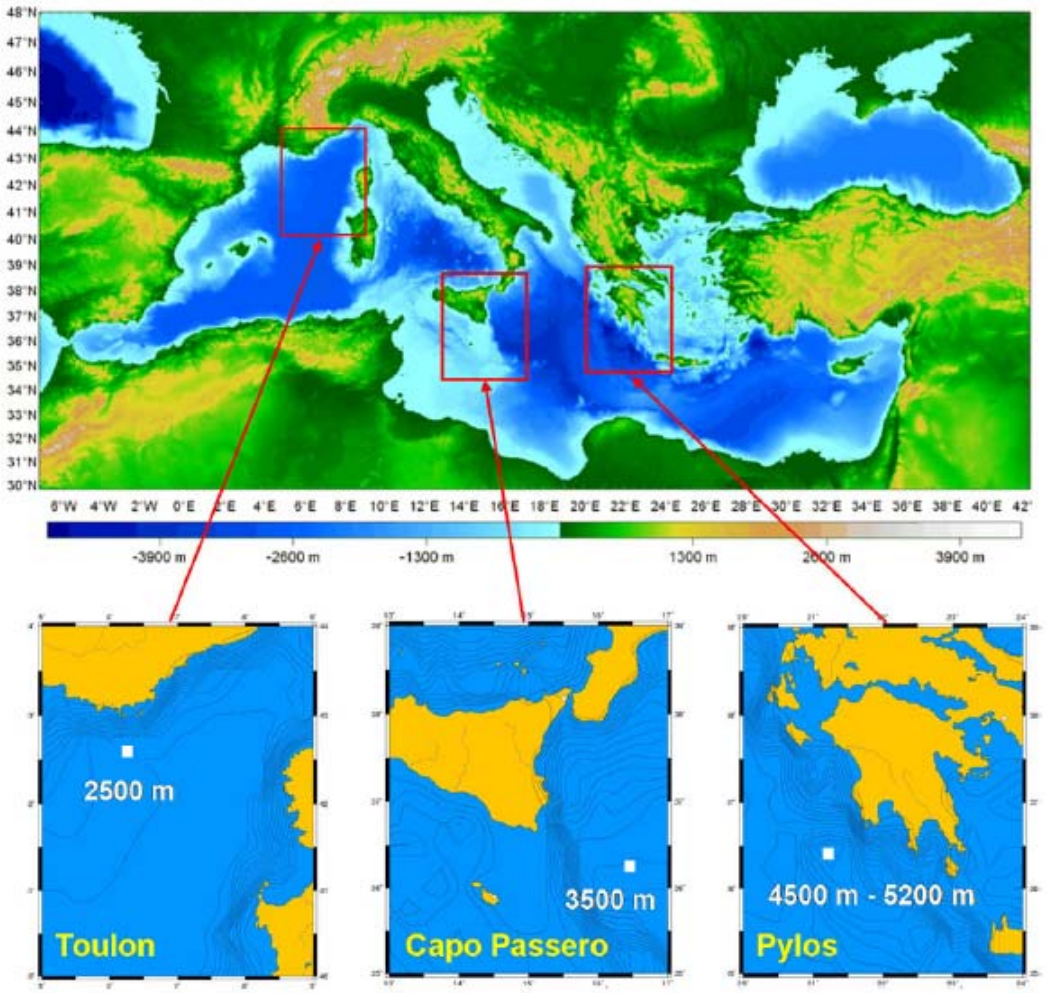

Figure 2.5 Map of three sites of KM3NET project in Mediterranean Sea.

A design study of the infrastructure was started in February 2006. The preparatory phase of the infrastructure has been started since March 2008. The three pilot projects from ANTARES, NEMO and NESTOR have been developed in order to deploy at depths from 2500 to 4500 metres

2.5.4 NEMO collaboration

The NEutrino Mediterranean Observatory (NEMO) collaboration has aimed in the design and construction of km^3 scale acoustic neutrino detection in the Mediterranean Sea. The NEMO uses the Catania test site which has a shore laboratory and a deep-sea laboratory. The first acoustic work in January 2005 was the monitoring and measurement of the acoustic noise background to determine the signal to noise ratio (SNR). Four TC-4042C RESON hydrophones are used for on-line monitoring of the sea environment. The mechanical and electronic design have been fully detailed in[54] which includes data analysis.

2.5.5 NESTOR collaboration

The Neutrino Extended Submarine Telescope with Oceanographic Research (NESTOR) is a deep-sea neutrino telescope in the southern sea off the coast of Greece. NESTOR has developed a deep-sea station which permanently connects to shore for several scientific researches. The construction and deployment was done in January 2002 at a depth of 4100 metres. The data from temperature, light attenuation, geomagnetic, pressure, water current and ocean bottom seismometer sensors were transferred to shore via fibre-optic cable [55-56].

2.6 ANTARES Collaboration

The astronomy with a Neutrino Telescope and Abyss environmental Research (ANTARES) collaboration built a large effective area water Cherenkov detector in the deep Mediterranean Sea optimised for the detection of high-energy neutrinos [57]. In addition, the ANTARES detector has also been designed to monitor and investigate the deep sea environment. The ANTARES neutrino telescope is located approximately 40 km south of the city of Toulon, France [58]. The detector site is installed at a water depth of 2500 metres and a geographic position of $42^{\circ}50'N$, $6^{\circ}10'E$. The map of ANTARES site is shown in [5] Figure 2.6.

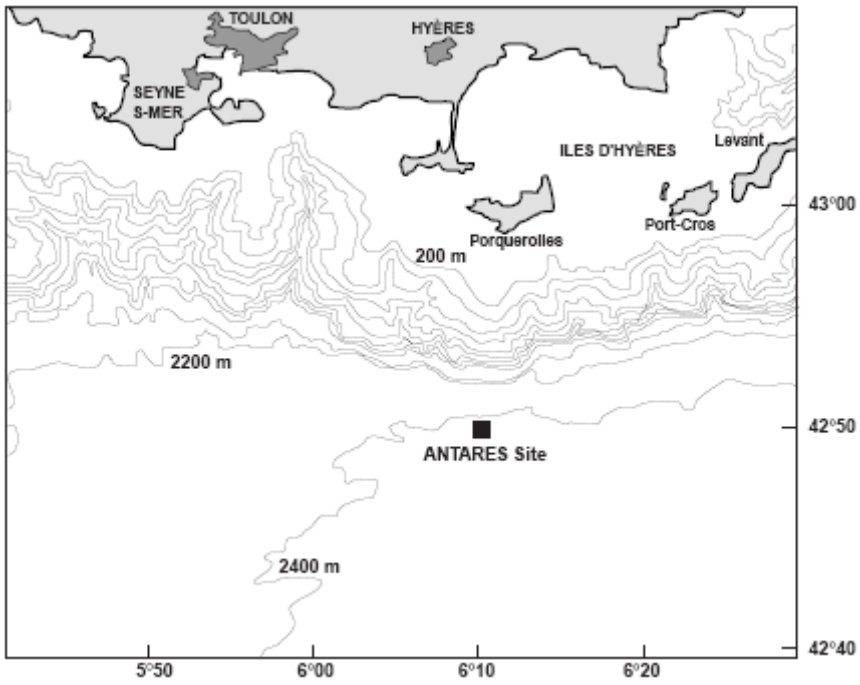

Figure 2.6 The map of ANTARES site.

The ANTARES is a large European neutrino telescope which collaborated with more than 200 scientists, engineers, technicians from France, Germany, Spain, Italy, the Netherlands, Romania and Russia.

2.6.1 AMADEUS detector

The ANTARES detectors consist of 12 vertical line structures, so-called *detection lines.* Each detection line holds 25 sensor storeys. The distance between each storey is 145 m. The first storey is held at 100 metres from the sea bed. Optical cables are used to link between each storey to the junction box which transmits data to the ground station. The optical cables are linked from the junction box to the onshore station about 42km away. The standard storey contains three optical modules (each one comprises a photomultiplier tube in a water pressure resistant glass sphere) and a local control module. In addition, for each module consists of many kinds of sensors and instruments (LED beacons, hydrophones, and compasses/tilt sensors) for timing and positioning calibration of the optical modules. An Instrumentation Line (IL) is designed for sensing and monitoring of the environment. The six storeys are held on the IL line. The ANTARES detector is shown in Figure 2.7. More details for the ANTARES detector has been presented by [59].

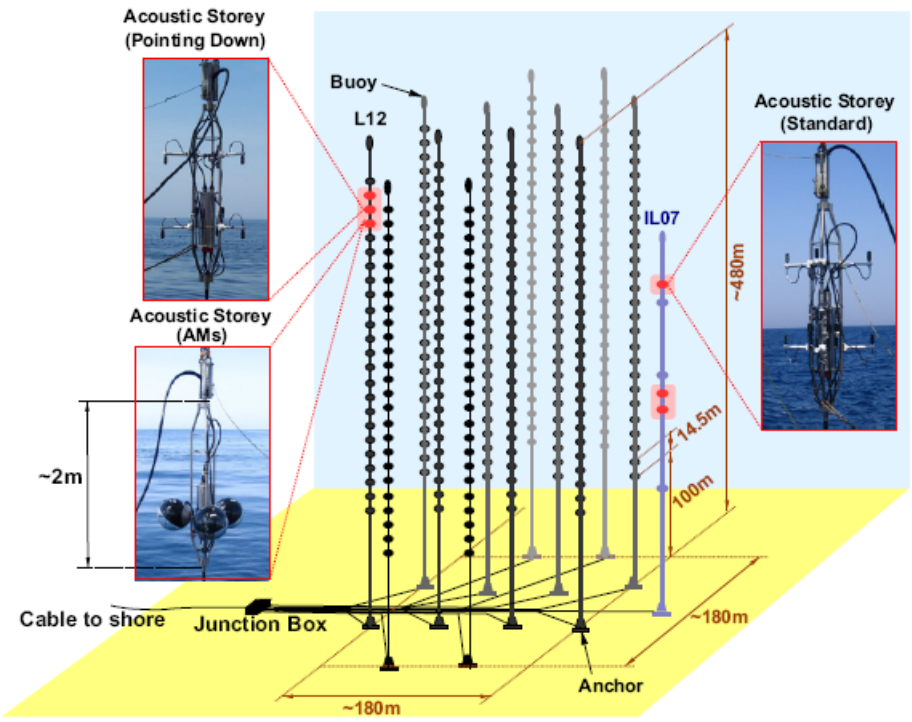

Figure 2.7 The ANTARES detector.

The Acoustic Detection Under the sea (AMADEUS) system is designed for acoustic detection of neutrinos in the deep sea. It replaced parts of the ANTARES detectors [60]. The AMADEUS system consists of six acoustic storeys. The first three are installed on the IL line and the sensors started operation in December 2007. The rest is held on the detection L12 which completely operated in May 2008.The 34 sensors of the AMADEUS site have fully been running to take data whilst the two hydrophones could not operate properly at the time of deployment.

The AMADEUS consists of two types of designed sensors, hydrophones and Acoustic Modules (AMs). Both types are designed based on piezo-electric sensing. The sensors on the IL line are grouped only the hydrophones whilst the L12 line holds the AM module at the lowest point. All of hydrophones are pointed up, except at the centre of L12 that are pointed down. The AMADEUS sensors are shown in Figure 2.8.

Two types of hydrophones are used in AMADEUS detector. Firstly, the commercial hydrophones from High Tech Inc (HTI) are equipped in three of five storeys whilst those in two storeys are designed and implemented by Erlangen Centre for Astroparticle Physics (ECAP). More information about the AMADEUS detector has been presented in [61].

Figure 2.8 Three different storeys of the AMADEUS detector.

As the ACoRNE collaboration and ECAP have successfully used the AMADEUS sensors for the deployment in 17 September 2011, the details will be presented in Chapter 7.

2.7 ACoRNE Collaboration

The acoustic Cosmic Ray Neutrino Experiment (ACoRNE) collaboration consists of researchers from many institutes. The University of Sheffield is the central organization and the laboratory is available there. The University of Northumbria, Imperial College London, University College London, and the University of Lancaster are the members of the ACoRNE collaboration.

The ACoRNE has received permission from the UK Ministry of Defence to use the Rona site as a test bed. The site is located between the Scottish mainland and the island of the Rona. The map of Rona site is shown in Figure 2.9.

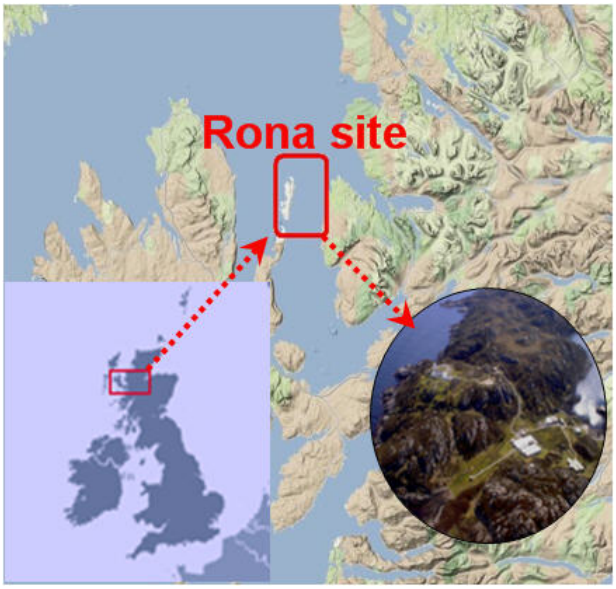

Figure 2.9 The map of Rona site at North West Scotland.

The coordinates of the eight-receiver hydrophone Rona array are shown in table A.1. The grid positions (x, y) are referred to the acoustic centre of the array. The z represents the depth from the surface. The buoy depth is the distance from the surface to the bottom buoy which is always two metres above the mounting plate 2 metres. The extension is the length of string between hydrophone and the bottom buoy. The cable length to shore is the length of cable which starts from the mounting plate on the sea bed to base station on the island. The three dimension simulation of Rona hydrophone array and the drawing of installation for a hydrophone are illustrated in Figure 2.10 and Figure 2.11, respectively. The details of Rona site will be clearly presented in Chapter 4.

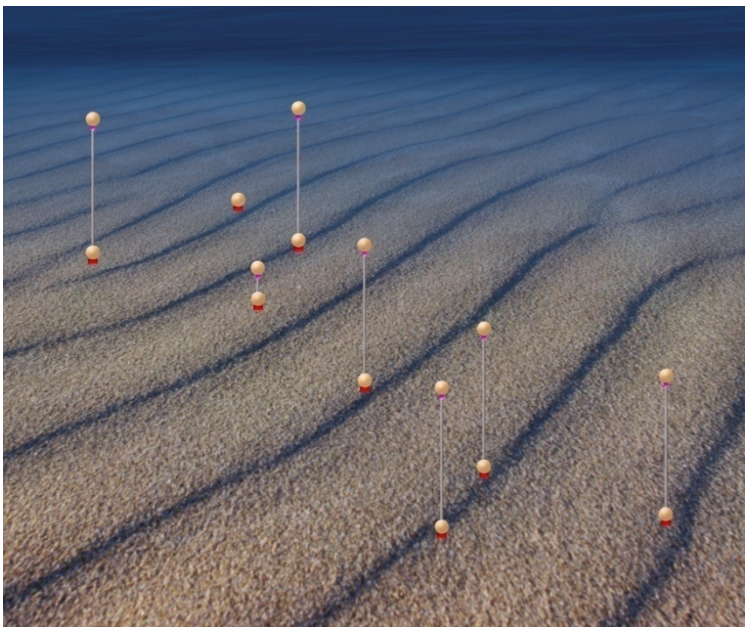

Figure 2.10 The three dimension simulation of Rona hydrophone array.

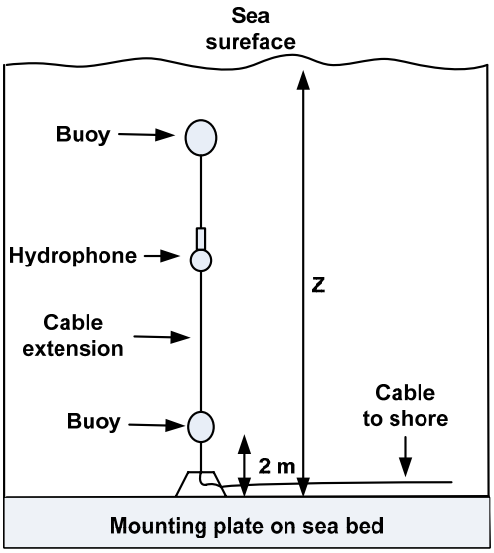

Figure 2.11 The installation of a hydrophone.

The simulation of particle cascades induced by neutrino interaction has been made by ACoRNE collaboration [62]. The main purpose of this research is to understand the characteristic radiation in kilometre scale arrays. The ACoRNE collaboration has been allowed by the Ministry of Defence to use the Rona site, West coast of Scotland, as a test bed for acoustic bipolar pulse injection. The Rona detector consists of an eight-hydrophone array which has been taking the data since December 2005. The deployment utilised a point source for injection of bipolar pulses into seawater. The data received is digitized with 140 kHz sampling rate and recorded to tape for each hydrophone. Unfortunately, 50% of recorded data was unusable because of power failure during measurements. The reason

for the unpredictable power failures on the hydrophones at the Rona site was discovered to be due to the fact that if the hot water was switched on the island, it would take the power from the hydrophones. This problem was fixed using un-interpretable power supplies.

The first data from deployment at the Rona site has been investigated and presented in [15, 63]. Signal processing techniques are applied to identify these pulses. A Butterworth high pass filter is utilised to filter low frequency components. The matched filter is also used for correlating signals. A Neural network is used to recognise the bipolar pulses.

Interestingly, a field trip has been made to the Rona site in August 2007. An omni-directional hydrophone was used as a point source to inject various pulses, step and sine signals, into sea water. The bipolar pulses are varied the amplitude between 10-25V. The bipolar pulses were injected in both continuous and single pulse format. The 20 kHz sine waves were also applied to the hydrophone at the amplitude 20-40 V. The objective of such sine wave signal testing was to measure the attenuation and ambient noise. The analysis of data and signal processing techniques were presented in [64]. The author recommended that two things that need to be improved for the next field trip. Firstly, the pulses were injected into seawater by hand. Human error could occur be occur when they were operating. The next trip should see the pulse generation automatically operated with a time stamp. Secondly, the amplitude of the pulses must be higher to make sure that the pulses will be receivable.

The last ACoRNE field trip was already deployed in September 2008. The ball hydrophone was utilised as a point source for injection of 10 kHz and 23 kHz bipolar pulses. The eight hydrophones in the Rona site were used as the receiving sensors, however, only seven hydrophones were operated properly. The route of this field trip and a boat are shown in the Figure 2.12.

For this trip, the injections of all signals were run automatically with a time stamp. It provided precisely recorded data. The pattern of signal injection was precisely setup using LABVIEW software. The sine signal was firstly sent into sea water, then the bipolar pulses were followed by variation of amplitude for each step. The deployment and data analysis of this ACoRNE field trip will be presented in Chapter 4.

Figure 2.12 Route of Rona field trip (left) and a boat used (right).

2.8 Limits on the neutrino flux from acoustic neutrino telescope

The SAUND collaboration have published the first diffuse neutrino flux limit based on their work on a United States Navy hydrophone array located in the Tongue of the Ocean, a deep basin situated near the Bahanas. They use a seven hydrophone subset of the total 52 hydrophone AUTEC array, arranged in a hexagonal pattern at depth between 1570 m and 1600 m. A novel techniques was employed by which calibration of the hydrophones was achieved by dropping weighted light bulbs into the sea from a stationary boat at the surface. Measuring the signal as the bulb imploded under pressure gave a rough estimation of the energy sensitivity of the array to a known source and allowed for timing calibration.

In addition to the AUTEC array performance evaluation a computer simulation was deployed to test the sensitivity of two hypothetical arrays. Each was comprised of hexagonal lattices of 1.5 km long strings, the strings being modelled to have continuous pressure sensitivity along their entire length. Array “A” is bounded by circle of radius 5 km with 500m nearest neighbour spacing. Array “B” is bounded by a circle of radius 50 km, with 5km spacing between strings. The results of this work are plotted in Figure 2.13 [64].

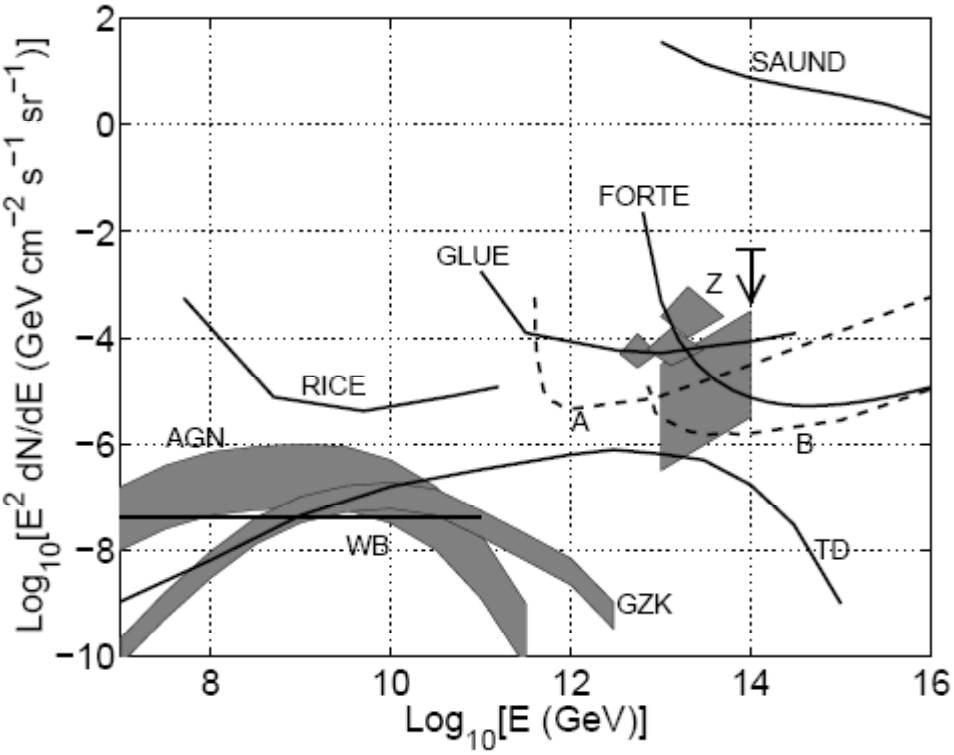

Figure 2.13 Limits on the neutrino flux for the AUTEC array.

2.9 Summary

The overview of neutrino telescopes has been discussed in more details. The formation and original sources of neutrinos have also been presented. The experimental approaches towards the UHE neutrino detection using several techniques have been described. The main purpose ofthe studies is to determine the suitable techniques that can detect neutrino pulses. The overview of previous experimental neutrino telescopefrom many collaborationshas briefly been presented. The main importanceis the ACoRNE and ANTARES collaborations as this research fully supports the ACoRNE previous works and uses the ANTARES detector as a test base. The comparison of attenuation between the distilled water and the seawater has been referred. The classification of noise background for acoustic particle detection is comprised into three groups by frequency ranges. The most effective to acoustic particle signal is the frequency range between 200 Hz to 50 kHz. The description of the sea-state by the wind speed at the sea surface from US Navy and Beaufort sea-state code has lastly been described in this chapter.More details about the sea campaign with ECAP at the ANTARES site are presented in Chapter 7.

Chapter 3

Single hydrophone Calibration

3.1 Introduction

The calibration of acoustic sensors is very important in acoustic detection in order to acquire accurate data allowing for sensitivity and time response of the sensors. An omni-directional hydrophone is used as a source of acoustic signal generation. Ideally, a hydrophone-generated acoustic signal would mimic its electrical input. However, a practical hydrophone cannot produce a linear output signal following its driving input. The transmitting hydrophone is modelled by signal processing techniques, so it is accurately predicted the acoustic output signal for a given driving input. From this idea, it is reversible and is applied to the require driving electrical signal in order to generate the artificial UHE neutrino-induced pulse. In ACoRNE previous works [15-16, 65] have shown that the signal processing technique can successfully be used to calibrate hydrophones. This can present in State Space or a transfer function [66].

This chapter presents a simple model of an omni-directional hydrophone using the state space equation that is very powerful tools for the analysis of linear system. However, as this model has more unknown variables, practically it is simpler to convert the system to transfer function.

A single ball hydrophone calibration for generation of artificial Ultra High Energy (UHE) neutrino-induced pulses is also investigated. Signal processing techniques are applied to hydrophone modelling in order to determine the correct electrical driving pulse for hydrophone that can generate acoustic bipolar pulse as needed.

A single channel acoustic generation module using 8-bit PIC microcontrollers for process and control has been designed and built [67]. The advantage of using embedded system over the personal computer is that it is very compact and reasonable cost. Moreover, power saving is most importance when experiments at fields as it can operate using battery power supply. The single hydrophone calibrator has been tested in water tank at the Sheffield University laboratory using PIC microcontroller module. The NI USB-6211 [68] data acquisition commercial module is used to generate a signal for comparison. The results from simulation and experiment are compared showing excellent agreement.

3.2 Hydrophone modelling

The understanding of the behaviour of acoustic transducers is fundamental to the transmission of acoustic signals. It is necessary to have a model of sufficient complexity such that it can accurately predict hydrophone response. In the case of a transmitting hydrophone for a given acoustic pulse, it is necessary to determine the correct electrical driving pulse.

A number of strategies can be used. With top end laboratory facilities it is possible to determine the full amplitude and phase response of the hydrophone over the full range of frequencies and use classical signal processing theory to determine the appropriate driving signal. Such measurements are however both costly and time consuming.

Another approach is to use the system identification theory such as state space models and transfer function models [69]. There have proved successful in creativity a simple electro-mechanical model of a hydrophone via state space analysis and converting to a transfer function for the actual fitting [70].

State space analysis is a powerful technique for the analysis of linear systems, such as amplifiers, filters and many types of transducers [71]. It is a time domain technique based on matrix representation of systems. It has the advantage of simplicity in combining models from different areas. Rather than using electrical analogies for electro-mechanical systems, the mechanical part of a system can be dealt with directly. State space analysis is very computationally robust, and can deal with very high order systems and with multiple inputs and outputs. Once the state space representation is known, standard algorithms can be used to determine the response of the system to arbitrary inputs and initial conditions. The states are degrees of freedom of the system, for example capacitor voltages and inductor currents for electrical systems and positions and velocities of masses for mechanical systems. The state space model of a system is defined by the pair of the state space equations [72-74] as shown in (3.1).

$$\dot{\mathbf{X}} = \mathbf{AX} + \mathbf{BU}$$
$$\mathbf{Y} = \mathbf{CX} + \mathbf{DU} \qquad (3.1)$$

Where $\mathbf{X}$ and $\dot{\mathbf{X}}$ are column vectors containing the states and their time derivatives respectively, $\mathbf{U}$ and $\mathbf{Y}$ are column vectors containing the inputs and outputs and

A, **B**, **C** and **D** are matrices containing physical parameters such as capacitance and mass. The state space equations of (3.1) can be realized with the block diagram of Figure 3.1.

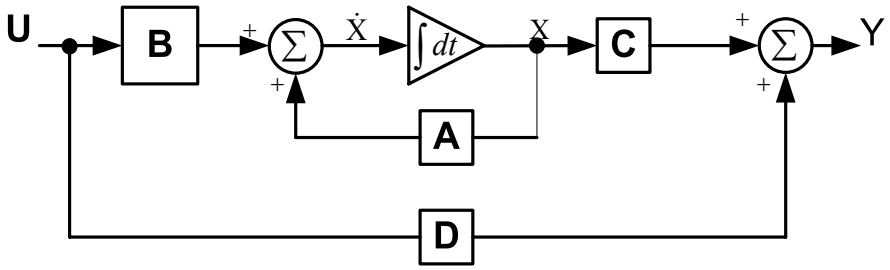

Figure 3.1 Block diagram of state space equation.

A hydrophone is a bilateral transducer that is associated with reversible physical effects [69]. In a reversible effect the same device can, for the example, convert mechanical energy into electrical energy and also convert electrical energy into mechanical energy. When the device converts electrical energy to mechanical energy, it is called a transmitter or sender. Conversely, when the device converts mechanical energy into electrical energy, it is called receiver or sensor.

Figure 3.2 shows a simple model of an omni-directional hydrophone consisting of two masses connected via springs with dampers (dashpots) and a capacitance in parallel with a current generator connected to an input/output via an external series resistor *R*. The physics is straightforward with the mechanical system coupled to the electrical system via the piezoelectric effect. For piezoelectric materials a displacement causes a charge separation and vice versa [75]. For our purposes we assume the constant $K = \frac{q}{x}$ $(\mathrm{C/m})$is omni-directional, a more detailed analysis would include the dependence on crystal orientation and use a tensor similar to the stress tensor. For a capacitor $q = CV$, it is assumed here that the two masses are coupled electrically in parallel and that the piezoelectric constants K_1 and K_2 for the two masses take account of any charge distribution between the capacitors.

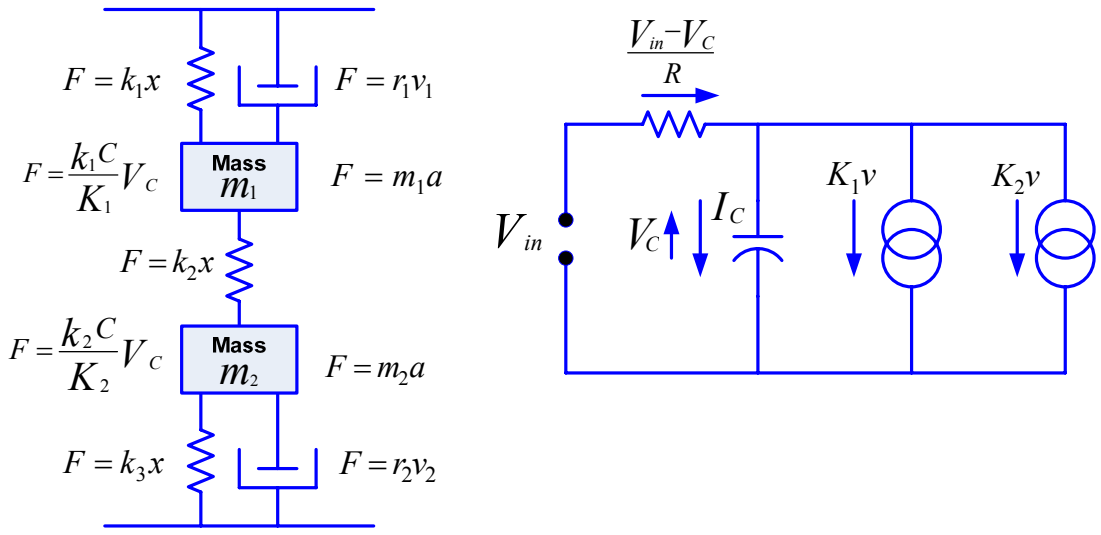

Figure 3.2 A simple model of a hydrophone.

This model can be used in both transmitter and detector mode. There are five states: the capacitor voltage V_C (x_1) and the velocities v_1 and v_2 of the two masses (x_2 and x_4) and positions – displacement from equilibrium (x_3 and x_5) of the two masses respectively. The inputs are the applied voltage, V_{in}, and external forces F_1 and F_2 on the two masses; and the outputs: velocity of the two masses (as the amplitude of sound is proportional to velocity rather than position) and the capacitor voltage [15].

For the piezo elements $Kx = q$ then $K\frac{dx}{dt} = Kv = \frac{dq}{dt} = i$ and that for the capacitor $q = CV$ and $\frac{dq}{dt} = C\frac{dV}{dt}$, by summing the currents through the capacitor is zero, this leads to equation (3.2a) describing the electrical system.

$$C\dot{x}_1 = \frac{u_1 - x_1}{R} - K_1 x_2 - K_2 x_4 \qquad (3.2a)$$

Where K_1 and K_2 are the piezo-electric constants, $(\mathrm{m/C})$, C the capacitance and R the electrical resistance. For the two mass mechanical system, the two masses are m_1 and m_2 with associated mechanical resistances r_1 and r_2 and spring constants k_1, k_2 and k_3. The external force on the hydrophone is u_2 (related to external pressure) which is shared between the two masses by the fraction f.

We can therefore write in equation (3.2b).

$$\frac{(k_1+k_2)\,C}{K_1}x_1 + fu_2 = m_1\dot{x}_2 + r_1x_2 + (k_1+k_2)x_3 - k_2x_5$$
$$\dot{x}_3 = x_2$$
$$\frac{(k_2+k_3)\,C}{K_2}x_1 + (1-f\,)u_2 = m_2\dot{x}_4 + r_2x_4 + (k_2+k_3)x_5 - k_2x_3 \tag{3.2b}$$
$$\dot{x}_5 = x_4$$

These expression scan be converted to state space form.

$$\mathbf{A} = \begin{bmatrix} -\frac{1}{RC} & -\frac{K_1}{C} & 0 & -\frac{K_2}{C} & 0 \\ \frac{(k_1+k_2)C}{K_1m_1} & -\frac{r_1}{m_1} & -\frac{(k_1+k_2)}{m_1} & 0 & \frac{k_2}{m_1} \\ 0 & 1 & 0 & 0 & 0 \\ \frac{(k_2+k_3)C}{K_2m_2} & 0 & \frac{k_2}{m_2} & -\frac{r_2}{m_2} & -\frac{(k_2+k_3)}{m_2} \\ 0 & 0 & 0 & 1 & 0 \end{bmatrix} \mathbf{B} = \begin{bmatrix} \frac{1}{RC} & 0 \\ 0 & \frac{f}{m_1} \\ 0 & 0 \\ 0 & \frac{(1-f)}{m_2} \\ 0 & 0 \end{bmatrix} \tag{3.3}$$

The desired outputs are the acoustic pressure in transmit mode and the hydrophone voltage in receive mode. The derivation of the acoustic pressure is complicated by the presence of an acoustic matching network between the hydrophone and the water. However the simple assumption that the coupling between the hydrophone and the water depends on a weighted sum of the two hydrophone velocities has proved very successful in practice and the model is capable of taking the complex coupling into account for the hydrophones tested, then **C** and **D** are defined in equation (3.4).

$$\mathbf{C} = \begin{bmatrix} 0 & c_1 & 0 & c_2 & 0 \\ 1 & 0 & 0 & 0 & 0 \end{bmatrix} \quad \mathbf{D} = \begin{bmatrix} 0 & 0 \\ 0 & 0 \end{bmatrix} \tag{3.4}$$

It is possible to use the state equations directly, however there are a large number of unknowns and the equation very over determined. In practice it is simpler to convert the system to a transfer function. This can be done as shown in the equation (3.5).

$$s\mathbf{X}(s) = \mathbf{A}\mathbf{X}(s) + \mathbf{B}\mathbf{U}(s)$$

$$(s\mathbf{I} - \mathbf{A})\,\mathbf{X}(s) = \mathbf{B}\mathbf{U}(s)$$

$$\mathbf{X}(s) = (s\mathbf{I} - \mathbf{A})^{-1}\mathbf{B}\mathbf{U}(s) \tag{3.5}$$

$$\mathbf{Y}(s) = \mathbf{C}(s\mathbf{I} - \mathbf{A})^{-1}\mathbf{B}\mathbf{U}(s) + \mathbf{D}\mathbf{U}(s) = (\mathbf{C}(s\mathbf{I} - \mathbf{A})^{-1}\mathbf{B} + \mathbf{D})\mathbf{U}(s)$$

hence $$H(s) = \mathbf{C}(s\mathbf{I} - \mathbf{A})^{-1}\mathbf{B} + \mathbf{D}$$

The calculation is rather tedious but is easily determined using symbolic maths software. In our case the symbolic MATLAB toolbox [76-77], which yields the transfer function in equation (3.6).

$$H(s) = \frac{b_3 s^3 + b_2 s^2 + b_1 s}{a_5 s^5 + a_4 s^4 + a_3 s^3 + a_2 s^2 + a_1 s + 1} \tag{3.6}$$

The transmit transfer function $H(s)$ indicates that the Pressure has terms depending on the first, second and third derivative of the hydrophone voltage (equating to velocity acceleration and rate of change of acceleration). The 5th order denominator allows for the two mechanical resonances at $\sqrt{k/m}$ and the low pass filtering effect of the RC circuit. The number of unknowns has now been reduced to eight. The relationship between the transfer function values and the physical hydrophone parameters is given in table 3.1.

Table 3.1 The coefficients of transfer function.

b_3	$C(K_1c_2(k_2+k_3)m_1 + K_2c_1(k_1+k_2)m_2)$
b_2	$C(K_1c_2r_1(k_2+k_3) + K_2c_1r_2(k_1+k_2))$
b_1	$C((K_1c_1 + K_1c_2 + K_2c_1 + K_2c_2)k_2 + (K_1c_2 + K_2c_1 + K_2c_2)k_1k_2 + (K_1c_1 + K_2c_1 + K_1c_2)k_2k_3 + (K_1c_2 + K_2c_1)k_1k_3))$
b_0	0
a_5	$CK_1K_2Rm_1m_2$
a_4	$K_1K_2(m_1m_2 + CRm_1r_2 + CRm_2r_1)$
a_3	$K_1K_2(m_1r_2 + m_2r_1 + CR(2k_1m_2 + 2k_2m_1 + 2k_2m_2 + 2k_3m_1 + r_1r_2))$
a_2	$K_1K_2(k_1m_2 + k_2m_1 + k_2m_2 + k_3m_1 + r_1r_2) + 2CR(k_1r_2 + k_2r_1 + k_2r_2 + k_3r_1))$
a_1	$CR(K_1k_2 + K_2k_2 + K_2k_1k_2 + K_1k_2k_3 + K_1K_2(2k_2 + 3k_1k_2 + 3k_1k_3 + 3k_2k_3)) + K_1K_2(k_1r_2 + k_2r_1 + k_2r_2 + k_3r_1)$
a_0	$(K_1K_2k_1k_2 + K_1K_2k_1k_3 + K_1K_2k_2k_3)$

More details about conversion between state space and transfer function representations in linear system is presented in ref [72].

3.3 Signal processing techniques for hydrophone calibration

The output signal response of linear time invariant (LTI) system to any input signal can be determined by using the convolution operator [78]. It states that if we know the impulse response of $h(t)$ a system, we can compute the output response $y(t)$ to any input $x(t)$, as shown in (3.7).

$$y(t) = x(t) * h(t) \tag{3.7}$$

Where $y(t)$ is output impulse response and the symbol * denotes convolution.
Alternatively, Fourier and inverse Fourier transforms can be used to transfer between domains (e.g. time to frequency and vice versa). When $Y(\omega)$ is the output response, $H(\omega)$ is the system function, and $X(\omega)$ is the input signal, as shown in (3.8).

$$Y(\omega) = H(\omega).X(\omega) \tag{3.8}$$

Ideally a Dirac delta function would be used as a driving signal as $X(\omega) = 1$ and $Y(\omega) = H(\omega)$. In practice however as an impulse or delta function cannot be easily created, a step signal is chosen in order to generate the step response of the system. The step response of the system is the time integral of its impulse response, hence the impulse response can be calculated from differentiation of a known step response. As mentioned, the output response signal results from the convolution between input signal and impulse response. Similarly, input signal can be calculated from de-convolution of the output response and system function as shown in (3.9). It is then transferred to the time domain using inverse Fourier transform as shown in (3.10).

$$X(\omega) = Y(\omega)/H(\omega) \tag{3.9}$$

$$x(t) = \frac{1}{2\pi}\int_{-\infty}^{\infty} X(\omega)e^{j\omega t}\, d(\omega) \tag{3.10}$$

The method, as described above, has three practical disadvantages [65]. Firstly, this method needs high signal-to-noise ratio as differentiation is used. Secondly, the step signal input must have a very fast rise time and a high signal to noise ratio. Lastly, the experiment needs to run in a large volume or an anechoic chamber to avoid reflections. The tank which is available in our workshop has limited volume and reflections soon arrive from the tank boundaries. To avoid the problems which are already mentioned above,

signal processing techniques are used. The block diagram of signal processing techniques for calibration is shown in Figure 3.3.

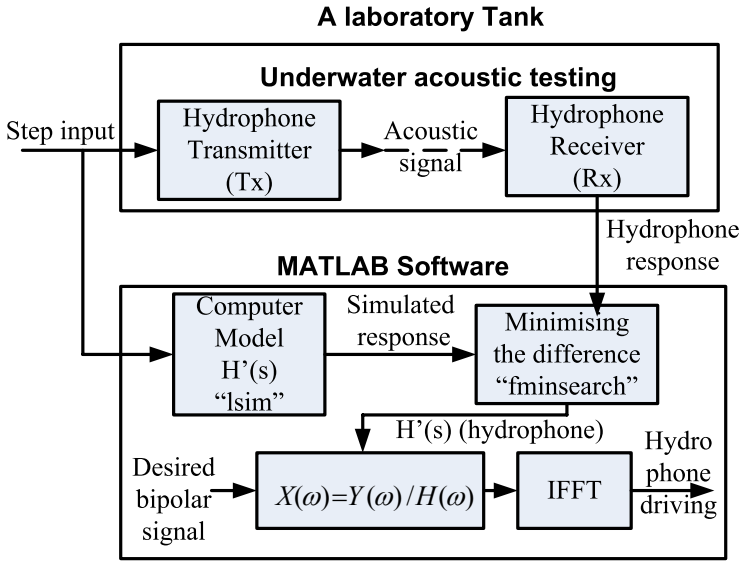

Figure 3.3 Signal processing techniques for calibration.

In practice, a step signal could not be perfectly generated due to the limitation of electronic components. Computer software is used to generate the mimic of a perfect step signal (generated in LabVIEW [79-80]) as shown in Figure 3.4. The step signal is sent to the transmitter hydrophone. The output signal is detected by a wide bandwidth (7 Hz- 80 kHz) receiver hydrophone, a Bruel&Kjaer type 8106 [81]. The hydrophone response is shown in Figure3.5. The known input to the hydrophone is injected into the LTI model and the output of the real and model hydrophone are fit by "fminsearch" using a Nelder Meade Simplex algorithm [82] which is a simplex method for finding a local minimum of a function of several variables. A simplex method is a pattern search that compares function values at the three vertices of a triangle. The worst vertex, where $f(x,y)$ is largest, is rejected and replaced with a new vertex. A new triangle is formed and the search is continued. The process generates a sequence of triangles which the function values at the vertices get smaller and smaller. The size of the triangles is reduced and the coordinates of the minimum point are found. In this research uses the default values for the number of iterations in "fminsearch". The default value is 200n, where n is the number of variables. The factor 200 is the result of experiments performed against quadratic functions.

Figure 3.6 shows that a fifth-order transfer function (TF) is sufficient to match the hydrophone in question but for other hydrophones higher order transfer functions may be needed. The actual fifth-order TF for this particular source hydrophone (frequency scaled

down by a factor of 2.8932×10^5) used in this model is shown in (3.11). The magnitude response and phase response of this hydrophone are plotted as shown in Figure 3.7 and Figure 3.8.

$$H(s) = \frac{-0.0085s^3 - 0.3974s^2 + 0.4520s}{2.2732s^5 + 1.9703s^4 + 6.4316s^3 + 3.2965s^2 + 4.1726s + 1} \quad (3.11)$$

In linear systems, a system is stable if all of the poles occur in the left half of the s-plane. From equation 3.11, all poles are in left haft of s-plane (s=-0.2685, s=-0.2019±1.2045i, s=-0.0973±1.0436i), then the system function is stable.

The system identification methods (it is an active area in control engineering and electrical engineering. In system identification, experimental measurements in terms of an input-output data of an unknown system are used to model the system mathematically) were initially attempted. These showed poor convergence and indeed no convergence at all. After some week work this was abandoned as no sensible result could be obtained. Towards the end of the project additional attempts were made to use system identification techniques by MSc student, Maria Coscollar. Similarly disappointing results were obtained.

Then, the propose procedure in Figure 3.3 is suitable as it can determine the hydrophone transfer function. In addition, the result from simulation using 'lsim' function shows that this modelling can produce the bipolar pulse as needed. The output bipolar pulses are applied by Fourier transform to plot in the frequency spectrum, the results show the peak frequency spectrum at the 10 kHz and 23 kHz as designed. Most important, this modelling has already experimented at the laboratory water tank, the result from experiment confirmed that the model can generate a good bipolar pulse.

Monte Carlo studies predict the neutrino interaction will produce bipolar pulses. Earlier studies predicted a pulse of around 10 kHz, whereas more recent studies predict a higher frequency of c. 23 kHz [16]. Both 10 and 23 kHz pulses have been investigated.

The input driving signal of 10 kHz, calculated from (3.9), results from replacing the fitted transfer function and the desired bipolar signal. An inverse Fourier transform is then used to convert the input driving signal from the frequency to time domain by (3.10), the signal is shown in Figure 3.9. To confirm this modelling the input driving signal is simulated and the output signal is shown in Figure 3.10. In order to validate the bipolar signals have a frequency response at the 10 kHz. The Fourier transform is applied to determine the

frequency spectrum of bipolar pulse. The output from Fourier transform is plotted showing the peak frequency response at the 10 kHz. The frequency spectrum of a 10 kHz bipolar pulse is illustrated in Figure 3.11. The 23 kHz bipolar pulse procedure replicates that of 10 kHz bipolar signal. The input signal for hydrophone driving is shown in Figure 3.12. Simulated and desired 23 kHz bipolar pulses are plotted in Figure 3.13. The Fourier transform is also applied to calculate the frequency response of a 23 kHz bipolar pulse. The frequency response of the 23 kHz bipolar pulse is plotted in Figure 3.14.

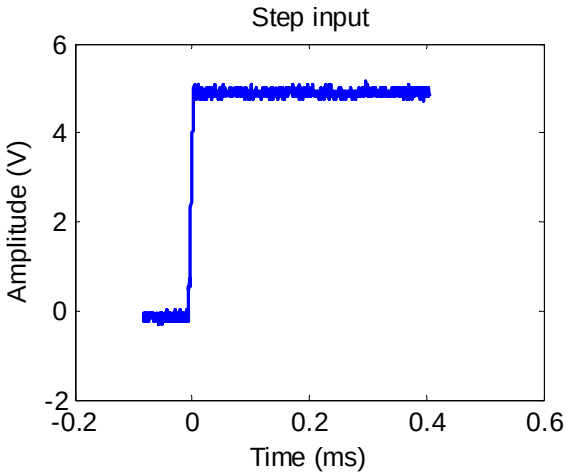

Figure 3.4 Input step signal.

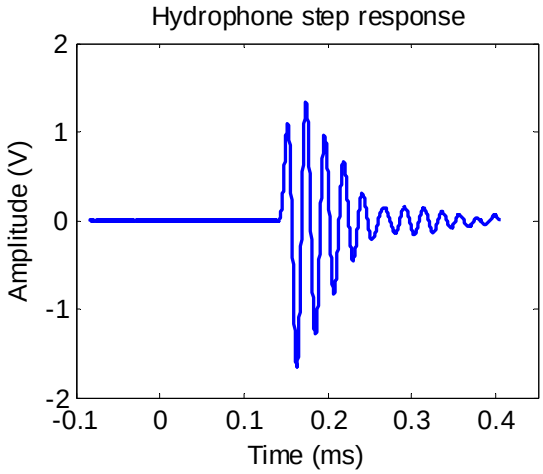

Figure 3.5 Hydrophone response.

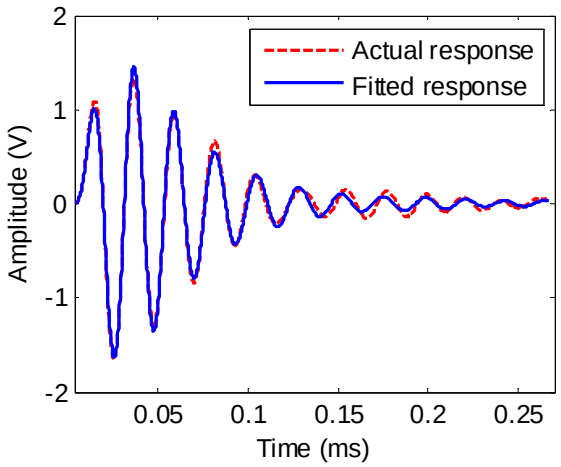

Figure 3.6 Fitting TF between measured and simulated step response.

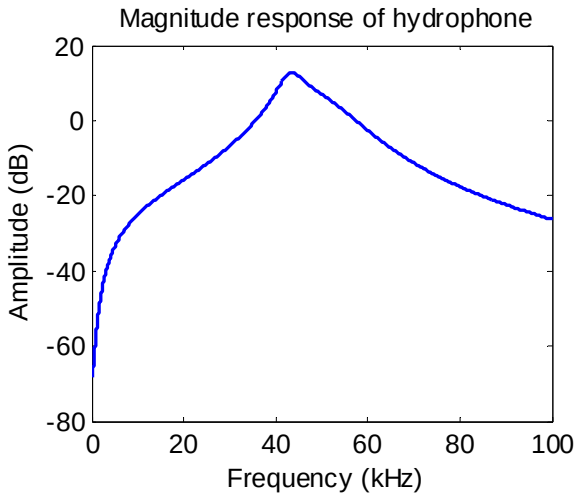

Figure 3.7 Magnitude response of hydrophone.

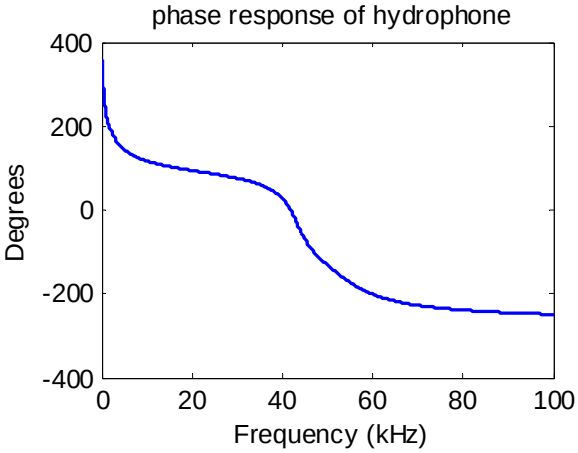

Figure 3.8 Phase response of hydrophone.

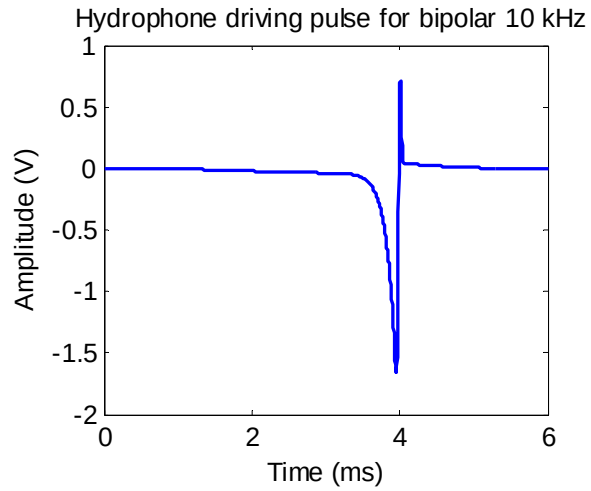

Figure 3.9 Input signal for hydrophone driving.

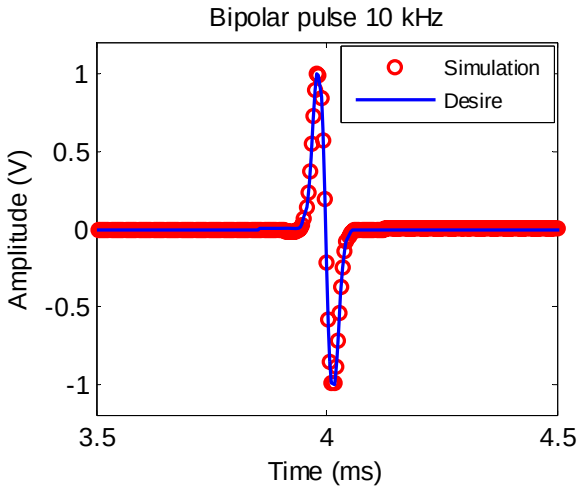

Figure 3.10 Simulated and desired 10 kHz bipolar pulses.

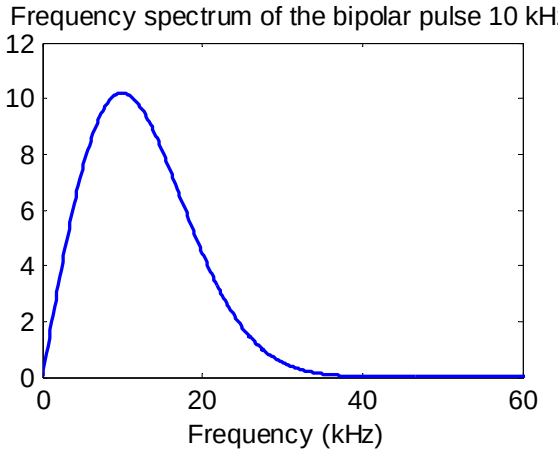

Figure 3.11 Frequency spectrum of the bipolar pulse 10 kHz.

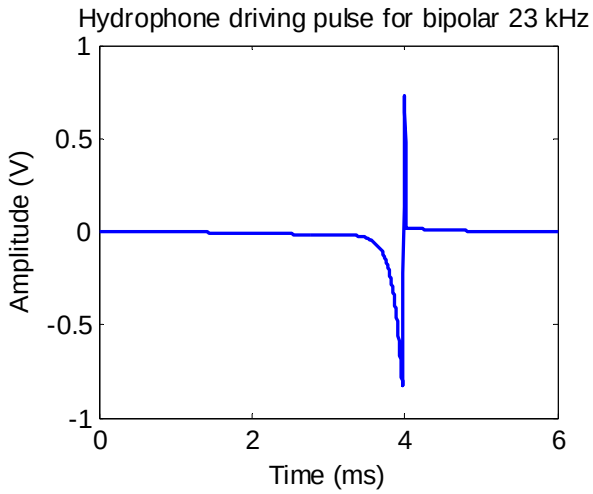

Figure 3.12 Input signal for hydrophone driving.

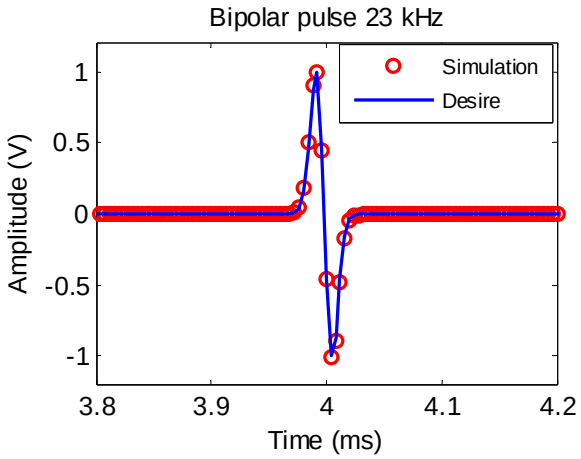

Figure 3.13 Simulated and desired 23 kHz bipolar pulses.

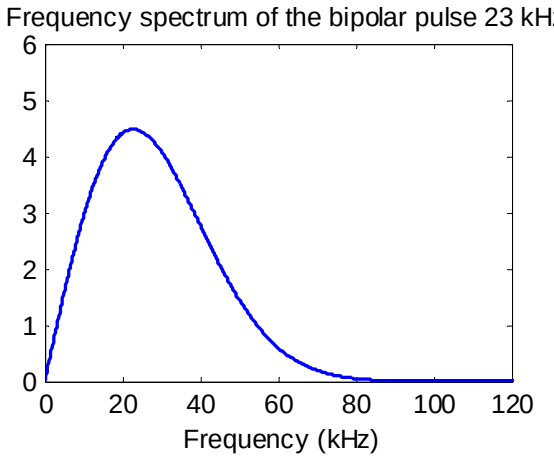

Figure 3.14 Frequency spectrum of the bipolar pulse 23 kHz.

3.4 Hardware design

Acoustic signals generated with MATLAB or LabVIEW software are of high quality (16 bits 500 kHz sampling rate), however the cost of such systems is quite expensive and

inconvenient to move and deploy on site. Furthermore the ultimate goal is to excite an array of hydrophones (of the order of 8 hydrophones) simultaneously which is both very expensive and technically challenging using LabVIEW. A number of alternative technologies were investigated. Simulations indicate that at least an 11 bit DAC needs to be used due to the noisy nature of the de-convolution process and obviously a sufficiently high sampling rate is needed (>200kHz).

A PIC18F4585 microcontroller from Microchip is chosen because it is very low cost, can be easily scaled to an array, be easily ruggedized for salt water and can run for many days on battery. A TLV5619 digital-to-analogue converter (DAC) chip is used to convert back to the analogue domain [83].The block diagram of a bipolar signal generation module using PIC microcontroller is shown in Figure 3.15.

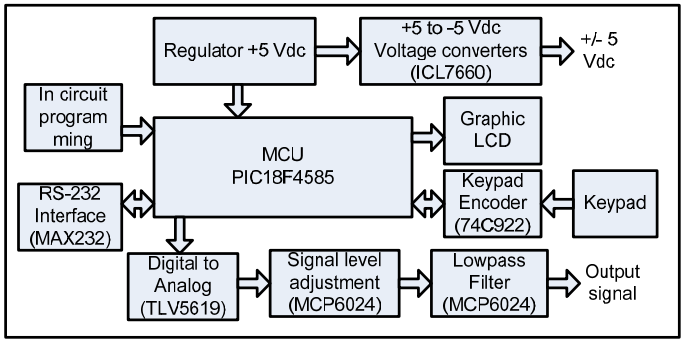

Figure 3.15 PIC module block diagram.

The PIC18F4585 starter kit module is used to develop the prototype in both software and hardware, as shown in Figure 3.16 [84]. MPLAB is software to develop and control PIC microcontrollers. The prototypical bipolar signal module was evolved and corrected until it is satisfactory and can operate as required.

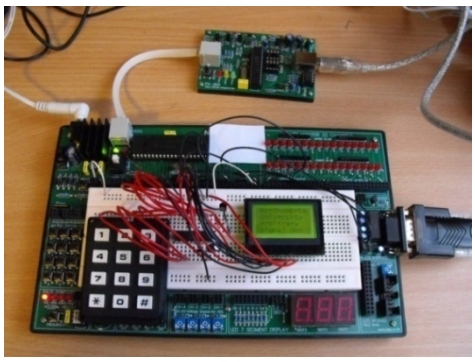

Figure 3.16 PIC starter kit module.

The Protell 99SE software is applied to draw schematic and also build printed circuit boards (PCB) files [85]. The PCB files are sent to the manufacturer for fabrication and sent back when they are finished. For the next step, all components are filled in PCB and also installed in box. The completed bipolar signal module is shown in Figure 3.17.

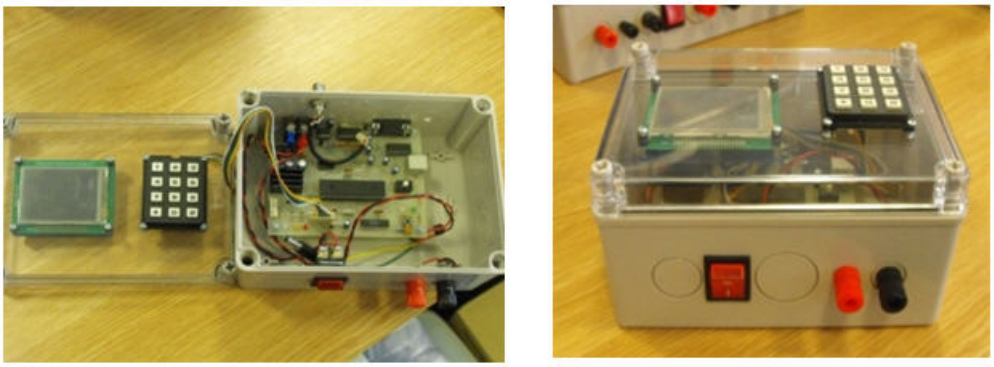

(a) (b)

Figure 3.17 PIC bipolar signal module (a) Inside module (b) Outside module.

Not only the bipolar signal module but also eight-channel array power amplifier module is built for amplification of signals which can drive eight hydrophones. The eight-channel power amplifier block diagram is illustrated in Figure 3.18. The PA94 high voltage power operation amplifier chip from APEX is designed and built for driving hydrophones [86]. The circuit is designed as an inverting amplifier circuit and gain of circuit is set to 10 times. The power amplifier module is shown in Figure 3.19

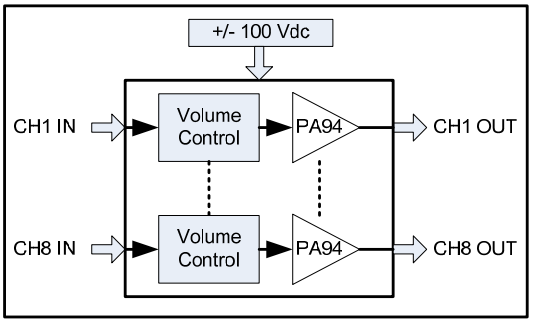

Figure 3.18 Power amplifier block diagram.

Figure 3.19 Power amplifier module.

The power supply module is comprised two parts, firstly a 240 VAC switching power supply is rectified and regulated to 12VDC to supply the PIC bipolar signal module and DC-to-DC Converter module when the system is tested in the laboratory. Secondly, a +12 to ±100Vdc DC-to-DC converter module converts the voltage from +12VDC to ±100VDC to supply the power amplifier module. In addition, this module is designed for use with a battery power supply when the system is deployed on sites. The power supply block diagram and power supply module are shown in Figure 3.20 and Figure 3.21 respectively.

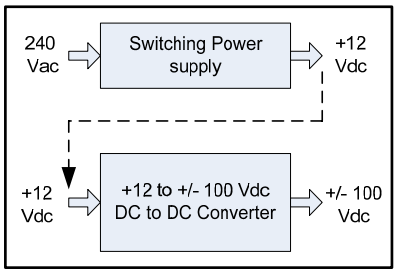

Figure 3.20 Power supply block diagram.

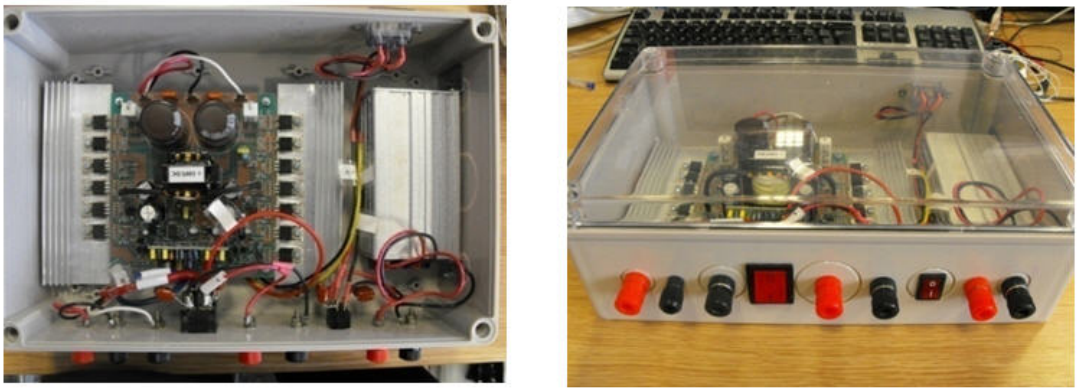

(a) (b)

Figure 3.21 Power supply module (a) Inside module (b) Outside module.

The block diagram of a single hydrophone calibrator is shown in Figure 3.22. Firstly, the acoustic driving pulse data or any signal data needs to be converted in the range between 0-4095 for 12-bit digital to analogue converter chip by MATLAB software [76]. The data is then transferred to flash program memory of the PIC via the serial port protocol or using the PICKIT2 programmer. The data is permanently kept in flash program memory until it is replaced by new data. The 12-bit digital data is sent to the DAC chip at the sampling rate of 250 kHz. The signal is amplified by a PA94 hydrophone power amplifier chip and sent out to the transmitter hydrophone in water tank. The acoustic signal is detected by the

acoustic receiver hydrophone and pre-amplified. Finally, the acoustic signal is recorded by digital storage oscilloscope.

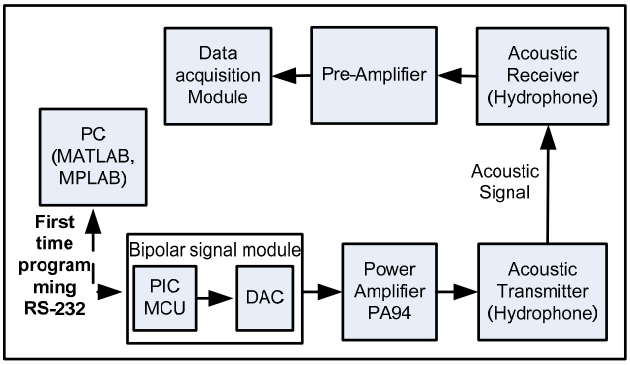

Figure 3.22 Block diagram of a single hydrophone calibrator.

3.5 Experiment and result

A single hydrophone calibrator system has to be tested in the water tank at the Sheffield University laboratory in order to verify the result from the simulation. The PIC module is used to generate 10 kHz and 23 kHz bipolar signals and the NI USB-6211 data acquisition module from National Instruments is use to validate the result from the PIC module. The NI USB-6211 and PIC modules are shown in Figure 3.23. The parameters used in this experiment are shown in table 3.2.

Table 3.2 Parameters setup in the experiment.

Parameters	PIC module	NI-USB6211
Resolution	12 bits	16 bits
Sampling rate	250 kS/s	250 kS/s
Sample number	1500 samples	1500 samples

The 10 kHz and 23 kHz driving pulses are generated from the PIC as shown in Figure 3.24 (a) 10 kHz and (b) 23 kHz. The output signal from PIC module is connected to power amplifier module to amplify the signal that can drive the hydrophone. The output signal from power amplifier module is directly connect to the ball transmitter hydrophone. The electrical signal is converted into pressure wave which is measured by a broad band Bruel&Kyaer (B&K) 8106 hydrophone which has a flat amplitude response and linear phase response over the frequencies of interest [81]. The hydrophone driving and output bipolar signals of 10 kHz and 23 kHz from PIC module are shown in Figure 3.25.

(a) (b)

Figure 3.23 Experimental modules (a) PIC module (b) NI-USB6211 module.

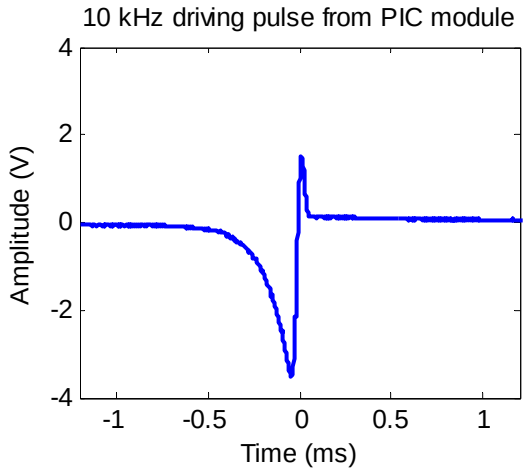

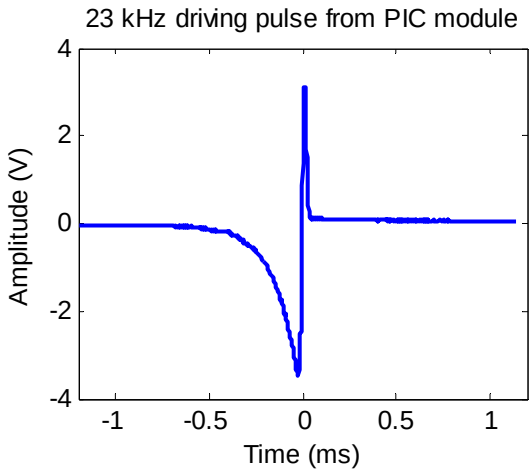

(a) (b)

Figure 3.24 Hydrophone driving signals from PIC module (a) 10 kHz (b) 23 kHz.

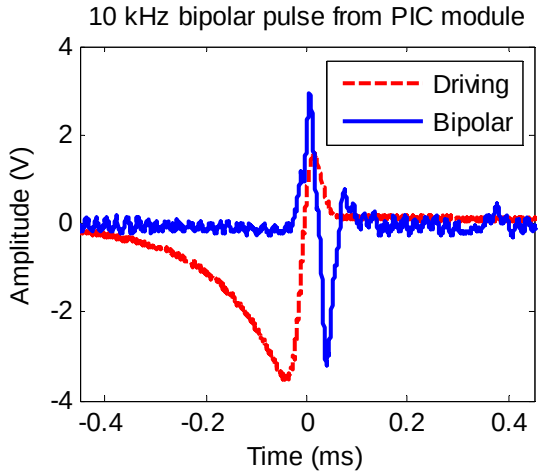

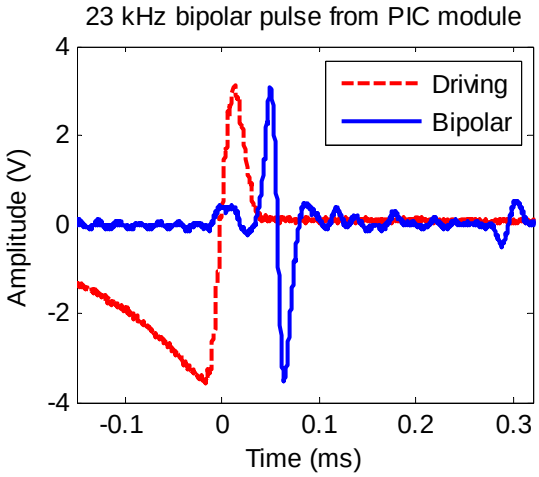

(a) (b)

Figure 3.25 Bipolar pulses from PIC module (a) 10 kHz (b) 23 kHz.

The NI USB-6211 module is similarly used to generate 10 kHz and 23 kHz hydrophone driving pulses for comparison the result from PIC module. The 10 kHz and 23 kHz driving

pulse from NI USB-6211 are plotted in the Figure 3.26 (a) 10 kHz, (b) 23 kHz. The sampling rate of the LabVIEW system is reduced to 250 kHz to enable more direct comparison of the two methods. As can be seen decent bipolar pulses are generated with both the PIC and NI modules. The results have shown that the PIC module can generate the similar bipolar pulses as NI commercial module. The hydrophone driving and output bipolar pulses from NI USB-6211 are illustrated in Figure 3.27, (a) 10 kHz, (b) 23 kHz.

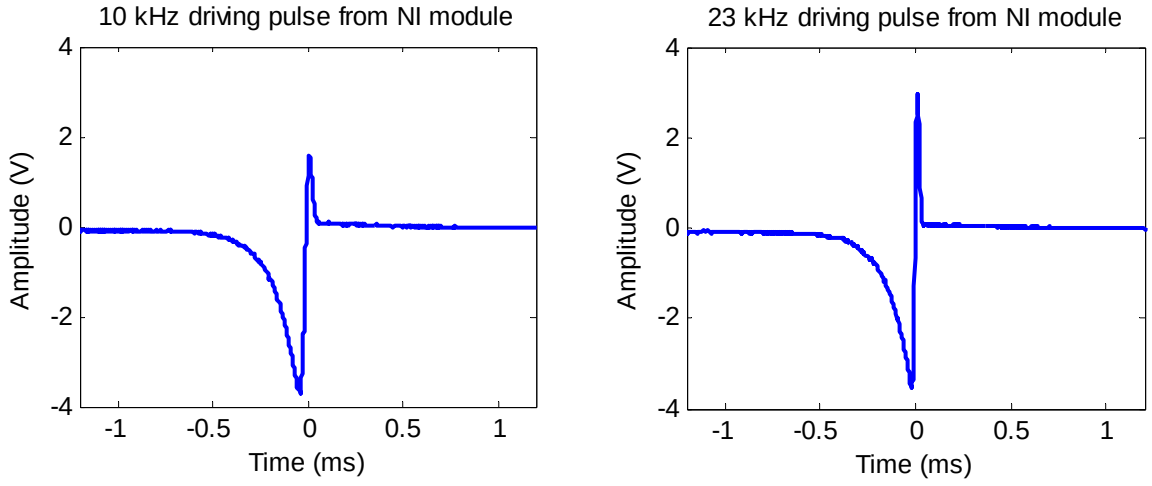

(a) (b)

Figure 3.26 Hydrophone driving signals from NI module (a) 10 kHz (b) 23 kHz.

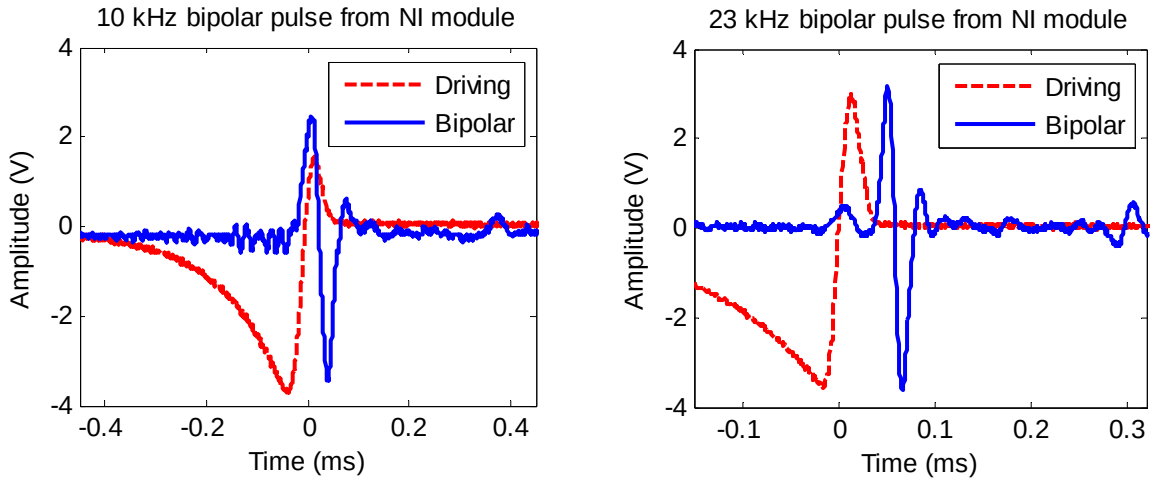

(a) (b)

Figure 3.27 Bipolar pulses from NI module (a) 10 kHz (b) 23 kHz.

3.6 Summary

A simple model of an omni-directional hydrophone has been presented. The state space equation has been applied to hydrophone modelling in order to find out the correct electrical driving pulse. It is possible to use the state equations directly, however there are a large number of unknown variables, and then the equation is very over determined. In practice, it is much simpler to convert state space to transfer function as that can be simply done using the MATLAB software toolbox.

Hydrophone calibration has been developed for generating an artificial UHE neutrino induced-pulse. Digital signal processing techniques have been applied to determine the correct electrical driving pulse to generate an artificial neutrino-induced pulse. The output signal response of LTI system to any input signal is determined by convolution. If we know the impulse response of a system, the output response can be calculated to any input.

We can also alternatively use the Fourier and inverse Fourier transforms to determine the electrical driving signal. However, an impulse function cannot be easily created, then the step signal is applied instead to compute the step response of a system. The step response of the system is the time integral of its impulse response, inversely the impulse response can be computed by the differentiation of known step response.

The output response signal is a result of convolution between input and impulse response, similarly the input signal can be inversely determined using de-convolution of the output response and system function. However, in practical work, the above method has some disadvantages. Firstly, a high signal-to-noise ratio is needed for the differentiation. Secondly, the step signal input must have a very fast rise time and a high signal to noise ratio. Finally, the experiment needs to operate in a large volume or an anechoic chamber to avoid reflection. To avoid these limitations, signal processing techniques are applied to determine the suitable electrical driving pulse.

In practice, the step signal is generated by LabVIEW software and sent via NIUSB-6211 module to the ball hydrophone. The hydrophone response is recorded by B&K 8106 receiver hydrophone. Using the same step input signal to simulate the step response using the “lsim” function from MATLAB, the output responses from simulation and experiment are fitted to find out the best match transfer function using “fminsearch” function. The de-convolution is used to calculate the input driving pulse from known output response and transfer function. The inverse Fourier transform is use to convert frequency domain to time domain for the input driving signal. Both 10 and 23 kHz input driving pulses are calculated

using the same processes. These signal data will be downloaded in to flash programme memory of microcontrollers to generate driving pulses for the hydrophone.

The 8-bit PIC microcontroller module has been built for generation of bipolar acoustic signal. The 12-bit digital to analogue converter chip is used to convert digital data signal from flash programme memory to analogue signals. The experiment has been done at the laboratory water tank in University of Sheffield. The 16-bit NI USB-6211 digital to analogue module is used to generate the same bipolar pulses for validation of the results.

The simulated and experimental results were shown and it was confirmed that the modelling can mimic the expected acoustic bipolar signal. The PIC module and the NI USB-6211 commercial module give very similar results. In addition, the PIC module is quite inexpensive and very convenient to deploy in the field. The laboratory experiment and results have already been published in [87].

The ACoRNE collaboration uses the Rona site, North West Scotland, as test site. The single hydrophone calibrator was deployed at the Rona site, with the depth around 200 metres, in order to test the system. The details of deployment, pattern of signal injection, data collection and data analysis from the Rona site will be presented in the next chapter.

Chapter 4

Analysis of single hydrophone signals in the Rona site

4.1 Introduction

In the previous chapter, a single hydrophone calibrator has presented which was measured in the laboratory water tank showing that it can generate artificial neutrino-induced signals. The next step, which needs to be done, is the deployment of the single hydrophone calibrator in the field to study the behaviour of such bipolar signals in shape and directivity.

As mentioned in Chapter 2, the Ministry of Defence has allowed the ACoRNE collaboration to use an eight-receiver hydrophone array at the Rona site (West coast of Scotland) as a test bed that is located at about 200 metres depth. In September 2008, ACoRNE had a field trip to deploy the single hydrophone calibrator at the Rona site.

This chapter will firstly present the calculation of sound attenuation in sea water. The ACoRNE attenuation parameterisations are compared with others. The 10 kHz and 23 kHz bipolar pulses are simulated using ACoRNE attenuation parameterisation. The simulation of the Rona hydrophone responses for 10 kHz and 23 kHz bipolar pulses are also discussed before detailing the field trip at the Rona site.

The deployment at the Rona site using a single hydrophone transmitter is presented. The 10 kHz, 23 kHz bipolar pulses and sine signal have been emitted into seawater. The details of signal injection and data collection techniques are also discussed in more details. Signal processing techniques have been applied to recognise the bipolar pulses which emitted in the Rona site.

4.2 Simulation of Attenuation in sea water

Acoustic attenuation in sea water has been investigated by many researchers. The attenuation of an acoustic pulse is caused by a combination of absorption and back scattering but the main effect is absorption. It is unlike the case with light where backscattering can be the dominant mechanism particularly in the blue part of the spectrum. The study of 0.2 – 100 kHz absorption of sound in sea water has been published by Francois and Garrison [88-89]. This is widely considered to be the “Gold Standard” but

only has predictions of magnitude, not phase. More recently, a simplified parameterisation, which retains the essential parameters on depth (z), salinity (S), temperature (T), and acidity (pH) of Francois and Garrison, has been presented by Ainslie and McColm [90]. Niess and Bertin [91] have published a complex attenuation formula based on Mediterranean conditions. ACoRNE [2] has presented a complex version of the Ainslie and McColm formulation, which retains the attenuation magnitude but introduces the phase shift predicted by Lieberman [92].

This research uses the ACoRNE parameterisations where the attenuation consists of three components: boric acid, magnesium sulphate and pure water. The ω_B and ω_{Mg} are the high pass filter for boric acid and magnesium sulphate respectively. The a_x values are the respective attenuation coefficients in dB/km. The attenuation parameterisations are illustrated as in equation (4.1).

$$\omega_B = 1560\pi\sqrt{\frac{S}{35}}e^{T/26}$$

$$\omega_{Mg} = 84000\pi e^{T/17}$$

$$a_B = \frac{1.893x10^{-4}}{2\pi}e^{\frac{pH-8}{0.56}}$$

$$a_{Mg} = \frac{0.52x10^{-3}}{2\pi}\left(1+\frac{T}{43}\right)\frac{S}{35}e^{\frac{-z}{6}} \qquad (4.1)$$

$$a_w = \frac{49x10^{-9}}{4\pi^2}e^{-\left(\frac{T}{27}+\frac{z}{17}\right)}$$

$$a_{dB/km} = \frac{a_B\omega_B S}{s+\omega_B} + \frac{a_{Mg}\omega_{Mg}S}{s+\omega_{Mg}} + a_w\omega^2 \quad \text{where as } s = i\omega$$

The comparison of the ACoRNE attenuation parameterisation with others is plotted in Figure 4.1. The first attenuation, the f^2 approximation assumes that the sea water behaves like a more viscous form of distilled water by decreasing the value of ω_0 to match the measured attenuation in the 10-100 kHz frequency region for the tropical waters. The sound velocity is 1500m/s. The optimised parameterisations for Mediterranean conditions are used for the other curves (T=15 °C, S= 37 ppt, pH = 7.9). The results of Niess&Bertin, Ainslie&McColm and ACoRNE are very close together as the same curve. The phase shift

□ □ □ □ □ □ □ □ □ □ □

figure.

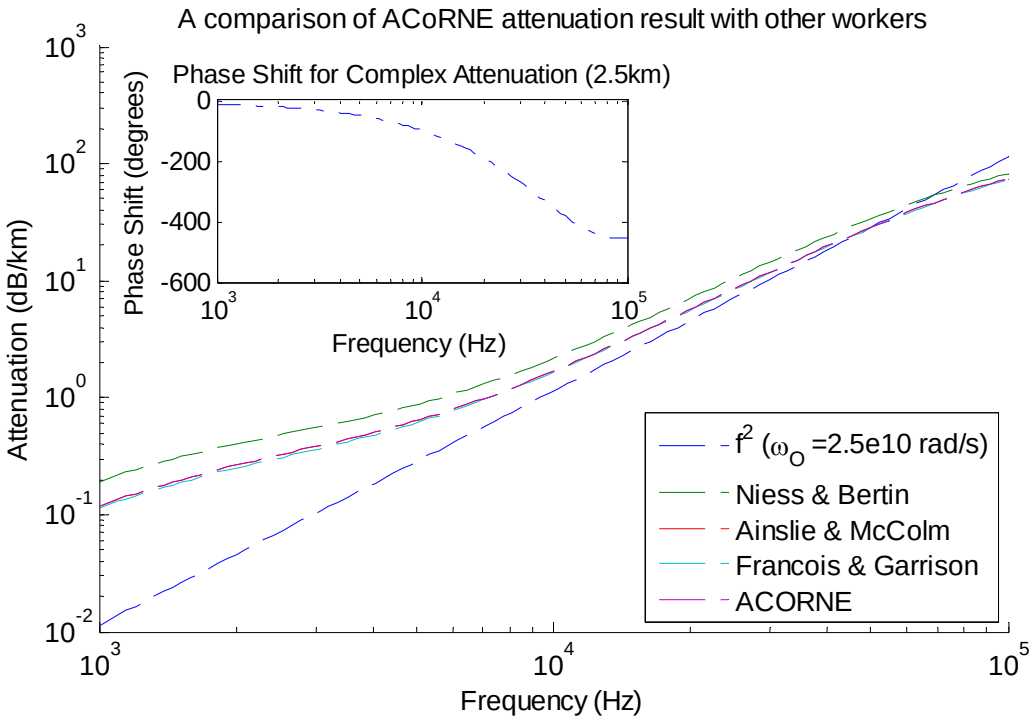

Figure 4.1 A comparison of ACoRNE attenuation result with other workers.

The comparison of sound attenuation from various attenuation parameterisations has already been plotted. The 10 kHz and 23 kHz bipolar pulses are simulated by ACoRNE attenuation parameterisation with varying distance from the source to observer in order to know the shape and amplitude of these signals at the detector. The output pulse can be determined by converting the pulse into the frequency domain by taking a Fourier transform, multiplying with the attenuation coefficient and taking the inverse Fourier transform. The optimised parameterisations for Mediterranean conditions are also used as same as the sound attenuated simulation. The distance (z) is varied with 100m, 500m, 1000m and 2500m. The output 10 kHz and 23 kHz pulses with varying the distance are shown in Figure 4.2 and Figure 4.3 respectively.

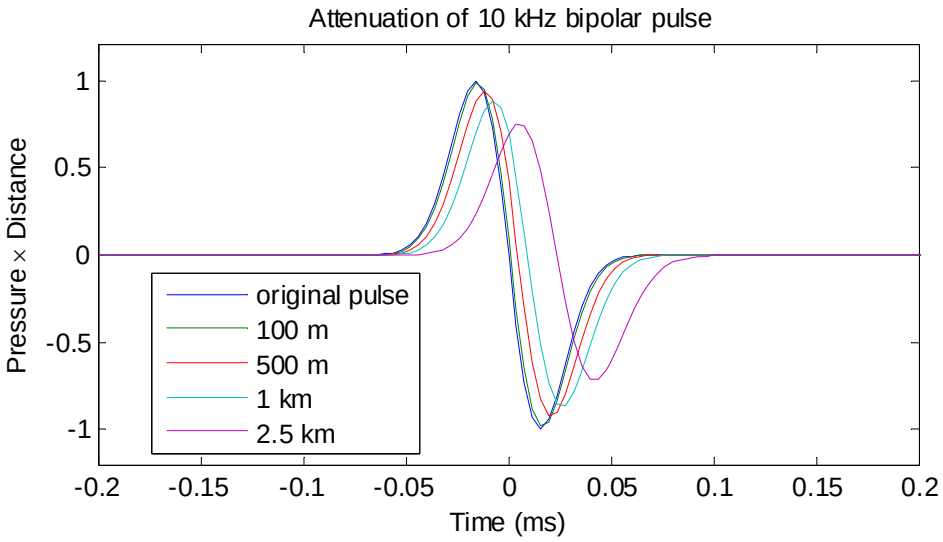

Figure 4.2 Attenuation of 10 kHz bipolar pulse.

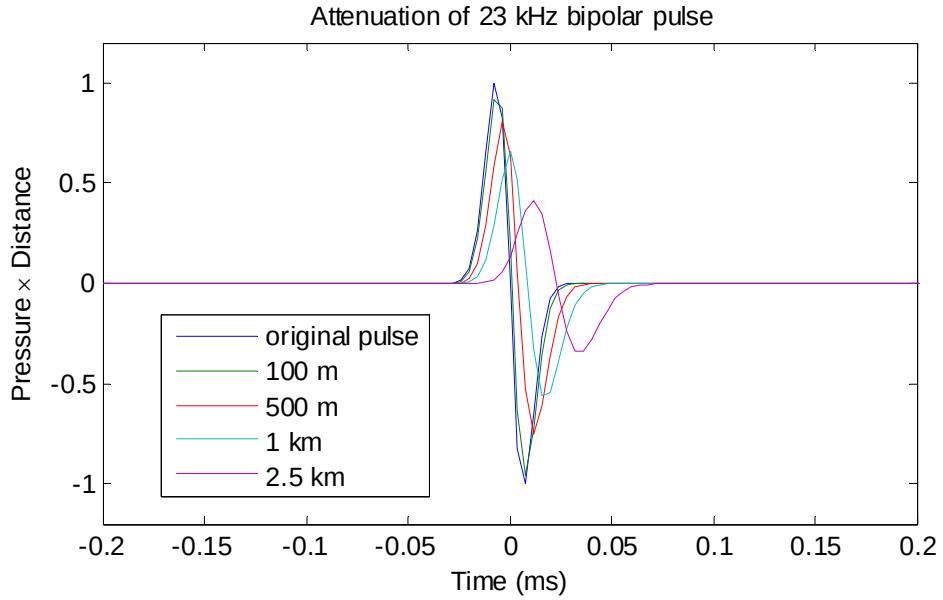

Figure 4.3 Attenuation of 23 kHz bipolar pulse.

It was hoped that the complex nature of the channel characteristic could be investigated in detail at Rona. However the non linear phase response of the hydrophones has rendered this impossible. This will be discussed briefly in the next section.

4.3 The response of the Rona hydrophones

The Rona hydrophones are a set of commercially available wide band sensors with flat frequency response up to resonance at 50 kHz. However, as they are part of a naval array, the exact specifications of the hydrophones are classified. Generally, only the amplitude response of hydrophones is given by the manufacturers. It is possible to infer the phase

response from the amplitude response. Ordinary differential equations are used to model the hydrophone transfer function as shown in (4.2).

$$\sum_{i=1}^{m} a_i \frac{d^i y}{dt^i} = \sum_{i=1}^{n} b_i \frac{d^i u}{dt^i} \tag{4.2}$$

Where u is the input, y is the output, a and b constants are determined by the physical parameters of the hydrophone and the maximum of n and m giving the order of the system. The amplitude response fitting from data sheet with 2nd, 3rd, 5th orders is shown in Figure 4.4. The phase response of 2nd, 3rd and 5th order is presented in Figure 4.5.

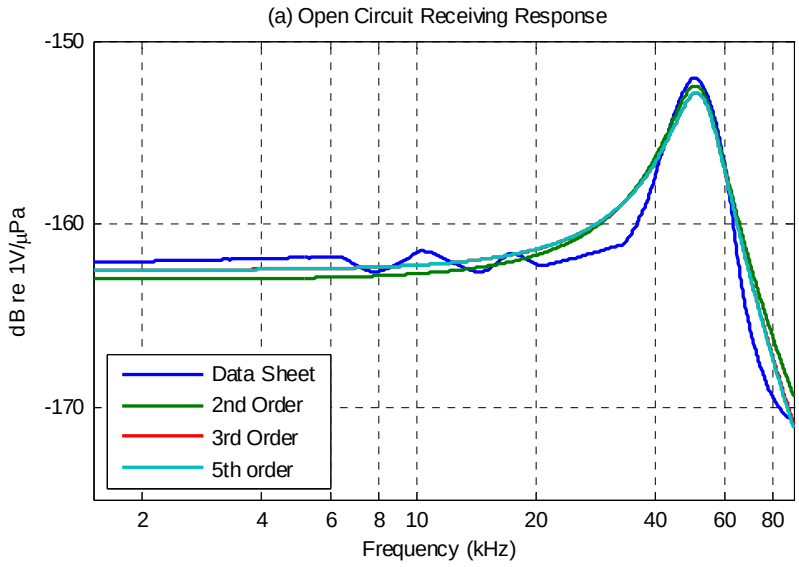

Figure 4.4 The simulated amplitude response of Rona hydrophone.

The simulation of the 10 kHz bipolar pulse through the 2nd, 3rd, 5th order response of the Rona hydrophones is illustrated in Figure 4.6. The Figure 4.7 shows the 23 kHz bipolar pulse response, however since the pulses were more than two times higher in frequency, the effect of non-linear phase response becomes very apparent and it can be seen the asymmetrical pulse.

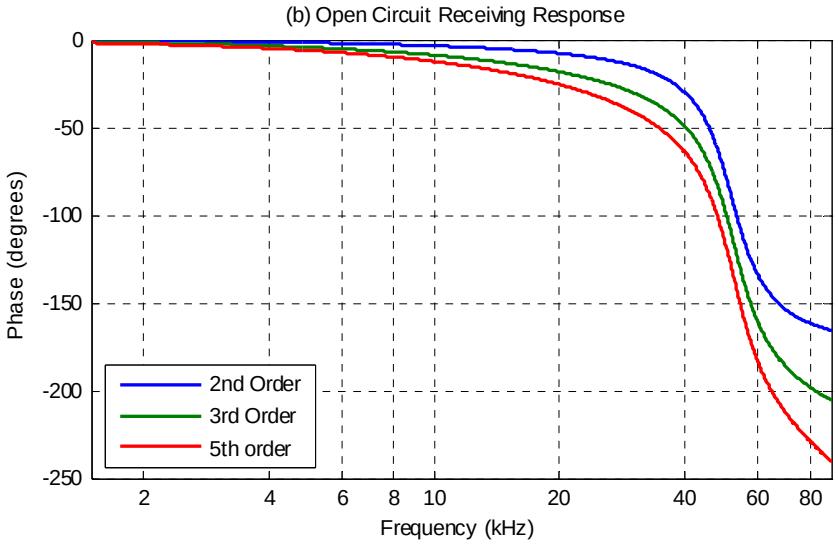

Figure 4.5 Simulated phase response of Rona hydrophone.

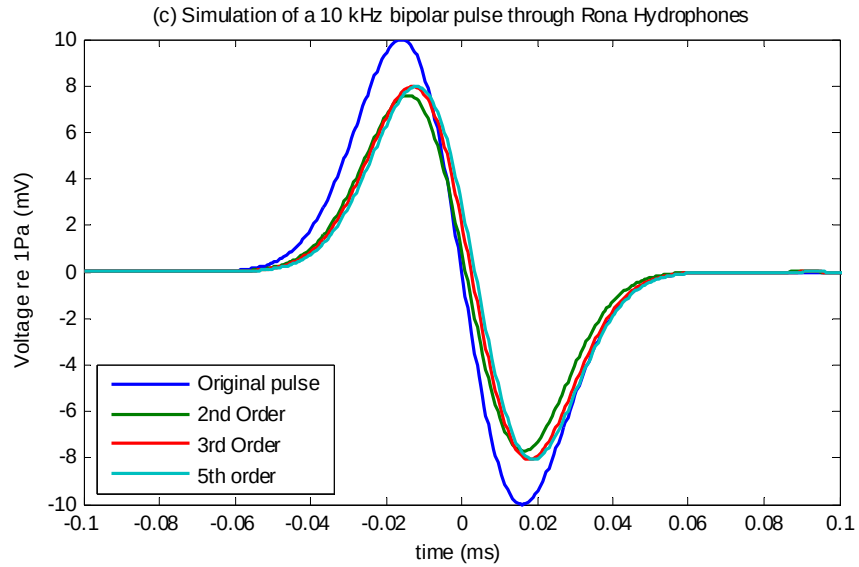

Figure 4.6 Simulated 10 kHz bipolar pulse.

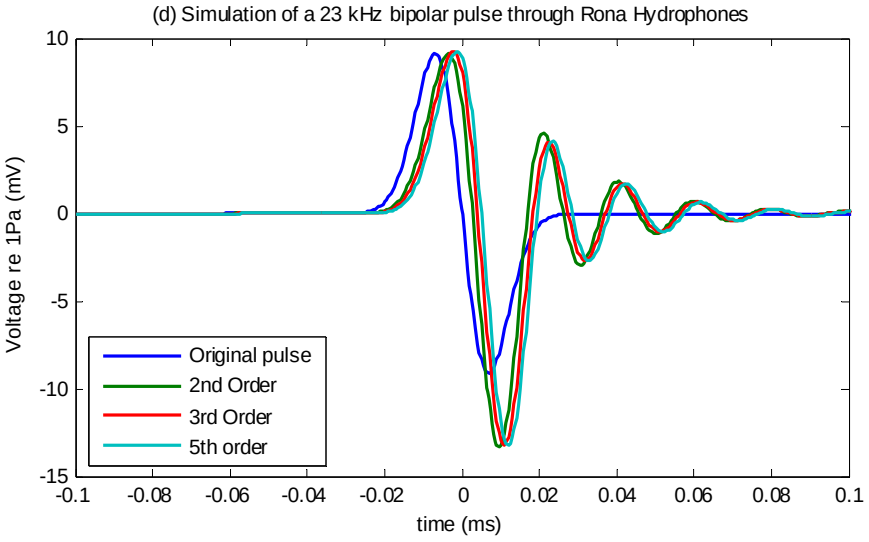

Figure 4.7 Simulated 23 kHz bipolar pulse.

4.4 Deployment at the Rona site

In 17th September 2008, ACoRNE utilised a single source hydrophone to inject both 10 and 23 kHz bipolar pulses in seawater at the Rona site. The eight-receiver hydrophone array is used to measure the signal injection, however the hydrophone number 8 is not activated. As a result of this problem, only 7 hydrophones are used in the measurement. The coordinates of this hydrophone array are illustrated in table A.1 in the appendix A. The route of the boat and the time injection are plotted in Figure 4.8.

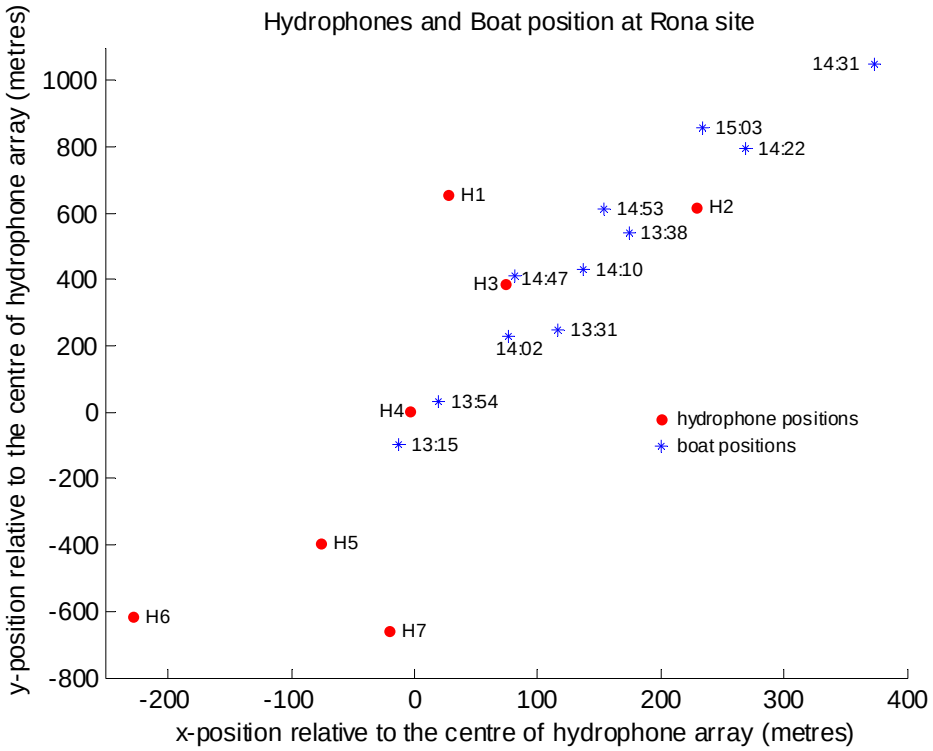

Figure 4.8 The route of the boat on the array during the day of 17 September 2008.

The pattern of injection begins with two single cycle sine waves with the amplitude 25 V. The single cycle sine waves are high amplitude as it is used in order to synchronise the clocks between the laptop on the boat and ground station of the Rona site. The delays are set up 20 seconds between both first and second single cycle sine waves.

Next, the 10 kHz bipolar signal is injected at a repetitive rate of 2 seconds per pulse whilst the amplitudes of these signals are adjusted every 100 seconds starting from 10, 15, 20, 25, 30 V. Then the single cycle sine waves are used again in the same manner as in the first step. The second step, the bipolar pulse is changed to 23 kHz instead of 10 kHz. However, the amplitudes of 23 kHz bipolar pulses are set up as same as the 10 kHz bipolar pulse. The details of injection are shown in Figure 4.9.

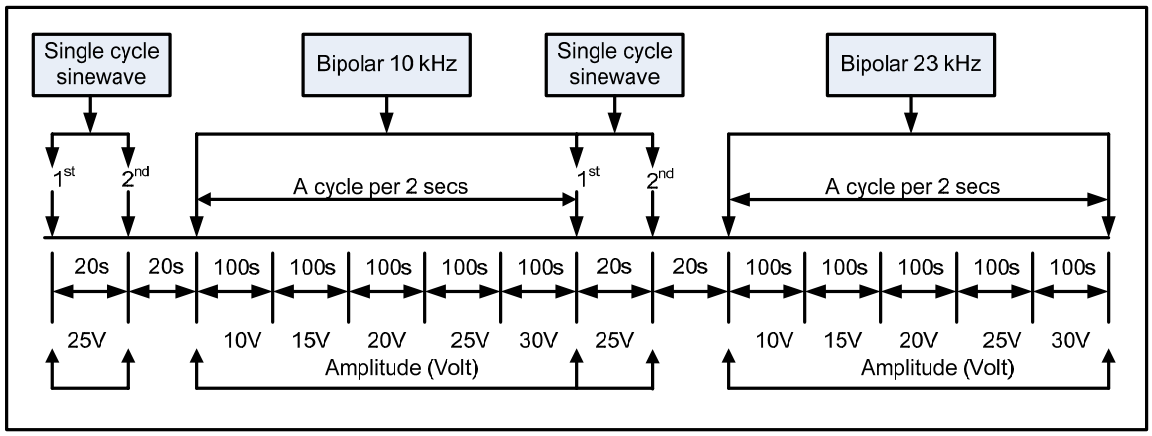

Figure 4.9 The pattern of injection at Rona site.

The collection of data is achieved by the data acquisition module on the island. The module is set the sampling rate at 140 kS/s, 16 bit resolution and recorded in ten minute files. The data is recorded in 9 sets. Each set comprises seven files (hydrophone 1 to hydrophone 7). The size of each data file is calculated by $140\frac{kS}{s} * 2\ bytes * 600s = 168\ Mbytes$.

4.5 Analysis of data

One of the major causes of noise in marine acoustic systems is wave noise which is dominated by low frequencies. The 85 % of the acoustic background energy was below 2.5 kHz [15].The graphic user interface (GUI) in MATLAB software is developed for the analysis. The raw data, which is recorded from the Rona site, is plotted in Figure 4.10.The hydrophones are labelled top to bottom from hydrophone 1 to 7, and y-axis is labelled in ADC counts. The first step in the analysis is simply to look for the pulses that should be there, but it could not resolve the signals.

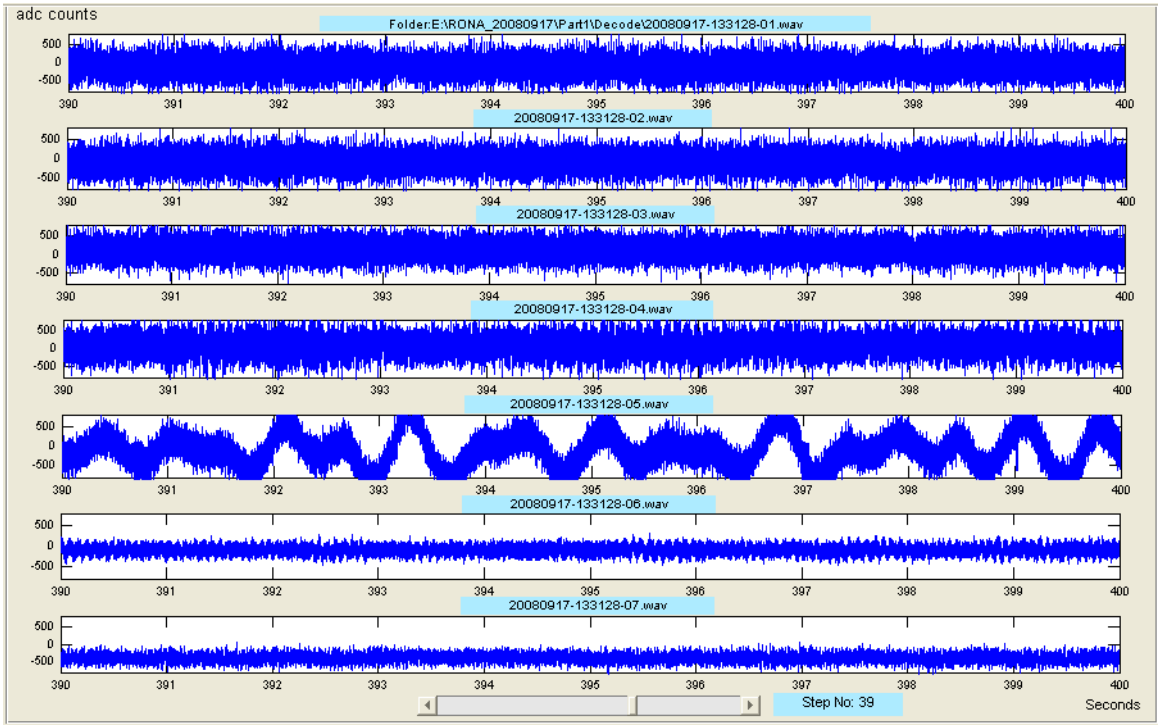

Figure 4.10 The raw data from the Rona site.

A 3rd order high pass Butterworth filter with a cut off of frequency 2.5 kHz is then used to remove the low frequency component of the data. The Figure 4.11 shows the output signal from the high pass filter. The output signal from the high pass filter is very clear when compared with the raw data, however it could still not be seen because the amplitude is very small.

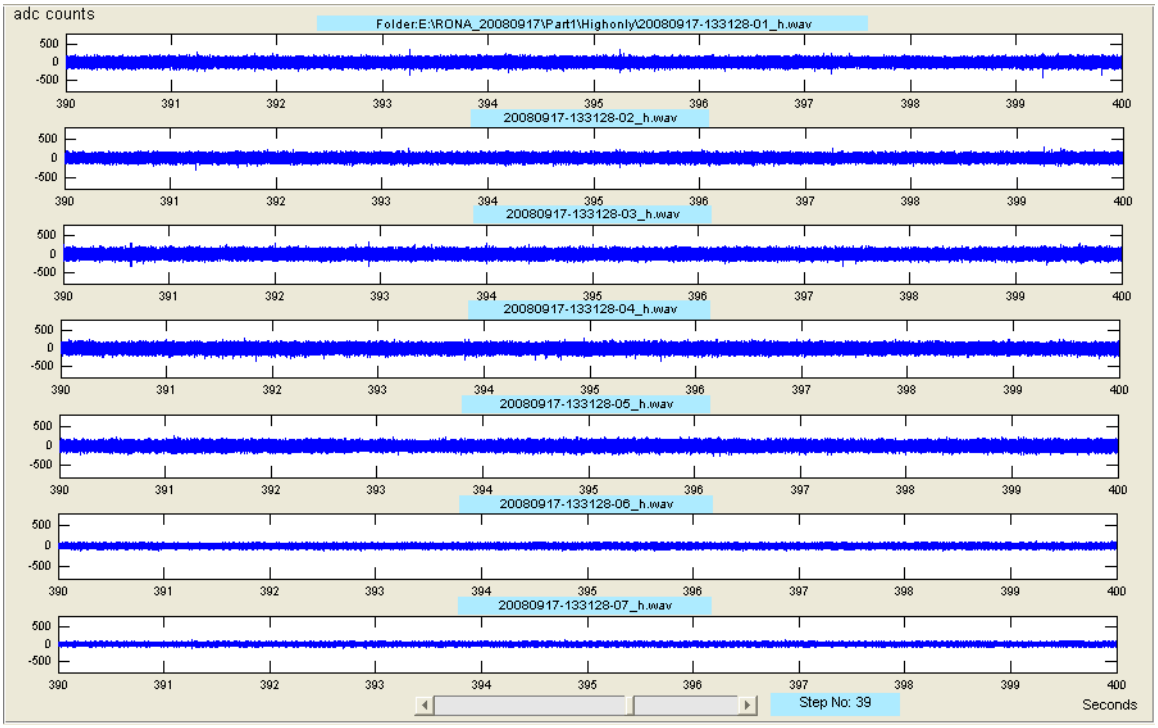

Figure 4.11 The output signal from high pass filter.

The matched filter is a technique of optimizing the signal to noise. The method is used to calculate the correlation between two signals that is called cross-correlation [93]. The output signal from the high pass filter is passed through the matched filter. The output signal from the matched filter is illustrated in Figure 4.12. A clear periodic signal can be seen especially in hydrophone 1 and 2.

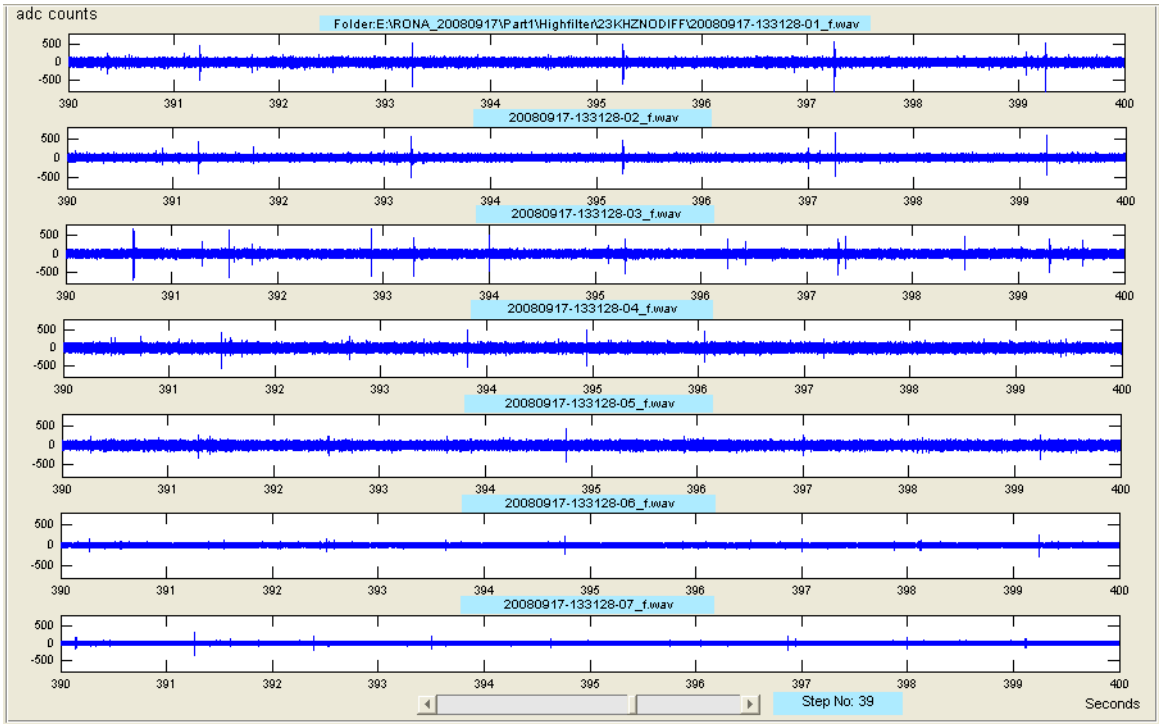

Figure 4.12 The output signal from matched filter.

Zooming of signals at the hydrophone 1 and 2, the Figure 4.13 and Figure 4.14 show the five pulses in ten seconds on the left hand windows. And the right hand windows, the first triggers for each hydrophone are zoomed to see the shape of pulse. This result confirmed that the pulses can be detected as following the pattern of injection.

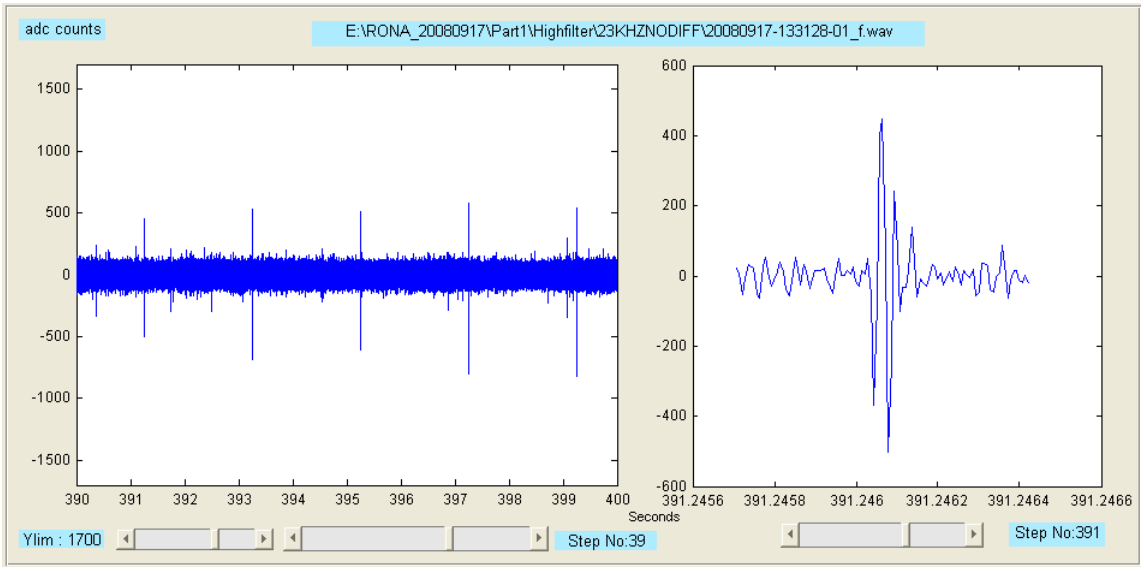

Figure 4.13 The 5 triggered pulse of hydrophone 1.

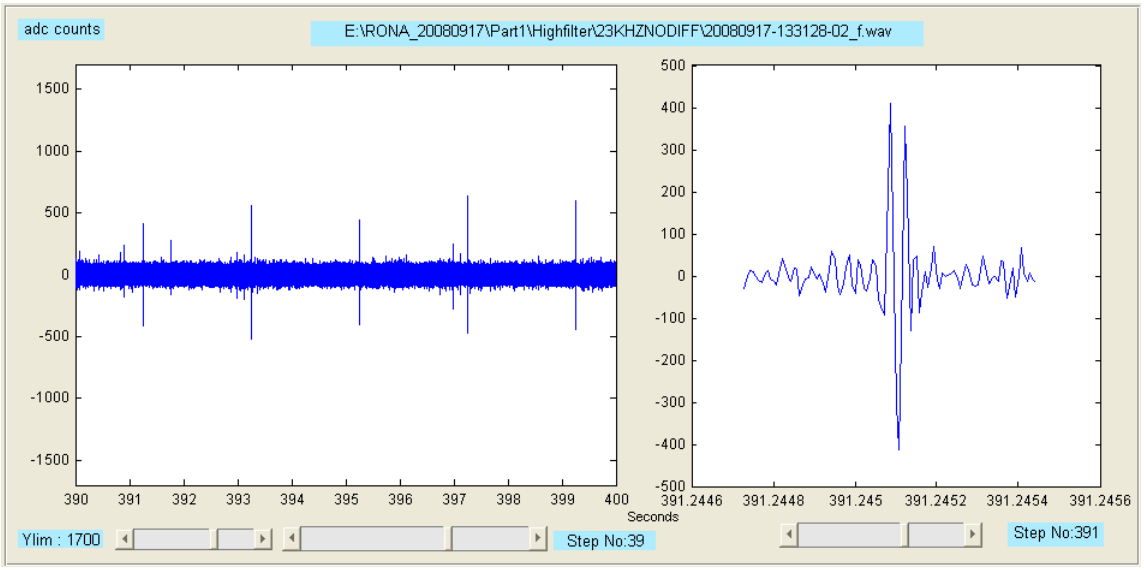

Figure 4.14 The five triggered pulse of hydrophone 2.

Data from hydrophones 1-7 was analysed, however only bipolar pulses from hydrophones 1, 2 and 3 were detected as they were closely the transmitter. Then, only data from hydrophones 1, 2 and 3 was compared to find out the similarity of the bipolar pulses from those hydrophones.

The comparison of bipolar pulse shape between each hydrophone has been done by using the cross correlation. The examples of signals from hydrophone 1, 2 and 3 from files "20080917-133128-0x.wave" are chosen for analysis. The 100 pulses for hydrophone 1, 2 and 3 are correlated for each hydrophone. However, the pulses of hydrophone 3 are separated into two parts, high intensity and low intensity, because the shape of pulses is significantly different between two parts.

Firstly, the dejittering of bipolar pulses needs to be made up from each hydrophone. The 100 pulses from hydrophone 1 are read by choosing the position of maximum pulse for the centre. However, the pulses are not always absolutely aligned. The cross correlation is applied to quantify how much each pulse has to move to best match another pulse. The 100 pulses have then been dejittered. The 100 pulses and the dejittering of 100 pulses from hydrophone 1 are shown in Figure 4.15, left windows and right windows respectively. The 100 pulses from hydrophone 2 are investigated using the same process as the hydrophone 1. The result from hydrophone 2 is shown in Figure 4.16. Surprisingly, the pulses from hydrophone 3 can be separated into two parts because the shape is slightly different. The first part is the pulses which have high amplitude injection (Approximately 20-30 Vpp). The second part is the pulses which have the amplitude between 10-20 Vpp from the source hydrophone. Figure 4.17 and Figure4.18 are shown the high amplitude pulse and low amplitude pulse from hydrophone 3 respectively.

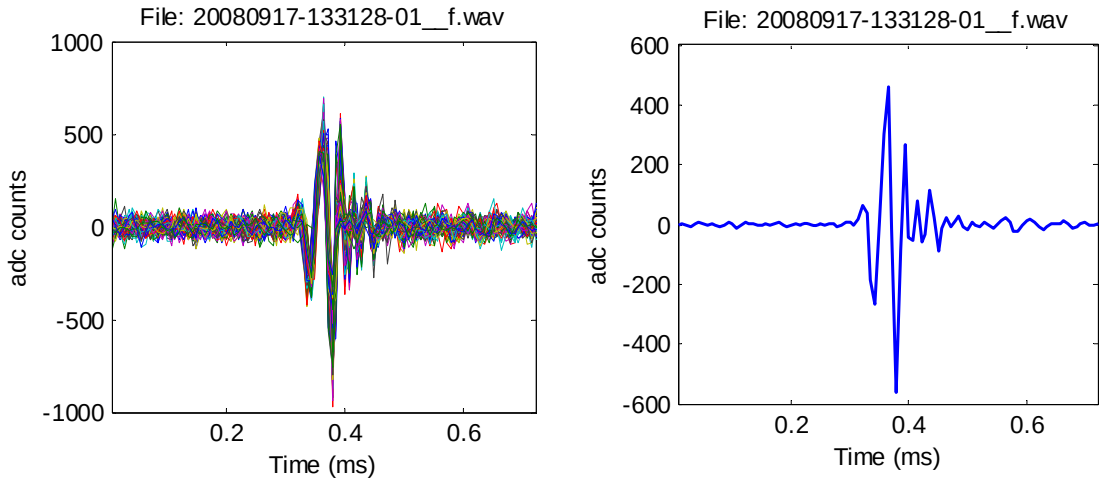

Figure 4.15 Triggered pulse of hydrophone 1.

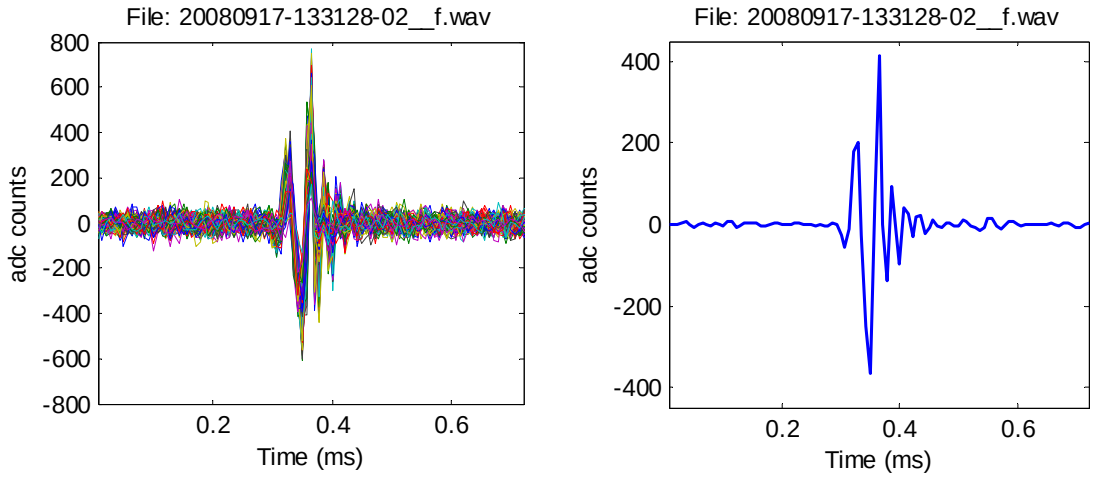

Figure 4.16 Triggered pulse of hydrophone 2.

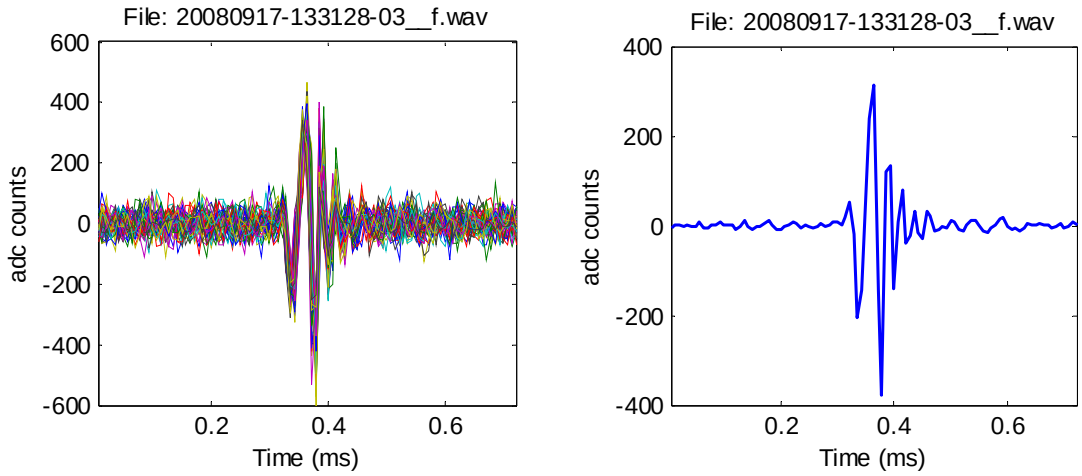

Figure 4.17 Triggered pulse of hydrophone 3 (high amplitude).

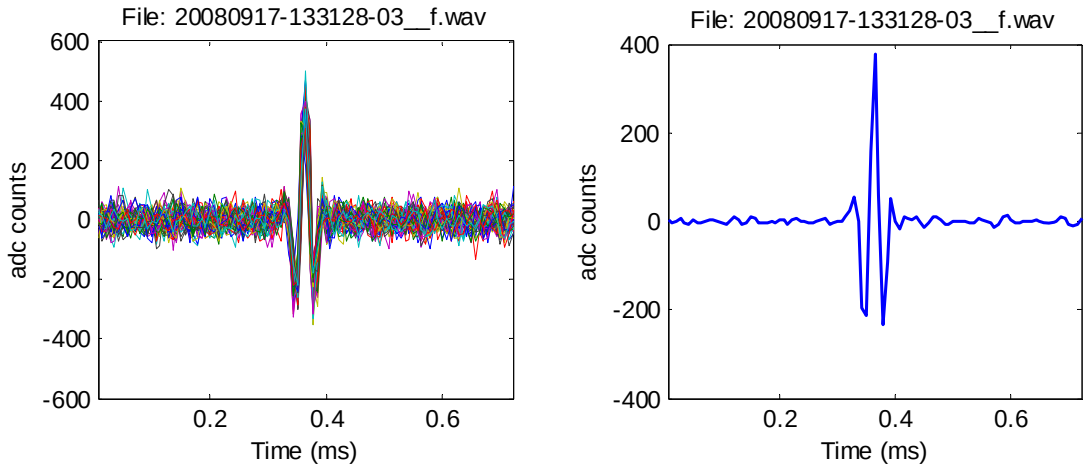

Figure 4.18 Triggered pulse of hydrophone 3 (low amplitude).

The non-linear phase response of the Rona receiver hydrophone already mentioned in the previous section, the results from hydrophone 1, 2 and 3 show non-bipolar pulses. These are almost certainly due to the non-linear phase response of the receiver hydrophone.

Finally, the cross correlation has been used to compare the average pulses from hydrophone 1, 2 and 3 in order to determine the similar bipolar pulse shapes. Looking at the table 4.1, the result from the cross correlation between hydrophone 1, 2 and 3 is illustrated.

Table 4.1 The cross correlation between hydrophone 1, 2 and 3.

Hydrophone	**1**	**2**	**3H**	**3L**
1	1			
2	-0.96	1		
3H	0.89	-0.95	1	
3L	-0.86	0.82	-0.78	1

With perfectly matched hydrophones the cross correlation would be one assuming an infinite signal to noise ratio. It looks as if hydrophones 1, 2 and 3H are well matched – producing good correlations. The negative values indicate pulse inversion –the signal from hydrophone 2 is inverted with respect to hydrophones 1 and 3H. This is most likely to be caused by the polarity of the hydrophone electrical connections being inverted. This is very common in practice as hydrophones are normally used in the frequency domain without concern for phase shifts. The behaviour of hydrophone 3 is very strange. There have however been problems with this hydrophone in the past and as the 3H and 3L signals were taken in single blocks not overlapping in time it is possible that there is a loose connection somewhere between hydrophone 3 and the DAQ causing this anomalous behaviour. In addition, the receiver hydrophones are a military array, so access to the hardware is impossible.

4.6 Summary

The simulation of 10 and 23 kHz bipolar pulse attenuation using the ACoRNE parameterization has also been investigated. The result of bipolar pulse from simulation has been plotted with varying the four values of distance. The phase and amplitude response of the Rona hydrophones has been studied to such signal characteristics.

The techniques of injection and data collection at the Rona site have been detailed. The investigation of data recorded has been reported. Signal processing techniques have been applied to resolve the bipolar pulse from the noise background. The result of MATLAB software analysis has shown the exact pattern of signal injected. Only signals from hydrophone 1, 2 and 3 are chosen for analysis using cross correlation. The correlated computation between hydrophone 1, 2 and 3 is well matched producing good correlations.

This chapter has already presented information regarding a single source hydrophone deployment at the Rona site. The simulation of eight-hydrophone array for deployment at the ANTARES site will be discussed in the next chapter.

Chapter 5

Simulation of hydrophone array

5.1 Introduction

The main aim of this research is the generation of acoustic bipolar pulses in seawater to mimic the interaction of neutrino-induced pulses. The transmitters have to be able to mimic such acoustic pulses in both directivity and shape. In addition, the ANTARES detector site is selected for deployment at a depth of 2475 m underwater. The important point is that the pulses have to be sent over considerable distances. At the Rona site, the hydrophones were very shallow c. 120 metres. Hence much more power will be needed for modern telescopes which need a large volume to detect the neutrino pulses. From these limitations, it is very important to study the behaviour of this acoustic pulse using the simulation software in order to be able to design and implement an acoustic transmitter system which will be able to reproduce an acoustic bipolar pulse with such characteristics.

This chapter will present the array simulation of acoustic signals, which will be emitted by eight hydrophones into sea water at the ANTARES site. The ACoRNE method [2] of computing natural complex attenuation is used to predict the 23 kHz bipolar pulse (shape and amplitude) at the ANTARES site.

Moreover, the calibration of an eight-hydrophone array, which will be performed at the ANTARES site, is presented. The new eight TC-4033 robust spherical reference hydrophones from Reson, are used for eight-channel transmitter hydrophones. The transfer function of the new hydrophones is determined by signal processing techniques. The new transfer function is simulated to confirm that the new hydrophones can produce acoustic bipolar pulses as needed.

The orthogonal pulse train will also be discussed in the last section. The main purpose is to investigate the feasibility of signal coding. This technique is very useful to apply in communication system and also in underwater acoustic detection as it can classify the signals emitted from array of hydrophones.

5.2 Simulation of acoustic array

In Chapter 2, the thermo-acoustic model was presented which is used as its source of the neutrino interaction in seawater. The computing method for acoustic signal for neutrino shower simulation and the calculation of the sound signal in seawater at the detector have been detailed in [2, 64, 93-94].

Before starting an array simulation, it might be useful to consider how many individual bipolar sources we need to use for generating a suitable pancake. To answer this question, the ACoRNE collaboration has presented the simulation of determination of the acoustic transmitter number that is suitable for generating of acoustic bipolar pulses. The simulation has shown that in the far field the amplitude of the acoustic signal drops by two orders of magnitude at 5 degrees out of the plane of the pancake. To investigate this, the study is made by a calibrator comprising multiple transmitters. The transmitters are equally space over a nominal 10 metres calibrator length, for instance a 10/n metre spacing for n transmitters. The simulation of the acoustic energy distribution as a function of angle is shown for a number of transmitting hydrophones when n = 2, 3, 4, 6, 8 and 10 respectively, namely 1 km from the neutrino interaction point. Moreover, the simulation has made up to 20 transmitters, however very small difference in the angular energy profile can be seen when n>10. Consequently, the number of 6 and 10 transmitters are suitable to accurately generate a pancake. The Figure 5.1 shows the results from simulation of predicted acoustic energy deposition profile. The figures are plotted as a function of the angle from the normal to the line array for differing numbers of transmitting elements arranged over 10 metres, where n=2 (top left), n=3 (top right), n=4 (middle left), n=6 (middle right), n=8 (bottom left) and n=10 (bottom right).

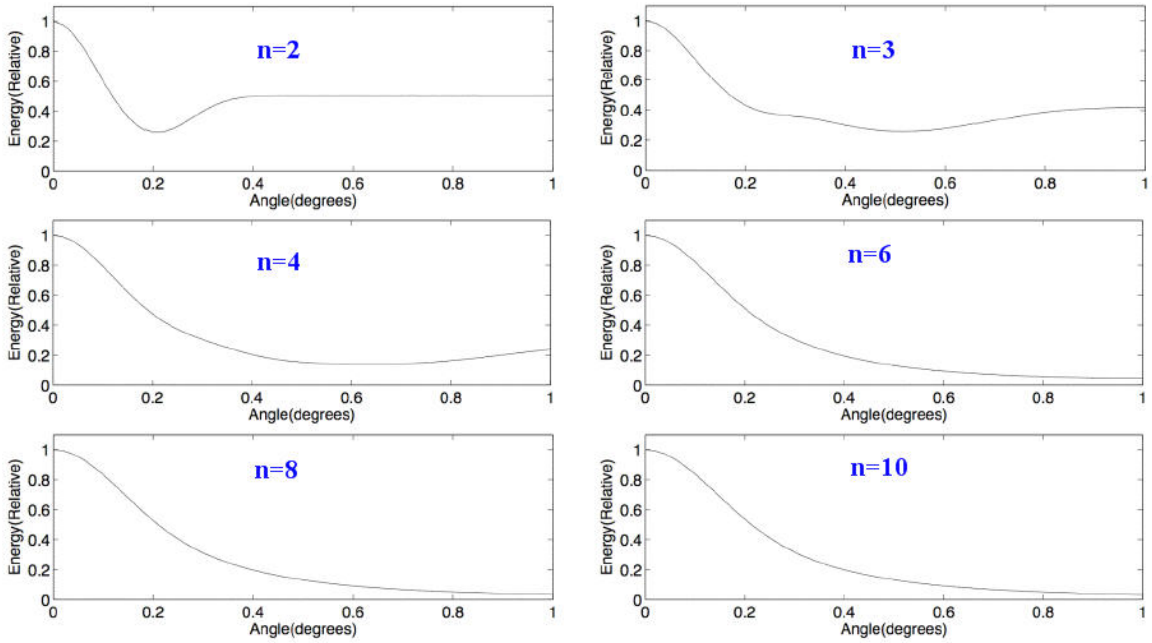

Figure 5.1 An acoustic energy deposition profile for differing number of transmitters.

The simulation method used by the ACoRNE collaboration including the complex attenuation effect in the seawater is assumed to simulate the eight-hydrophone array system [93]. It is used to study the array design and size in order to achieve the best approximation to the real UHE neutrino-induced pulse properties in the transmission of the artificial bipolar pulse. It is referenced to the bipolar pulse signal shape and directivity at the acoustic receiver sensors belonging to the ANTARES system. The details on a formation of the acoustic signals already mentioned in the section 2.3.

For the simulation, the shower points are generated in polar coordinate. Then the shower points are split in eight sphere storeys (number of hydrophones). The shower points are converted to Cartesian coordinates in order to calculate the distance from the original point of the shower to the observer point. Then, the energy of showers calculates from the histogram of flight times to the observer (time=distance/velocity of sound). Finally, the pressure pulse is the derivative of time to the observer.

The deposited energy is binned in a cylinder of ten metres in length and 2.5 cm in width that gives approximated characteristics to the bipolar signal created for the neutrino interaction, referred to bipolar pulse shape and directivity. This is used as a reference to compare it with the array shower generation which uses the same size as the cylinder simulation but it is split in eight spheres with equal centres along the ten metres in length. The length is also compared for eight and six metres in order to study the length with the best approximation in shape and ‘pancake’ angle to neutrinos bipolar pulse.

The coordinate system is chosen such that the neutrino interacts at the origin and travels vertically along the z axis where the value of z increases with depth and the origin. The point (0, 0 ,$-Z_p$) is chosen such that the maximum 'pancake' occurs at 0°. For the analysis the observer is positioned at 2475 metres from the shower in the centre of the acoustic pancake along the x axis, simulating the deployment of the ANTARES detector, the array simulation system for eight metre length shower is shown in Figure 5.2. For the simulation, a 10^{11} GeV shower energy deposition is chosen which was used in previous studies for comparison.

The array has been simulated to determine the length that allows the most directive angle maintaining the bipolar pulse shape. An energy equivalent to a 10^{11} GeV shower is shared between eight spheres for 4, 6, 8 and 10 metres array length and also a uniform energy distribution along a 10 metre cylinder is shown for comparison. The observer is located far away at 2475 metres from the source. The result from simulation (Figure 5.3) is plotted showing the relation between pulse energy at the receiver and angular spread of pancake with angle from 0º to 1º. Figure 5.4 shows the result of pancake spread varying with the angle between 0º to 1º. The highest amplitude of bipolar signal as a function of time is at 0º.

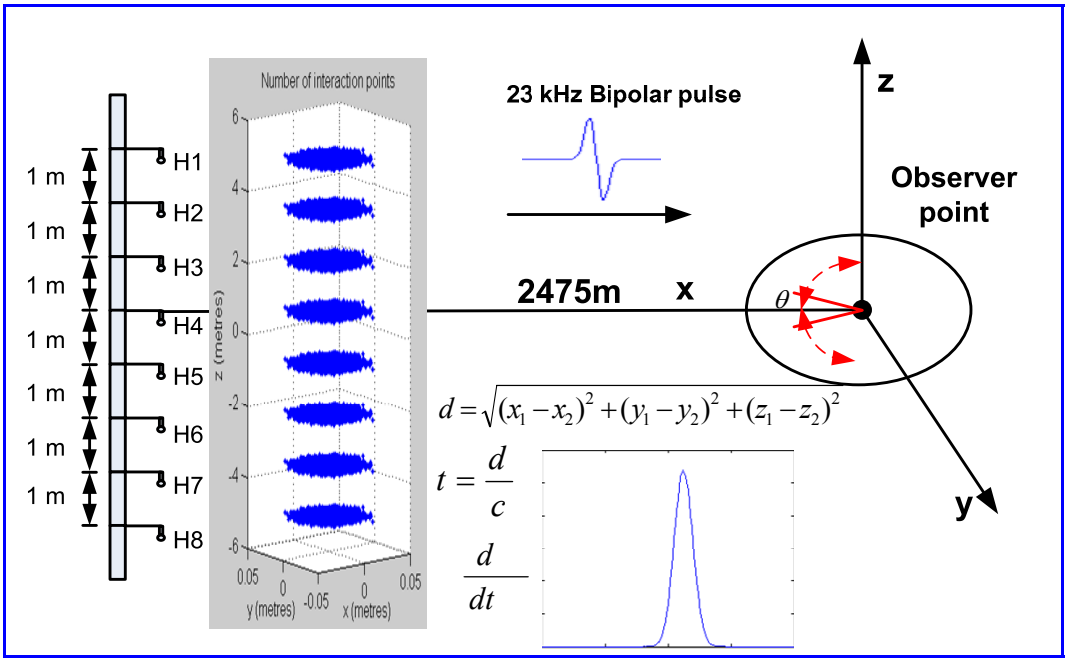

Figure 5.2 Simulation of the 8 hydrophone array transmission to ANTARES detector.

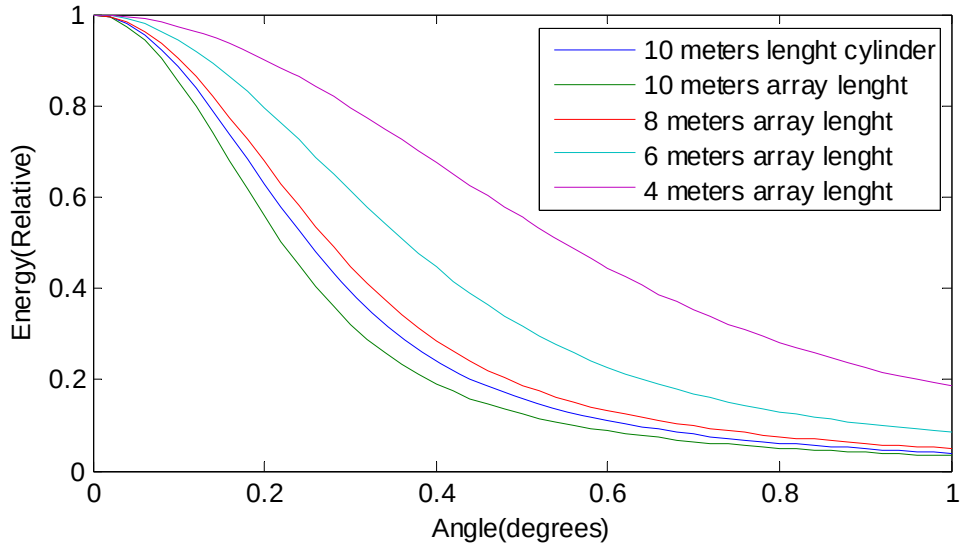

Figure 5.3 Energy vs angle at 2475 metres from 10^{11} GeV of thermal energy shower deposition, under Mediterranean Sea conditions.

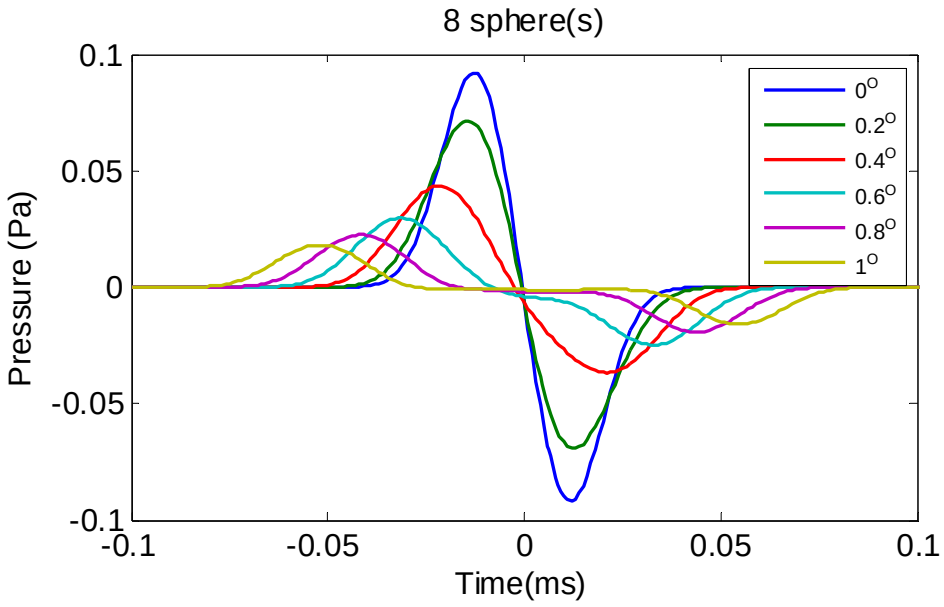

Figure 5.4 The simulation of bipolar pulse with varying angle.

5.3 Hydrophone array calibration

ACoRNE has bought eight new TC-4033 robust spherical reference hydrophones from Reson. The TC-4033 has uniform omni-directional characteristics from 1 Hz to 140 kHz. The specification of the TC-4033 transmitting sensitivity is illustrated in Figure 5.5. The certificate of calibration from Reson has been attached in Appendix E. The TC-4033 offers excellent acoustic characteristic and durability, which makes it ideal for a wide range of applications and for calibration purpose. In addition, it can operate at the depth up to 900

metres in seawater. The eight TC-4033 hydrophones using in this research are shown in Figure 5.6.

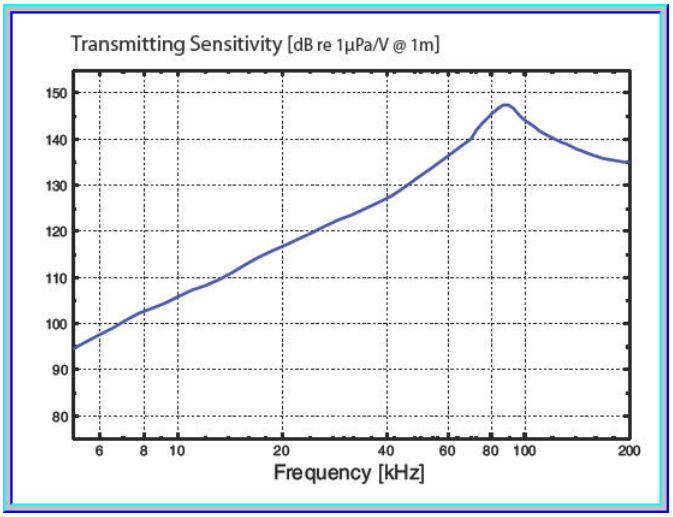

Figure 5.5 Transmitting sensitivity of TC-4033 hydrophones.

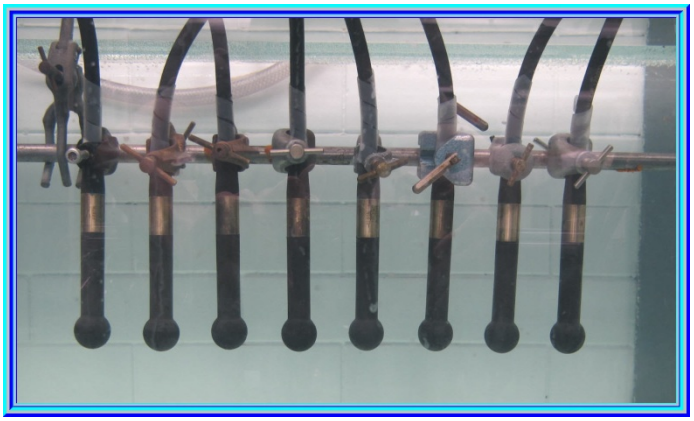

Figure 5.6 TC-4033 Reson hydrophones.

The array of eight TC-4033 hydrophones is used as a transmitter whereas a B&K 8106 is used as receiving hydrophone for testing in the laboratory. The B&K 8106 has a flat frequency response and omni-directional over a wide frequency range7 Hz to 80 kHz with receiving sensitivity -173 dB re 1 V/µPa. A 10 dB preamplifier with 7 Hz high-pass filter is included for signal conditioning over long underwater cables. The B&K 8106 hydrophone and its receiving sensitivity are shown in Figure 5.7 and 5.8 respectively.

Figure 5.7 Bruel & Kjaer 8106 hydrophone.

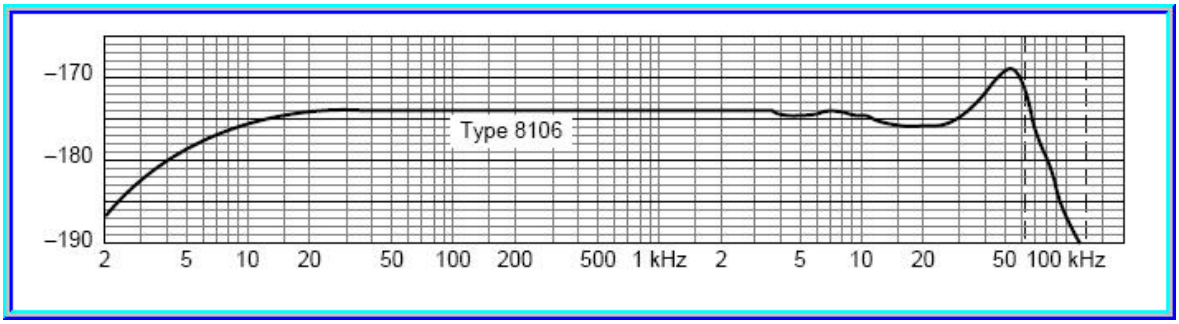

Figure 5.8 Receiving sensitivity of B&K 8108 hydrophone.

The signal processing techniques for a single hydrophone (ball hydrophone) calibration have already presented in Chapter 3. However, the ACoRNE has obtained eight TC-4033 hydrophones which are used as an array transmitter. Hence, the hydrophone array calibration needs to be repeated again in order to confirm that it can produce the bipolar pulses as required.

The calibration of hydrophone array uses the same process as that described for a single hydrophone in Chapter 3. However, all TC-4033s are new hydrophones which already calibrated from Reson Company. The certificate of hydrophone calibration has been attached in Appendix E.

In order to get a step response from a TC-4033 hydrophone, a step signal is generated by the PXI-6713 NI DAC module and sent to the power amplifier. The signal from the power amplifier module is sent to the TC-4033 hydrophone. The step response is received by B&K 8106 and recorded with the TDS2002B digital storage oscilloscope. The step response is applied to determine the transfer function of the TC-4033 hydrophone as presented in Chapter 3.The fitting of a transfer function between an actual step response and a simulated step response for the TC-4033 hydrophone is shown in Figure 5.9.

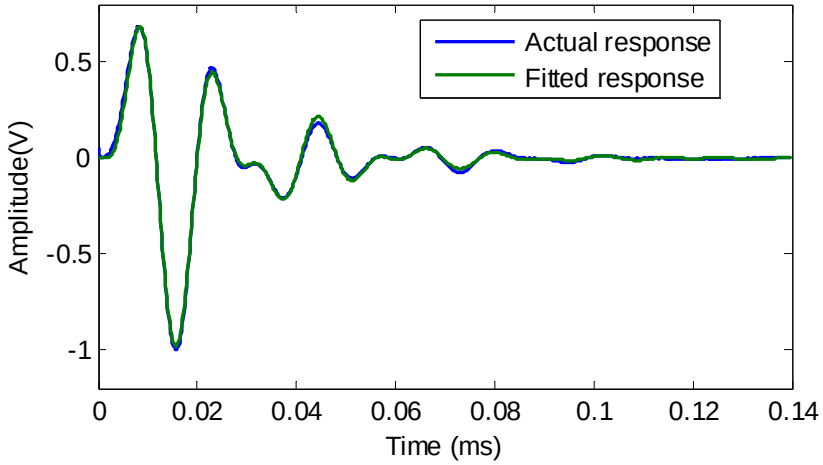

Figure 5.9 Fitting TF between measured and simulated step response.

The best match fifth-order transfer function (frequency scaled down by a factor of 50×10^3) from "*fminsearch"* MATLAB software function is shown in equation (5.1).

$$H(s) = \frac{0.0531s^2 - 0.0027s - 0.0019}{0.000063464s^5 + 0.0004318s^4 + 0.0115s^3 + 0.053028s^2 + 0.4063 + 1} \qquad (5.1)$$

From equation 5.1, all poles are in left haft of s-plane (s=-2.9128, s=-0.8593±10.9974i, s=-1.0863±6.5785i), then the system function is stable.

The 23 kHz input driving signal for the TC-4033 hydrophone, calculated from equation (3.9), is determined from replacing fitted transfer function and the desired bipolar signal. An inverse Fourier transform then calculates the input driving signal from frequency domain to time domain by equation (3.10). The 23 kHz input driving pulse for TC-4033 hydrophone is plotted in Figure 5.10. In order to confirm this hydrophone can produce 23 kHz bipolar pulse as needed, then the "*lsim"* function is used to simulate the output of 23 kHz bipolar pulse. The output from simulation is shown in Figure 5.11.

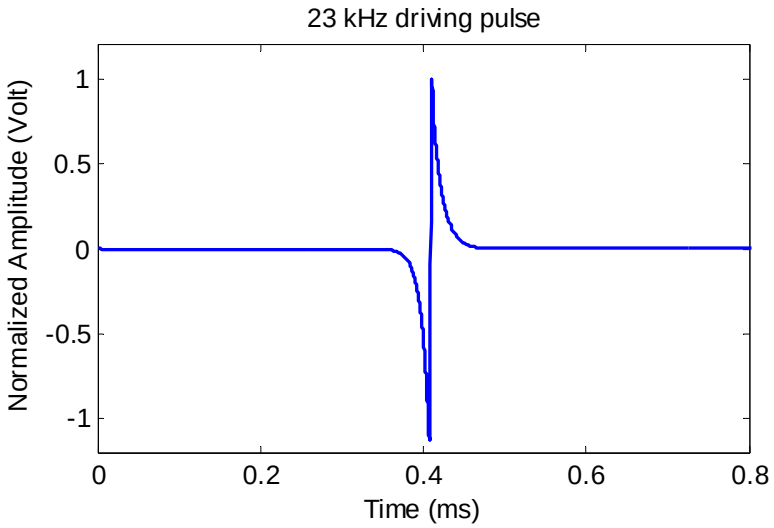

Figure 5.10 The 23 kHz driving bipolar pulse.

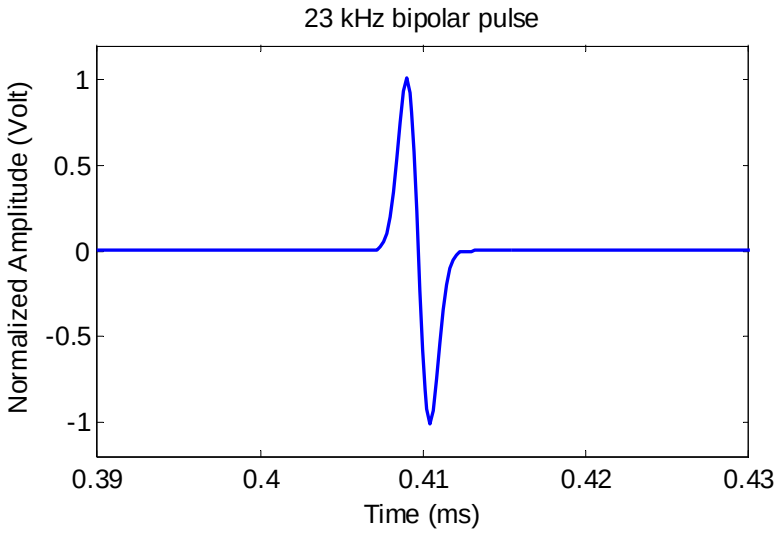

Figure 5.11 The 23 kHz simulated bipolar pulse for TC-4033 hydrophone.

5.4 Orthogonal pulses

Obtaining satisfactory underwater acoustic communication (UAC) has been challenging because of various limitations [95-98]. The Doppler Effect occurs when a sound source moves, the acoustic radiation pattern changes, thereby producing changes to the generated frequencies as perceived by a stationary observer. The resulting frequency heard by the observer is not the source's output frequency but that increased by the resulting drop in the wavelength. On the other hand, when the source is moving away from the observer, the frequency received by the observer is lower than the actual frequency. When sound impinges upon a surface, a portion of its energy is absorbed by the surface and the remainder bounces back or becomes reflected from the surface. This phenomenon is called the reflection. The other limitation of underwater acoustic communication and detection is

refraction which the direction of the advancing wave front is bent away from the straight line of travel. Refraction occurs as the result of the difference in the propagation velocity as the wave travels from one medium to a different medium. The diffraction occurs when a sound wave travels through a barrier, some of the sound being reflected back, some continues onward and some of the sound bends or diffracts over the surface.

The other obstacle to acoustic communication underwater is the inter-symbol interference (ISI) [99]. It is the distortion of a symbol signal which interferes with other symbols. This causes the overlap of individual pulses to the degree that the receiver cannot reliable distinguish between changes of state. The cause of ISI is usually multipath propagation [100]and bandwidth limitation [101-103].The multipath propagation is a signal from a transmitter reaches the receiver via various different paths as a result of reflection, refraction and atmospheric effects and so on.

Moreover, the need for high speed and accurate data transmission in underwater communications is growing. Researchers have attempted to develop in each part of UAC especially channel equalization, channel modelling, multi-carrier modulation, underwater networking and so on. Each must be considered in selecting the appropriate signalling for a UAC system [104].

It is not only underwater communications that have limitations but also under water acoustic detection is difficult because the seawater has bandwidth limitation [105-107]. Especially, this research has been studying the feasibility of neutrino detection in sea water. When several bipolar pulses are emitted into sea water at the same time, one finds overlapping and interference between this signals. As a result, it is a difficulty in recognising and reconstructing the bipolar pulses emitted.

To study the possibility of solving these limitations in underwater acoustic communication and detection, orthogonal pulses were used to deploy at sea in order to investigate the possibility of coding signals.

The ten sets of orthogonal signals are firstly generated by MATLAB software with 1000 samples for each set. Orthogonal signals are resulted from the 5^{th} order Butterworth filter of the Hanning window multiplying with the band limited Gaussian noise. Figure 5.12 shows the ten sets of orthogonal signals. The Figure 5.13 shows separately plots for the ten orthogonal sets.

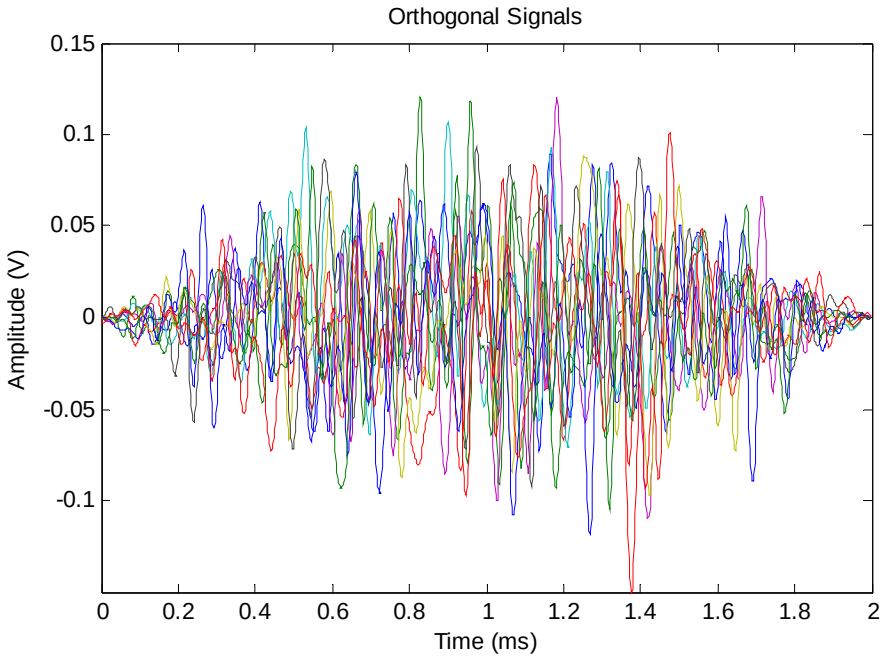

Figure 5.12 Ten sets of orthogonal signals.

The two groups of ten set orthogonal signals are created from the same signals. However, for each group is added by different Gaussian noise to mimic the sea noise. The first group and second group of orthogonal signals with added noise are plotted in Figure 5.14 and Figure 5.15, respectively.

The main idea of this technique uses the cross correlation between those of two groups of signals in order to determine a score of one for the matched signals, ideally a score of zero for unmatched signals. In practice, this simulation, using 0.32 for a unmatched score. A one thousand time of ten sets are calculated to find out the distribution of data. The histogram is used in order to show the different score of cross-correlation. The results from simulation is plotted in Figure 5.16.

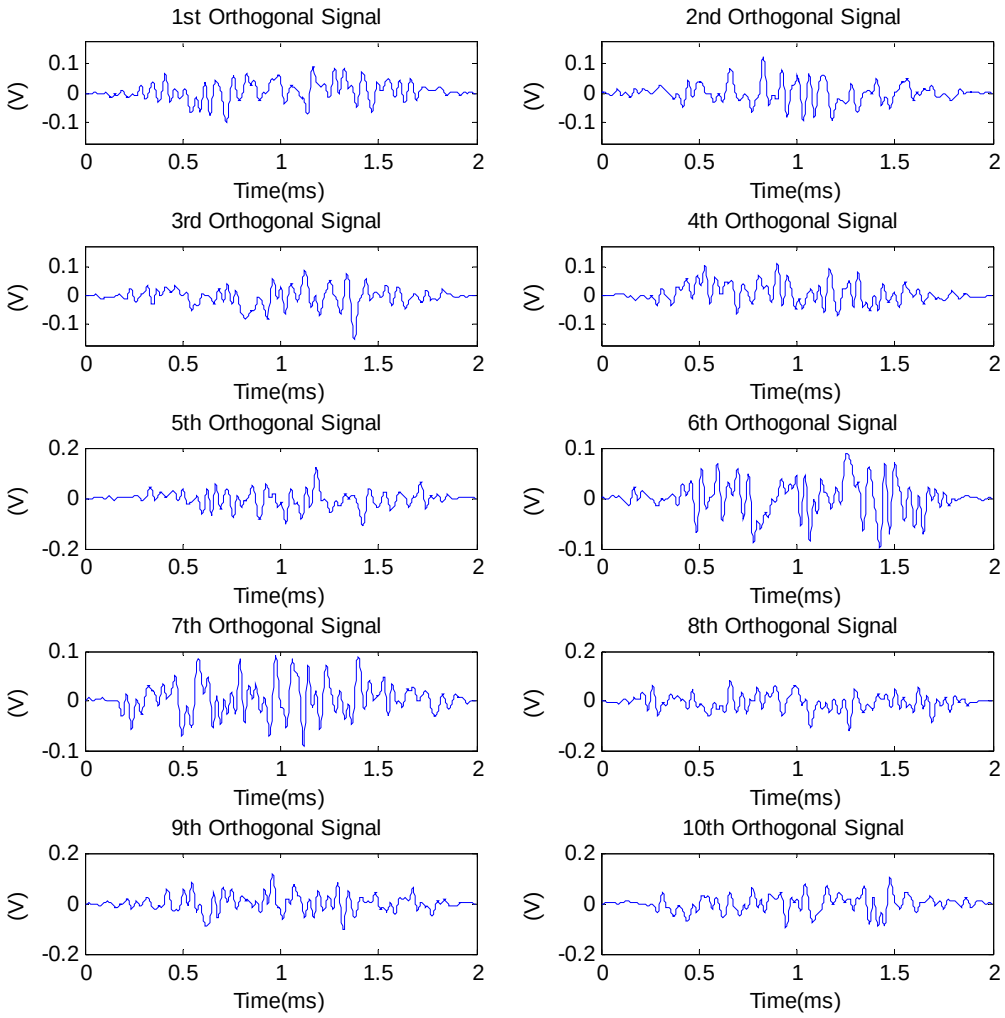

Figure 5.13 Ten sets of orthogonal signal which are separately plotted for each set.

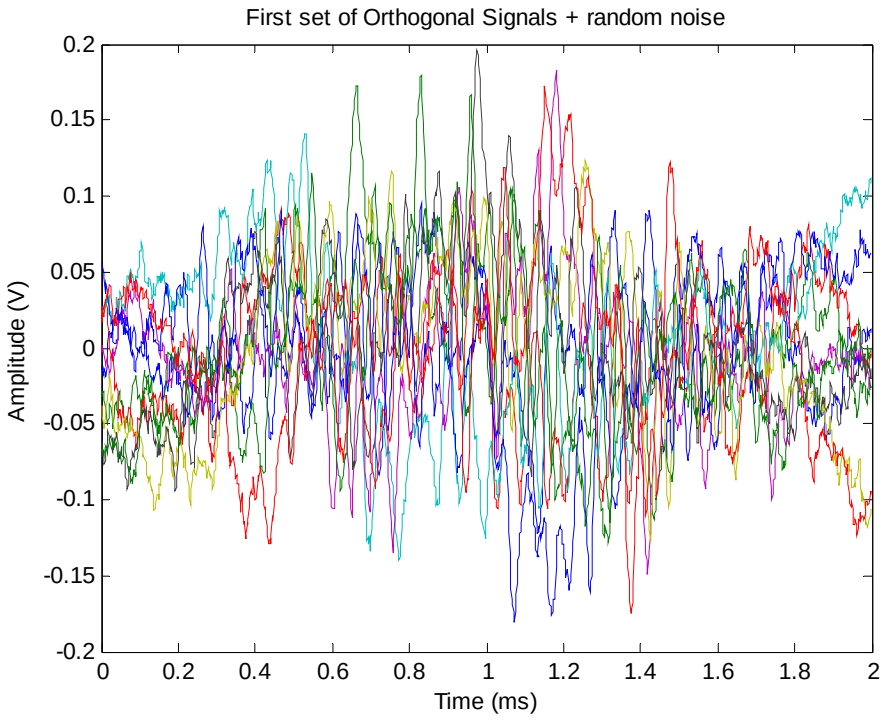

Figure 5.14 First set of orthogonal signals with random noise.

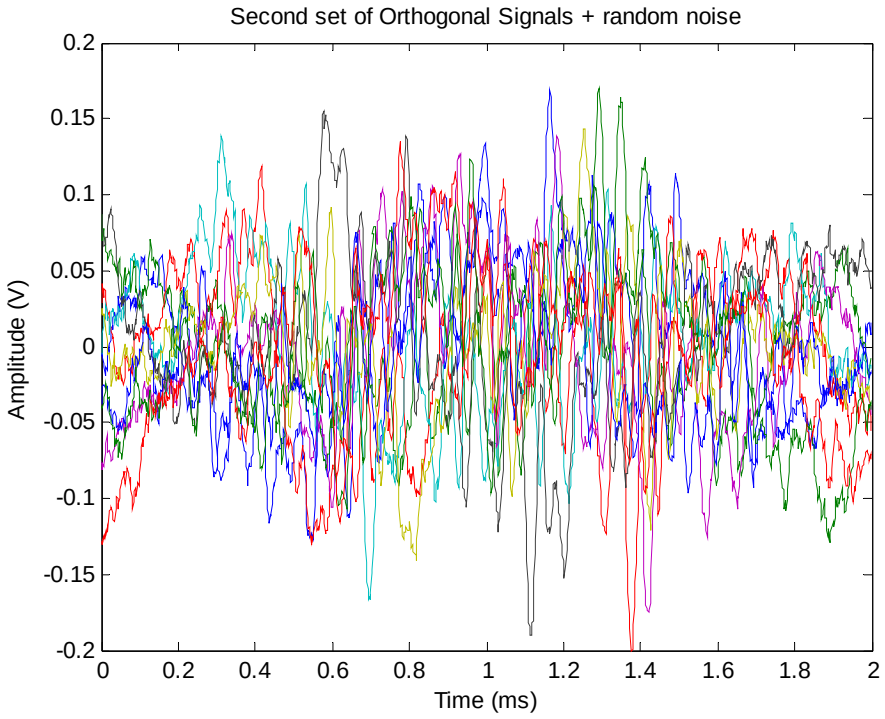

Figure 5.15 Second set of orthogonal signals with random noise.

Figure 5.16 shows histograms of the cross-correlation output between ten sets of orthogonal signals adding with Gaussian noise. The simulation uses the same signals but changing adding Gaussian noise for one thousand times to see the distribution of data.

In the case of the cross-correlation without noise, if it is different signals, the result score should equal 0.3 ($R_{xy} = 0.3$ if $x \neq y$) and if it is the same signal, the result score should equal 1 ($R_{xy} = 1$ if $x = y$). However, the results show in Figure 5.16 with adding noise, so it is spread out between 0.2 and 0.4 for the different signals. It is between 0.8 and 1.2 in the case that both signals are matched together.The results from simulation have shown that each set of orthogonal signal is identified by this technique.

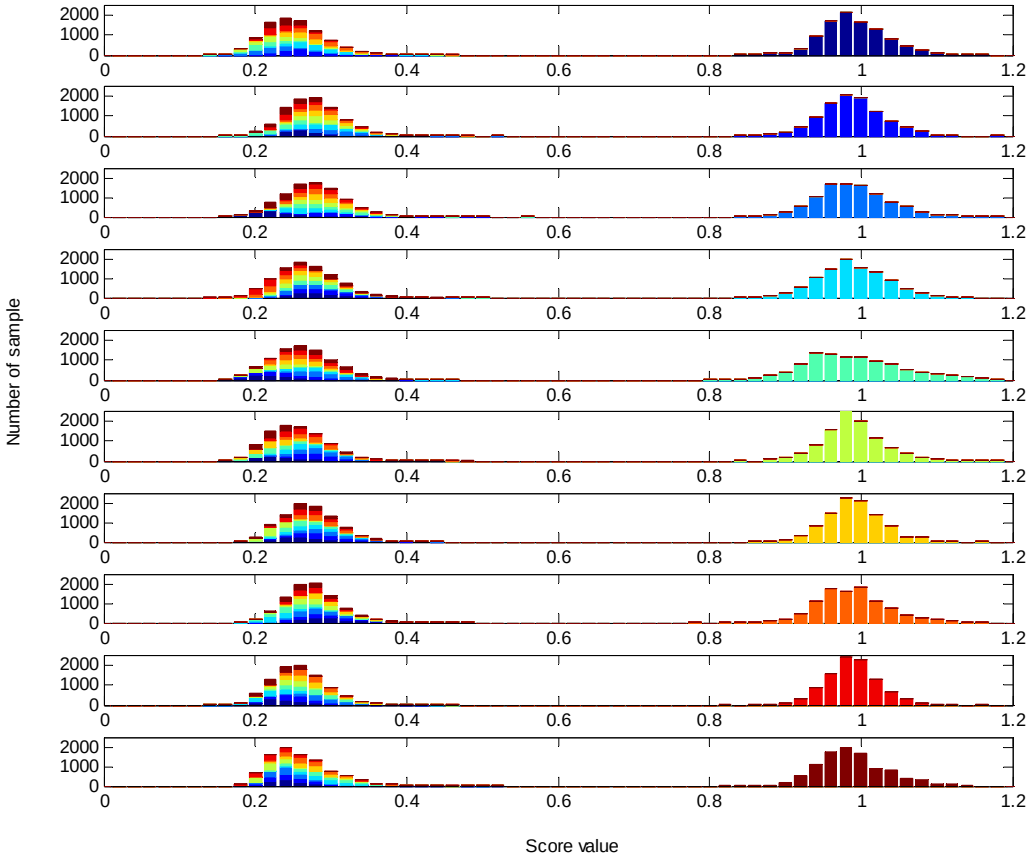

Figure 5.16 The simulated results of orthogonal signals.

This technique is very useful for researchers in underwater acoustic communication and detection, especially in the area of acoustic neutrino detection when bipolar pulses are sent by an array of hydrophones. The signals emitted have interference due to the band limitation of seawater, it becomes more difficult to classify for each of signal. This technique will then be applied in order to recognise and reconstruct signals in neutrino detection. The ten sets of orthogonal signals are deployed at the ANTARES site in order to study the feasibility of this technique to classify the signals. The deployment of orthogonal signal sets is presented in Chapter 7.

5.5 Summary

In this chapter, the simulation of acoustic hydrophone array calibration has been presented for neutrino detection. The results show that the eight hydrophones arranged over an eight metres spacing structure can mimic the anticipated pancake behaviour predicted from neutrino-induced showers as well as the acoustic bipolar pulse shape and amplitude at the ANTARES system. The simulation results have been published in ref [108].

The calibration of an eight-channel hydrophone transmitter array has been discussed. Signal processing techniques have been applied to calculate the transfer function of new TC-4033 Reson hydrophones which will be used for the sea operation. More details of hydrophone array calibration and laboratory experiment are presented in next chapter. The results of the sea campaign using an eight-channel hydrophone transmitter array, which are already deployed at ANTARES site, are presented in the Chapter 7.

The study of orthogonal pulses has been discussed in this chapter. The example ten sets of sine signals have been used in this study. The result from simulation has shown that we can classify the matched signal for each signal of orthogonal sets. This is very useful for underwater acoustic communication and detection. The ten sets of orthogonal signals are emitted in the ANTARES site to study the feasibility of this technique in practice, more details about the deployment will be discussed in Chapter 7.

Chapter 6

Embedded system design for arbitrary waveform generation

6.1 Introduction

A simulation of array transmitters has already been carried out in the previous chapter. An experiment is very important in order to confirm the result with the simulation. The main aim of this research is to generate bipolar pulses which mimic the neutrino-like pulses. Hence, the design and implementation of an electronic module that can re-produce acoustic bipolar pulses is very challenging. This chapter presents the design and implementation of a dsPIC33FJ256MC710-I/P (dsPIC), 16-bit digital signal controller, embedded arbitrary waveform generation module. In addition, a laboratory experiment for an eight-hydrophone array system using the dsPIC module is also presented. To validate the results from the dsPIC module, the a PXI-6713 digital to analogue converter commercial module from National Instruments has been used.

6.2 Hardware design

The eight-channel waveform generation module is designed and built using 16-bit digital signal controllers. The dsPICs from Microchip Technology supports 256 KB flash program memory and 30 KB data ram, are used as Central Processing and Control Units (CPCUs). The module consists of nine dsPIC chips, the first chip is designed as a master control to interface with eight dsPIC slaves via the Inter-Integrated Circuit (I^2C) protocol. The 0.5 μs fast settling time digital to analogue converter (DAC) chips, type DAC8822, are used to convert digital data to analogue signals. The MCP6024 operational amplifiers (op amp) are used to convert current from the DAC chips to voltage (I/V converter) and to amplify in the last stage.

The master control is interfaced with many peripheral devices, for instance, RS232, Key control, LCD display and in-circuit programming (ICP). The operation of the system starts with all the waveforms that are downloaded into the flash program memory of each slave module. Users can control output signals using key control and the status of the operation is shown on a LCD display. The methods of communication between master and slaves can operate by two methods. Firstly, the I^2C interface is designed to transfer data between master and slaves. Secondly, interrupt triggers are used to turn slaves on in order to

generate the rapid waveform. Using interrupt triggers, the dsPIC master unit can control the different time delays in micro-seconds between each slave. The block diagram of the dsPIC module is shown in Figure 6.1.

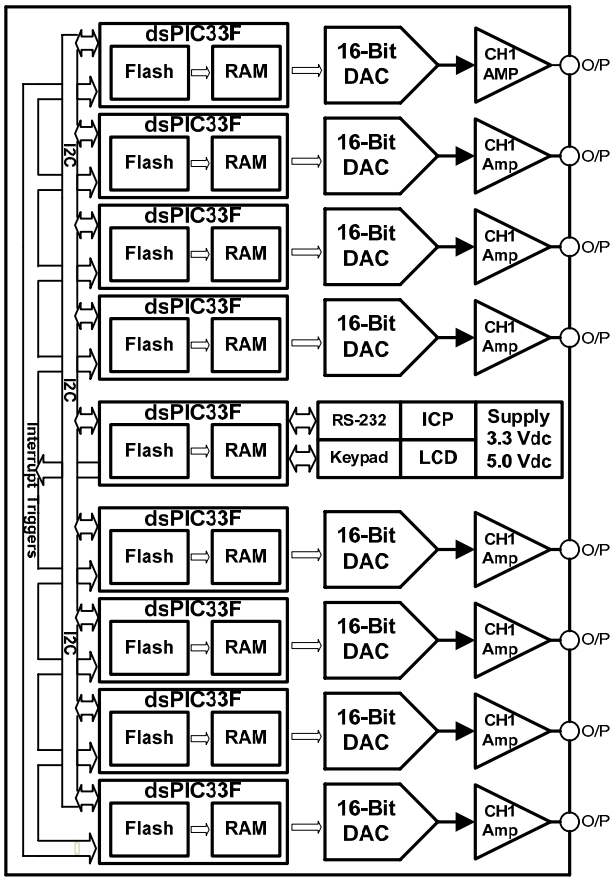

Figure 6.1 Block diagram of dsPIC module.

The first step is started from studying of dsPIC33F starter kit board using a CCS C compiler as a software control. The dsPIC33F starter kit is shown in Figure 6.2. The dsPIC33F is initially interfaced to a DAC8822 DAC chip which solders on the SSOP28 PCB adapter. When the development of source codes is finished, the next step is to design the schematic and PCB for the dsPIC33F module. The Altuim software is used for the main schematic and PCB design. The Altium software itself is more powerful in the design of PCB, especially in 3D graphic design. The dsPIC PCB board is simulated in the 3D graphic design before the fabrication to make sure that the module has the expected appearance. The 3D graphic design of PCB is plotted in Figure 6.3. The Gerber files are sent to the PCB manufacture to fabricate following the schematic and PCB design needed. The most important challenge was the soldering of dsPIC33F TQFP100 0.5mm lead pitch package. All the components are assembled onto the PCB following the schematic which was already tested before the fabrication. The metal and acrylic box is built to support the PCB board, the complete dsPIC33F module is shown in Figure 6.4.

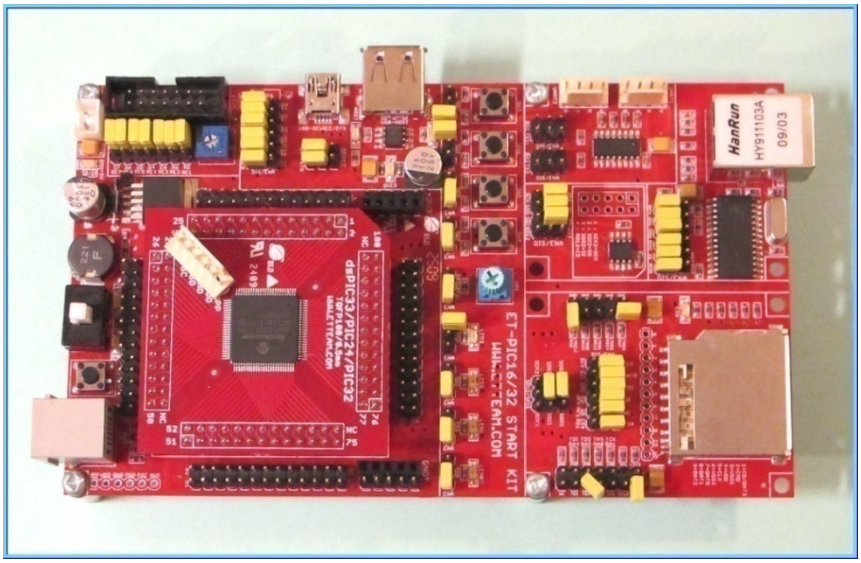

Figure 6.2 The dsPIC33F starter kit board.

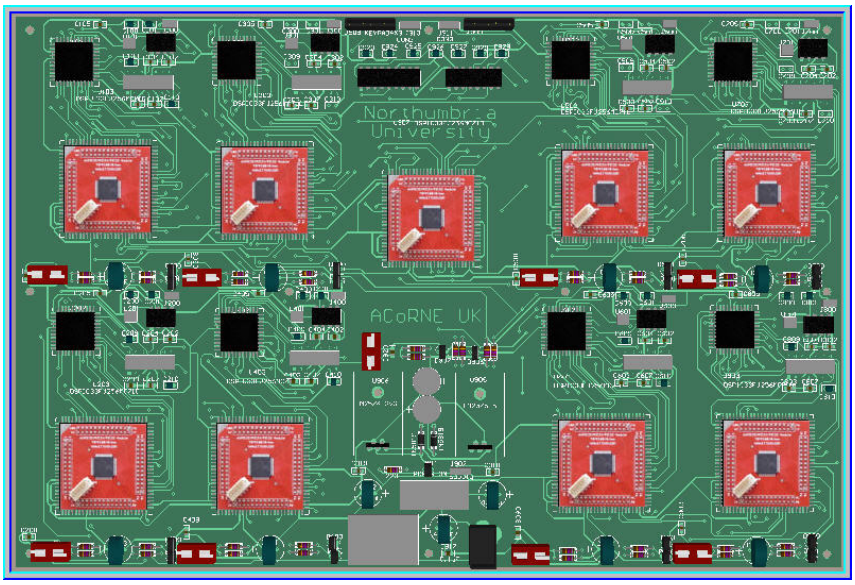

Figure 6.3 The 3D graphic design of dsPIC33F module.

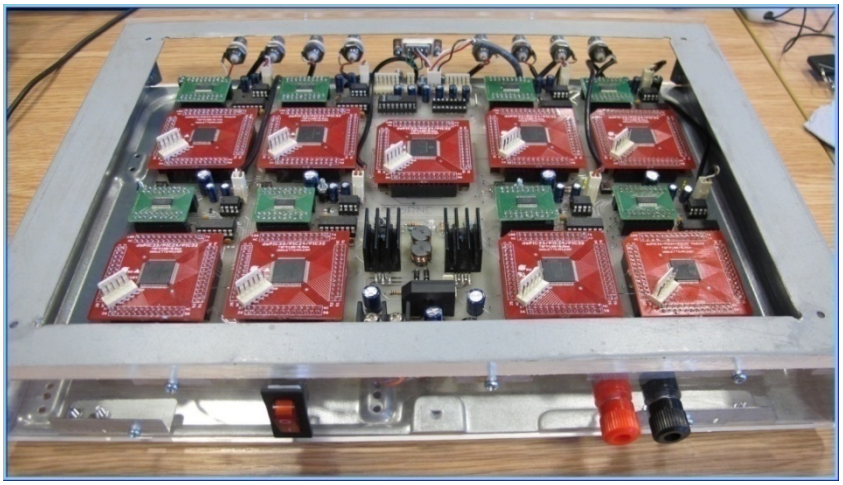

Figure 6.4 The dsPIC33F arbitrary waveform generation module.

CCS C compiler software is developed to control nine dsPIC33F digital signal controllers; one master and eight slaves. When the power switch is turned on, the program runs to mode selections which consist of three modes; sine wave, bipolar and orthogonal options. Next step, programme runs to a sub function that it is chosen. Time delays are calculated to trigger eight slaves starting sending digital data to DAC chips. For eight slaves, when triggering signals received, digital data is loaded from flash programme memory to data RAM. Finally, digital data is sent to DAC chips to convert digital signal to analogue signal. Flowchart diagram of dsPIC software is shown in Figure 6.5.

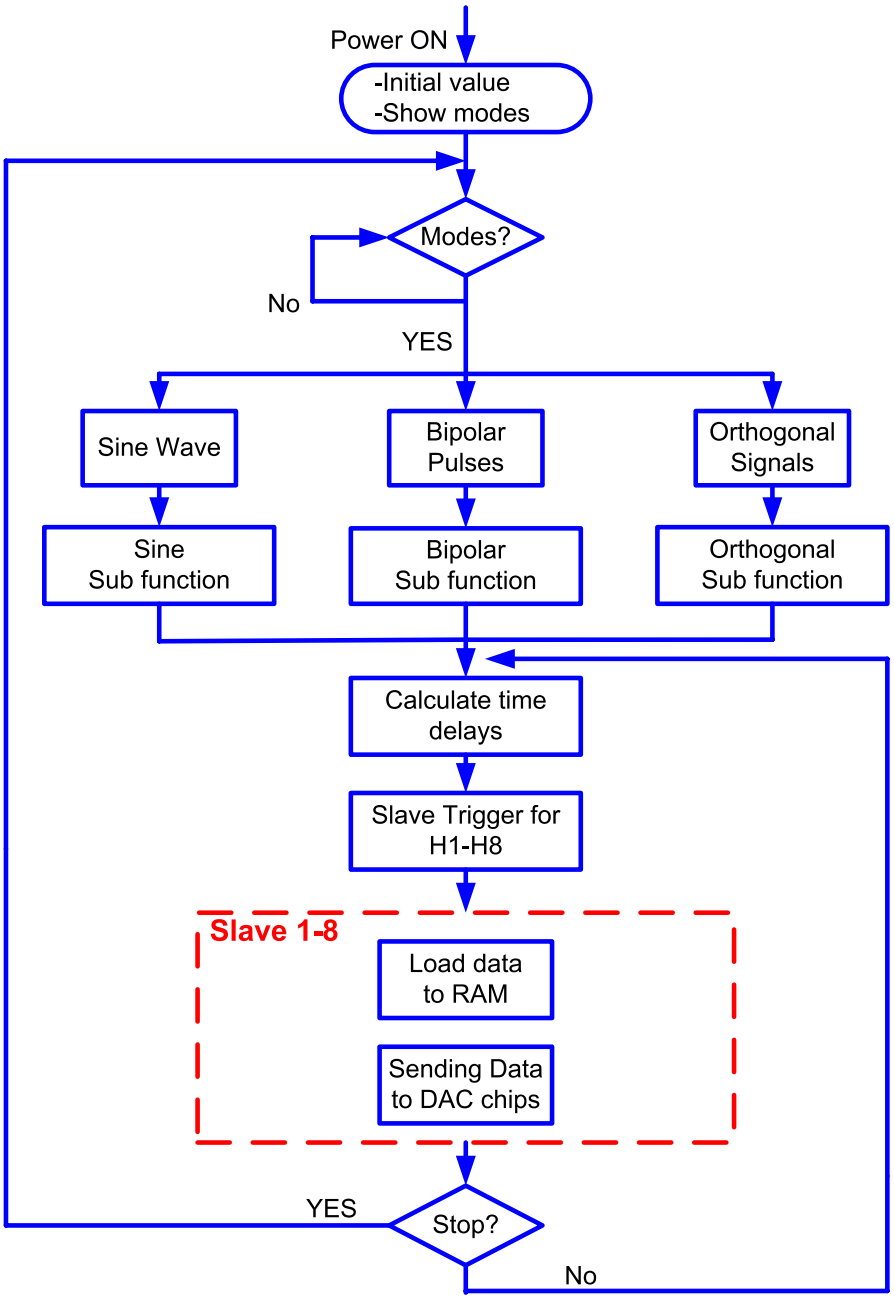

Figure 6.5 Flowchart of dsPIC software.

6.3 An hydrophone array calibration

6.3.1 Experiment at the laboratory

In the experiment, an acoustic underwater detection system comprises the eight-channel dsPIC arbitrary waveform generation module, an eight-channel PXI-6713 commercial high speed digital to analogue module, an eight-channel power amplifier module, eight TC4033 transmitter hydrophones from Reson, a B&K-8106 hydrophone receiver, a B&K-2690 conditioning amplifier and data acquisition modules (TDS2002B storage oscilloscope and NI PCI-6254 16-bit resolution commercial data acquisition). The block diagram of the acoustic underwater detection and the real system in the laboratory are illustrated in Figure 6.6 and Figure 6.7, respectively.

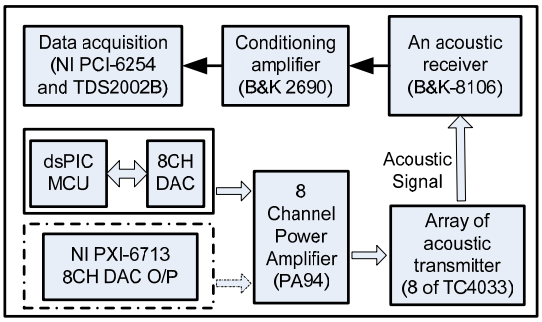

Figure 6.6 Block diagram of the underwater acoustic detection.

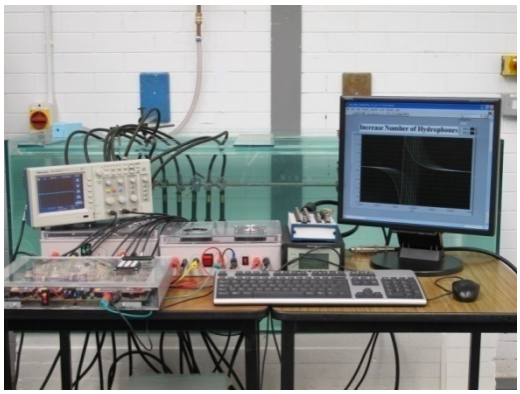

Figure 6.7 The acoustic underwater detection system.

A 60x150x60 cm water tank is used for experimentsin acoustic underwater detection at the Northumbria University laboratory. Due to the limited dimensions of the water tank, the hydrophone array is installed in the horizontal direction in order to test in the longest dimension. The dimension drawing of water tank and hydrophone installation are illustated in Figure 6.8 and Figure 6.9, respectively.

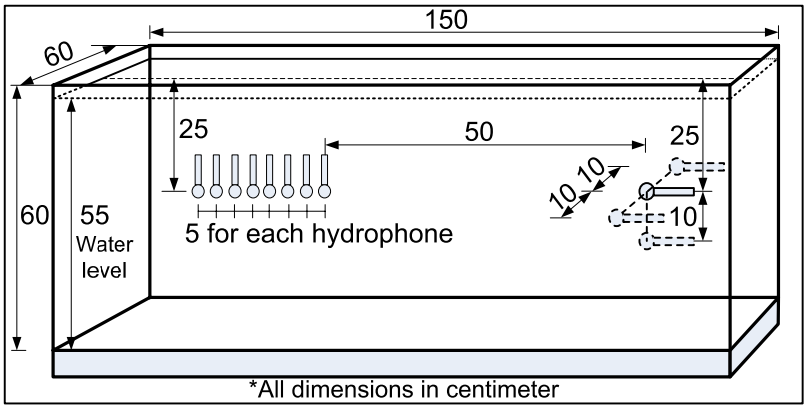

Figure 6.8 Drawing of water tank at the laboratory.

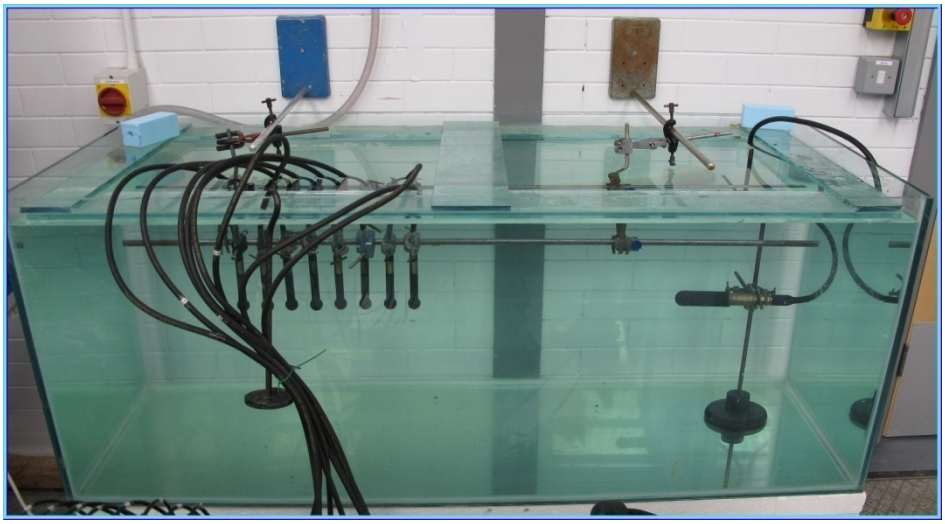

Figure 6.9 The installation of eight hydrophones in laboratory water tank.

6.3.2 Laboratory experiment result

The first experiment is the calibration of each hydrophone using the same driving pulse and distance. The signal output voltage from dsPIC and NI PXI-6713 are set to 4.1 V. The driving pulse is then amplified by the power amplifier with a gain of 17. The output signal from power amplifier is then about 70 V which is sufficient to drive the hydrophones in the laboratory and the field.

The testing for calibration of the hydrophone is started with the dsPIC module. Hydrophone number 1 (H1) is firstly tested and then H2 is also tested but using the same distance (50 cm between transmitter and receiver) with H1. The received bipolar signals from H1 to H8 are plotted in the Figure 6.10. The plot starts from the H1 signal in the left

hand side until the H8 signal in the right hand side. The hydrophones are extremely well matched.

The NI PXI-6713 is also used to validate the result with dsPIC module. The process of calibration is tested in the same way as the dsPIC module at the same distance. The result of received signals using PXI-6713 is plotted in Figure 6.11.

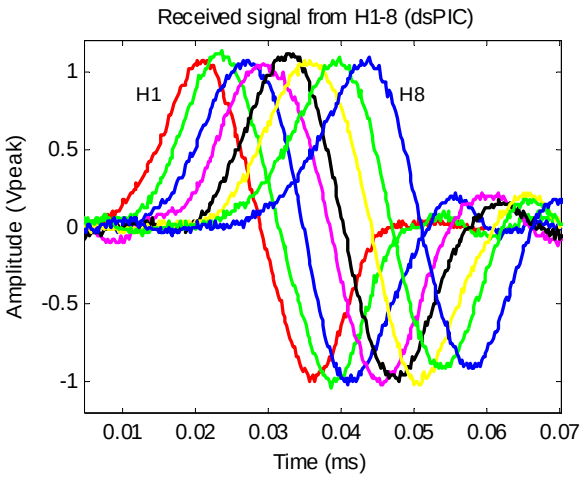

Figure 6.10 Received bipolar pulses from hydrophone 1-8 using dsPIC module.

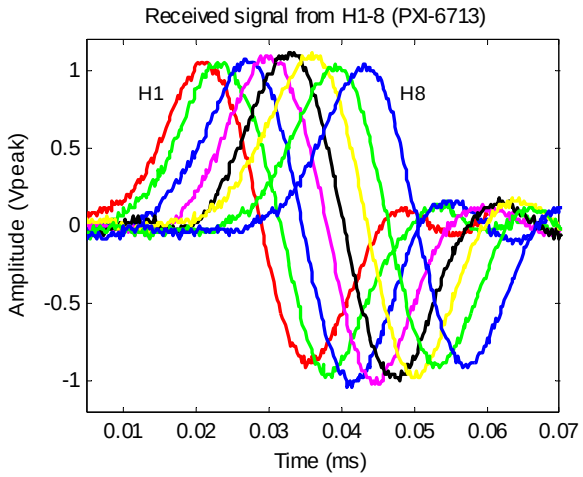

Figure 6.11 Received bipolar pulses from hydrophone 1-8 using PXI-6713 module.

The second experiment is the study of the hydrophone array operation, synchronisation between eight transmitter hydrophone in order to understand the direction and shape of the signals at the receiver. In this experiment, the receiver hydrophone is set at three positions. The first position is directly aligned to the centre of the hydrophone transmitters (0 degree of pancake direction). Another two positions are set in the left and bottom side with 10 cm from the centre point to examine off axis behaviour. The three positions of receiver hydrophone are illustrated in Figure 6.12.

The measurements start with setting the hydrophone receiver at the centre point. A bipolar signal is individually sent from hydrophone number 1 (H1) to hydrophone number 8 (H8) to establish the amplitude of the received signal for each hydrophone.

In the next step, signals from H1-H8 are simultaneously sent to the receiver. In this step, it is very important to set the delay time between each hydrophone transmitter to synchronize the pulses at the receiver. As the distance between hydrophones are 5 cm, and the velocity of sound in water approximately 1500 m/s, the delay time is set to 33.3 μs.

The measurements are repeated with the same procedure but the receiver is moved to the left and bottom points. The PXI-6713 is also tested with the same step to validate the result with dsPIC module. The result data from measurements is recorded in table 6.1.

The measurements show that the case of placing eight hydrophones at the centre position can achieve the highest value because it is the best synchronous position for eight signals when compared to the left and bottom positions. The result are displayed in table 6.1. If the hydrophones were truly omni-directional then the "Left" and "bottom" column should show identical values. The variations are however slight being of the order of a few percent.

Moreover, in the case of the individual sending hydrophone at the centre position, the results show the relation between the fall off in sound amplitude with distance. The relative pressure amplitude and relative distance of each hydrophone position on the experiment is compared with the theoretical model (Pressure α 1/r). The comparison of relation between pressure and distance of data from theory, dsPIC and PXI-6713 modules is plotted in Figure 6.13.

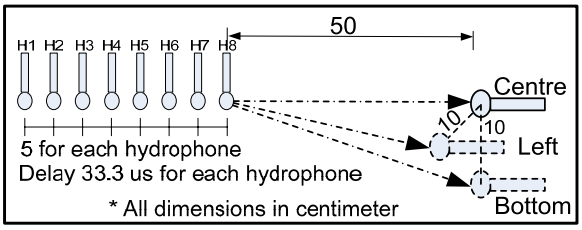

Figure 6.12 Three positions of received hydrophone.

Table 6.1 Comparison received bipolar pulses between PXI-6713 and dsPIC module.

Hydrophone	PXI-6713			dsPIC module		
	Centre	Left	Bottom	Centre	Left	Bottom
H1	1.54	1.46	1.56	1.68	1.54	1.58
H2	1.64	1.60	1.66	1.76	1.62	1.60
H3	1.84	1.76	1.74	1.86	1.74	1.72
H4	1.98	1.84	1.80	1.96	1.92	1.86
H5	2.30	2.06	2.08	2.30	2.04	2.10
H6	2.46	2.24	2.30	2.48	2.22	2.30
H7	2.56	2.28	2.36	2.58	2.30	2.32
H8	2.86	2.64	2.78	2.88	2.70	2.74
Calculation H1+...+H8	17.18	15.88	16.28	17.50	16.08	16.22
Measurement H1-H8	16.4	15.0	15.8	16.6	14.8	16.00
	*All units are in Vp-p					

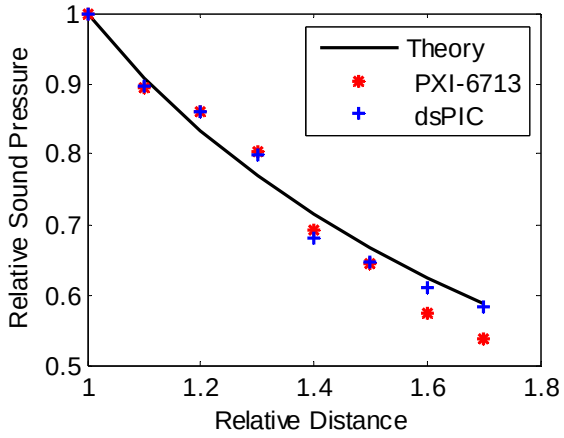

Figure 6.13 The relation between distance and pressure.

Figure 6.14 shows the received signal at the centre point by increasing the number of hydrophone transmitters from two hydrophones to eight hydrophones (lowest amplitude to highest amplitude). The graph shows that the received signal amplitude is determined by the addition of the received signal amplitudes of each hydrophone.

The comparison of received signal between dsPIC and PXI module for 8 hydrophones is plotted in Figure 6.15. The receiver is placed in the centre. The result shows that it is little different between the signal which came from the dsPIC and PXI modules.

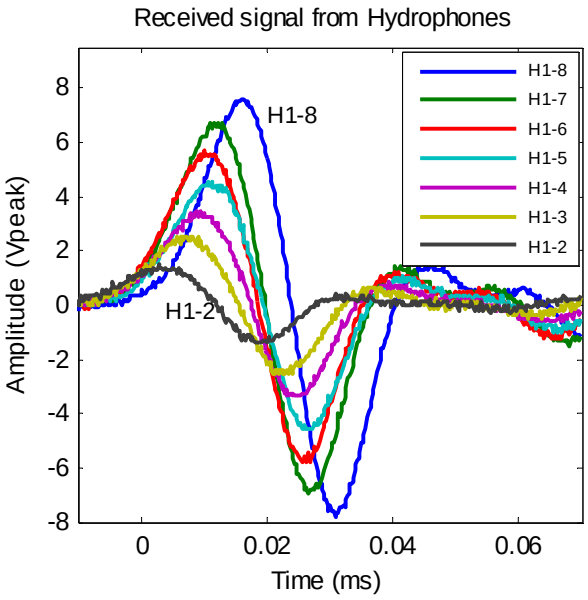

Figure 6.14 The received bipolar signal by increasing number of hydrophones.

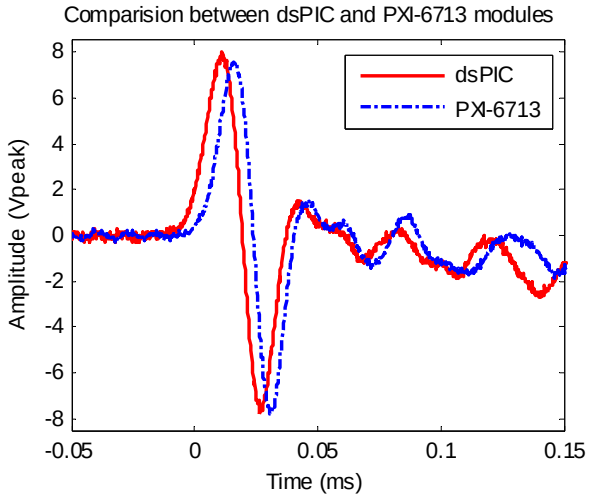

Figure 6.15 The comparison received signal between dsPIC and PXI module by 8 hydrophones.

6.4 Summary

The design and implementation of an eight-channel arbitrary signal generator module using the dsPIC33F digital signal controllers have fully been detailed. The eight-hydrophone array system has already been tested in the laboratory water tank using a dsPIC33F signal generation module. The NI PXI-6713 is used to confirm the operation of the dsPIC33F module that it is able to generate the bipolar pulses needed. The first experiment is mainly hydrophone calibration in order to know the characteristic and the frequency response for each hydrophone. Secondly, an eight-hydrophone array is tested for the operation in order to study the synchronisation of bipolar pulses from eight

hydrophones. Data from the experiments is plotted and shows that the dsPIC33F module can generate bipolar pulses fully as well as PXI-6713commercial module. In addition, synchronisation of the hydrophone array has been plotted in the table showing excellent results.

As mentioned in Chapter 1, the main contribution of this research is the design and implementation of an eight-channel hydrophone transmission array. The work has established excellent laboratory experimental results. The hydrophone transmission array has been deployed at the ANTARES site. The details of sea operation and data analysis are presented in the next chapter.

Chapter 7

The deployment and analysis at the ANTARES site

7.1 Introduction

The measurements using an acoustic array at the ANTARES site are the result of a joint project of the ACoRNE collaboration, which has the Northumbria University as a leading participant in this project, and the Erlangen Centre for Astroparticle Physics (ECAP), Erlangen-Nuremberg University, Germany. The deployment has been done during a sea campaign on the vessel Tethys II in 17th September 2011. The aim of this project is to test an array of eight hydrophones which emit bipolar acoustic signals into the sea water to mimic the neutrino interaction. More details of the sea campaign has been presented by [109]

7.2 An acoustic array construction

The construction of an acoustic array mechanical structure is designed and built by ECAP at the Erlangen-Nuremberg University laboratory. It is made by aluminium profile which is a strong material, easy to assemble and carry to appropriate sites, such as from Erlangen-Nuremberg, Germany to La Seyne, France. The array construction is designed as T shape. It consists of five two-metre long aluminium rods, four of them are used for holding hydrophones, the rest is used as a heading to hold the construction to the stern A-frame of the vessel. The distance for each hydrophone is set to one metre long. The acoustic array construction is shown in Figure7.1. More details of an array construction drawing has been presented in Appendix D.

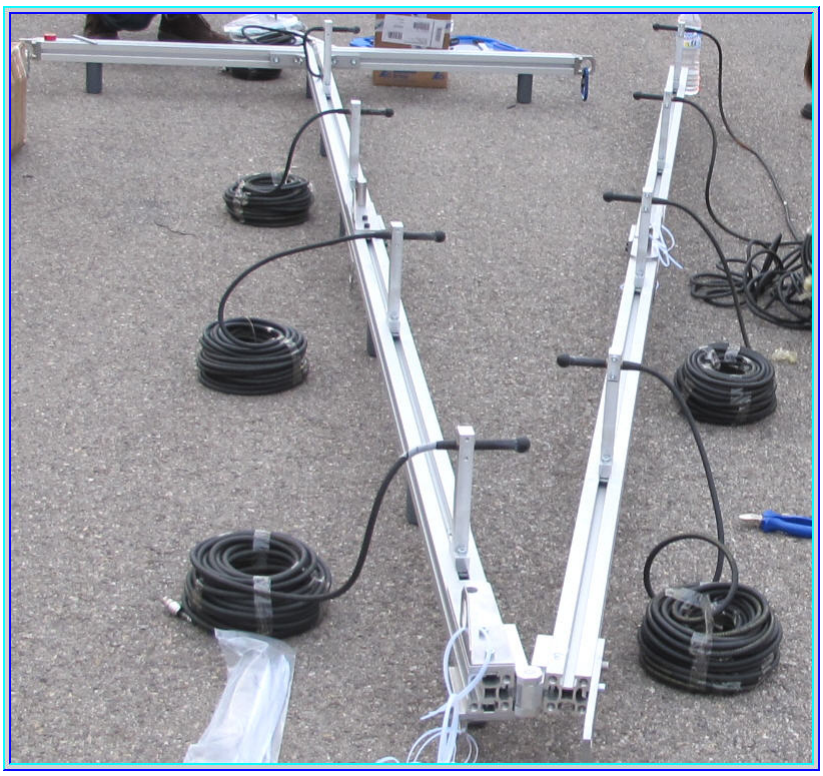

Figure 7.1 Construction of eight-hydrophone array.

7.3 On-site operation

The operation started early at the dock of the Ifremer site in La Seyne about 7:00 am (local time) on 17th September 2011. The five aluminium rods were assembled to two parts and connected together using a joint which can rotate to the same direction in order to keep it short as possible. This is an advantage when the array construction is carried to the vessel and suspended into seawater. In addition, the acoustic array construction had been pre-mounted in Erlangen to make sure that all parts fitted correctly together. The eight hydrophones were held at the positions which were one metre of distance for each of them. The twenty metre long hydrophone cables were attached to the aluminium rods using cable ties. The rest of the cables ending were tied together and prepared to connect to a power amplifier module. The acoustic array was lifted over the ship's side manually.

The ship took more than two hours from the coast to the site. The testing of the acoustic array was run between 21:00 and 22.00 (local time). Other research groups continued to perform at the mooring line until 3.00 (local time) in the morning. The ship anchored nearly La Seyne for the night and sailed back to the site at about 8:00 (local time). Unfortunately, the weather of the sea became seriously rough, and then measurements could not be continued. As a result, the decision was made by the captain to return the

vessel to the dock of the Ifremer site in La Seyne at about noon. Figure 7.2 shows the deployment as the ANTARES site.

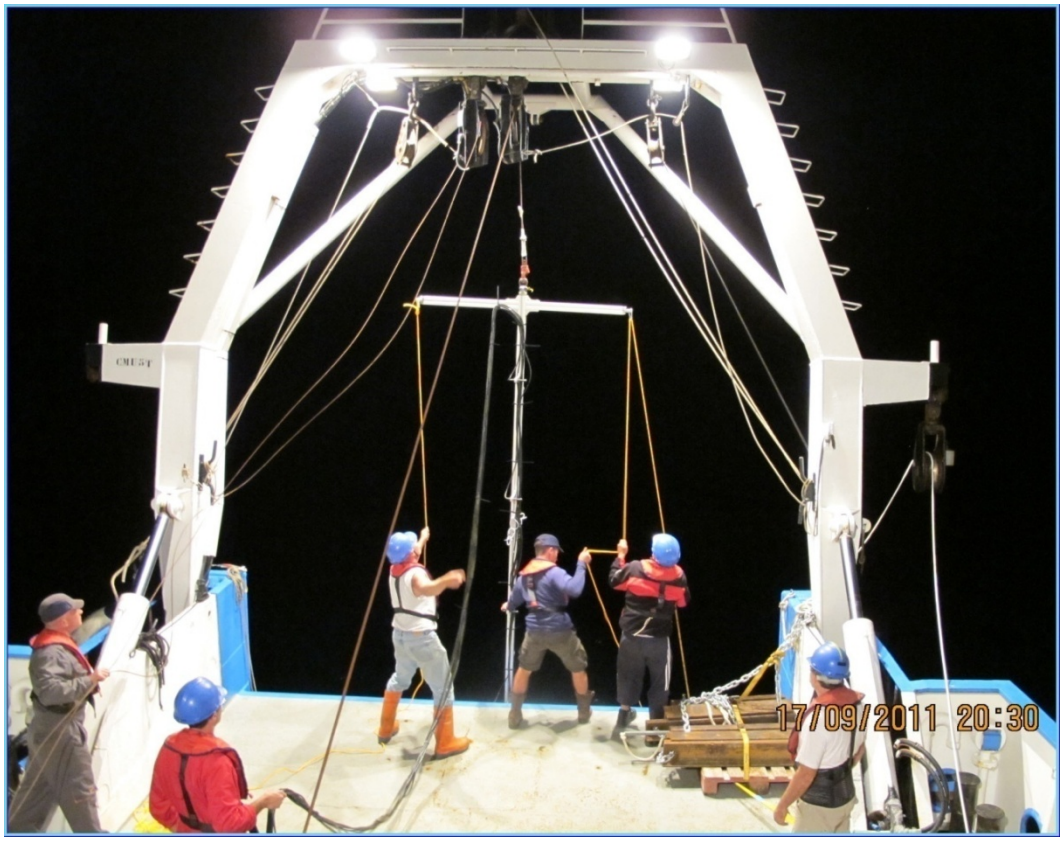

Figure 7.2 The deployment at the ANTARES site on 17th September 2011.

7.3.1 Signal emission

In this deployment, three types of signals are emitted with the hydrophone array.

- **Sine wave**

  The sine wave is useful for calibration and to verify attenuation, since in the worst case the bipolar signal is too weak to be detected. Three sine wave frequencies were chosen for the emission; 5 KHz, 10 KHz, 15 KHz.

- **Bipolar pulse**

  The 23 KHz bipolar signal is sent to study the expected neutrino interaction in sea water.

- **Pulse trains of "orthogonal signals"**

  The ten sets of orthogonal signals are sent to investigate the possibility of coding signals. More details of orthogonal signals have been discussed in the Chapter 5.

It might be difficult to position the hydrophones precisely enough along the array to calculate the exact time delay between the hydrophone emissions for constructive

interference. To solve this problem, the measurements are taken with several delays within a reasonable range.

The plan for the emission of the signals is to position the vessel at 1 nautical mile (1 NM = 1.15 miles or 1852 metres) from the AMADEUS sensor with a bearing such that the vessel drifts away from the detectors for safety reasons. In order to avoid the hydrophone array being obstructed by other materials, the vessel is aligned to move with the stern towards AMADEUS sensors. The drawing of the ANTARES detector position is plotted in Figure 7.3.

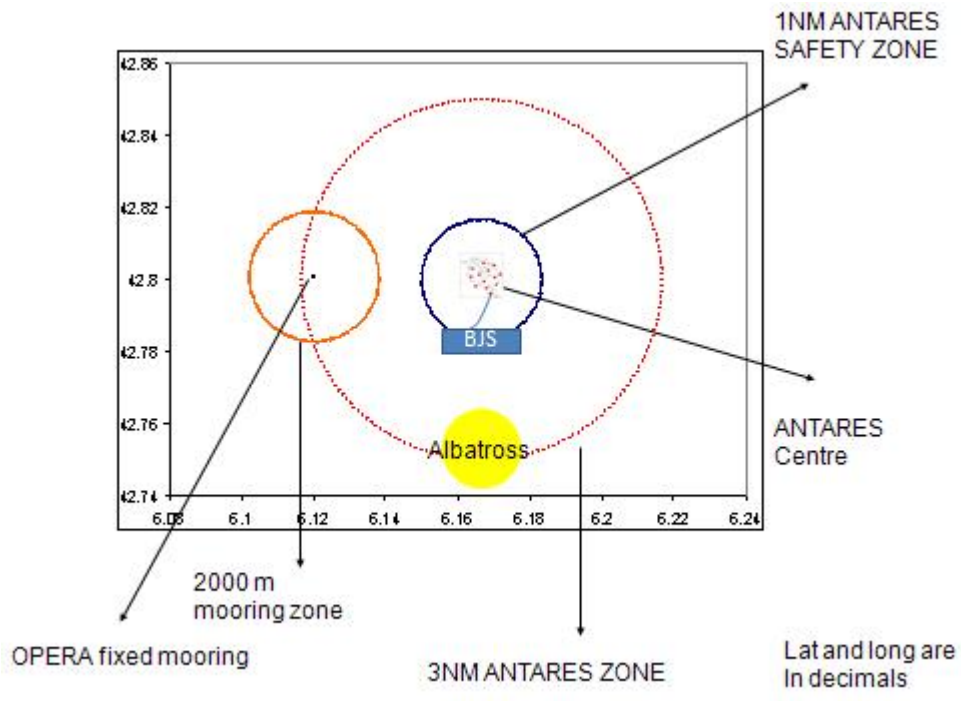

Figure 7.3 The map of the ANTARES detector site.

The signal direction is varied over a certain range by varying the delay times of the signal emission. The calculation of delay times is made by approximating the depth of the AMADEUS sensors on Line 12 of 2100 metres, and scanning the distance over the range from 1400-2200 metres with a step size of 20 metres. Hence, the delay times start from 555 μs at a distance of 1400 metres to 460 μs at a distance of 2200 metres. The planned position for deployment is shown in Figure 7.4.

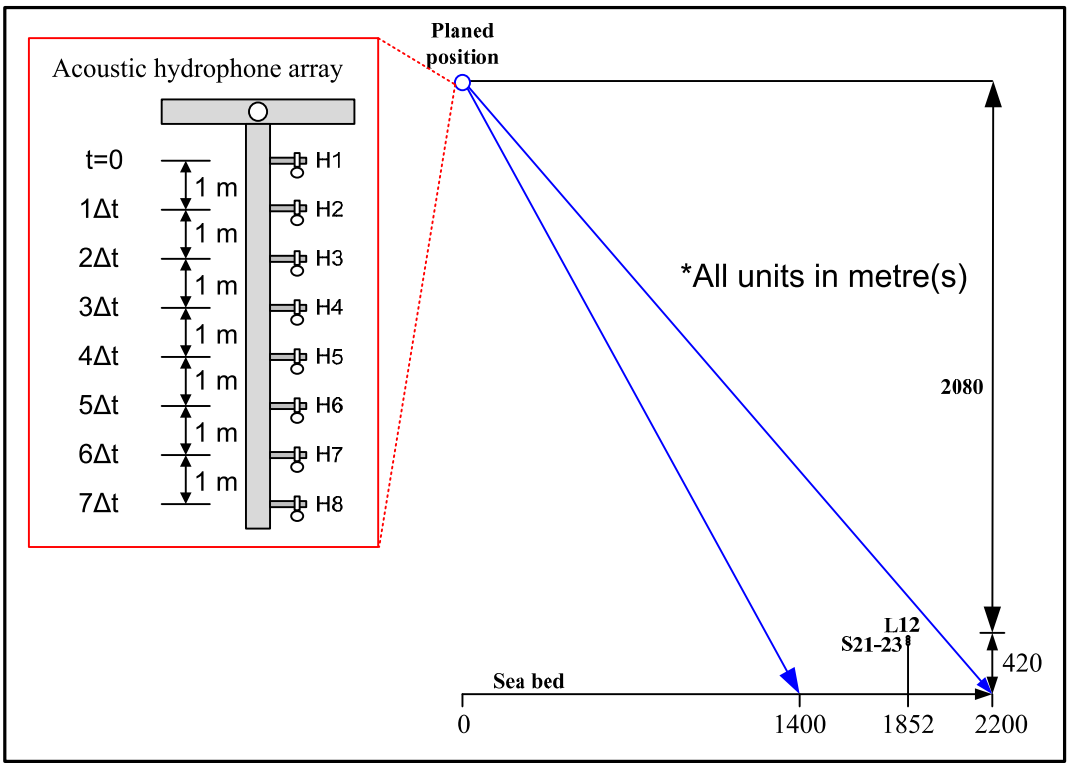

Figure 7.4 Planned position for the deployment.

Due to the limitation of time and the sea conditions, the emission of signals is shorter than intended. Firstly, the dsPIC33F module is used to generate signals as previously mentioned. 5, 10 and 15 kHz sine waves are firstly sent into seawater in order to measure the sea attenuation and it is very useful for the recognition of the signal emitted. The bipolar pulses are the second signal which followed the sine wave. Ten sets of orthogonal signal to investigate the possibility of coding signals are finally emitted by the dsPIC module. Secondly, the PCI-6713 commercial module is automatically set by LabVIEW software that repeats the same step as the dsPIC33F module had done. However, all of orthogonal signal sets are not injected into seawater due to the limitation of time and the weather condition. The UTC time, local time and step of sea operation in 17th September 2011 are shown in the table 7.1.

Table 7.1 Time table of sea operation on 17th September 2011.

UTC time	Local time	Operation
18:25	20:25	Arrive at the site; setup the construction of hydrophone array to stern A-frame
18:45	20:45	Sets up electronics and software
18:52	20:52	Stop running engine, ship drifts
19:00	21:00	Start measurement using dsPIC module: • 1 scan cycle for each of 5,10,15 kHz sine signal • 3 scan cycle for bipolar pulse • 1 scan cycle for each set of orthogonal signals (10 sets).
19:35	21:35	Start measurement using PCI-6713 module: • 3 scan cycle for 5 kHz sine signal. • 1 scan cycle for each of 10 and 15 kHz sine signal. • 3 scan cycle for bipolar pulse. • No orthogonal signal, due to the limitation of time and the sea condition became very rough.
20:00	22:00	Finishing measurement.

7.4 Data analysis

7.4.1 Vessel position analysis

First of all, the plan for the deployment is to start the ship position at 1NM from the ANTARES detector with a bearing point away from the sensor for the safety reason. It is planned to orient the ship with the stern toward ANTARES detector as this way the hydrophones point towards the sensors without obstructing objects.

Unfortunately, at the setting up time, the position of the ship actually is far away from the intended location. Hence the actual distance from the hydrophone array to the detector is too great approximately 1.285NM or 2.38 km. In addition, the ship is oriented with the bow towards the current, with the result that the bow is towards the ANTARES sensor. At the start point, the distance from the ship to the ANTARES detector is about 2.488km with

the bearing 142º. The vessel drifts with the bow towards the current until the finish of measurements. At the end, the ship is 2.859km from the sensor site with bearing of 139º. From 18:25:45 (UTC time) to 20:00:47 (UTC time), the vessel drifts far around 481 metres in 95 minutes with the direction of drift 315º (NW).

Due to the rough sea wave condition, it is estimated that the stern of the ship moved up and down about 2 metres during the experiment. As we know, the length of Tethys II is about 24.90 metres, then the angle of sine α is calculated from $sine \propto = \frac{2}{24.9}$, then $\propto \approx 4 - 5°$, assuming the vessel rotates around a point at half its length. It is not clear how the array, hanging from the stern A-frame with the top part about 2 metres below the surface, reacts to this movement. The position of Tethys II at the deployment time is shown in table 7.2. The comparison of vessel position from planned point, started point and ended pointed is drawn in Figure 7.5.

Table 7.2 The position of Tethys II at the operation time.

UTC time	Position Tethys II	Distance from ANTARES	Bearing of ANTARES
18:25:45	42.814504N, 6.146822E	2.38km	140º
19:00:45	42.815683N, 6.146703E	2.488km	142º
20:00:47	42.817544N, 6.142636E	2.859km	139º

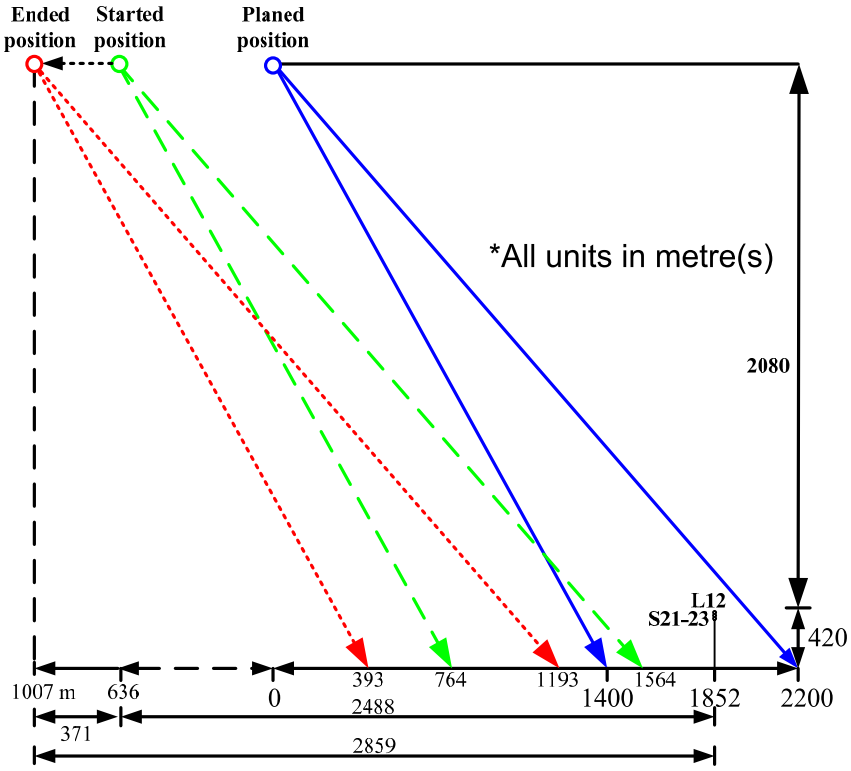

Figure 7.5 Comparison of vessel positions at the ANTARES site.

7.4.2 The simulation of expected sine signal

According to the deployment at the ANTARES site, unfortunately as we were well away from our planned position there is no hope of seeing bipolar pulses as the beam is way too narrow. There is some chance of detecting the sine signals emitted, as there are multiple peaks in the interference pattern at the receiver location.

The simulation of the sine signal emission into sea water at the ANTARES site is developed in MATLAB software using the same values as the sea operation at the ANTARES site. The first and most important parameter is the distance from the started point to the end point which has already been plotted in Figure 7.5. The scanning delay time is started from 461µs to 555 µs for the cycle scan of 1400-2200 metres. Hydrophone sensitivity for each frequency (5, 10 and 15 kHz) is also included to calculate the response of this signal. The transmitting sensitivity from the TC-4033 Reson hydrophone datasheet is 100, 106 and 110 dB re 1µPa/V @ 1m for the frequencies 5, 10 and 15 kHz respectively. The sea attenuation using the ACoRNE parameters which were already mentioned in Chapter 4 was also applied to this simulation.

The results from the simulation are illustrated in the Figure 7.6, 7.7 and 7.8 for frequencies of 5, 10 and 15 kHz respectively. It is found that 15 kHz signal has the highest amplitude at around 34 mPa at the receiver sensors, accordingly this analysis will focus on 15 kHz signal. The ambient noise amplitude at the ANTARES site has been stated in the reference [21]as being highly variable but the mean level is about 10 mPa in the frequency range from 10 to 50 kHz or 20 mPa for 1 to 50 kHz. This would give a RMS value of around 0.5mV or 1mV for the respective frequency range.

As the ambient noise level is about 10-20 mPa at the ANTARES sensors, so the sine wave signals at the frequencies 5 and 10 kHz are more difficult to detect than that at 15 kHz, as it has the highest amplitude of about 34mPa. However, this simulation is calculated on the basis that eight hydrophones have to be able to synchronise at 100% to get this amplitude. Hence if the synchronisation of eight hydrophones could not synchronise 100%, then the amplitude of the received signal might be lower than the simulated value.

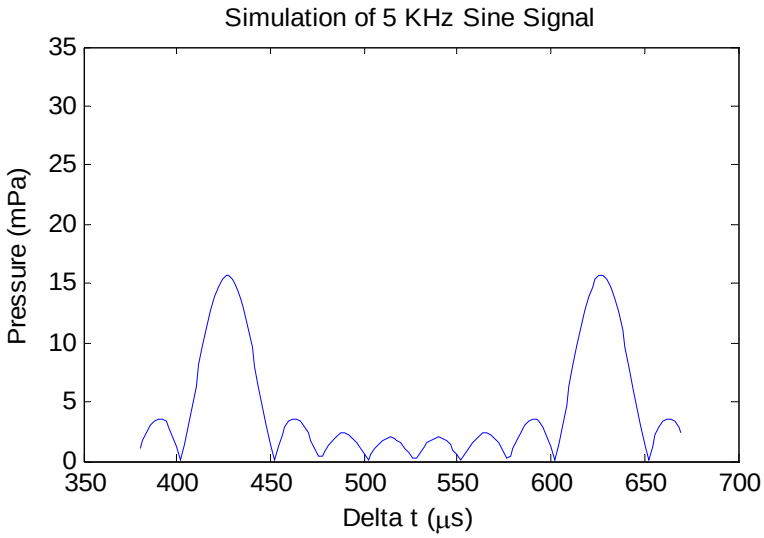

Figure 7.6 Simulation of 5 kHz expected sine signal at the received sensor.

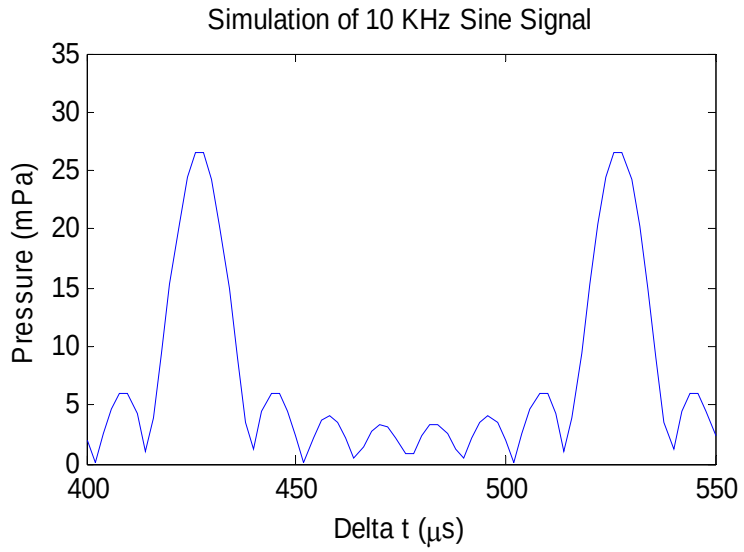

Figure 7.7 Simulation of 10 kHz expected sine signal at the received sensor.

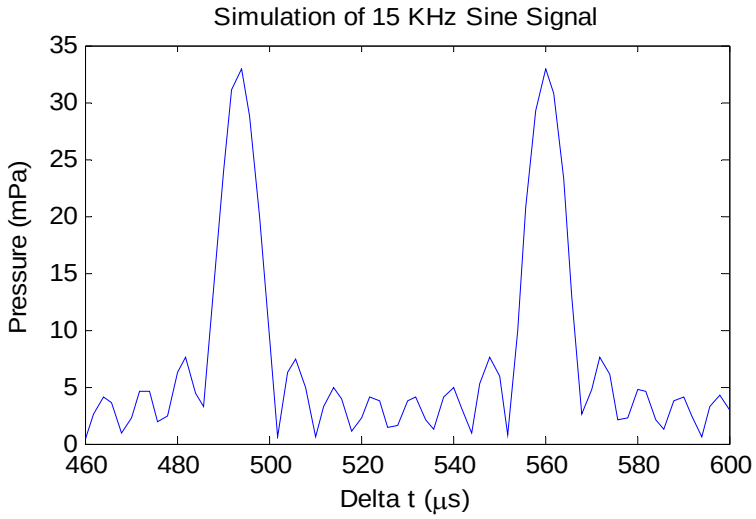

Figure 7.8 Simulation of 15 kHz expected sine signal at the received sensor.

7.4.3 ANTARES detector and data acquisition system.

Data is taken from 18 sensors on three storeys on line 12. On the line, the acoustic sensors are on storeys 21, 22 and 23 the positions at 390, 405 and 419 metres above sea floor respectively. The storey number 21 is untypical as it contains so-called acoustical modules that is quite difficult to handle the data. Six sensors are grouped for each storey, storey number 22 consists of sensor numbers 18 to 23, and the sensor numbers 30-35 are held on the storey number 23.

The sampling rate of the ANTARES DAQ system is 250kS/s, resulting in a large data record during the measurement time. All files for each sensor are separately cut to reduce the file size in order to make it convenient for saving and sending. The data files recorded during the time 19:00to 20:00 (UTC time) are chosen for data analysis. All data files are

separated into six groups, in each group consists of the data from the sensor number 18 to 23 and number 30 to 35 that recorded the data at the same time. All files are recorded in .bin format, for the average file size is about 600MB, then the average total file size for data analysis is around 6x12x600MB ≈ 43200MB or 43GB.

The first step of analysis is simply to look at the data plotted using MATLAB software as a main program. Unfortunately, data for each file is lost after minute average because of ANTARES DAQ recorded system. The examples of data from sensor number 18 are plotted in Figure 7.9 to Figure 7.12.

The author has contacted the ANTARES DAQ administrator to find out what was the cause of data lost. The answer has been confirmed from the administrator that the DAQ is not able to record the full data in real time as that would be over 20MB/s. Moreover, the DAQ system has an on-line matched filter, which accepts bipolar signals. This filter usually reduces the amount of data by a factor of 100. For this sea campaign, it lost the filter and wrote roughly half the data to disk. The ANTARES DAQ system is set up the data filtering based on time slices of 0.105 second, so the data in one time slice is either accepted if the filter conditions are met or discarded. In addition, roughly the first 10 seconds are written to disk for each run, so it could see holes in the data with lengths in multiples of 0.105 seconds. However, the applied filter is not 100% efficient, but it should be rather efficient for the signal shapes sent during this sea campaign.

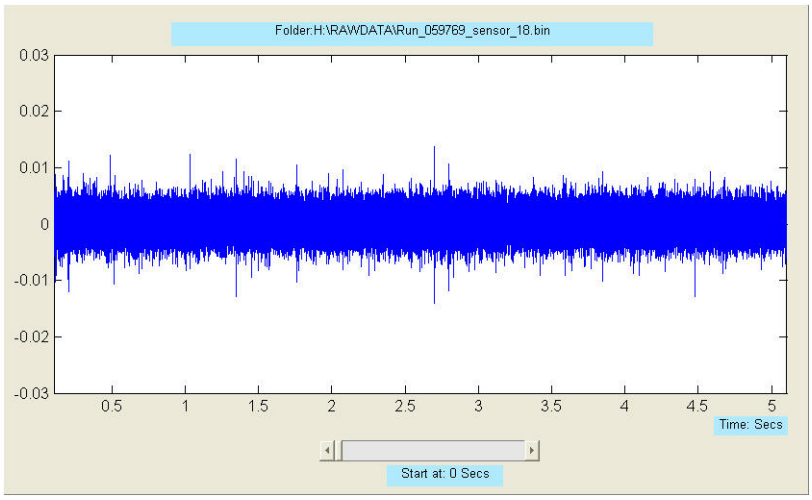

Figure 7.9 Sensor number 18 with the time from 0-5 seconds.

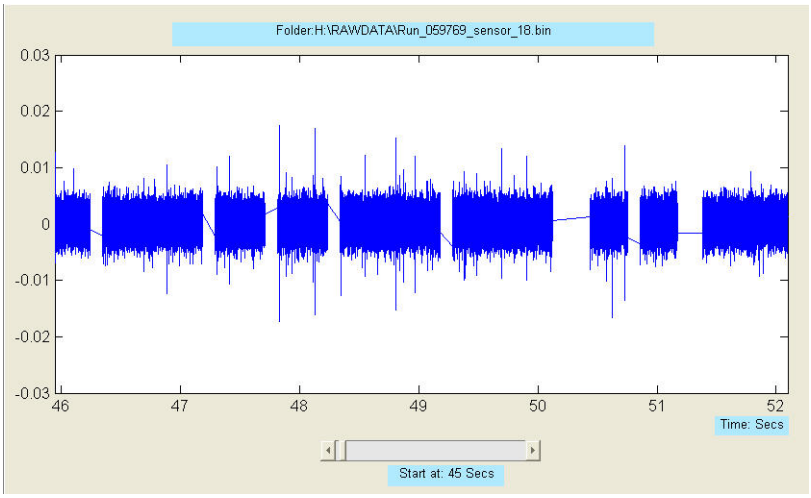

Figure 7.10 Sensor number 18 with the time between 46-52 seconds.

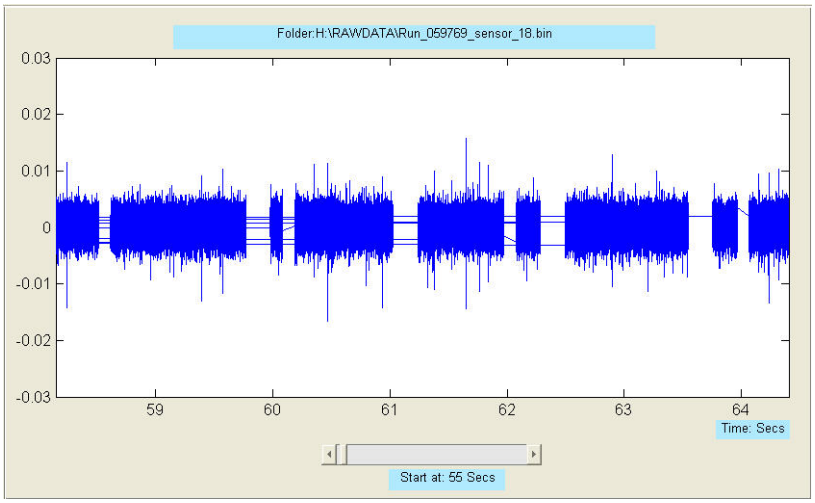

Figure 7.11 Sensor number 18 with the time between 58-64 seconds

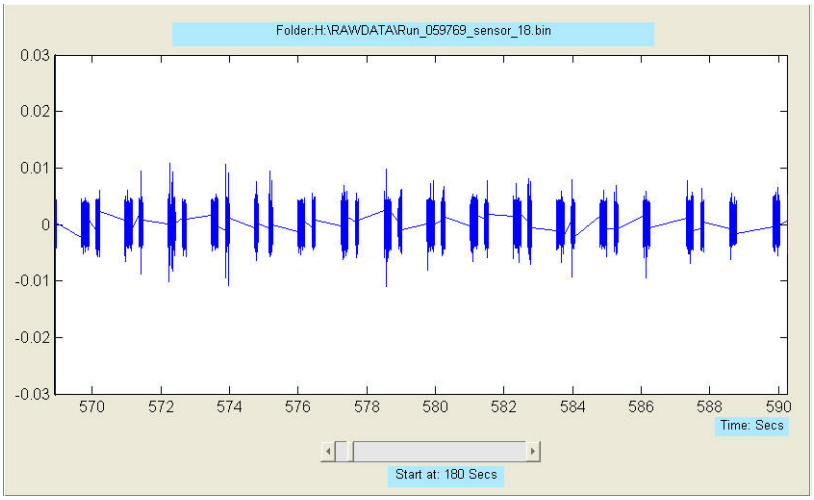

Figure 7.12 Sensor number 18 with the time between 570- 590 seconds.

7.4.4 Raw data analysis attempts

At this point, the data analysis has found limitations. The first is that the position of ship was far away from detectors, hence the amplitude of the signal received is very weak. Secondly, the recorded data is lost after one minute for each file, so it is quite difficult to recognise the signal. However, the data analysis is still needed to be continued although it is unlikely to see the signal emitted.

The main purpose of the next step is to establish the chance to see the sine signal within the recorded data. The simulated sine signal for the ANTARES site is used to add to the real recorded data that included noise and signal from the sea operation in order to know the possibility of sine signal detection. The simulated sine signal for the ANTARES site is plotted in Figure 7.13.

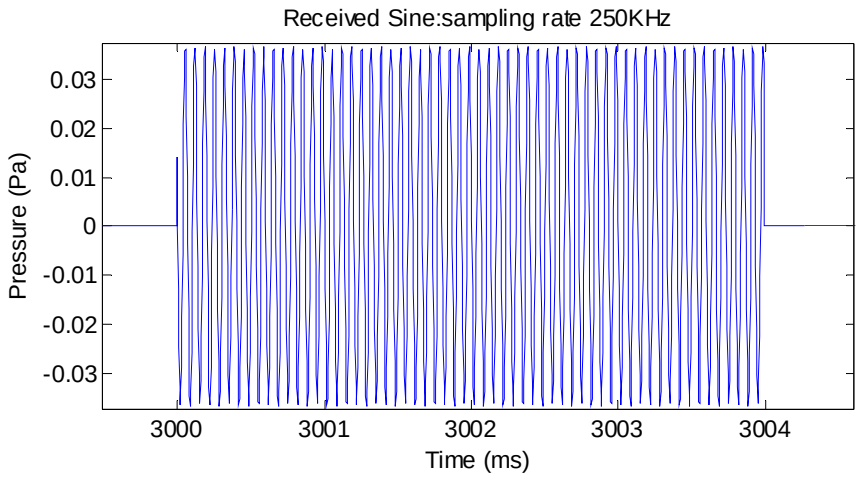

Figure 7.13 The simulation of sine signal received at the receiver.

According to the simulation of sine emitted into seawater at the ANTARES site in the previous section, it has confirmed that the 15 kHz is the highest pulse compared with 5 and 10 kHz sine signals. Then this section we will focus on the 15 kHz sine signal to find out the probability of detecting such signals emitted at the ANTARES site. The 15 kHz simulated sine signal with 1000 sample length is added to the real ANTARES data at the position 1000ms and 3000ms of time axis, as shown in the Figure 7.14.

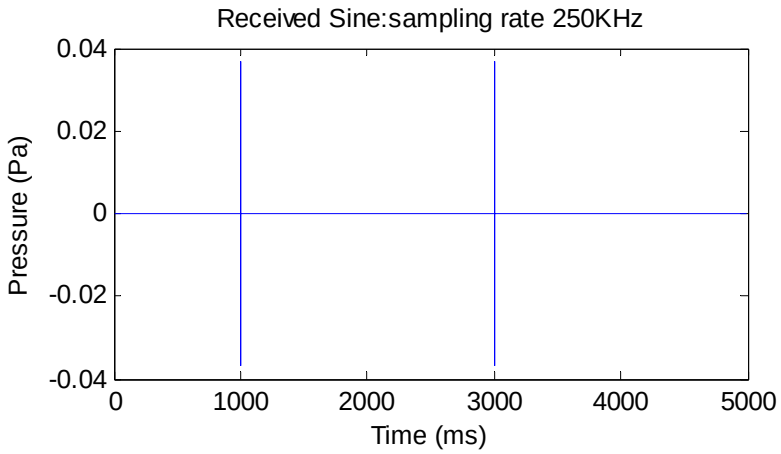

Figure 7.14 Adding sine signal at 1000ms and 3000ms time axis.

The recorded ANTARES data from file 'Run_059774_sensor_18.bin' is used in this calculation. The example of ANTARES data is plotted in Figure 7.15 (top). Two sets of 15 kHz simulated sine signal are added with ANTARES data and plotted in Figure 7.15 (middle).

The 3rd order Butterworth band pass filter [110] with low frequency cut off at 14 kHz and high frequency cut off at 16 kHz is applied to filter the other frequencies and noise background out. The advantage of a Butterworth filter is that it is maximally flat (has no ripples) in the pass-band, and rolls off towards zero in the stop-band. MATLAB software has provided the "*butter function*" to calculate the filter coefficients which are used with the *"filter function"* that has been provided by MATLAB software.

Then, the ANTARES data added with sine signal is filtered. The output band pass filter illustrated in Figure 7.15 (bottom).

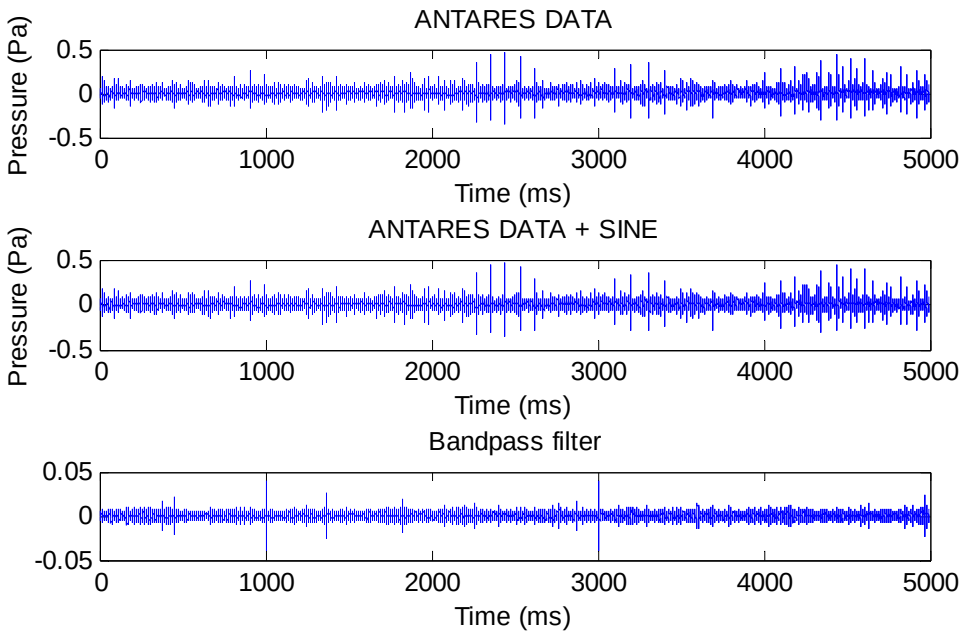

Figure 7.15 The plot of ANTARES data (top), ANTARES data add with sine (middle) and the output from band pass filter (bottom).

The next technique to optimise the signal to noise ratio is to use a matched filter which uses the correlation between two data sets. The first set is the known signals whilst the other is the signal set that needs to be compared. In this simulation, the simulated sine signal is the known signal that needs to be emitted into seawater and the output from the band pass filter is the signals that needs to be correlated.

The output from the band pass filter is applied to the match filter in order to find out the matched signal. The output from the match filter is plotted in Figure 7.16 (top).

The Hilbert transform is an operator to calculate the envelope of signals. It removes the oscillations and keeps the signal envelope which is very useful for the detection of signals in this study [111].

The final stage, the output from a match filter is calculated by use of the Hilbert transform. The output has shown exactly the positions of signals at the 1000ms and 3000ms time axis. The results are plotted in Figure 7.16 (bottom).

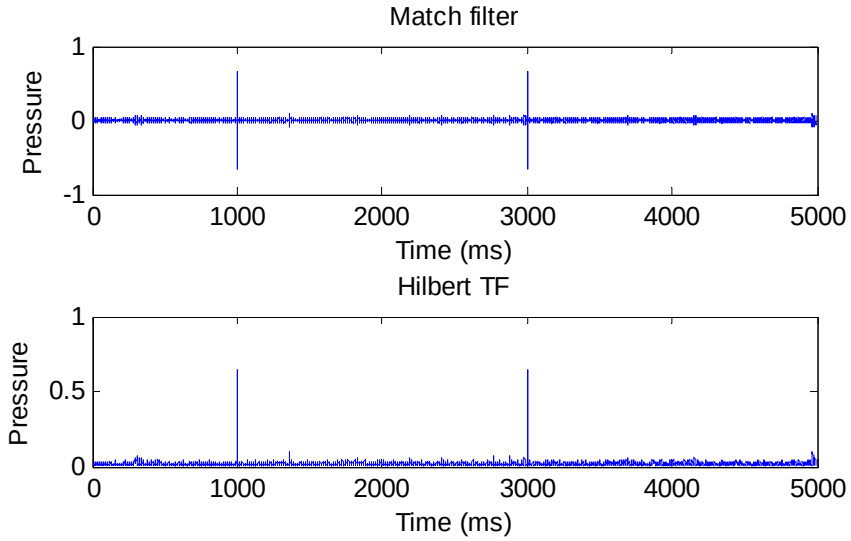

Figure 7.16 Output from match filter (top) and output from Hilbert transform (bottom).

The 15 kHz sine signal with the amplitude of about 34 mPa is used in the calculation and confirmed that signals can be detected at this level of amplitude. This simulation has changed the amplitude of 15 kHz sine signals in order to know how the minimum level of the sine signal amplitude that is detectable. The amplitude of sine signals decreases from 34 mPa to 10, and 5 mPa.

The results from simulation show that when the amplitude of sine signal reduces to 10 mPa, the sine signal can still be clearly detected. The output signal from the Hilbert transform for 15 kHz sine signal with the amplitude 10 mPa is plotted in Figure 7.17. However, for the sine signal with amplitude 5 mPa, the output from the Hilbert transform in the Figure 7.18, can be seen but the level of signal is nearly lost in the noise background, it is quite difficult to reliably detect the signals at this level.

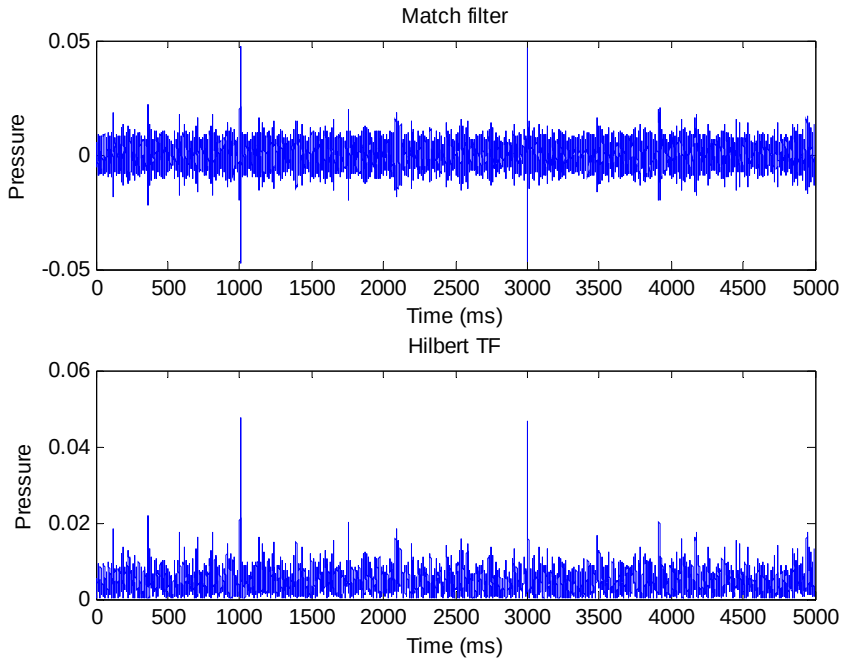

Figure 7.17 Signal outputs when 15 kHz sine signal amplitude is 10mPa.

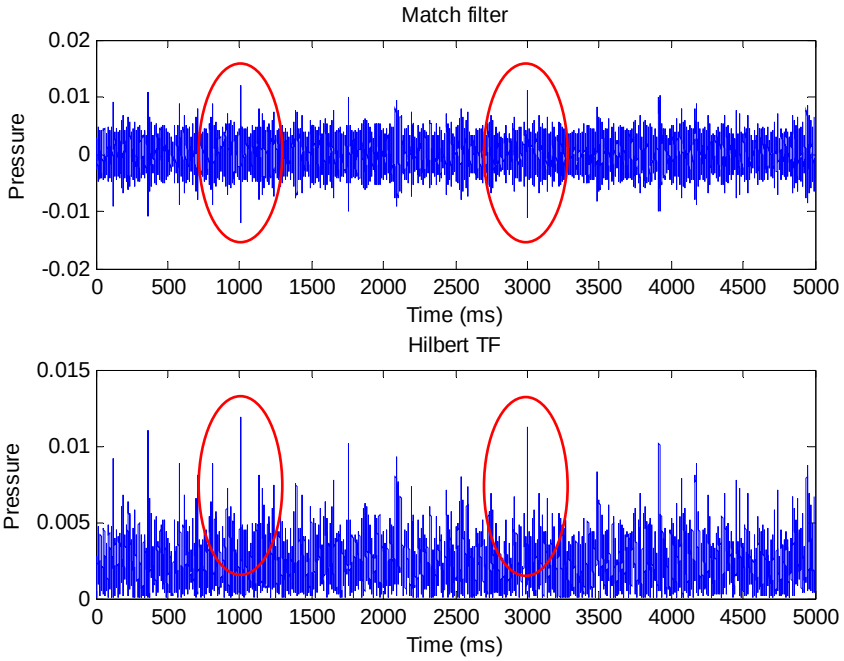

Figure 7.18 Signal outputs when 15 kHz sine signal amplitude is 5mPa.

The detection limits for sine signals was also been simulated for 5 and 10 kHz. 10 kHz sine signals with amplitude of 10 mPa are plotted in Figure 7.19. The outputs from the match filter and the Hilbert transform show that the signal can be clearly detected, however the noise background is still high but lower than signal emitted. When reducing the amplitude of 10 kHz sine signal to 5 mPa as shown in the Figure 7.20, the noise background around

the signals is higher than the signals at time. The detection at this level is more affected by noise.

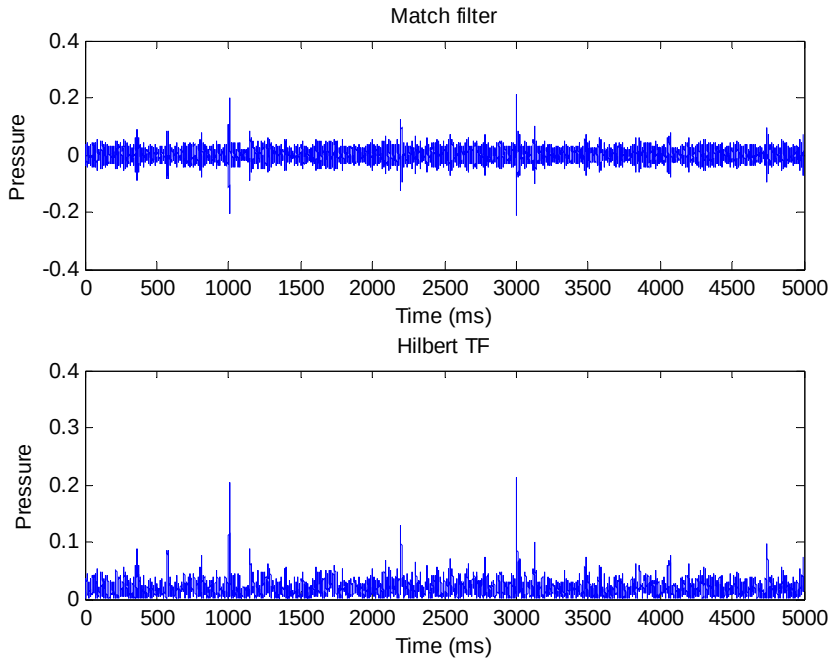

Figure 7.19 Signal outputs when 10 kHz sine signal amplitude is 10mPa.

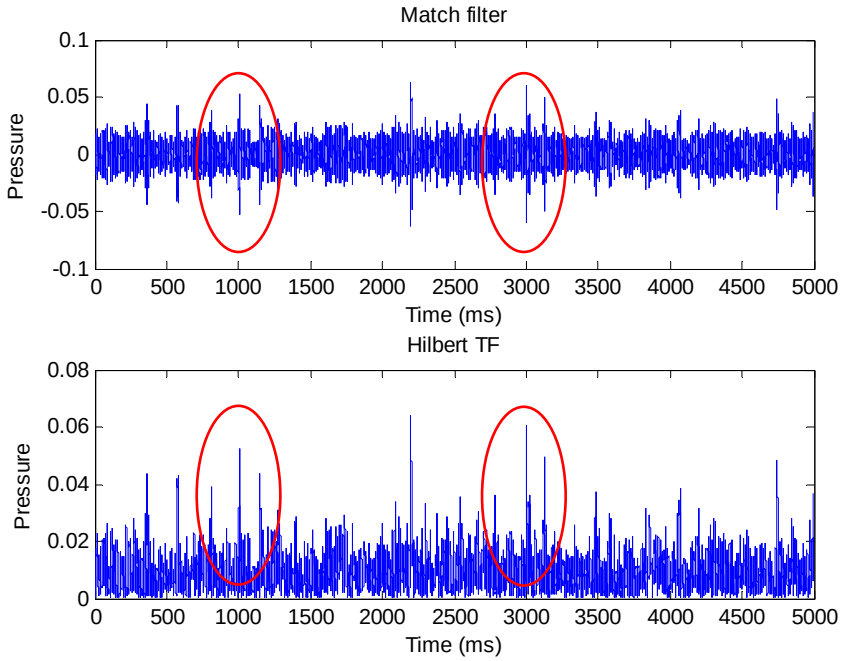

Figure 7.20 Signal outputs when 10 kHz sine signal amplitude is 5mPa.

Looking at the 5 kHz sine signal with amplitude of 15 mPa, the outputs from the match filter and Hilbert transform show that the simulation cannot detect the signals needed. At the lower frequency, the signal is much more affected by noise background. Figure 7.21

shows the output from simulation that the sine signals cannot be detected as they are affected by low frequency noise background, the possibility of detection for a 5 kHz sine signal is much more difficult than those of higher frequency.

To conclude, the 15 kHz sine signal is easiest to detect as it has the highest amplitude pulse and smallest noise background. The 10 kHz sine signal is possible to detect as well as the 15 kHz sine signal, although the amplitude is lower than for 15 kHz. However, the 5 kHz sine signal is unlikely to be detected as it is affected by the low frequency noise background.

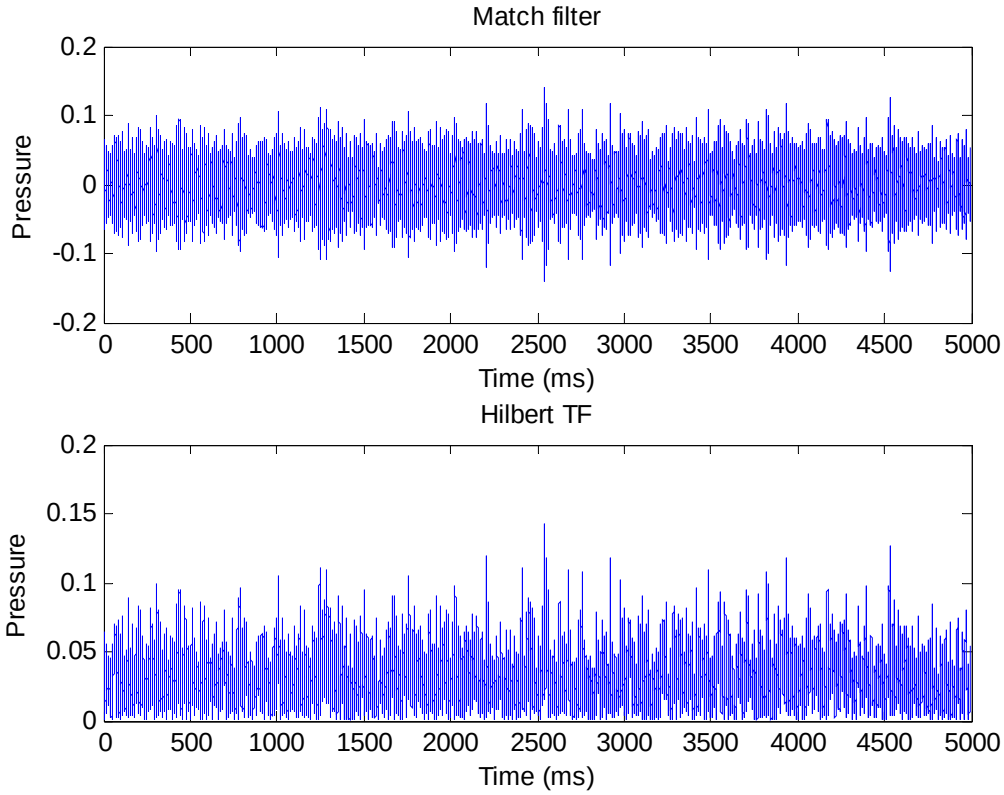

Figure 7.21 Signal outputs when 5 kHz sine signal amplitude is 15mPa.

The signal processing techniques as mentioned above have been applied to analyse the data from sea operation that shows on Table B.3 in Appendix B. All data files have been analysed, especially sine signals and artificial neutrino-induced pulses. That were recorded by sensor numbers 18-23 and sensor numbers 30-35. As a result of the vessel was far away from the planned point, the received signals are very weak. In additional, the ANTARES DAQ system could not record at the full data length, then all data files were lost after one minute length. Unfortunately, the sine waves and bipolar pulses could not be detected.

However, we have learned more experiences from this sea campaign and it would be very useful to develop the system for deployment in the next sea operation. The ACoRNE and ECAP collaboration have planned to improve a hydrophone array calibrator for neutrino detection, especially increasing the amplitude of signal emission. The new sea campaign will be on summer 2013 at the ANTARES site.

7.5 Summary

The sea campaign at the ANTRES site has been presented. The main purpose of this sea operation was to test a transmitter array of hydrophones that generates artificial neutrino-induced acoustic pulses in sea water. Work started with the design and implementation of an eight-metre array construction which was built at the ECAP collaboration, Erlangen University Germany. On site operation was fully detailed throughout the measuring time. Three types of signals were injected into sea water with varying the time delays. Each type of signal was scanned over the range from 1400-2200 metres to make sure it would be acquired by the detector.

5,10 and 15 kHz sine signals were firstly injected for testing the sea attenuation and were very useful for signal recognition. Then, bipolar signals and pulse trains of orthogonal signals were produced by the dsPIC module. The same types of signals were also sent by a NI commercial module in order to validate the results. Signal processing techniques were applied to recognise such types of signals. However, the signals received were very weak, as a result of the vessel being far away from the position planned. In addition, the ANTARES DAQ system could not record full real-time data and the recorded data files were lost after one minute length. As a result of these limitations, no signal could be detected. However, the deployed data is still very useful in order to study the noise background of sea water and much has been learned for future sea campaigns. The deployment and data analysis have been presented in [112].

Chapter 8

Conclusion and Future Work

8.1 Conclusion

The objective of this research was to design and implement an eight-hydrophone transmitter array which was used to generate acoustic bipolar signal into sea water in order to simulate the artificial UHE neutrino interaction in sea water. As Northumbria University is a member of the ACoRNE collaboration, this research had full support of our collaborators in order to investigate the acoustic detection of neutrinos.

To continue the work of the ACoRNE collaboration, the investigation of a single hydrophone calibration was firstly important to understand the sensor's response. Practically, the nature of the hydrophone itself could not produce output signal following a given driving input. Hence signal processing techniques were applied to hydrophone modelling in order to determine the hydrophone transfer function that could be able to produce the bipolar pulses needed.

The ACoRNE collaboration used the National Instruments commercial module as bipolar generating source which needed to operate via a laptop or desktop every time. It was inconvenient to deploy this system in the field as it required main power to support throughout an operational time. To solve this limitation, a bipolar acoustic generation module was built using 8-bit PIC microcontrollers for processing and control. This module was designed to run with 12 VDC making the system convenient to operate that can run directly from a 12 VDC battery. The module was very compact and easy to transport to the fields. In addition to the acoustic generation module an eight channel power amplifier module used for driving hydrophones was also designed and built. Eight PA-94 high voltage inverting operation amplifier chips with an adjustable gain were used in this module. The power amplifier module was powered by a 12 VDC to ± 100 VDC converter power supply module that was also built to support operation from a 12 VDC battery.

Calibration of a single hydrophone for generation of artificial Ultra High Energy (UHE) neutrino-induced pulses was carried out. Both 10 kHz and 23 kHz signals were used in this experiment. Signal processing techniques were applied to hydrophone modelling. A bipolar acoustic generator module was used for generating bipolar pulses and control. The NI USB-6211 commercial module from National instruments was used for comparison.

The modelling was compared to experimental data generated in a laboratory water tank at the Sheffield University workshop. The result from simulation and experiment were compared showing excellent agreement.

In September 2008, the ACoRNE collaborators were allowed to utilise a hydrophone array situated between the Scottish mainland and the island of Rona for the deployment. The NI module and LabVIEW software were developed for generation of acoustic bipolar pulses. A single ball hydrophone was used as a point source for injection of both 10 kHz and 23 kHz bipolar signals. The Rona seven-hydrophone array was used as a receiver. The raw data was directly recorded using a sampling rate of 140 kHz. From this data, signal processing techniques were applied to identify the pulses. A Butterworth high pass filter was used to filter low frequency components (<2.5kHz). A matched filter was also utilized for correlating signals. The GUI MATLAB software is used to analyse and plot these pulses. The result shows that the calibrator pulses can be detected and identified.

Prediction of the characteristics of the eight-hydrophone transmission array system for deployment at the ANTARES site has been developed using the ACoRNE collaboration computing method which uses the complex attenuation parameters in the sea water to simulate the array system. The linear hydrophone array simulation shows that eight hydrophones arranged over an eight metres spacing structure can mimic the anticipated pancake behaviour predicted from neutrino-induced showers as well as the acoustic bipolar pulse shape and amplitude at the ANTARES system.

In order to evaluate the actual behaviour of the acoustic neutrino detector in the field, an acoustic transmitter array is needed to send artificial acoustic neutrino-induced pulses through the sea. An eight-channel arbitrary waveform generator module was designed and built using 16-bit dsPIC microcontrollers. Signal Processing techniques were applied to calibrate the hydrophone transmitter array. The behaviour of an acoustic transducer array was examined in a laboratory water tank to study shape and direction of such a signal in water. The result was validated against the PXI-6713 commercial module.

Finally, the array system seven metres in length was deployed at the ANTARES site. 23 kHz bipolar pulses were sent into sea water to simulate a neutrino interaction. Other types of signal were also emitted. Signal processing techniques were applied to the data acquired in order to recognise the signals emitted. However, the vessel was far away from the intended position, and the signal received was thus very weak. In addition, the technical problem of the ANTARES DAQ system that it was not able to record the full

real-time data, so the recorded data files was partly lost after one minute. Due to these limitations, no signals could be detected. However, the deployed data is still very useful in order to study the noise background of sea water.

8.2 Future work

The main objective of this research was the design and implementation of an eight-hydrophone transmission array for the generation of acoustic bipolar signals that mimic neutrino interaction in sea water. Much work has been done with excellent results, both simulated and practical works, especially in the respect of hardware implementation and laboratory experiments. However, there is some further work that still needs to be done in the future in order to improve the efficiency of the hydrophone transmission array.

All electronic modules have been successfully implemented with full functions as needed. However, the size of modules is still large so all PCB design sizes need to be reduced. Electronic SMD devices are suitable in order to reduce dimensions and costs. In addition, compact electronic modules are very convenient to carry for testing in the field.

Laboratory experiments have been done using the laboratory water tank. But it would be better if the future work can operate in a larger structure such as a swimming pool that allows the direct signal from hydrophone to be measured for a longer period of time before reflected sound arrives.

Future practical work would involve a further sea campaign at the ANTARES site. As a result of the vessel being too far away from the planned position, signals received at the detector were very weak. As the transmitter is coherent the energy in the pancake is 8^2or 64 times greater than for a single hydrophone. The answer to this problem is, the vessel must be exactly placed at the position planned, however this is often difficult in practice.

As a result of swell, a vessel always moves up and down during the measurement, causing the transmit array to swing like a pendulum. An array construction should be designed to include tilt sensors to measure the angular movement of the hydrophones in order to synchronise the output signals from the eight hydrophones. A GPS module with a control loop to direct the signal to the correct location is needed to include in the data logger. Because the ANTARES site is very deep, and planned neutrino telescopes may well be even deeper (>4km if the Greek site is chosen for KM3NET) the hydrophone output signal needs to be higher by a factor of at least 5 and ideally 10. In addition, the array transmitter should be designed with a feedback receiver hydrophone on a vessel. It is very useful for checking the operation of signal generation module and signals from each hydrophone to make sure that they work properly.

Appendix A. Rona array position

The table A.1 shows the position of the hydrophone array at the Rona site which was uses as a test bed for ACoRNE collaboration. More detail about Rona site has been described in Chapter 2 and Chapter 4.

Table A.1 The coordinates of the Rona hydrophone array.

Hydro phone No.	Grid Position			WGS 84 Latitude	WGS 84 Longitude	Buoy Depth	Exten-sion	Cable length to shore
	x (m)	y (m)	z (m)					
H1	27.6204	655.0056	225	N 57° 33.9163′	W 05° 55.7129′	223	130	3469
H2	228.6494	619.9275	229	N 57° 33.9037′	W 05° 55.5097′	227	128	4300
H3	73.3558	388.8460	228	N 57° 33.7746′	W 05° 55.6517′	226	30	3855
H4	-3.9945	2.6211	227	N 57° 33.5645′	W 05° 55.7067′	225	130	4033
H5	-76.1565	-393.9459	219	N 57° 33.3490′	W 05° 55.7559′	217	130	4388
H6	-228.5946	-614.5854	217	N 57° 33.2256′	W 05° 55.8956′	215	130	4557
H7	-20.8801	-657.8689	222	N 57° 33.2088′	W 05° 55.6853′	220	130	5206

Table A.2 shows the routes of the signal injection at the Rona site. The latitude and longitude position was recorded from the commercial GPS on a boat with the time. The grid positions (x, y), which have a relation to grid position centre of hydrophone array in table A.1, are calculated from both latitude and longitude.

Table A.2 The routes of the signal injection at Rona site.

Step no.	Grid position		WGS 84 Latitude	WGS 84 Longitude	Time
	x (m)	y (m)			
1	-13.136	-98.199	N 57° 33.51′	W 5° 55.71′	13:15
2	116.84	247.6	N 57° 33.7′	W 5° 55.6′	13:31
3	173.86	541.84	N 57° 33.86′	W 5° 55.56′	13:38
4	19.286	30.096	N 57° 33.58′	W 5° 55.685′	13:54
5	75.924	231.37	N 57° 33.69′	W 5° 55.64′	14:02
6	137.54	432.36	N 57° 33.80′	W 5° 55.59′	14:10
7	268.56	796.7	N 57° 34.00′	W 5° 55.584′	14:22
8	373.22	1051	N 57° 34.14′	W 5° 55.39′	14:31
9	81.361	411.44	N 57° 33.787′	W 5° 55.645′	14:47
10	154.04	613.65	N 57° 33.898′	W 5° 55.584′	14:53
11	234.26	860.05	N 57° 33.033′	W 5° 55.518′	15:03

The table A.3 is illustrated the patterns of the signal injection at the Rona site, in 17th September 2008, which comprises types of signals, amplitude and the time of beginning.

Table A.3 Details of the signal injection.

Step no.	Tyne of signal	Amplitude (Volt)	Started time
1.	Sine wave (10 kHz)	30	13:21:38
2.	Bipolar (10 kHz)	10	13:22:25
		15	13:24:05
		20	13:25:45
		25	13:27:25
		30	13:29:05
3.	Sine wave (23 kHz)	30	13:30:45
4.	Bipolar (23 kHz)	10	13:31:25
		15	13:33:05
		20	13:34:45
		25	13:36:25
		30	13:38:05
5.	Sine wave (10 kHz)	30	13:53:27
6.	Bipolar (10 kHz)	10	13:54:10
		15	13:55:50
		20	13:57:30
		25	13:59:10
		30	14:00:50
7.	Sine wave (23 kHz)	30	14:02:30
8.	Bipolar (23 kHz)	10	14:03:10
		15	14:04:50
		20	14:06:30
		25	14:08:10
		30	14:09:50
9.	Sine wave (10 kHz)	30	14:12:49
10.	Bipolar (10 kHz)	10	14:13:32
		15	14:15:12
		20	14:16:52
		25	14:18:32
		30	14:20:12
11.	Sine wave (23 kHz)	30	14:21:52
12.	Bipolar (23 kHz)	10	14:22:32
		15	14:24:12
		20	14:25:52
		25	14:27:32
		30	14:29:12
13.	Sine wave (10 kHz)	30	14:47:36
14.	Bipolar (10 kHz)	10	14:48:23
		15	14:50:03
		20	14:51:43
		25	14:53:23
		30	14:55:03
15.	Sine wave (23 kHz)	30	14:56:43
16.	Bipolar (23 kHz)	10	14:57:23
		15	14:59:03
		20	15:00:43
		25	15:02:23
		30	15:04:03

Appendix B. ANTARES deployment position data

Table B.1 shows the position data for the vessel during the sea operation at the ANTARES site [109]. The data was recorded from a UPS logger. The column “index” refers to the data points of the UPS logger in the table. During the measurements, the vessel was drifting. At the end of the table, the speed (in km/h) picks up, at this point, the measurements were finished and the vessel sailed to the next destination.

Table B.1 Dates, times and positions of vessel during measurement at ANTARES site.

Index	UTC date	UTC time	Latitude	N/S	Longitude	E/W	Altitude	Speed	heading
105	09/17/11	18:45:45.00	42.815370	”N”	6.147464	”E”	46.12	0	329.19
106	09/17/11	18:46:45.00	42.815383	”N”	6.147454	”E”	45.99	1	274.2
107	09/17/11	18:47:45.00	42.815384	”N”	6.147441	”E”	45.91	0	318.64
108	09/17/11	18:48:45.00	42.815432	”N”	6.147383	”E”	47.46	0	302.37
109	09/17/11	18:49:45.00	42.815454	”N”	6.147337	”E”	46.36	0	296.8
110	09/17/11	18:50:45.00	42.815507	”N”	6.147193	”E”	48.77	0	293.36
111	09/17/11	18:51:45.00	42.815514	”N”	6.147171	”E”	46.47	0	299.6
112	09/17/11	18:52:45.00	42.815529	”N”	6.147136	”E”	46.19	0	309.67
113	09/17/11	18:53:45.00	42.815543	”N”	6.147113	”E”	45.98	0	293.93
114	09/17/11	18:54:45.00	42.815551	”N”	6.147089	”E”	46.5	0	304
115	09/17/11	18:55:45.00	42.815579	”N”	6.147032	”E”	⌟ 4.6	0	309.4
116	09/17/11	18:56:45.00	42.815607	”N”	6.146984	”E”	45.6	0	299.6
117	09/17/11	18:57:45.00	42.815622	”N”	6.146949	”E”	45.31	0	282.86
118	09/17/11	18:58:45.00	42.815633	”N”	6.146887	”E”	47.01	0	257.85
119	09/17/11	18:59:45.00	42.815628	”N”	6.146860	”E”	48.99	0	295.25
120	09/17/11	19:00:45.00	42.815683	”N”	6.146703	”E”	51.32	0	296.39
121	09/17/11	19:01:47.00	42.815940	”N”	6.145997	”E”	32.27	8	106.26
122	09/17/11	19:02:47.00	42.815830	”N”	6.146508	”E”	39.5	0	338.25
123	09/17/11	19:03:47.00	42.815870	”N”	6.146487	”E”	40.6	0	347.51
124	09/17/11	19:04:47.00	42.815910	”N”	6.146474	”E”	44.6	0	241.21
125	09/17/11	19:05:47.00	42.815845	”N”	6.146313	”E”	52.41	0	322.6
126	09/17/11	19:06:47.00	42.815865	”N”	6.146292	”E”	50.06	0	274.2
127	09/17/11	19:07:47.00	42.815865	”N”	6.146280	”E”	49.98	0	260.16
128	09/17/11	19:08:47.00	42.815856	”N”	6.146207	”E”	48.15	0	293.93
129	09/17/11	19:09:47.00	42.815864	”N”	6.146183	”E”	48.68	0	327.24
130	09/17/11	19:10:47.00	42.815878	”N”	6.146171	”E”	49.96	0	283.73
131	09/17/11	19:11:47.00	42.815906	”N”	6.146013	”E”	50.97	0	4.33
132	09/17/11	19:12:47.00	42.815919	”N”	6.146014	”E”	50.92	0	328.19
133	09/17/11	19:13:47.00	42.815946	”N”	6.145991	”E”	52.08	0	309.37
134	09/17/11	19:14:47.00	42.816010	”N”	6.145884	”E”	54.67	0	305.48
135	09/17/11	19:15:47.00	42.816087	”N”	6.145738	”E”	48.44	0	297.32
136	09/17/11	19:16:47.00	42.816109	”N”	6.145680	”E”	47.27	0	315.36
137	09/17/11	19:17:47.00	42.816149	”N”	6.145626	”E”	43.91	0	325.52
138	09/17/11	19:18:47.00	42.816164	”N”	6.145612	”E”	46.6	0	257.92
139	09/17/11	19:19:47.00	42.816153	”N”	6.145543	”E”	40.54	0	314.45
140	09/17/11	19:20:47.00	42.816195	”N”	6.145485	”E”	41.41	0	309.26

Table B.1 Dates, times and positions of vessel during measurement at ANTARES site (Continued).

Index	UTC date	UTC time	Latitude	N/S	Longitude	E/W	Altitude	Speed	heading
141	09/17/11	19:21:47.00	42.816259	”N”	6.145377	”E”	45.41	0	315.71
142	09/17/11	19:22:47.00	42.816294	”N”	6.145331	”E”	45.68	0	288.16
143	09/17/11	19:23:47.00	42.816303	”N”	6.145293	”E”	47.53	0	320.67
144	09/17/11	19:24:47.00	42.816344	”N”	6.145247	”E”	48.48	0	309.4
145	09/17/11	19:25:47.00	42.816373	”N”	6.145200	”E”	49.47	0	320.67
146	09/17/11	19:26:47.00	42.816393	”N”	6.145177	”E”	49.95	0	309
147	09/17/11	19:27:47.00	42.816496	”N”	6.145004	”E”	61.18	0	337.19
148	09/17/11	19:28:47.00	42.816548	”N”	6.144974	”E”	59.34	0	315.33
149	09/17/11	19:29:47.00	42.816583	”N”	6.144927	”E”	61.01	0	303.88
150	09/17/11	19:30:47.00	42.816612	”N”	6.144868	”E”	60.52	0	329.88
151	09/17/11	19:31:47.00	42.816652	”N”	6.144837	”E”	58.73	0	318.97
152	09/17/11	19:32:47.00	42.816699	”N”	6.144780	”E”	58.86	0	320.67
153	09/17/11	19:33:47.00	42.816720	”N”	6.144757	”E”	59.34	2	311.87
154	09/17/11	19:34:47.00	42.817118	”N”	6.144152	”E”	39.57	12	358.34
155	09/17/11	19:35:47.00	42.817161	”N”	6.144150	”E”	32.98	0	162.15
156	09/17/11	19:36:47.00	42.817063	”N”	6.144193	”E”	54.98	0	318.93
157	09/17/11	19:37:47.00	42.817090	”N”	6.144162	”E”	51.83	0	287.33
158	09/17/11	19:38:47.00	42.817098	”N”	6.144127	”E”	50.86	0	343.31
159	09/17/11	19:39:47.00	42.817124	”N”	6.144116	”E”	52.09	0	287.33
160	09/17/11	19:40:47.00	42.817132	”N”	6.144081	”E”	51.13	0	293.92
161	09/17/11	19:41:47.00	42.817148	”N”	6.144032	”E”	52.17	0	8.97
162	09/17/11	19:42:47.00	42.817154	”N”	6.144033	”E”	51.44	1	309.67
163	09/17/11	19:43:47.00	42.817168	”N”	6.144010	”E”	51.24	0	296.31
164	09/17/11	19:44:47.00	42.817227	”N”	6.143848	”E”	47.12	0	291.1
165	09/17/11	19:45:47.00	42.817250	”N”	6.143766	”E”	45.79	0	274.67
166	09/17/11	19:46:47.00	42.817255	”N”	6.143691	”E”	46.73	0	275.23
167	09/17/11	19:47:47.00	42.817262	”N”	6.143590	”E”	50.33	0	289.89
168	09/17/11	19:48:47.00	42.817277	”N”	6.143532	”E”	48.48	0	285.69
169	09/17/11	19:49:47.00	42.817294	”N”	6.143448	”E”	47.88	0	267.18
170	09/17/11	19:50:47.00	42.817292	”N”	6.143385	”E”	49.62	0	317.2
171	09/17/11	19:51:47.00	42.817320	”N”	6.143350	”E”	50.7	0	282.49
172	09/17/11	19:52:47.00	42.817330	”N”	6.143289	”E”	50.99	0	299.6
173	09/17/11	19:53:47.00	42.817344	”N”	6.143254	”E”	50.7	1	297.28
174	09/17/11	19:54:47.00	42.817387	”N”	6.143141	”E”	44.13	2	291.92
175	09/17/11	19:55:47.00	42.817451	”N”	6.142922	”E”	48.16	0	278.85
176	09/17/11	19:56:47.00	42.817464	”N”	6.142813	”E”	48.13	0	316.51
177	09/17/11	19:57:47.00	42.817498	”N”	6.142770	”E”	45.58	0	297.32
178	09/17/11	19:58:47.00	42.817520	”N”	6.142711	”E”	44.41	0	288.15
179	09/17/11	19:59:47.00	42.817529	”N”	6.142674	”E”	46.26	0	299.52
180	09/17/11	20:00:47.00	42.817544	”N”	6.142636	”E”	48.79	0	296.39
181	09/17/11	20:01:47.00	42.817606	”N”	6.142467	”E”	51.72	0	287.1
182	09/17/11	20:02:47.00	42.817621	”N”	6.142398	”E”	48.38	0	284.49
183	09/17/11	20:03:47.00	42.817631	”N”	6.142349	”E”	48.75	0	255.75
184	09/17/11	20:04:47.00	42.817626	”N”	6.142324	”E”	49.32	0	293.66
185	09/17/11	20:05:47.00	42.817641	”N”	6.142278	”E”	47.55	0	310.6
186	09/17/11	20:06:47.00	42.818235	”N”	6.141332	”E”	43.93	16	215.17
187	09/17/11	20:07:47.00	42.816205	”N”	6.139382	”E”	46.04	19	204.4
188	09/17/11	20:08:47.00	42.813477	”N”	6.137695	”E”	48.01	18	218.09
189	09/17/11	20:09:47.00	42.811188	”N”	6.135249	”E”	53.21	20	228.38
190	09/17/11	20:10:47.00	42.809096	”N”	6.132040	”E”	42.15	21	230.48

The table B.2 shows the GPS data out from the computer screen in the cabin of vessel (Tethys II). The "compass" reading shows the heading of the vessel.

Table B.2 Dates, times, positions and direction of vessel during deployment at ANTARES site.

Index	UTC date	UTC time	Latitude	Longitude	Compass
1	09/17/11	19:02:42	42N48.951	6E08.787	-
2	09/17/11	19:04:17	42N48.954	6E08.783	-
3	09/17/11	19:04:46	42N48.954	6E08.782	-
4	09/17/11	19:06:52	42N48.956	6E08.772	-
5	09/17/11	19:09:52	42N48.957	6E08.763	171
6	09/17/11	19:13:07	42N48.963	6E08.749	158
7	09/17/11	19:13:42	42N48.979	6E08.716	163
8	09/17/11	19:13:57	42N48.980	6E08.724	163
9	09/17/11	19:26:37	42N48.995	6E08.699	155
10	09/17/11	19:33:42	42N49.020	6E08.662	138
11	09/17/11	19:34:47	42N49.025	6E08.655	146
12	09/17/11	19:42:17	42N49.039	6E08.625	153
13	09/17/11	19:54:37	42N49.051	6E08.575	166
					Mean:157

The table B.3 shows the time stamp at the transmitted and recorded points. The first column shows start and finish time stamp at the transmitter whereas the second column presents the types of signal emission. The data file names, hydrophone number 18-23 and 30-35, are illustrated in the third column. The local time at the ground station, the length of data and size of file are shown in the fourth column.

Table B.3 Time comparison at the transmitting and recording points.

Time stamp at the transmitters (Local time)	**Types of signals**	**Data file names**	**Time stamp at DAQ (Local time/length/ Bytes)**
21:01:30-21:10:22	Sine wave (dsPIC)	Run_059769_sensor_18 Run_059769_sensor_19 Run_059769_sensor_20 Run_059769_sensor_21 Run_059769_sensor_22 Run_059769_sensor_23 Run_059769_sensor_30 Run_059769_sensor_31 Run_059769_sensor_32 Run_059769_sensor_33 Run_059769_sensor_34 Run_059769_sensor_35	(20:59:13 /9m 52s /2000167525)
21:10:46-21:15:26 21:15:48-21:31:18	Bipolar pulses (dsPIC) Orthogonal signals (dsPIC)	Run_059771_sensor_18 Run_059771_sensor_19 Run_059771_sensor_20 Run_059771_sensor_21 Run_059771_sensor_22 Run_059771_sensor_23 Run_059771_sensor_30 Run_059771_sensor_31 Run_059771_sensor_32 Run_059771_sensor_33 Run_059771_sensor_34 Run_059771_sensor_35	(21:09:29 /9m 50s /2002541045)
		Run_059772_sensor_18 Run_059772_sensor_19 Run_059772_sensor_20 Run_059772_sensor_21 Run_059772_sensor_22 Run_059772_sensor_23 Run_059772_sensor_30 Run_059772_sensor_31 Run_059772_sensor_32 Run_059772_sensor_33 Run_059772_sensor_34 Run_059772_sensor_35	(21:19:43 /14m 40s /2000517408)

Table B.3 Time comparison at the transmitting and recording points (Continued).

Time stamp at the transmitters (Local time)	**Types of signals**	**Data file names**	**Time stamp at DAQ (Local time/length/ Bytes)**
Started 21:35:36- 21:48:13	5 kHz sine signal (NI module)	Run_059773_sensor_18 Run_059773_sensor_19 Run_059773_sensor_20 Run_059773_sensor_21 Run_059773_sensor_22 Run_059773_sensor_23 Run_059773_sensor_30 Run_059773_sensor_31 Run_059773_sensor_32 Run_059773_sensor_33 Run_059773_sensor_34 Run_059773_sensor_35	(21:34:47 /14m 37s /2000989906)
Started 21:49:43-21:51:03 21:51:42- 21:53:02 21:53:54- 21:58:53	10 kHz sine signal (NI module) 15 kHz sine signal (NI module) Bipolar pulses (NI module)	Run_059774_sensor_18 Run_059774_sensor_19 Run_059774_sensor_20 Run_059774_sensor_21 Run_059774_sensor_22 Run_059774_sensor_23 Run_059774_sensor_30 Run_059774_sensor_31 Run_059774_sensor_32 Run_059774_sensor_33 Run_059774_sensor_34 Run_059774_sensor_35	(21:49:49 /12m 45s /1768397950)
Due to the time limitation, then we could not emit orthogonal pulses using NI module			

Appendix C. Schematic and PCB designs

The schematics and PCB for the eight-channel acoustic signal generation module and eight-channel power amplifier module are designed by the Protell99SE software. Figure C.1 shows the schematic of power supply. The circuit is designed to support both AC and DC supplies which are very convenient for testing in the laboratory. In addition, this module is designed to use a battery power supply that is very suitable for testing at sites. The voltage output consists of two levels using LM2576T-05 and LM2576-3.3 switching power regulator IC chips. That at 5.0 V is designed to supply the peripheral devices, keypad interface (74C922), serial interface (MAX3232), positive to negative voltage converter (ICL7660), operation amplifier (MCP6024) and so on. That at 3.3 V is supplied to a master chip and eight slave controllers, dsPIC33FJ256MC710-I/P digital signal controllers. The 16-bit digital to analogue converter (DAC8822) chips also use 3.3 V for operation.

Figure C.2 shows the schematic of a master controller and eight slave controllers. The main function of the master controller is the interface and control with eight-slave controllers. Data transfer between master and slaves is done via the Inter-Integrated Circuit (I^2C) which was invented by Phillips Corporation [89 NXP Semiconductor 2012]. The original speed of this protocol in 1982 was 100 kHz. This protocol has been developed by new technology; consequently, the current version of this protocol can run up to 5 MHz. The advantage of I^2C protocol requires only a two-wire system for communication, Serial Data (SDA) and Serial Clock (SCL). The eight output signals from the master controllers are connected to interrupt pin of each slave controller for triggering purposes.

The eight slave controller schematics are simplified into each box. The full schematic of each slave controller is plotted in Figure C.3.The main function of each slave controller is controlled by master controller

Another functions of the master controller are the interfacing with the keypad encoder (74C922) for the user interface. The MAX3232 is used by the master controller to interface via the serial port of the computer. The Figure C.4 is the schematic of the keypad encoder and serial port interface with a computer.

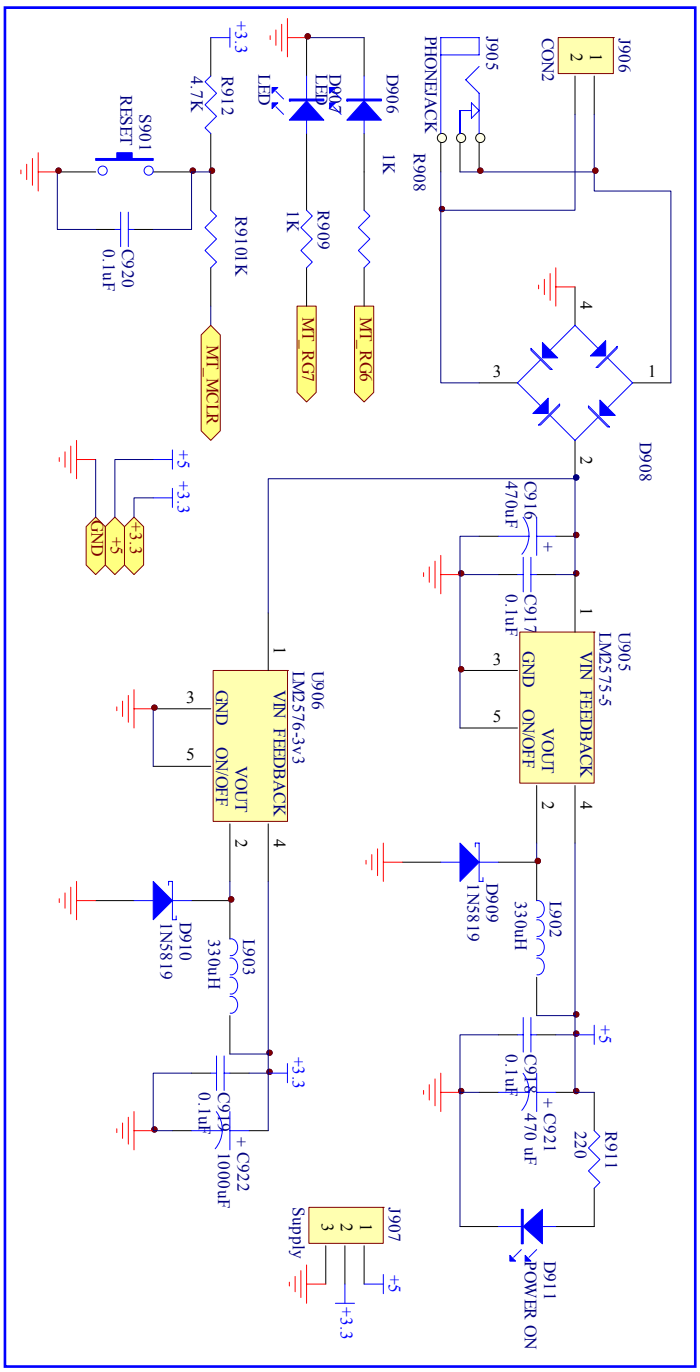

Figure C.1 Power supply schematic of dsPIC module.

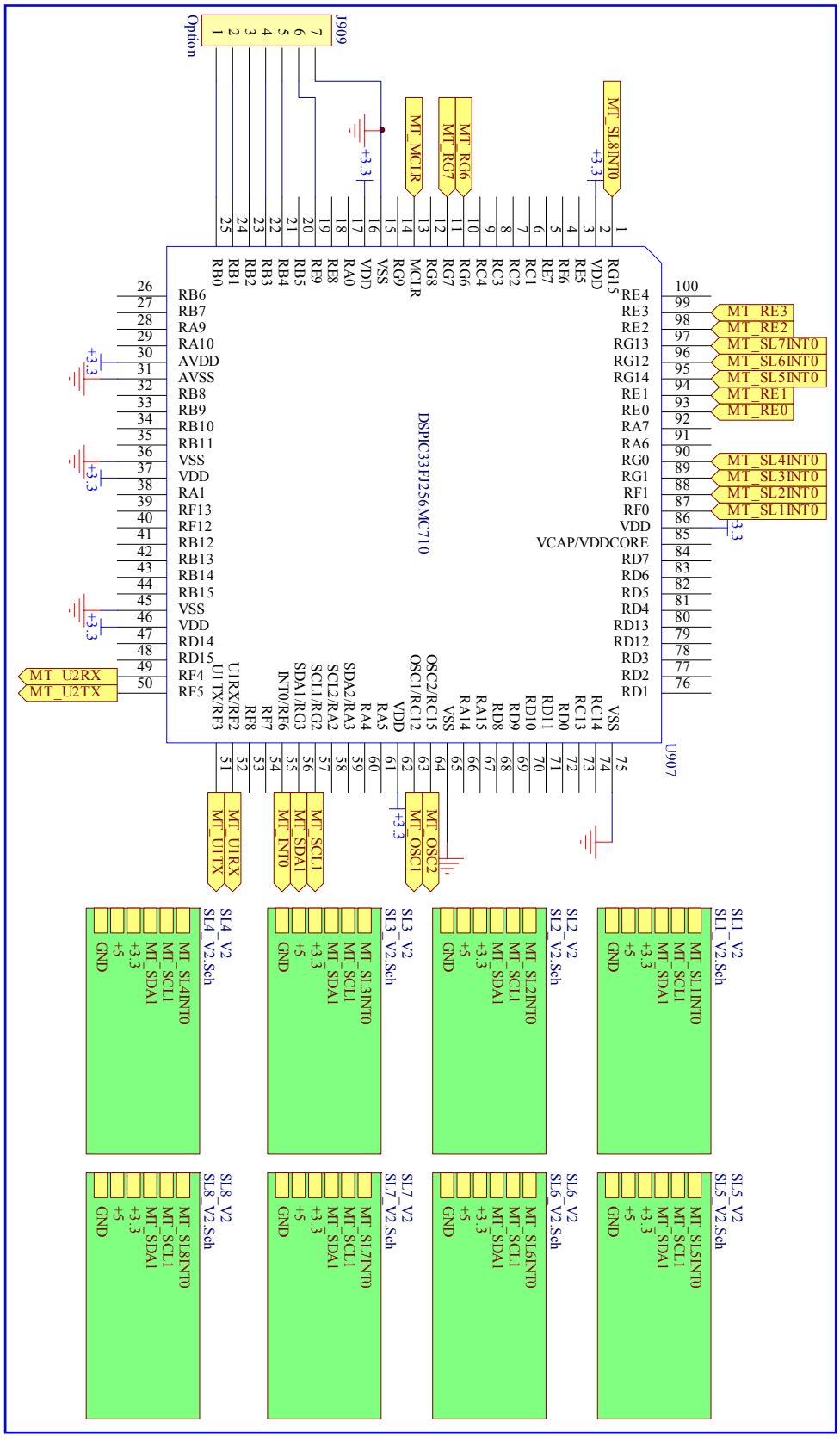

Figure C.2 Schematic of dsPIC33 master control and eight-slave module.

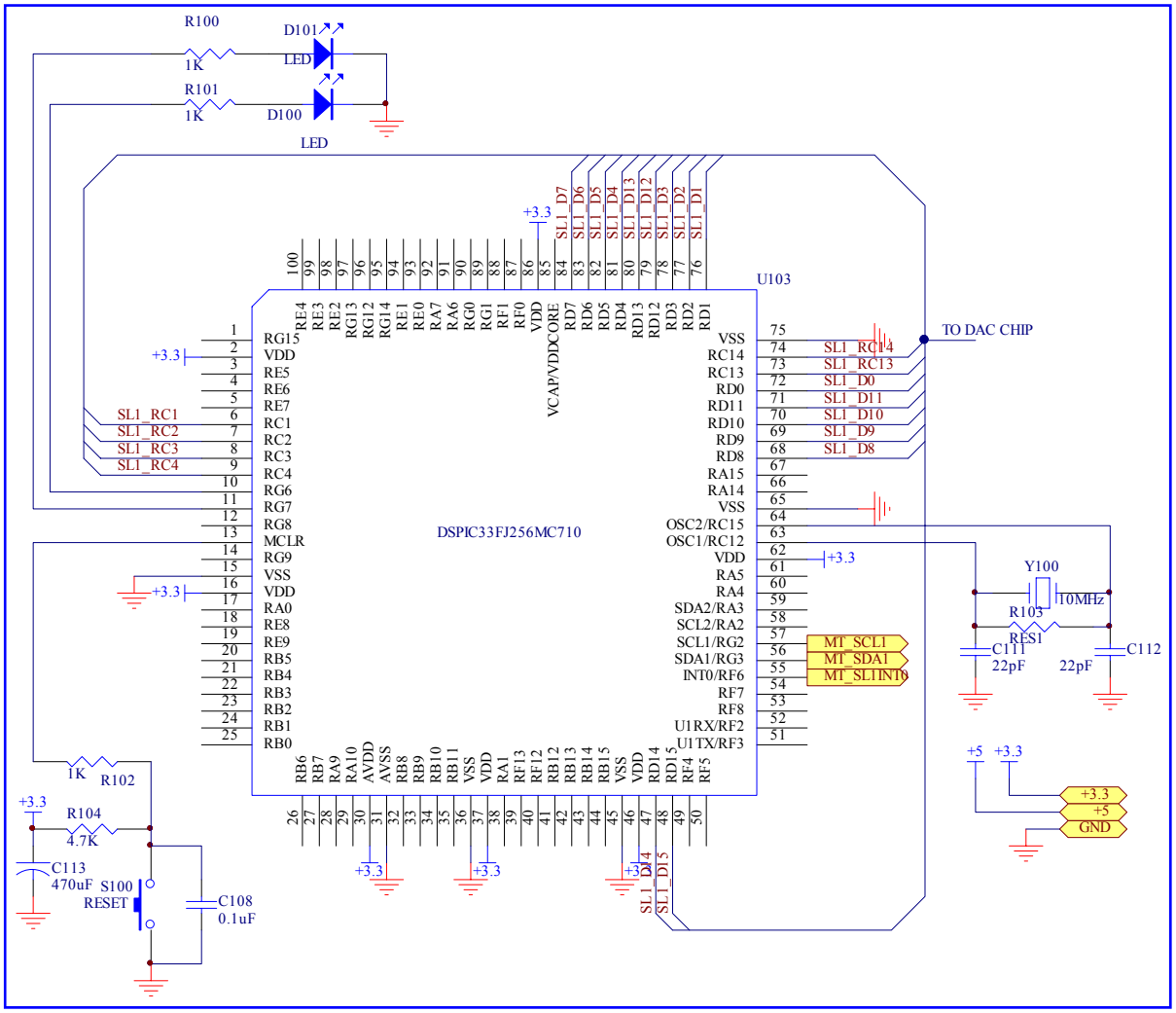

Figure C.3 Schematic of dsPIC33 slave controller.

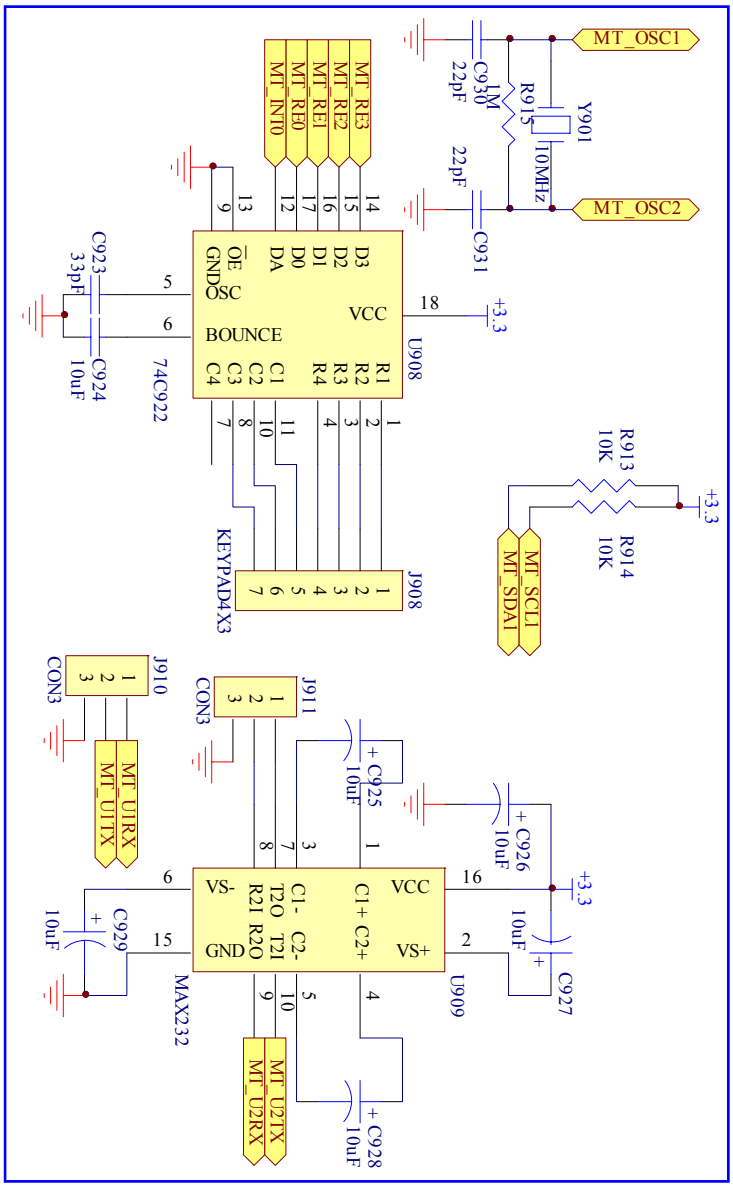

Figure C.4 Schematic of keypad and RS-232 interface.

Figure C.5 shows the schematic of a 16-bit digital to analogue converter using DAC8822 (compatible with AD5547). The acoustic signal generation module consists of eight parts of digital to analogue converter. The DAC8822 receives the digital data from a dsPIC slave controller and converts data to an analogue signal. The DAC8822 is designed as current type output, it is needed to convert current to voltage (I/V) by operation amplifiers (MCP6024 or compatible). The output voltage ($\boldsymbol{V_{out}}$) from the digital to analogue converter, can be calculated from the equation (C.1).

$$V_{out} = \left(\frac{D}{32768} - 1\right) \times V_{ref} \qquad \text{(C.1)}$$

Where D is the 16-bit digital data that is sent from a dsPIC controller. The table C.1 shows the output voltage and digital data of the DAC8822.

Table C.1 Digital data and voltage output of AD8822.

Digital data in binary	Voltage output
1111 1111 1111 1111	+ V_{REF}(32,767/32,768)
1000 0000 0000 0001	+ V_{REF}(1/32,768)
0000 0000 0000 0000	0
0111 1111 1111 1111	-V_{REF}(1/32,768)
0000 0000 0000 0000	- V_{REF}

The dsPIC33F is set to run at a maximum frequency of 40 MHz for sending digital data to DAC chips. Consequently, a high slew rate for the I/V converter is needed, typically 7V/µs (MCP6024 can support). The problem has been found when the author firstly used the low value of slew rate with the LM324 it could not generate the necessary signal. The DAC8822 is designed in bipolar mode, the positive and negative power supply is connected to the circuit. Because the main power supply is only the positive, so aICL7660 CMOS switched voltage converter from positive to negative is used to supply the -5V to the MCP6024 operation amplifier. The ISL6002 2.5VDC voltage reference is connected to the DAC8822 for external reference voltage.

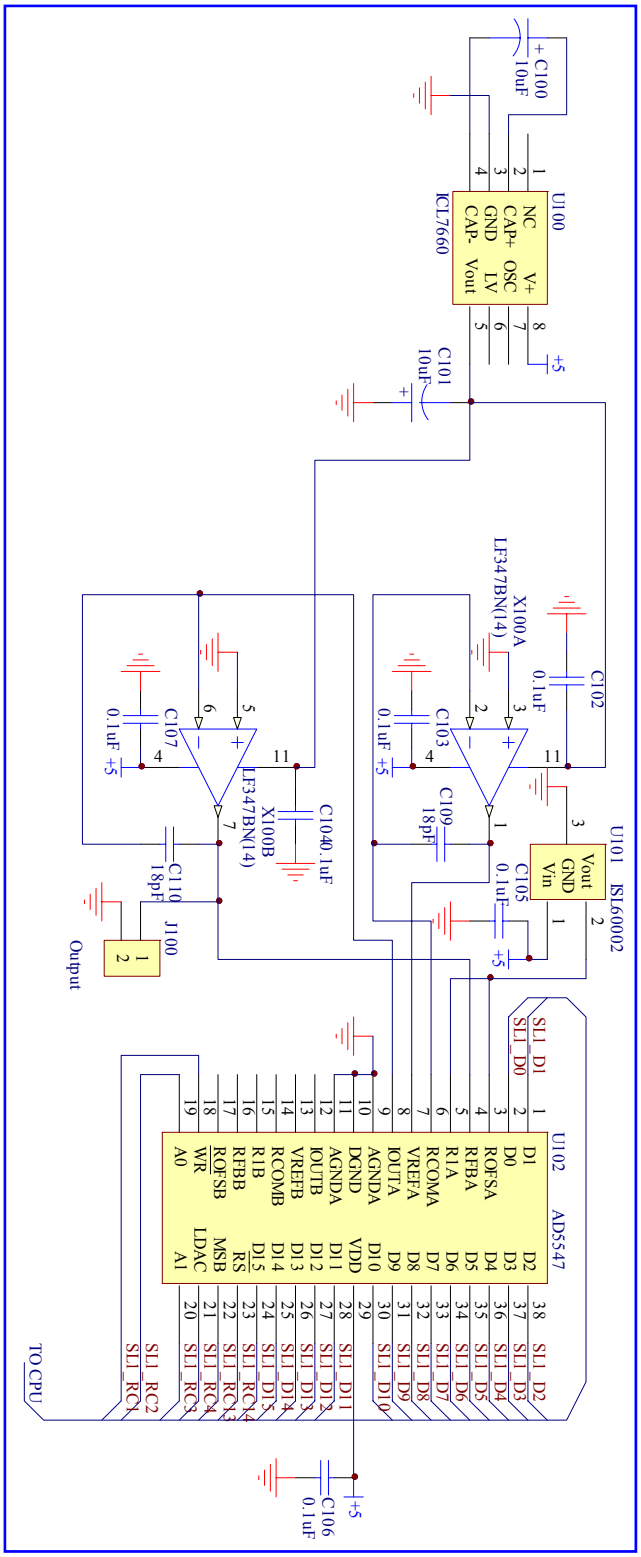

Figure C.5 Schematic of digital to analogue converter.

Figure C.6 shows the schematic of a PA94 CMOS high voltage power amplifier for driving continuous output currents up to 100mA. The PA94 can operate at the high voltage supply ,typically 900V (±450V), as such is very useful for driving hydrophones. In this research the maximum voltage used was ±100 V. The other interest is the high slew rate of this

chip with 500V/μS supported. The operation is designed using an inverting amplifier circuit with few components needed. The gain can easily be changed by a resistor feedback in the inverting amplifier circuit. The power amplifier module consists of eight modules of power amplifier circuit which are designed to drive the eight-channel hydrophone array.

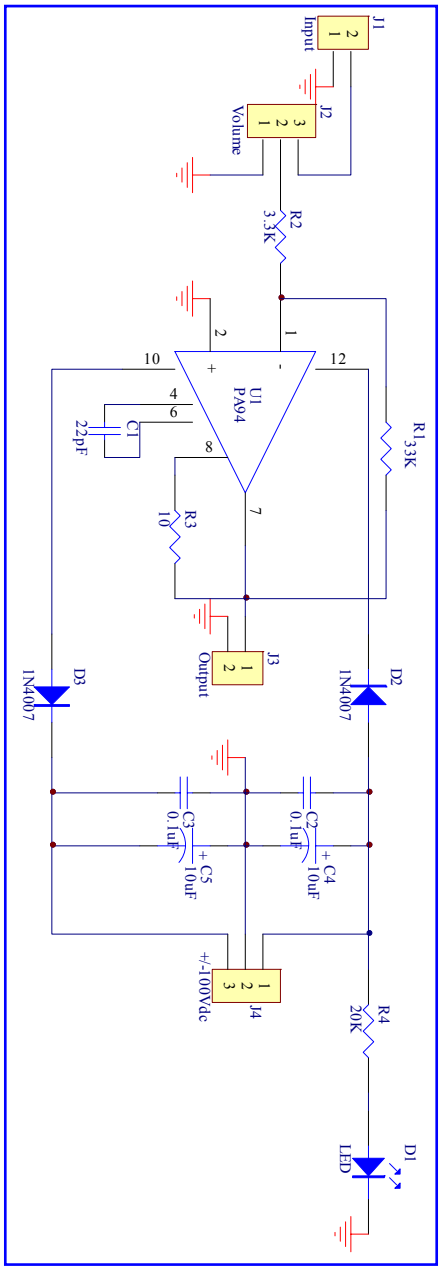

Figure C.6 Schematic of PA94 power amplifier module.

The schematics, as shown in the previous pages, are included in one circuit and updated to PCB file as shown in Figure C.7. The PCB of the eight-channel signal generation module is designed using Protell99SE software. The Gerber file is sent to manufacturer for fabrication, then all the electronic components are assembled on to a PCB. Figure C.8

shows the assembling of PCB at the Northumbria University laboratory. Finally, all electronic components and the PCB are built in the box as shown in the Figure C.9. Figure C.10 shows the completed eight-channel power amplifier module that was used in the laboratory and deployed at the site.

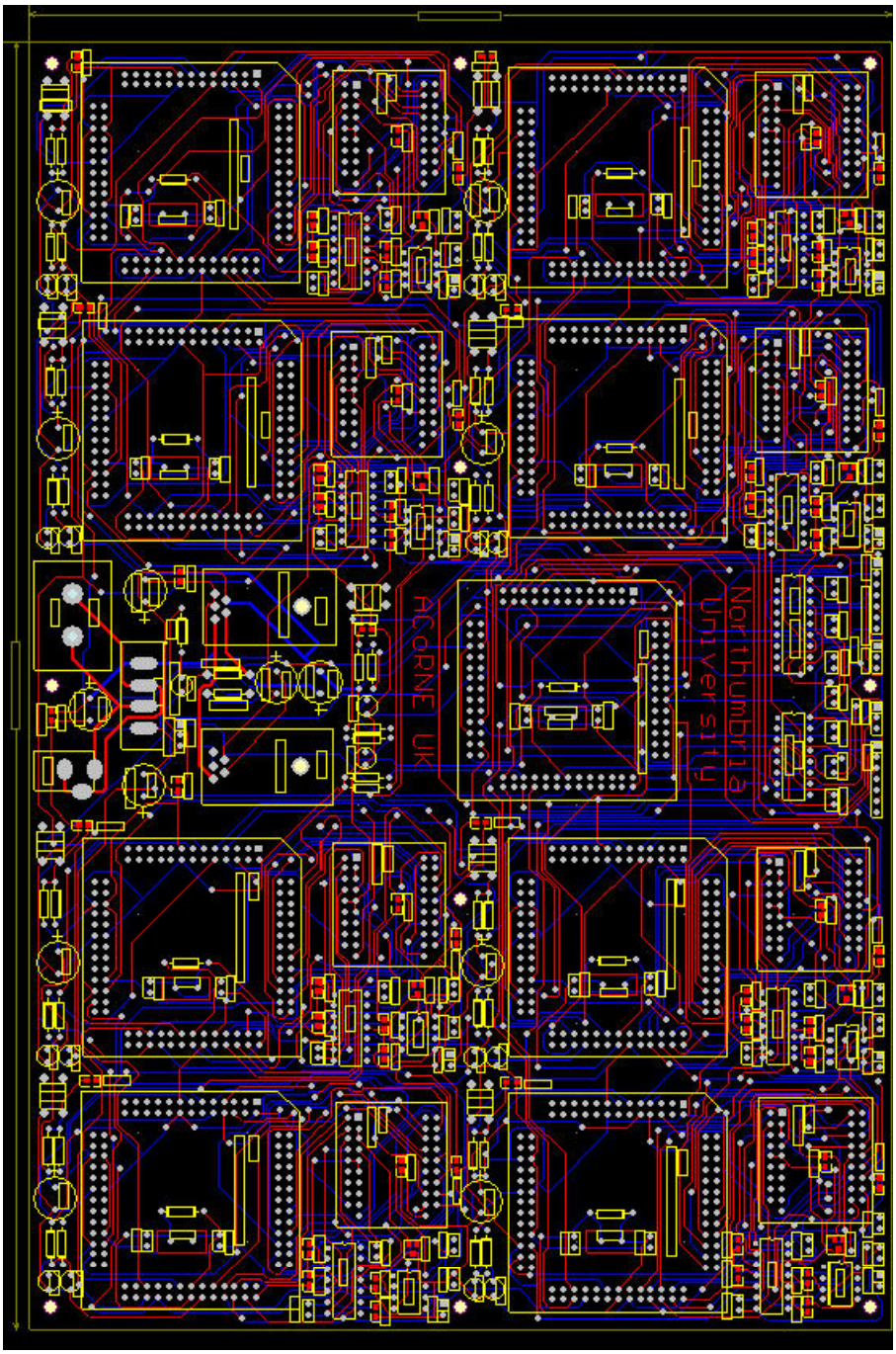

Figure C.7 PCB of dsPIC module.

Figure C.8 The assembling of dsPIC signal generation module.

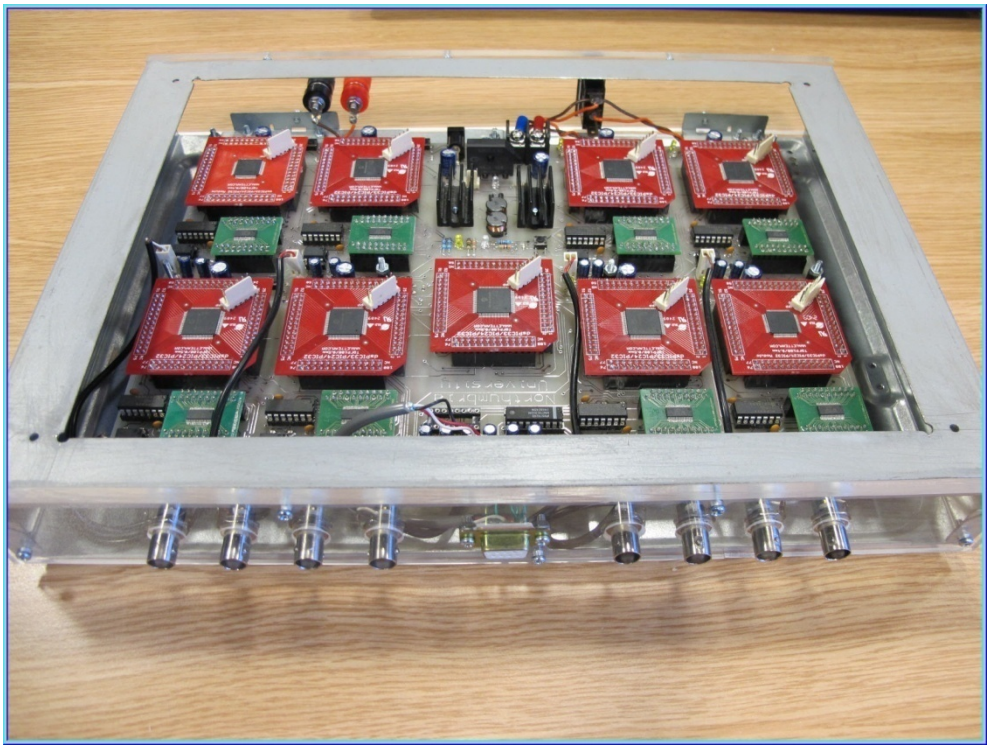

Figure C.9 The eight-channel dsPIC signal generation module.

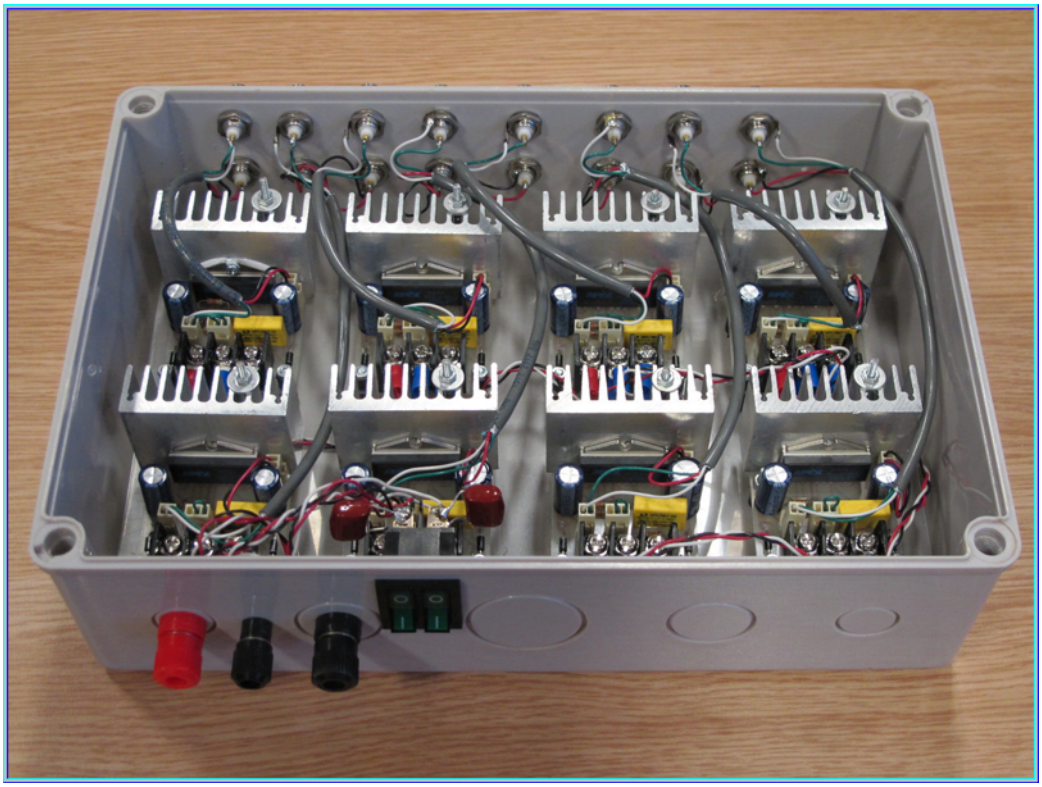

Figure C.10 Completed power amplifier module.

Figure C.11 shows the deployment of eight-channel acoustic transmitter on the vessel (Tethys II) at the ANTARES site, in the Mediterranean Sea.

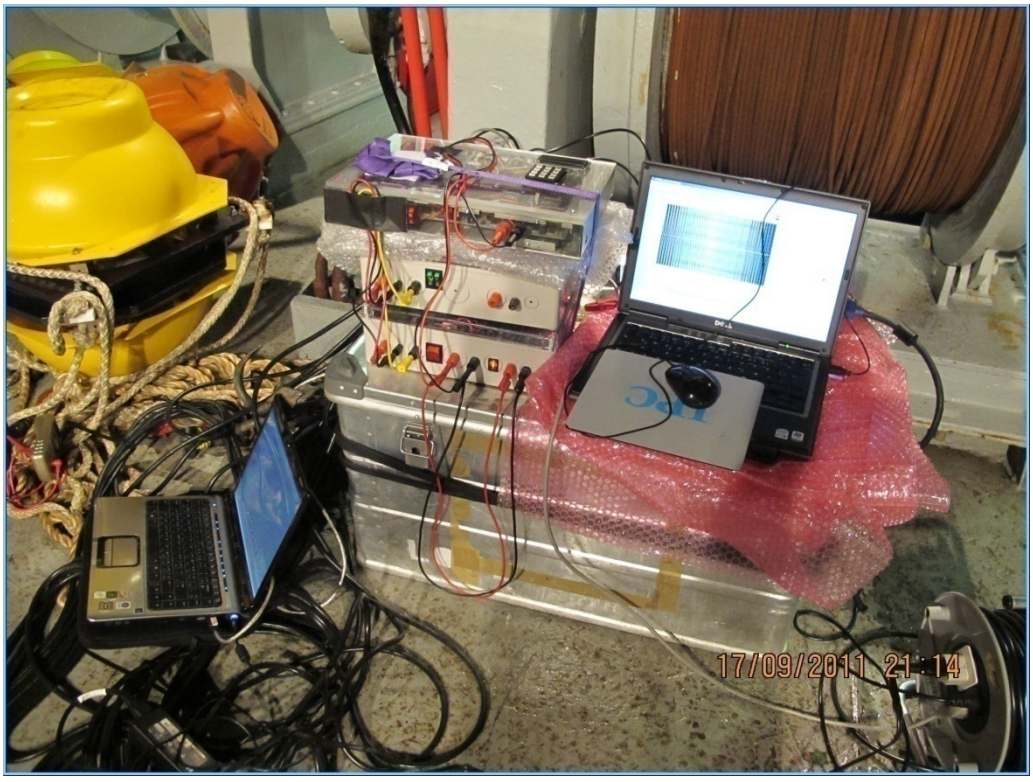

Figure C.11 The sea operation on the Tethys II at the ANTARES site.

Appendix D. Drawing of an array construction

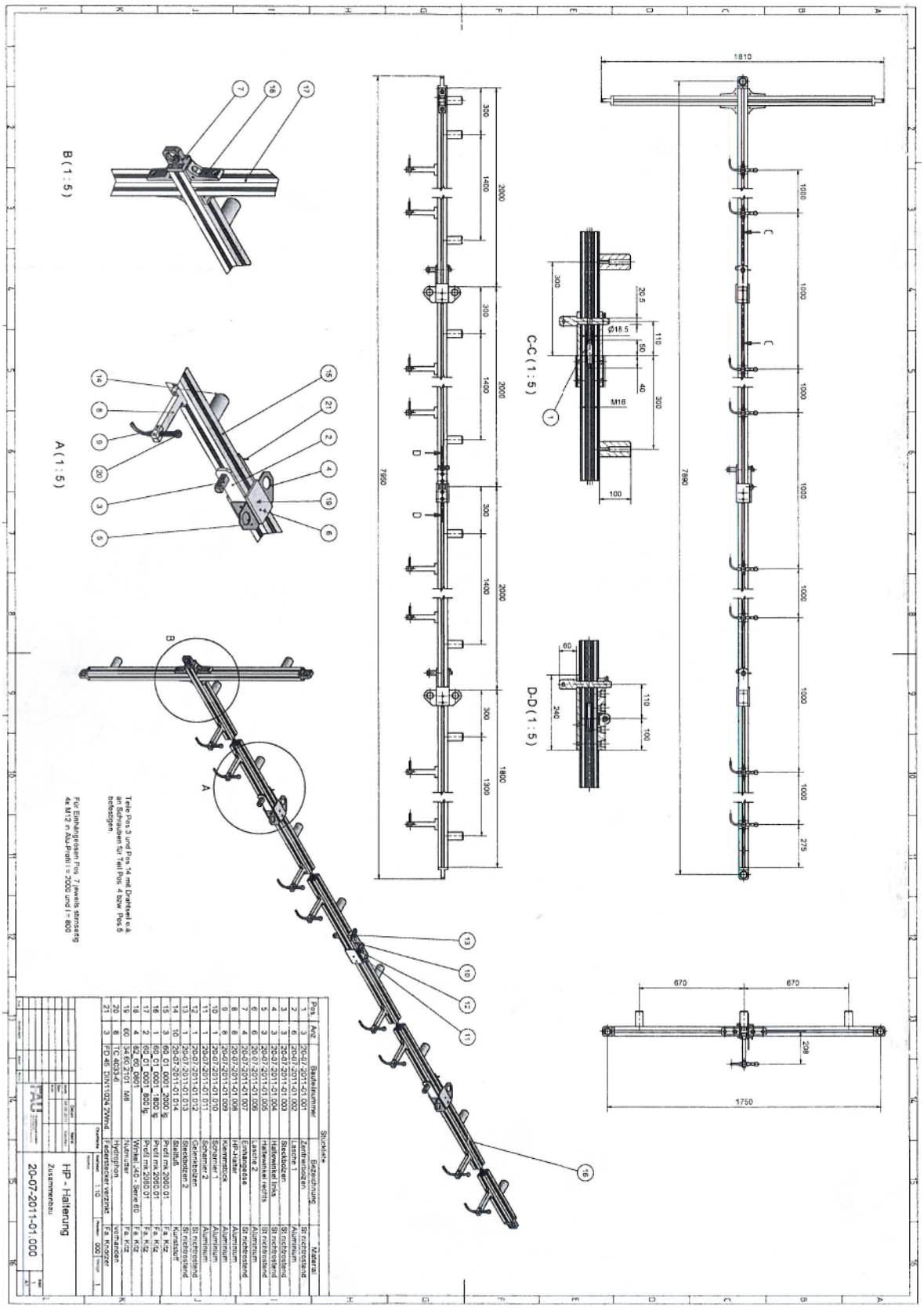

Figure D.1 Drawing of hydrophone array construction part I.

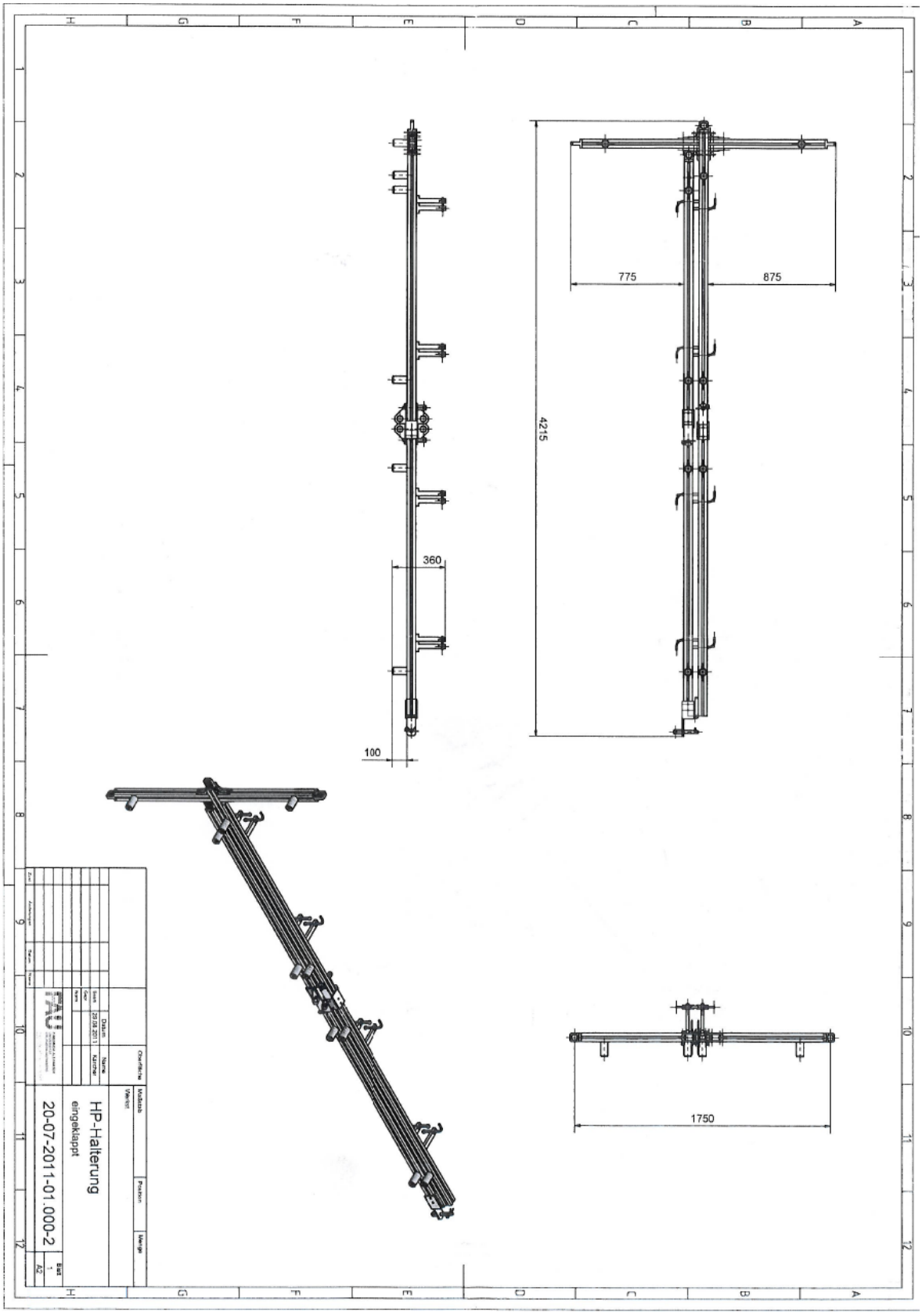

Figure D.2 Drawing of hydrophone array construction part II.

Appendix E. Sensitivity of TC-4033 hydrophone

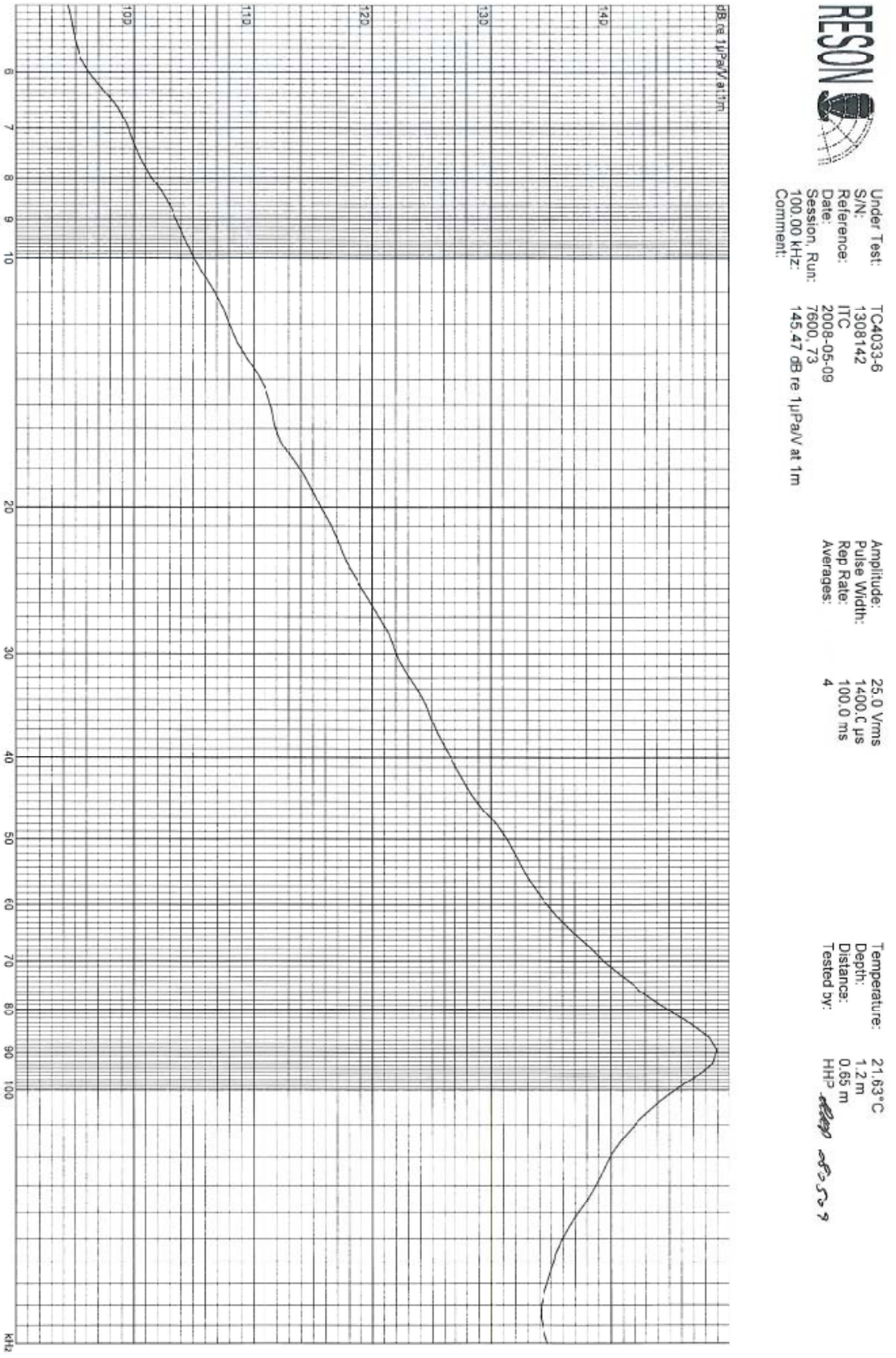

Figure E.1 Certificate of TC-4033 hydrophone calibration.

Appendix F. Software

LabVIEW is short for Laboratory Virtual Instrument Engineering Workbench. It is a powerful and flexible graphical development environment created by National Instruments, which is a company that creates hardware and software products that use computer technology to help engineers and scientists take measurements, control processes, and analyse and store data. LabVIEW consists of two parts, block diagram and front panel. The block diagram window contains program code that exists in a graphical form. The front panel window is graphical user interface that consists of various types of controls and indicators.

In this research the system includes LabVIEW software with USB-6211 16-bit two-channel digital to analogue converter and PXI-6713 or PCI-6713 12-bit eight-channel digital to analogue converter hardware modules to validate the results from the experiments in the laboratory and deployment in the field. The Figure F.1shows the block diagram window that consists of source codes to generate the eight-channel bipolar pulses. The math script is used to calculate the delay times between each hydrophone, then the bipolar pulse data is sent to build the waveform.

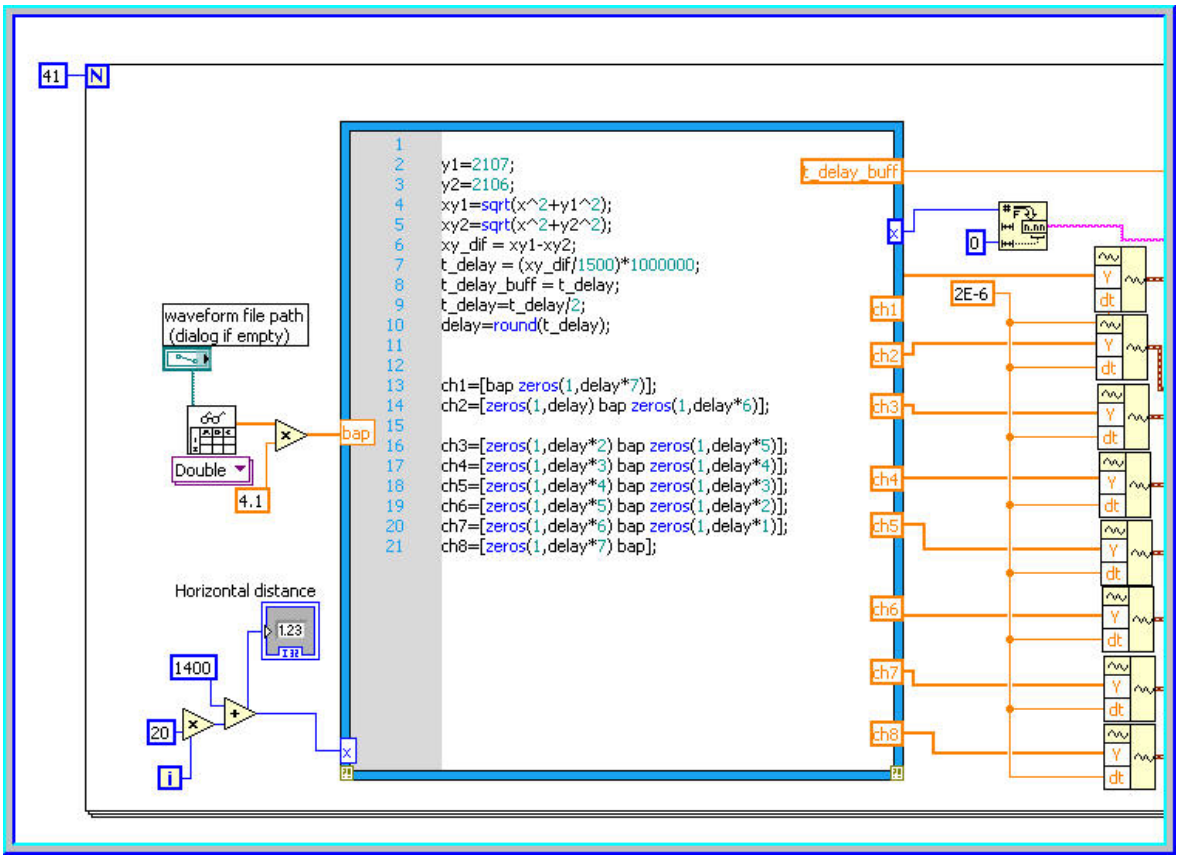

Figure F.1 LabVIEW software for eight-channel hydrophone transmitter (part I).

Figure F.2 shows the source codes that continue from the part one in Figure F.1. All eight waveforms of bipolar pulse are combined in the array, then eight waveforms are sent to the DAQmx to convert data from digital to analogue signals. Finally, all waveforms are sent to the terminal box (BNC-2110) which connects to a power amplifier to gain amplitude of waveforms for driving the hydrophone. In the experiments for the eight-channel transmitter, the sampling rate of PXI-6713 is set to 500 kS/s with sufficient speed to generate a good bipolar signal.

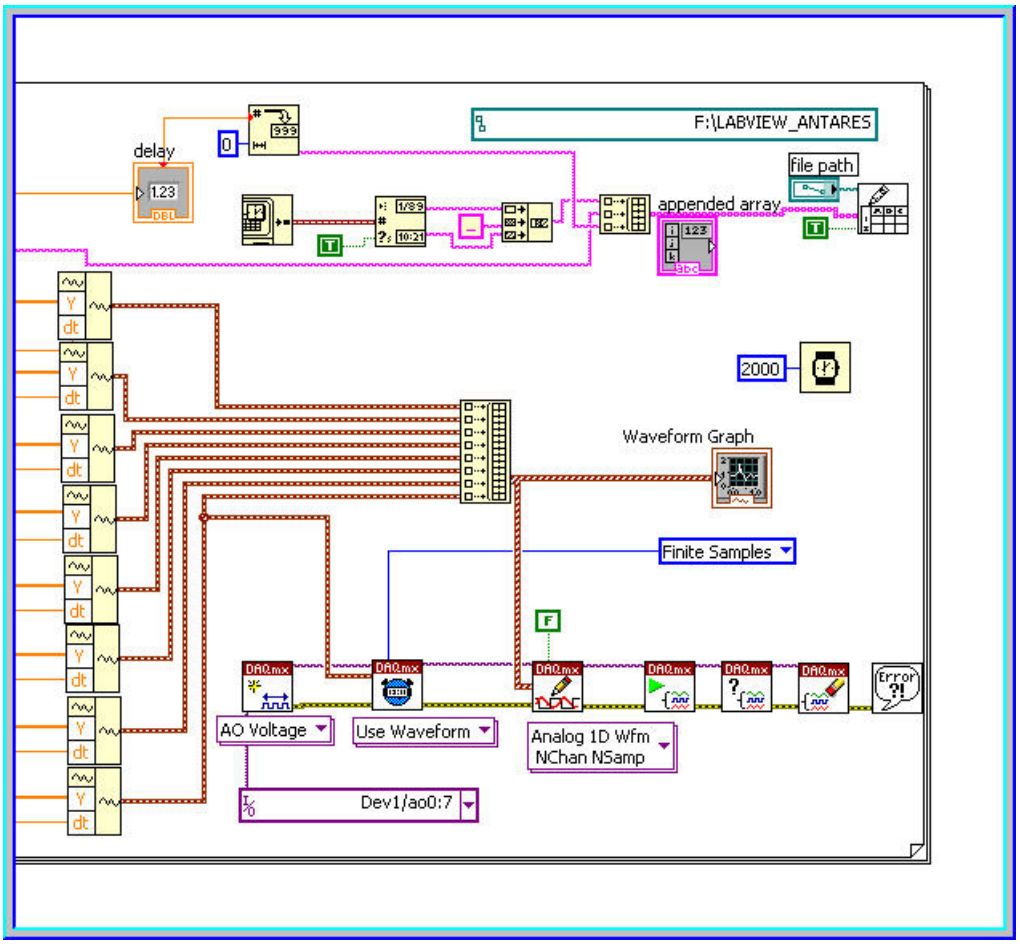

Figure F.2 LabVIEW software for eight-channel hydrophone transmitter (part II).

The front panel has the window for user interface and graphical outputs. It is very useful and convenient to change parameters and data. The Figure F.3 shows the eight input driving pulses that are send to the eight hydrophones via the PXI-6713 module. More details of the experiment at the laboratory have been presented in Chapter 6.

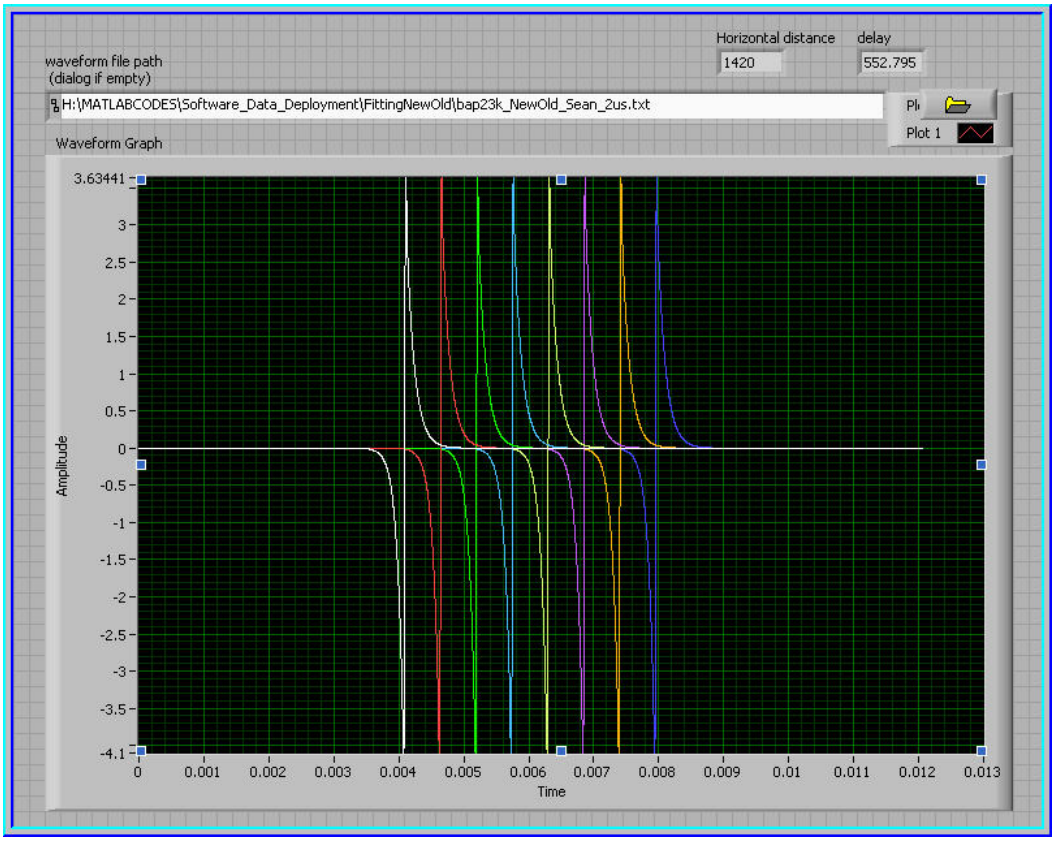

Figure F.3 Front panel of LabVIEW software with eight-channel driving pulses.

To control 16-bit digital signal controllers, the high-level C language has been developed using CCS C compiler with dsPIC33F starter kit board. The control software comprises two parts: master control and slave control. Master control is mainly interfaced with eight slaves via I^2C protocol. User interface and PC communication are functioned by master module whilst eight slave modules are commanded for generating arbitrary waveforms by master module. The source codes for master module and slave modules which deployed at the ANTARES site, has been added.

```
/*********************************************/
/* ******        Sourcecode for dsPIC master control  ***/
/* **********          Using CCS C compiler          ***/
/***   Deployment at the ANTARES site 17/09/2011****/
/* *******By Wichian Ooppakaew *****************/

/*********************************************/
#include <33FJ256MC710.h>
#fuses HS,PR_PLL,NOWDT,NOCOE,NODEBUG,
NOWRTB, NOPUT,NOWRTSS, NOWRT, NOPROTECT,
NORSS

#use delay(crystal=10000000,clock=40000000)
#use rs232(baud=9600,uart1,stream=rs232_1)
#use rs232(baud=9600,uart2,stream=rs232_2)
#use i2c(master, I2C1,force_hw,slow)
#include <stdlib.h>
#include <math.h>
#include <M_I2C.h>

/*************************************/
#include <lcd_dspic.h>
        //1234567890123456
#define msg0 "   Hy-Phone II  "
#define msg1 "SignalGeneration"
char str[17];
/*************************************/
/* The delay values must start from 1 up*/
//#define Delay_Shift 3  // unit in micro second
//#define Hydro_Delay (Delay_Shift-1) // in u
#define BUFFER_SIZE 32
BYTE buffer[BUFFER_SIZE];
BYTE next_in =0,next_out = 0;
unsigned int8  digit;
unsigned int8 keydata,keypress,mode;
unsigned int8 i,count,delay_buff[4];
unsigned int16
Hydro_Delay_Loop_Show,Hydro_Delay_Loop_Run;
unsigned int16
thousand_buff,hundred_buff,ten_buff,unit_buff,distance,buff;
unsigned int16 array_time(unsigned int16 x)
{
float xy1_sum,xy2_sum,xy_dif,t_delay,t_delay_ret,x_range;
x_range = x;
xy1_sum=sqrt((pow(x_range,2)+(pow(2107,2))));
xy2_sum=sqrt((pow(x_range,2)+(pow(2106,2))));
xy_dif = xy1_sum-xy2_sum;
t_delay = xy_dif/1500.0;
t_delay_ret = (t_delay*1000000.0);
return((int16)t_delay_ret);
}
/*************************************/
void lcd_string(char *s, int delay)
{
 while(*s!=0)
        {
         lcd_text(*s++);
         delay_ms(delay);
        }
}
void strcpy(char *s1, char *s2)
{
        while(*s1++ = *s2++);
}
/*************************************/

#int_ext0
void ext0_isr()
{
        keypress=input_e();
        keypress=keypress&0x0f;
    switch (keypress)
        {
                case 0:     keypress=1;
                break;
                case 1:     keypress=2;
                break;
                case 2:     keypress=3;
                break;
                case 8:     keypress=7;
                break;
                case 9:     keypress=8;
                break;
                case 10:  keypress=9;
                break;
                case 13:  keypress=0;
                break;
                // *=12,#=14
        }
        mode=keypress;
}
#int_rda
void rs232_isr1()
{
   int t;
        buffer[next_in] = fgetc(rs232_1);
        t=next_in;
        next_in=(next_in+1) % BUFFER_SIZE;
        if(next_in == next_out)
           next_in = t;
}

#define bkbhit (next_in!=next_out)

BYTE bgetc()
{
        BYTE c;
        while(!bkbhit);
        c=buffer[next_out];
        next_out=(next_out+1) % BUFFER_SIZE;
        return(c);
}
#int_rda2
void rs232_isr2()
{
        digit=fgetc(rs232_2);
        //rs1_flag = FALSE;
        //fputc(digit,rs232_2);
        //output_a(digit);
}
void delay_06us(void)
{
        delay_us(0); //
        delay_us(0);
        delay_us(0);
        delay_us(0);
        delay_us(0);
        delay_us(0);
        delay_us(0);
        delay_us(0);
}

void delay_05us(void)
{
        delay_us(0); //
        delay_us(0);
        delay_us(0);
        delay_us(0);
        delay_us(0);
        delay_us(0);
}
void delay_02us(void)
{
        delay_us(0); //
        delay_us(0);
        delay_us(0);
}

void main(void)
{
  int i;
  unsigned int16
max_distance,min_distance,min_distance_buff;
  char string_buff[5];
  char ranges_buff[4];
```

```
  char mode_buff[3];
  unsigned int8 inner_count,ortho_count;
  mode=0xff;
  //Hydro_Delay_Loop_Run = 666-30;
  set_tris_g(0xff06);
  set_tris_f(0xfff0);
  output_low(PIN_F0);
  output_low(PIN_F1);
  output_low(PIN_G1);
  output_low(PIN_G0);
  //enable_interrupts(INT_RDA);
  //enable_interrupts(INT_RDA2);
  enable_interrupts(INT_EXT0);
  enable_interrupts(INTR_GLOBAL);
  init_i2c();
  lcd_init();

/***********************************************/
/***********Show Initial LCD**********************/
              lcd_command(LINE1);
                //1234567890123456
              strcpy(str,"   Hy-Phone II  ");
              lcd_string(str,0);
              lcd_command(LINE2);
              strcpy(str,"Signal Generator");
              lcd_string(str,0);
              delay_ms(1000);
              lcd_command(LINE2);
              strcpy(str,"BioNicBot @RMUTT");
              lcd_string(str,0);
              delay_ms(1000);
 while(TRUE)
 {
 switch(mode)
              {
 case 0xff:  delay_ms(1000);
              lcd_command(LINE1);
                           //1234567890123456
              strcpy(str,"  STATUS: STOP  ");
              lcd_string(str,0);
              lcd_command(LINE2);
              strcpy(str,"Mode 1,4,7 and 8");
              lcd_string(str,0);
              output_high(PIN_G6);
              output_high(PIN_G7);
              //output_high(PIN_F0);
              delay_ms(500);
              output_low(PIN_G6);
              output_low(PIN_G7);
              //output_low(PIN_F0);
              delay_ms(500);
               break;

case 7: // Orthogonal 10 sets
              mode=0xff;
              lcd_command(LINE1);
              strcpy(str,"Insert x-min   ");
              lcd_string(str,0);
                //1234567890123456
              lcd_command(LINE2);
                //1234567890123456
              strcpy(str,"Value =        m");
              lcd_string(str,0);
              count=0;
              mode=0xff;
              while(count<4)
               {
                 while(mode==0xff)
              {
              }
              ranges_buff[count]=mode;
              itoa(ranges_buff[count],10,string_buff);
              lcd_command(0xc9+count);
              lcd_text(string_buff[0]);
              mode=0xff;
              count=count+1;
              }
              delay_ms(500);
              distance = 0;
              thousand_buff = 0;
              hundred_buff = 0;
              ten_buff = 0;
              unit_buff = 0;
              buff = ranges_buff[0];
              thousand_buff = buff*1000;
              buff = ranges_buff[1];
              hundred_buff=buff*100;
              buff = ranges_buff[2];
              ten_buff = buff*10;
              buff = ranges_buff[3];
              unit_buff = buff*1;
              distance =(thousand_buff+hundred_buff+ten_buff+unit_buff);
                                                          // Test showing
              itoa(distance,10,string_buff);
              lcd_clear();
              lcd_command(LINE2);

                //1234567890123456
              strcpy(str,"x min =        m");
              lcd_string(str,0);
              lcd_command(0xCa);
              lcd_text(string_buff[0]);
              lcd_text(string_buff[1]);
              lcd_text(string_buff[2]);
              lcd_text(string_buff[3]);
              delay_ms(2000);
              min_distance =distance;
              min_distance_buff = min_distance;
              // getting maximum value
              lcd_command(LINE1);
              strcpy(str,"Insert x-max   ");
              lcd_string(str,0);
                //1234567890123456
              lcd_command(LINE2);
               //1234567890123456
              strcpy(str,"Value =        m");
              lcd_string(str,0);
              count=0;
              mode=0xff;
              while(count<4)
              {
                while(mode==0xff)
              {

              }
              ranges_buff[count]=mode;
              itoa(ranges_buff[count],10,string_buff);
              lcd_command(0xc9+count);
              lcd_text(string_buff[0]);
              mode=0xff;
              count=count+1;
                }
              delay_ms(500);
              distance = 0;
              thousand_buff = 0;
              hundred_buff = 0;
              ten_buff = 0;
              unit_buff = 0;
              buff = ranges_buff[0];
              thousand_buff = buff*1000;
              buff = ranges_buff[1];
              hundred_buff=buff*100;
              buff = ranges_buff[2];
              ten_buff = buff*10;
              buff = ranges_buff[3];
              unit_buff = buff*1;
              distance =
              (thousand_buff+hundred_buff+ten_buff+unit_buff);
                                                    // Test
              showingitoa(distance,10,string_buff);
              lcd_clear();
              lcd_command(LINE2);
                //1234567890123456
              strcpy(str,"x max =        m");
              lcd_string(str,0);
```

```
            lcd_command(0xCa);
            lcd_text(string_buff[0]);
            lcd_text(string_buff[1]);
            lcd_text(string_buff[2]);
            lcd_text(string_buff[3]);
            delay_ms(2000);
□           □           □           □           □           □
    max_distance =distance;
            ortho_count=1;
do
{
 switch (ortho_count)
{

            case 1:
            write_slave(slave01,0x01);
            write_slave(slave02,0x01);
            write_slave(slave03,0x01);
            write_slave(slave04,0x01);
            write_slave(slave05,0x01);
            write_slave(slave06,0x01);
            write_slave(slave07,0x01);
            write_slave(slave08,0x01);
            break;

            case 2:
            write_slave(slave01,0x02);
            write_slave(slave02,0x02);
            write_slave(slave03,0x02);
            write_slave(slave04,0x02);
            write_slave(slave05,0x02);
            write_slave(slave06,0x02);
            write_slave(slave07,0x02);
            write_slave(slave08,0x02);
            break;

            case 3:
            write_slave(slave01,0x03);
            write_slave(slave02,0x03);
            write_slave(slave03,0x03);
            write_slave(slave04,0x03);
            write_slave(slave05,0x03);
            write_slave(slave06,0x03);
            write_slave(slave07,0x03);
            write_slave(slave08,0x03)
            break;

            case 4:
            write_slave(slave01,0x04);
            write_slave(slave02,0x04);
            write_slave(slave03,0x04);
            write_slave(slave04,0x04);
            write_slave(slave05,0x04);
            write_slave(slave06,0x04);
            write_slave(slave07,0x04);
            write_slave(slave08,0x04);
            break;

            case 5:
            write_slave(slave01,0x05);
            write_slave(slave02,0x05);
            write_slave(slave03,0x05);
            write_slave(slave04,0x05);
            write_slave(slave05,0x05);
            write_slave(slave06,0x05);
            write_slave(slave07,0x05);
            write_slave(slave08,0x05);
            break;

            case 6:
             write_slave(slave01,0x06);
            write_slave(slave02,0x06);
            write_slave(slave03,0x06);
            write_slave(slave04,0x06);
            write_slave(slave05,0x06);
            write_slave(slave06,0x06);
             write_slave(slave07,0x06);
             write_slave(slave08,0x06);
            break;

case 7:
write_slave(slave01,0x07);
write_slave(slave02,0x07);
write_slave(slave03,0x07);
write_slave(slave04,0x07);
write_slave(slave05,0x07);
write_slave(slave06,0x07);
write_slave(slave07,0x07);
write_slave(slave08,0x07);
break;

case 8:
write_slave(slave01,0x08);
write_slave(slave02,0x08);
write_slave(slave03,0x08);
write_slave(slave04,0x08);
 write_slave(slave05,0x08);
 write_slave(slave06,0x08);
write_slave(slave07,0x08);
 write_slave(slave08,0x08);
break;

case 9:
write_slave(slave01,0x09);
write_slave(slave02,0x09);
write_slave(slave03,0x09);
 write_slave(slave04,0x09);
 write_slave(slave05,0x09);
write_slave(slave06,0x09);
 write_slave(slave07,0x09);
 write_slave(slave08,0x09);
break;

case 10:
write_slave(slave01,0x0a);
write_slave(slave02,0x0a);
write_slave(slave03,0x0a);
write_slave(slave04,0x0a);
write_slave(slave05,0x0a);
write_slave(slave06,0x0a);
 write_slave(slave07,0x0a);
write_slave(slave08,0x0a);
break;

}

//inner_count = 1;
 //do
 //{    // do 10 time injection
do
{
itoa(min_distance,10,string_buff);
lcd_command(LINE2);
  //0123456789012345
strcpy(str,"x=    m; t=   us");
lcd_string(str,0);
lcd_command(0xC2);
lcd_text(string_buff[0]);
 if(min_distance!=0)
 lcd_text(string_buff[1]);
lcd_text(string_buff[2]);
if(min_distance>999)
 lcd_text(string_buff[3]);
Hydro_Delay_Loop_RUN = array_time(min_distance);
Hydro_Delay_Loop_Show = Hydro_Delay_Loop_RUN;
itoa(Hydro_Delay_Loop_RUN,10,string_buff);
lcd_command(0xCB);
lcd_text(string_buff[0]);
lcd_text(string_buff[1]);
lcd_text(string_buff[2]);
if(min_distance==0)
Hydro_Delay_Loop_Run=Hydro_Delay_Loop_Run-32;
else if((min_distance>250)&&(min_distance<750))
```

```
Hydro_Delay_Loop_Run=Hydro_Delay_Loop_Run-30;
else if((min_distance>750)&&(min_distance<1250))
Hydro_Delay_Loop_Run=Hydro_Delay_Loop_Run-28;

else if((min_distance>1250)&&(min_distance<1750))
Hydro_Delay_Loop_Run=Hydro_Delay_Loop_Run-27;

else if((min_distance>1750)&&(min_distance<2250))
Hydro_Delay_Loop_Run=Hydro_Delay_Loop_Run-22;

else if((min_distance>2250)&&(min_distance<2750))
Hydro_Delay_Loop_Run=Hydro_Delay_Loop_Run-20;

else if((min_distance>2750)&&(min_distance<3250))
Hydro_Delay_Loop_Run=Hydro_Delay_Loop_Run-18;

else if((min_distance>3250)&&(min_distance<4250))
Hydro_Delay_Loop_Run=Hydro_Delay_Loop_Run-14;

else if((min_distance>4250)&&(min_distance<4750))
Hydro_Delay_Loop_Run=Hydro_Delay_Loop_Run-14;

else if(min_distance>4750)
Hydro_Delay_Loop_Run=Hydro_Delay_Loop_Run-11;

lcd_command(LINE1);
//1234567890123456
strcpy(str,"M7 Set=      Run");
lcd_string(str,0);
itoa(ortho_count,10,string_buff);
lcd_command(0x87);
lcd_text(string_buff[0]);

if(ortho_count==10)
lcd_text(string_buff[1]);
//itoa(inner_count,10,string_buff);
//lcd_command(0x8b);
//lcd_text(string_buff[0]);
//if(inner_count == 10)
lcd_text(string_buff[1]);

if(min_distance==0)
fprintf(rs232_2,"M7:x=0000 t=666");
else
fprintf(rs232_2,"M7:x=%d
t=%d",min_distance,Hydro_Delay_Loop_Show);

output_high(PIN_F0); // Ch1
// delay between 1 and 2 about 380 ns (without delay)
delay_us(Hydro_Delay_Loop_Run);
output_high(PIN_F1); // Ch2
// delay between 2 and 3 about 380 ns (without delay)
delay_us(Hydro_Delay_Loop_Run);
output_high(PIN_G1); // Ch3
// without delay ch4 faster than ch3 300ns
delay_us(Hydro_Delay_Loop_Run);
output_high(PIN_G0); // Ch4
// without delay ch5 faster than ch4 200ns
delay_us(Hydro_Delay_Loop_Run);
output_high(PIN_G14);// Ch5
// delay between 5 and 6 about 80 ns (without delay)
delay_us(Hydro_Delay_Loop_Run);
output_high(PIN_G12);// Ch6
// without delay ch7 faster than ch6 200ns
delay_us(Hydro_Delay_Loop_Run);
output_high(PIN_G13);// Ch7
// without delay ch8 faster than ch7 13us
delay_us(13);//compensated delay
// after compensated with 13us delay =340 ns
delay_us(Hydro_Delay_Loop_Run);
output_high(PIN_G15);// Ch8
delay_ms(5);
output_low(PIN_F0);  //Ch1
output_low(PIN_F1);  //Ch2
output_low(PIN_G1);  //Ch3
output_low(PIN_G0);  //Ch4
output_low(PIN_G14);// Ch5
output_low(PIN_G12);// Ch6
output_low(PIN_G13);// Ch7
output_low(PIN_G15);// Ch8
delay_ms(1000);
lcd_command(LINE1);

 //1234567890123456

strcpy(str,"SEND 1-8: Done  ");
lcd_string(str,0);
delay_ms(1000);
min_distance=min_distance+20;

}while((mode!=0)&&(min_distance < max_distance));
min_distance = min_distance_buff;
//inner_count = inner_count+1;
//}while((mode != 0)&& (inner_count<11)); //inner loop
ortho_count=ortho_count+1;

if(ortho_count==11)
ortho_count=1;
}while(mode !=0);
mode=0xff;
break;

case 8: // Sine 5kHz, 10kHz ,15kHz
mode=0xff; // Mode 2 put 1 metre delay between them.
lcd_command(LINE1);
strcpy(str,"Insert x-min   ");
lcd_string(str,0);
 //1234567890123456
lcd_command(LINE2);
 //1234567890123456
strcpy(str,"Value =       m");
lcd_string(str,0);
count=0;
mode=0xff;
while(count<4)
 {
while(mode==0xff)
{

}
ranges_buff[count]=mode;
itoa(ranges_buff[count],10,string_buff);
lcd_command(0xc9+count);
lcd_text(string_buff[0]);
mode=0xff;
count=count+1;
 }
delay_ms(500);
distance = 0;
thousand_buff = 0;
hundred_buff = 0;
ten_buff = 0;
unit_buff = 0;
buff = ranges_buff[0];
thousand_buff = buff*1000;
buff = ranges_buff[1];
hundred_buff=buff*100;
buff = ranges_buff[2];
ten_buff = buff*10;
buff = ranges_buff[3];
unit_buff = buff*1;
distance =
(thousand_buff+hundred_buff+ten_buff+unit_buff);
// Test showing

itoa(distance,10,string_buff);
lcd_clear();
lcd_command(LINE2);

  //1234567890123456
strcpy(str,"x min =       m");
lcd_string(str,0);
lcd_command(0xCa);
lcd_text(string_buff[0]);
```

```
lcd_text(string_buff[1]);
lcd_text(string_buff[2]);
lcd_text(string_buff[3]);
delay_ms(2000);
min_distance =distance;
min_distance_buff = min_distance;
// getting maximum value
lcd_command(LINE1);
strcpy(str,"Insert x-max   ");
lcd_string(str,0);
  //1234567890123456
lcd_command(LINE2);
 //1234567890123456

strcpy(str,"Value =        m");
lcd_string(str,0);
count=0;
mode=0xff;
while(count<4)
{
while(mode==0xff)
{
}
ranges_buff[count]=mode;
itoa(ranges_buff[count],10,string_buff);
lcd_command(0xc9+count);
lcd_text(string_buff[0]);
mode=0xff;
count=count+1;
}
delay_ms(500);
distance = 0;
thousand_buff = 0;
hundred_buff = 0;
ten_buff = 0;
unit_buff = 0;
buff = ranges_buff[0];
thousand_buff = buff*1000;
buff = ranges_buff[1];
hundred_buff=buff*100;
buff = ranges_buff[2];
ten_buff = buff*10;
buff = ranges_buff[3];
unit_buff = buff*1;
distance =
(thousand_buff+hundred_buff+ten_buff+unit_buff);
// Test showing
itoa(distance,10,string_buff);
lcd_clear();
lcd_command(LINE2);
//1234567890123456
strcpy(str,"x max =        m");
lcd_string(str,0);
lcd_command(0xCa);
lcd_text(string_buff[0]);
lcd_text(string_buff[1]);
lcd_text(string_buff[2]);
lcd_text(string_buff[3]);
delay_ms(2000);

max_distance =distance;
ortho_count=1;
do{
switch (ortho_count)
{
case 1:  write_slave(slave01,0x0b);
write_slave(slave02,0x0b);
write_slave(slave03,0x0b);
 write_slave(slave04,0x0b);
 write_slave(slave05,0x0b);
 write_slave(slave06,0x0b);
 write_slave(slave07,0x0b);
 write_slave(slave08,0x0b);
break;

case 2:  write_slave(slave01,0x0c);
 write_slave(slave02,0x0c);
write_slave(slave03,0x0c);
write_slave(slave04,0x0c);
write_slave(slave05,0x0c);
write_slave(slave06,0x0c);
write_slave(slave07,0x0c);
write_slave(slave08,0x0c);
break;


case 3:  write_slave(slave01,0x0d);
 write_slave(slave02,0x0d);
write_slave(slave03,0x0d);
write_slave(slave04,0x0d);
write_slave(slave05,0x0d);
write_slave(slave06,0x0d);
write_slave(slave07,0x0d);
 write_slave(slave08,0x0d);
break;
}
inner_count = 1;
 //do
  //{     // do 10 time injection
do
{
itoa(min_distance,10,string_buff);
lcd_command(LINE2);
  //0123456789012345
strcpy(str,"x=    m; t=   us");
lcd_string(str,0);
lcd_command(0xC2);
lcd_text(string_buff[0]);
if(min_distance!=0)
{
lcd_text(string_buff[1]);
lcd_text(string_buff[2]);
}
if(min_distance>999)
lcd_text(string_buff[3]);
Hydro_Delay_Loop_RUN = array_time(min_distance);
Hydro_Delay_Loop_Show = Hydro_Delay_Loop_RUN;
itoa(Hydro_Delay_Loop_RUN,10,string_buff);
lcd_command(0xCB);
lcd_text(string_buff[0]);
lcd_text(string_buff[1]);
lcd_text(string_buff[2]);
if(min_distance==0)
Hydro_Delay_Loop_Run=Hydro_Delay_Loop_Run-32;


else if((min_distance>250)&&(min_distance<750))
Hydro_Delay_Loop_Run=Hydro_Delay_Loop_Run-30;

else if((min_distance>750)&&(min_distance<1250))
Hydro_Delay_Loop_Run=Hydro_Delay_Loop_Run-28;

else if((min_distance>1250)&&(min_distance<1750))
Hydro_Delay_Loop_Run=Hydro_Delay_Loop_Run-27;

else if((min_distance>1750)&&(min_distance<2250))
Hydro_Delay_Loop_Run=Hydro_Delay_Loop_Run-22;

else if((min_distance>2250)&&(min_distance<2750))
Hydro_Delay_Loop_Run=Hydro_Delay_Loop_Run-20;

else if((min_distance>2750)&&(min_distance<3250))
Hydro_Delay_Loop_Run=Hydro_Delay_Loop_Run-18;

else if((min_distance>3250)&&(min_distance<4250))
Hydro_Delay_Loop_Run=Hydro_Delay_Loop_Run-14;

else if((min_distance>4250)&&(min_distance<4750))
Hydro_Delay_Loop_Run=Hydro_Delay_Loop_Run-14;

else if(min_distance>4750)
Hydro_Delay_Loop_Run=Hydro_Delay_Loop_Run-11;

lcd_command(LINE1);
```

```
 //1234567890123456
strcpy(str,"M8 Set=      Run");
lcd_string(str,0);
itoa(ortho_count,10,string_buff);
lcd_command(0x87);
lcd_text(string_buff[0]);
if(ortho_count==10)
lcd_text(string_buff[1]);
//itoa(inner_count,10,string_buff);
//lcd_command(0x8b);
//lcd_text(string_buff[0]);
//if(inner_count == 10)
//  lcd_text(string_buff[1]);

if(min_distance==0)
fprintf(rs232_2,"M8:x=0000 t=666");
else
fprintf(rs232_2,"M8:x=%d
t=%d",min_distance,Hydro_Delay_Loop_Show);
output_high(PIN_F0); // Ch1

// delay between 1 and 2 about 380 ns (without delay)
delay_us(Hydro_Delay_Loop_Run);
output_high(PIN_F1); // Ch2

// delay between 2 and 3 about 380 ns (without
delay)delay_us(Hydro_Delay_Loop_Run);

output_high(PIN_G1); // Ch3
// without delay ch4 faster than ch3 300ns
delay_us(Hydro_Delay_Loop_Run);
output_high(PIN_G0); // Ch4

// without delay ch5 faster than ch4 200ns
delay_us(Hydro_Delay_Loop_Run);
output_high(PIN_G14);// Ch5

// delay between 5 and 6 about 80 ns (without delay)
delay_us(Hydro_Delay_Loop_Run);
output_high(PIN_G12);// Ch6

// without delay ch7 faster than ch6 200ns
delay_us(Hydro_Delay_Loop_Run);
output_high(PIN_G13);// Ch7

// without delay ch8 faster than ch7 13us
delay_us(13);//compensated delay
// after compensated with 13us delay =340 ns
delay_us(Hydro_Delay_Loop_Run);
output_high(PIN_G15);// Ch8
delay_ms(5);
output_low(PIN_F0);  //Ch1
output_low(PIN_F1);  //Ch2
output_low(PIN_G1);  //Ch3
output_low(PIN_G0);  //Ch4
output_low(PIN_G14);// Ch5
output_low(PIN_G12);// Ch6
output_low(PIN_G13);// Ch7
output_low(PIN_G15);// Ch8
delay_ms(1000);
lcd_command(LINE1);
//1234567890123456
strcpy(str,"SEND 1-8: Done  ");
lcd_string(str,0);
delay_ms(1000);
min_distance=min_distance+20;
}while((mode!=0)&&(min_distance < max_distance));
min_distance = min_distance_buff;
//inner_count = inner_count+1;
//}while((mode != 0)&& (inner_count<4)); //inner loop
ortho_count=ortho_count+1;
if(ortho_count==4)
ortho_count=1;
}while(mode !=0);
mode=0xff;
break;

case 4: mode=0xff; // Bipolar pulse 23kHz
write_slave(slave01,0x00);
write_slave(slave02,0x00);
write_slave(slave03,0x00);
write_slave(slave04,0x00);
write_slave(slave05,0x00);
write_slave(slave06,0x00);
write_slave(slave07,0x00);
write_slave(slave08,0x00);
lcd_command(LINE1);
strcpy(str,"Insert x-min   ");
lcd_string(str,0);
 //1234567890123456
lcd_command(LINE2);
 //1234567890123456
strcpy(str,"Value =       m");
lcd_string(str,0);
count=0;
mode=0xff;
while(count<4)
{

while(mode==0xff)
{

}
ranges_buff[count]=mode;
itoa(ranges_buff[count],10,string_buff);
lcd_command(0xc9+count);
lcd_text(string_buff[0]);

mode=0xff;

count=count+1;

 }
delay_ms(500);
distance = 0;
thousand_buff = 0;
hundred_buff = 0;
ten_buff = 0;
unit_buff = 0;
buff = ranges_buff[0];
thousand_buff = buff*1000;
buff = ranges_buff[1];
hundred_buff=buff*100;
buff = ranges_buff[2];
ten_buff = buff*10;
buff = ranges_buff[3];
unit_buff = buff*1;
distance =
(thousand_buff+hundred_buff+ten_buff+unit_buff);
// Test showing
itoa(distance,10,string_buff);
lcd_clear();
lcd_command(LINE2);
 //1234567890123456
strcpy(str,"x min =       m");
lcd_string(str,0);
lcd_command(0xCa);
lcd_text(string_buff[0]);
lcd_text(string_buff[1]);
lcd_text(string_buff[2]);
lcd_text(string_buff[3]);
delay_ms(2000);
min_distance =distance;
min_distance_buff = min_distance;
// getting maximum value
lcd_command(LINE1);
strcpy(str,"Insert x-max   ");
lcd_string(str,0);
//1234567890123456
lcd_command(LINE2);
  //1234567890123456
strcpy(str,"Value =       m");
lcd_string(str,0);
count=0;
mode=0xff;
```

```
while(count<4)
 {
  while(mode==0xff)
{
}
ranges_buff[count]=mode;
itoa(ranges_buff[count],10,string_buff);
lcd_command(0xc9+count);
lcd_text(string_buff[0]);
mode=0xff;
count=count+1;
 }
delay_ms(500);
distance = 0;
thousand_buff = 0;
hundred_buff = 0;
ten_buff = 0;
unit_buff = 0;
buff = ranges_buff[0];
thousand_buff = buff*1000;
buff = ranges_buff[1];
hundred_buff=buff*100;
buff = ranges_buff[2];
ten_buff = buff*10;
buff = ranges_buff[3];
unit_buff = buff*1;
distance =
(thousand_buff+hundred_buff+ten_buff+unit_buff);
// Test showing
itoa(distance,10,string_buff);
lcd_clear();
lcd_command(LINE2);
//1234567890123456
strcpy(str,"x max =        m");
lcd_string(str,0);
lcd_command(0xCa);
lcd_text(string_buff[0]);
lcd_text(string_buff[1]);
lcd_text(string_buff[2]);
lcd_text(string_buff[3]);
delay_ms(2000);
max_distance =distance;
do{
itoa(min_distance,10,string_buff);
lcd_command(LINE2);
 //0123456789012345
strcpy(str,"x=    m; t=   us");
lcd_string(str,0);
lcd_command(0xC2);
lcd_text(string_buff[0]);
if(min_distance!=0)
{
lcd_text(string_buff[1]);
lcd_text(string_buff[2]);
}
if(min_distance>999)
lcd_text(string_buff[3]);
Hydro_Delay_Loop_RUN = array_time(min_distance);
Hydro_Delay_Loop_Show = Hydro_Delay_Loop_RUN;
itoa(Hydro_Delay_Loop_RUN,10,string_buff);
lcd_command(0xCB);
lcd_text(string_buff[0]);
lcd_text(string_buff[1]);
lcd_text(string_buff[2]);
if(min_distance==0)
Hydro_Delay_Loop_Run=Hydro_Delay_Loop_Run-32;
else if((min_distance>250)&&(min_distance<750))
Hydro_Delay_Loop_Run=Hydro_Delay_Loop_Run-30;
else if((min_distance>750)&&(min_distance<1250))
Hydro_Delay_Loop_Run=Hydro_Delay_Loop_Run-28;
else if((min_distance>1250)&&(min_distance<1750))
Hydro_Delay_Loop_Run=Hydro_Delay_Loop_Run-27;
else if((min_distance>1750)&&(min_distance<2250))
Hydro_Delay_Loop_Run=Hydro_Delay_Loop_Run-22;
else if((min_distance>2250)&&(min_distance<2750))
Hydro_Delay_Loop_Run=Hydro_Delay_Loop_Run-20;
else if((min_distance>2750)&&(min_distance<3250))
Hydro_Delay_Loop_Run=Hydro_Delay_Loop_Run-18;
else if((min_distance>3250)&&(min_distance<4250))
Hydro_Delay_Loop_Run=Hydro_Delay_Loop_Run-14;
else if((min_distance>4250)&&(min_distance<4750))
Hydro_Delay_Loop_Run=Hydro_Delay_Loop_Run-14;
else if(min_distance>4750)
Hydro_Delay_Loop_Run=Hydro_Delay_Loop_Run-11;
lcd_command(LINE1);
//1234567890123456
strcpy(str,"Mode 4  Running ");
lcd_string(str,0);
if(min_distance==0)
fprintf(rs232_2,"M4:x=0000 t=666");
else
fprintf(rs232_2,"M4:x=%d
t=%d",min_distance,Hydro_Delay_Loop_Show);
output_high(PIN_F0); // Ch1

// delay between 1 and 2 about 380 ns (without delay)
delay_us(Hydro_Delay_Loop_Run);
output_high(PIN_F1); // Ch2

// delay between 2 and 3 about 380 ns (without delay)
delay_us(Hydro_Delay_Loop_Run);
output_high(PIN_G1); // Ch3

// without delay ch4 faster than ch3 300ns
delay_us(Hydro_Delay_Loop_Run);
output_high(PIN_G0); // Ch4

// without delay ch5 faster than ch4 200ns
delay_us(Hydro_Delay_Loop_Run);
output_high(PIN_G14);// Ch5

// delay between 5 and 6 about 80 ns (without delay)
delay_us(Hydro_Delay_Loop_Run);
output_high(PIN_G12);// Ch6

// without delay ch7 faster than ch6 200ns
delay_us(Hydro_Delay_Loop_Run);
output_high(PIN_G13);// Ch7

// without delay ch8 faster than ch7 13us
delay_us(13);//compensated delay
// after compensated with 13us delay =340 ns
delay_us(Hydro_Delay_Loop_Run);
 output_high(PIN_G15);// Ch8
delay_ms(5);
output_low(PIN_F0);  //Ch1
output_low(PIN_F1);  //Ch2
output_low(PIN_G1);  //Ch3
output_low(PIN_G0);  //Ch4
output_low(PIN_G14);// Ch5
output_low(PIN_G12);// Ch6
output_low(PIN_G13);// Ch7
output_low(PIN_G15);// Ch8
delay_ms(1000);
lcd_command(LINE1);
 //1234567890123456
strcpy(str,"SEND 1-8: Done  ");
lcd_string(str,0);
delay_ms(1000);
min_distance=min_distance+20;
if(min_distance>max_distance)
{
 min_distance = min_distance_buff;
}
}while(mode != 0);
mode=0xff;
break;
case 1: mode=0xff;
write_slave(slave01,0x00);
write_slave(slave02,0x00);
write_slave(slave03,0x00);
write_slave(slave04,0x00);
write_slave(slave05,0x00);
```

```
write_slave(slave06,0x00);
write_slave(slave07,0x00);
write_slave(slave08,0x00);
while(mode!=0x00)
 {
lcd_command(LINE1);
strcpy(str,"Insert No Hydro ");
lcd_string(str,0);
//1234567890123456
lcd_command(LINE2);
//1234567890123456
strcpy(str,"Hydro Number=   ");
lcd_string(str,0);
while(mode==0xff)
{
}
mode_buff[0]=mode;
itoa(mode_buff[0],10,string_buff);
lcd_command(0xce);
lcd_text(string_buff[0]);
delay_ms(1000);
switch(mode)
{
case 1: mode=0xff;
 lcd_command(LINE1);
//1234567890123456
strcpy(str,"Hydro Number 1  ");
lcd_string(str,0);
lcd_command(LINE2);
strcpy(str,"SEND Ch1:RUNNING");
lcd_string(str,0);
output_high(PIN_F0); // Ch1
delay_ms(100);
output_low(PIN_F0);  //Ch1
lcd_command(LINE2);
//1234567890123456
strcpy(str,"SEND Ch1: Done  ");
lcd_string(str,0);
delay_ms(1000);
break;
case 2: mode= 0xff;
lcd_command(LINE1);
//1234567890123456
strcpy(str,"Hydro Number 2  ");
lcd_string(str,0);
lcd_command(LINE2);
strcpy(str,"SEND Ch2:RUNNING");
lcd_string(str,0);
output_high(PIN_F1); // Ch2
delay_ms(100);
output_low(PIN_F1);  //Ch2
lcd_command(LINE2);
//1234567890123456
strcpy(str,"SEND Ch2: Done  ");
lcd_string(str,0);
delay_ms(1000);
break;
case 3: mode= 0xff;
lcd_command(LINE1);
//1234567890123456
strcpy(str,"Hydro Number 3  ");
lcd_string(str,0);
lcd_command(LINE2);
strcpy(str,"SEND Ch3:RUNNING");
lcd_string(str,0);
output_high(PIN_G1); //Ch3
delay_ms(100);
output_low(PIN_G1);  //Ch3
lcd_command(LINE2);
//1234567890123456
strcpy(str,"SEND Ch3: Done  ");
lcd_string(str,0);
delay_ms(1000);
break;
case 4: mode= 0xff;
lcd_command(LINE1);
//1234567890123456
strcpy(str,"Hydro Number 4  ");
lcd_string(str,0);
lcd_command(LINE2);
strcpy(str,"SEND Ch4:RUNNING");
lcd_string(str,0);
output_high(PIN_G0);
delay_ms(100);
output_low(PIN_G0);  //Ch4
lcd_command(LINE2);
//1234567890123456
strcpy(str,"SEND Ch4: Done  ");
lcd_string(str,0);
delay_ms(1000);
break;
case 5: mode= 0xff;
lcd_command(LINE1);
//1234567890123456
strcpy(str,"Hydro Number 5  ");
lcd_string(str,0);
lcd_command(LINE2);
strcpy(str,"SEND Ch5:RUNNING");
lcd_string(str,0);
output_high(PIN_G14);//Ch5
delay_ms(100);
output_low(PIN_G14);// Ch5
lcd_command(LINE2);
//1234567890123456

strcpy(str,"SEND Ch5: Done  ");
lcd_string(str,0);
delay_ms(1000);
break;

case 6: mode= 0xff;
lcd_command(LINE1
//1234567890123456
strcpy(str,"Hydro Number 6  ");
lcd_string(str,0);
lcd_command(LINE2);
strcpy(str,"SEND Ch6:RUNNING");
lcd_string(str,0);
output_high(PIN_G12);// Ch6
delay_ms(100);
output_low(PIN_G12);// Ch6
lcd_command(LINE2);
//1234567890123456
strcpy(str,"SEND Ch6: Done  ");
lcd_string(str,0);
delay_ms(1000);
break;

case 7: mode= 0xff;
lcd_command(LINE1);
//1234567890123456
strcpy(str,"Hydro Number 7  ");
lcd_string(str,0);
lcd_command(LINE2);
strcpy(str,"SEND Ch7:RUNNING");
lcd_string(str,0);
output_high(PIN_G13);// Ch7
delay_ms(100);
output_low(PIN_G13);// Ch7
lcd_command(LINE2);
//1234567890123456
strcpy(str,"SEND Ch7: Done  ");
lcd_string(str,0);
delay_ms(1000);
break;
case 8: mode= 0xff;
lcd_command(LINE1);
//1234567890123456
strcpy(str,"Hydro Number 8  ");
lcd_string(str,0);
lcd_command(LINE2);
strcpy(str,"SEND Ch8:RUNNING");
lcd_string(str,0);
output_high(PIN_G15);//Ch8
delay_ms(100);
```

```
output_low(PIN_G15);// Ch8
lcd_command(LINE2);
//1234567890123456
strcpy(str,"SEND Ch8: Done  ");
lcd_string(str,0);
delay_ms(1000);
break;
default:  mode=0x00;
lcd_command(LINE1);
strcpy(str,"Insert No Hydro ");
lcd_string(str,0);
//1234567890123456
lcd_command(LINE2);
//1234567890123456
strcpy(str,"Only No.1-8 or 0");
lcd_string(str,0);
delay_ms(1000);
break;
} // end of sub switch
}   // end of while
mode = 0xff;
break; // main case 1
} // end switch
 }

} // end main of Master control



/*********************************************/
/************  Source codes for Slaves**************/
/******For Slave 1- 8 only changing I2C address*******/
/*********************************************/
#include <33FJ256MC710.h>

#fuses XT,PR_PLL,NOWDT,NOCOE,NODEBUG,
NOWRTB, NOPUT, NOWRTSS, NOWRT, NOPROTECT,
NORSS
#use delay(crystal=10000000,clock=40000000)
#use i2c(SLAVE, I2C1,slow,address=0x52)

// I2C Slave addresses
// SL1=0x52                    //SL2=0x54
// SL3=0x56                    //SL4=0x58
// SL5=0x6A                    //SL6=0x6C
// SL7=0x6E                    //SL8=0x60
#define __2us__

#include "dsPIC_23K_2us.c"
#include "ortho_dspic01.c"
#include "ortho_dspic02.c"
#include "ortho_dspic03.c"
#include "ortho_dspic04.c"
#include "ortho_dspic05.c"
#include "ortho_dspic06.c"
#include "ortho_dspic07.c"
#include "ortho_dspic08.c"
#include "ortho_dspic09.c"
#include "ortho_dspic10.c"
#include "sine05khz.c"
#include "sine10khz.c"
#include "sine15khz.c"
void dac_on(void);
#define AD5547_WR               PIN_C1
#define AD5547_A0   PIN_C2
#define AD5547_A1  PIN_C3
#define AD5547_LDAC PIN_C4
#define AD5547_MSB  PIN_C13
#define AD5547_RS  PIN_C14
#define AD5547_DATAPORT PORTD
unsigned int16 dataram_16bit[2000];
BYTE address,buffer[0x10],data1;

#INT_SI2C
void ssp_interupt()
{
        BYTE incoming, state;
        state = i2c_isr_state();
        if(state < 0x80)
        {
                incoming = i2c_read();
                if(state == 1)
                {
                        address = incoming;
                }
                if(state == 2)
                {
                        data1 = incoming;
                }
        }
        if(state == 0x80)
        {
                i2c_write(buffer[address]);
        }
}

#INT_EXT0
void ext0_interupt()
{
        dac_on();
        output_high(PIN_G6);
        output_high(PIN_G7);
        delay_ms(300);
        output_low(PIN_G6);
        output_low(PIN_G7);
}

void init_i2c()
{
  output_float(PIN_G2);
  output_float(PIN_G3);
}
void dac_on(void)
{
 int16 count;
 for(count=0;count<2000;count++)
{
/* Free running mode */
output_d(dataram_16bit[count]);

#if defined(__1us__)
// 5 delay(0) to get 1Ms/s
delay_us(0); //
 delay_us(0);//
 delay_us(0);
 delay_us(0);
 delay_us(0);

 #elif defined(__2us__)
  // 1 and 5 zero is for 500khz
 delay_us(1); //
 delay_us(0);//
 delay_us(0);
 delay_us(0);
delay_us(0);
delay_us(0);

#elif defined(__4us__)
delay_us(3);
delay_us(0);
delay_us(0);
delay_us(0);
delay_us(0);
delay_us(0);

#elif defined(__sine__)
delay_us(0); //
delay_us(0);//
 delay_us(0);
delay_us(0);
delay_us(0);

#endif

 /* Control mode
```

```
output_d(count);
output_low(AD5547_WR);
output_high(AD5547_WR);
output_high(AD5547_LDAC);
output_low(AD5547_LDAC);

*/
 }
}

void main(void)
{
  int16 count;
  set_tris_g(0xff0f);
 /*-----Control mode------*/
  output_high(AD5547_WR);
  output_low(AD5547_LDAC);
  output_high(AD5547_RS);
  output_low(AD5547_MSB);
  output_low(AD5547_A0);
 output_low(AD5547_A1);
  setup_adc_ports(no_analogs);
  init_i2c();
  enable_interrupts(INTR_GLOBAL);
  enable_interrupts(INT_SI2C);
  enable_interrupts(INT_EXT0);

  /*initial data for DAC */
  output_low(AD5547_WR);
  output_high(AD5547_LDAC);
  data1=0xff;
  while(TRUE)
 {
switch(data1)
{
case 0x00:
for(count=0;count<2000;count++)
{
   dataram_16bit[count]=dsPIC_23K_2us[count];
}
data1=0xff;
break;

case 0x01:
for(count=0;count<2000;count++)
{
   dataram_16bit[count]=ortho_dspic01[count];
}
data1=0xff;
break;
case 0x02:
for(count=0;count<2000;count++)
{
dataram_16bit[count]=ortho_dspic02[count];
}
data1=0xff;
break;
case 0x03:
for(count=0;count<2000;count++)
{
    dataram_16bit[count]=ortho_dspic03[count];
}
  data1=0xff;
break;
case 0x04:
for(count=0;count<2000;count++)
{
dataram_16bit[count]=ortho_dspic04[count];
}
  data1=0xff;
break;
case 0x05:
 for(count=0;count<2000;count++)
{
dataram_16bit[count]=ortho_dspic05[count];
}
data1=0xff;
break;
case 0x06:
 for(count=0;count<2000;count++)
{
dataram_16bit[count]=ortho_dspic06[count];
}
 data1=0xff;
break;

case 0x07:
for(count=0;count<2000;count++)
{
dataram_16bit[count]=ortho_dspic07[count];
}
  data1=0xff;
break;
case 0x08;
for(count=0;count<2000;count++)
{
dataram_16bit[count]=ortho_dspic08[count];
}
 data1=0xff;
break;
case 0x09:
for(count=0;count<2000;count++)
{
dataram_16bit[count]=ortho_dspic09[count];
}
 data1=0xff;
break;
case 0x0a;
for(count=0;count<2000;count++)
{
dataram_16bit[count]=ortho_dspic10[count];
}
data1=0xff;
break;
case 0x0b:
for(count=0;count<2000;count++)
{
dataram_16bit[count]=sine05khz[count];
}
 data1=0xff;
break;
case 0x0c:
for(count=0;count<2000;count++)
{
dataram_16bit[count]=sine10khz[count];
}
data1=0xff;
break;
case 0x0d:
for(count=0;count<2000;count++)
{
dataram_16bit[count]=sine15khz[count];
}
data1=0xff;
break;
}
 }
}

//**********END OF PROGRAM**********//
```

References

[1] R. J. Urick, *Principles of underwater sound*: McGraw-Hill, 1975.

[2] S. Bevan, A. Brown, S. Danaher, J. Perkin, C. Rhodes, T. Sloan, L. Thompson, O. Veledar, and D. Waters, "Study of the acoustic signature of UHE neutrinos interactions in water and Ice," *Nuclear Instruments and Methods in Physics Research A,* vol. 607, pp. 398-411, 2009.

[3] M. Ardid, "ANTARES: A system of underwater sensors looking for neutrinos," in *Sensor technologies and applications,2007*, Valencia, Spain, 2007, pp. 192-197.

[4] M. B. Cabo, "Acoustic for underwater neutrino telescopes," PhD thesis Universitat Politecnica De Valencia, 2011, p. 122.

[5] K. Graf, "Experiment Studies within ANTARES towards Acoustic Detection of Ultra-High Energy Neutrinos in the Deep-Sea," PhD thesis, University of Erlangen-Nurnberg, 2008, p. 137.

[6] L. F. Thompson, "ARENA 2008 acoustic detection conference summary," *Nuclear Instruments and Methods in Physics Research A,* vol. 604, pp. S244-S248, 2009.

[7] S. Anvar, "FPGA-based system-on-chip designs for real-time application in particle physics," in *Real Time Conference,2005 14th IEEE-NPSS*, 2005, pp. 682-687.

[8] P. E. Doust and J. F. Dix, "The impact of improved transducer matching and equalization techniques on the accuracy and validity of underwater acoustic measurements," *Institute of Acoustics,* vol. 23, 2001.

[9] J. Vandenbroucke, G. Gratta, and N. Lehtinen, "Experimental study of acoustic Ultra-High-Engergy neutrino detection," *The Astrophysical journal,* vol. 621, pp. 301-312, March 2005.

[10] M. Ardid, M. Bou-Cabo, V. Espinosa, J. Martinez-Mora, F. Camarena, and J. Alba, "Calibration of sensors for acoustic detection of neutrinos," *Journal of Physics: Conference Series,* vol. 81, pp. 1-6, 2007.

[11] M. Ardid, M. Bou-Cabo, F. Camarena, V. Espinosa, and G. Larosa, "Use of parametric acoustic sources to generate neutrino-like signals," *Nuclear Instruments and Methods in Physics Research A,* vol. 604, pp. S208-S211, 2009.

[12] M. Ardid, S. Adrian, M. Bou-Cabo, and G. Larosa, "R&D studies for the development of a compact transmitter able to mimic the acoustic signature of a UHE neutrino interaction," *Nuclear Instruments and Methods in Physics Research A,* vol. 662, pp. S206-S209, 2012.

[13] S. Adrian, M. Ardid, M. Bou-Cabo, G. Larosa, C. D. Llorens, and J. A. Martinez-Mora, "Development of a compact transmitter array for the acoustic neutrino detection calibration," in *Mobile Adhoc and Sensor Systems (MASS), 2011 IEEE 8th International Conference*, Valencia, Spain, 2011, pp. 916-921.

[14] D. Schlosberg, "Calibration of a directional hydrophone in a hydroacoustic tank using the Prony method," in *OCEANS'97. MTS/IEEE Conference*, Dartmouth, NS, 1997, pp. 1339-1342.

[15] S. Danaher, "First data from ACoRNE and signal processing techniques," *Journal of physics: Conference Series,* vol. 81, pp. 1-5, 2007.

[16] L. F. Thompson, "Future plans for the ACoRNE collaboration," *Journal of physics: Conference Series,* vol. 81, pp. 1-5, 2007.

[17] E. Kuntsal, "A preamplifier, steerable, multichannel line array hydrophone: ITC - 8255," in *OCEANS 2000 MTS/IEEE Conference and Exhibition*, Santa Barbara, CA, 2000, pp. 1287-1288.

[18] S. P. Robinson and G. R. DORE, "Uncertainties in the calibration of hydrophone at NPL by the three-transducer spherical-wave reciprocity method in the frequency range 10 kHz to 500 kHz," National Physical Laboratory, UK1994.

[19] T. Karg, "Detection of ultra high energy neutrinos with an underwater very large volume array of acoustic sensors: A simulation study," PhD thesis, University of Erlangen-Nurnberg, 2006, p. 137.

[20] Y. Fukuda, T. Hayakawa, E. Ichihara, K. Inoue, and K. Ishihara, "Evidence for oscillation of atmospheric neutrinos," *Physical Review Letters,* vol. 81, pp. 1562-1567, 1998.

[21] G. A. Askariyan, B. A. Dolgoshein, A. N. Kalinovsky, and N. V. Mokhov, "Acoustic detection of high energy particle showers in water," *Nuclear Instruments and Methods in Physics Research A,* vol. 164, pp. 267-278, 1979.

[22] J. G. Learned, "Acoustic radiation by charged atomic particles in liquids: an analysis," *Physical Review D,* vol. 19, p. 3293, 1979.

[23] ACoRNE Collaboration, "Acoustic cosmic ray neutrino experiment," in http://www.hep.shef.ac.uk/research/acorne/, Last accessed date: 15 April 2012.

[24] A. D. Pierce, *An introduction to its Physical Principles and Applications*. New York: McGraw-Hill, 1981.

[25] N. W. Ashcroft and N. D. Mermin, "Solid state physics," Thomson Learning, 1976, pp. 492-494.

[26] N. G. Lehtinen, S. Adam, G. Gratta, T. K. Berger, and M. J. Buchkingham, "Sensitivity of an underwater acoustic array to ultra-high energy neutrinos," *Astroparticle Physics,* vol. 17, pp. 279-292, 2002.

[27] P. Tkalich and C. E. S, "On mechanism of wind wave noise generation," in *OCEAN'98 Conference*, France, 1998, pp. 1378-1381.

[28] N. Kurahashi and G. Gratta, "High-frequency ambient noise as background to deep ocean transient signal detection," *Atmospheric and Oceanic Physics,* vol. 1, pp. 1-5, 2007

[29] E. Andres, P. Askebjer, S. W. Barwick, and R. Bay, "The AMANDA neutrino telescope: principle of operation and first results," *Astroparticle Physics,* vol. 13, pp. 1-20, 2000.

[30] A. Achterberg, M. Ackermann, J. Adams, J. Ahrens, and K. Andeen, "First year performance of the IceCube neutrino telescope," *Astroparticle Physics,* vol. 26, pp. 155-172, October 2006.

[31] M. Merch, "The IceCube detector: A large sensor network at the south pole," *IEEE Pervasive Computing* vol. 9, pp. 43-47, 2010.

[32] S. R. Klein, "IceCube: A cubic kilometer radiation detector," *IEEE Transactions on Nuclear Science,* vol. 56, pp. 1141-1147, 2009.

[33] J. A. Aguilar, A. Albert, F. Ameli, M. Anghinolfi, G. Anton, and S. Anvar, "First results of the instrumentation line for the deep-sea ANTARES neutrino telescope," *Astroparticle Physics,* vol. 26, pp. 314-324, October 2006.

[34] V. V. Elewyck, "Detection of inclined and horizontal showers in the Pierre Auger observatory," in *AIP conference*, 2005, pp. 187-189.

[35] D. Z. Besson, "Status of the RICE experiment," *Journal of physics: Conference Series,* vol. 81, pp. 1-4, 2008.

[36] A. Silvestri, "Status of the ANITA and ANITA-lite," *Astroparticle Physics: arXiv:astro-ph/0411007v2,* pp. 1-9, 2004.

[37] V. Aynutdnov, A. Avrorin, V. Balkanov, I. Belolaptikov, and N. Budnev, "The Baikal neutrino experiment: status, selected physics results, and perspectives," *Nuclear Instruments and Methods in Physics Research A,* vol. 588, pp. 99-106, April 2008.

[38] I. A. Samarai, J. Busto, B. Combettes, A. G. Dehanine, and G. Hallewell, "New developments of scintillating crystal-based hybrid single photon detector (X-HPDs) for charged particle and neutrino detection application," in *International conference*

on Advancements in Nuclear Instrumentation Measurement Methods and their Application (ANIMMA), 2009, pp. 1-7.

[39] E. D. Wolf, "KM3NeT, a new generation neutrino telescope," *Nuclear Instruments and Methods in Physics Research A,* vol. 588, pp. 86-91, April 2008.

[40] C. Bigongiari, "Km3NeT, a deep sea challenge for neutrino astronomy," in *International conference on Sensor technologies and applications* Valencia, Spain, 2007, pp. 248-253.

[41] E. Migneco, S. Aiello, A. Aloisio, F. Ameli, I. Amore, and M. Anghinolfi, "Recent achievements of the NEMO project," *Nuclear Instruments and Methods in Physics Research A,* vol. 588, pp. 111-118, April 2008.

[42] F. Ameli, "Data acquistion and transport for NEMO project," in *15th IEEE-NPSS Real time conference* Batavia, IL, 2007, pp. 1-6.

[43] G. Aggouras, E. G. Anassontzis, A. E. Ball, G. Bourlis, and W. Chinowsky, "Operation and performance of the NESTOR test dectector," *Nuclear Instruments and Methods in Physics Research A,* vol. 552, pp. 420-439, November 2005.

[44] T. A. Demidova, "Current meter measurements in studies of near-buttom background conditions in vicinity of planned NESTOR neutrino telescope," in *IEEE 5th Working Conference on Current Measurement* FL, USA, 1995, pp. 259-264.

[45] S. Boser, C. Bohm, and F. Descamps, "The South pole acoustic test seup: calibrations and lake test," *Journal of physics: Conference Series,* vol. 81, pp. 1-6, 2007.

[46] J. Vandenbroucke, N. Lehtinen, Y. Zhao, and G. Gratta, "Acoustic detection of ultra-high energy neutrinos," in *OCEANS 2003*, 2003.

[47] N. Kurahashi, "Updates from the study of acoustic Ultra-high energy neutrino detection phase II," *Nuclear Instruments and Methods in Physics Research A,* vol. 604, pp. S127-S129, 2009.

[48] V. Aynutdinov, A. Avrorin, and V. Balkanov, "High enegy neutrino acoustic detection activities in Lake Baikal: Status and results," *Nuclear Instruments and Methods in Physics Research A,* vol. 604, pp. S130-S135, 2009.

[49] V. Aynutdinov, A. Avrorin, and I. Belolaptikov, "Acoustic search for high-energy neutrinos in the Lake Baikal: Results and Plans," *Nuclear Instruments and Methods in Physics Research A,* vol. 662, pp. S210-S215, 2012.

[50] U. Emanuele, "Time calibration of the KM3NeT neutrino telescope," in *Neclear science symposium and medical imaging conference*, Valencia, Spain, 2011, pp. 1852-1856.

[51] P. Bagley, A. Holford, A. Jamieson, and M. Priede, "KM3NeT conceptual design for a deep-sea research infrastructure incopratiing a very large volume neutrino telescope in the Mediterranean Sea," 2011.

[52] P. Bagley, J. Craig, A. Holford, and A. Jamieson, "KM3NeT Technical design report for a deep-sea research infrastructure in the Mediterranean Sea incorporating a very large volume neutrino telescope," 2011.

[53] E. Migneco, "Progress and latest results from Baika, Nestor, NEMO and KM3NeT," *Journal of Physics: Conference Series 136,* pp. 1-6, 2008.

[54] g. Riccobene, "Long-term measurements of acoustic background noise in very deep sea," *Nuclear Instruments and Methods in Physics Research A,* vol. 604, pp. S149-S157, 2009.

[55] E. G. Anassontzis, "NESTOR deep sea neutrino telescope: Deployment and results," in *XIII International symposium on very high energy cosmic ray interactions*, January 2006, pp. 279-286.

[56] P. K. F. Grieder, "NESTOR Neutrino telescope status report," in *Nuclear Physics B*. vol. 97, 2001, pp. 105-108.

[57] M. Circella, "The construction of ANTARES, the first undersea neutrino telescope," *Nuclear Instruments and Methods in Physics Research A,* vol. 602, pp. 1-6, 2009.

[58] R. Lahmann, "The acoustic detection system of the ANTARES neutrino telescope in the Mediterranean Sea," in *Sensor technologies and applications, 2007*, Valencia, Spain, 2007, pp. 221-226.

[59] K. Graf, "Studies of acoustic neutrino detection methods with ANTARES," *Nuclear Instruments and Methods in Physics Research A,* vol. 626, pp. S217-S220, 2011.

[60] R. Lahmann, "Status and recent results of the acoustic neutrino detection test system AMADEUS," *Nuclear Instruments and Methods in Physics Research A,* vol. 662, 2012.

[61] R. Lahmann, "Deep-sea acoustic neutrino detector and the AMADEUS system as a multi-purpose acoustic array," *Nuclear Instruments and Methods in Physics Research A,* vol. 602, pp. 255-261, 2009.

[62] J. Perkin, "Simulating the sensitivity of hypothetical km3 hydrophone arrays to fluxes of UHE neutrinos," *Journal of physics: Conference Series,* vol. 81, pp. 1-6, 2007.

[63] S. Bevan, "An Investigation into the Feasibility of a Sea Water and Ice Based Acoustic UHE Neutrino Telescope." vol. PhD thesis: University College London, 2008.

[64] J. D. Perkin, "The acoustic detection of Ultra High Energy Neutrinos." vol. PhD thesis: University of Sheffield, 2007, p. 140.

[65] O. Veledar, "Hydrophone-based calibration for seawater acoustic detection of UHE neutrinos," *Nuclear Instruments and Methods in Physics Research A,* vol. 604, pp. 212-214, June 2009 2009.

[66] S. T. Karris, *Signals and Systems with MATLAB computing and simulink modeling* California: Orchard Publications, 2003.

[67] MicrochipTechnology, "Microchip PIC18F2480/2580/4480/4580 Data Sheet," in *http://ww1.microchip.com/downloads/en/DeviceDoc/39637d.pdf*, 2009 Last accessed date: 11 March 2012.

[68] NationalInstruments, "USB-6211 16-Bit, 250 kS/s M Series Multifunction DAQ, Bus-Powered datasheet" in *http://sine.ni.com/nips/cds/print/p/lang/en/nid/203224*, 2011 Last accessed date: 15 April 2012.

[69] J. P. Bentley, *Principles of measurement systems*, 4 ed.: Pearson, Prentice Hall, 2005.

[70] S. Danaher, "Signal processing for acoustic neutrino detection in water," in *The international Workshop (ARENA 2005)*, Desy, Zeuthen, Germany, 2005, pp. 75-86.

[71] W. S. Levine, *Control Systems Fundamentals*: CRC Press, 2000.

[72] R. K. Bansal, A. K. Goel, and M. K. Sharma, "MATLAB and its applications in engineering," Pearson Education India, 2009.

[73] J. D. Aplevich, "The essentials of linear state-space systems ": John Wiley &Sons, 1999, p. 320.

[74] S. K. Mitra, "Digital signal processing: A computer-based approach," New York: McGraw-Hill, 1998.

[75] C. L. Naumann, G. Anton, K. Graf, J. Hobl, A. Kappes, U. F. Katz, R. Lahmann, and K. Salomon, "Understanding piezo based sensors for acoustic neutrino detection," *Journal of physics: Conference Series,* vol. 81, pp. 1-6, 2007.

[76] MATHWORKS, "MATLAB USER GUIDE," in *http://www.mathworks.co.uk/help/techdoc/*, Last accessed date: 20 May 2012.

[77] MathWorks,"MATLAB user's guide," in *http://www.mathworks.co.uk/help/techdoc/ref/ss2tf.html*, Last accessed date: 29 July 2012.

[78] V. K. Ingle and J. G. Proakis, *Digital Signal Processing Using MATLAB*. USA: Bookware Companion Series, 2007.

[79] R. H. Bishop, "LabVIEW 8 Student Edition," 2007, p. 619.

[80] NationalInstrments, "Getting Started with the NI LabVIEW," in *http://digital.ni.com/manuals.nsf/websearch/6DD40C65B07DCE3F8625776000685F6C*, Last accessed date: 25 March 2012.

[81] Bruel&Kjaer, "Product data Hydrophones- Types 8103,8104,8105,8106," in *http://www.bksv.com/doc/bp0317.pdf*, Last accessed date: 20 May 2012.

[82] J. H. Mathews and K. K. Fink, "Numerical methods using MATLAB," Prentice Hall, 2004.

[83] TexasInstruments, "TLV5619 2.7V TO 5.5 V 12-BIT PARALLEL DIGITAL-TO-ANALOG CONVERTER," in *http://www.ti.com/lit/ds/symlink/tlv5619.pdf*, 2004 Last accessed date: 15 March 2012.

[84] InovationExperiment, "NX-887 PIC18F4580 STARTER KIT," in *http://www.inex.co.th/inexstore/index.php?page=shop.product_details&flypage=flypage.tpl&product_id=80&category_id=22&option=com_virtuemart&Itemid=11*, 2010 Last accessed date: 15 March 2012.

[85] Altium, "Altium Designer Training for Schematic Capture and PCB Editing," in *http://www.altium.com/training/en/manuals-and-downloads.cfm*, 2011 Last accessed date: 15 March 2012.

[86] CirrusLogic, "PA94 high voltage power operational amplifiers," in *http://www.cirrus.com/en/pubs/proDatasheet/PA94U_N.pdf*, 2011 Last accessed date: 20 May 2012.

[87] W. Ooppakaew and S. Danaher, "Hydrophone calibration based on microcontrollers for acoustic detection of UHE neutrinos," *Nuclear Instruments and Methods in Physics Research A,* vol. 662, pp. S249-S253, 2012.

[88] R. E. Francois and G. R. Garrison, "Sound absorption based on ocean measurements: Part I: Pure water and magnesium sulfate contributions," *Journal of the acoustical society of America,* vol. 72, pp. 896-907, 1982.

[89] R. E. Francois and G. R. Garrison, "Sound absorption based on ocean measurements: Part II: Boric acid contribution and equation for total absorption," *Journal of the acoustical society of America,* vol. 72, pp. 1879-1890, 1982.

[90] M. A. Ainslie and J. G. McColm, "A simplified formula for viscous and chemical absorption in sea water," *Journal of the acoustical society of America,* vol. 103, pp. 1671-1672, 1998.

[91] V. Niess and V. Bertin, "Underwater acoustic detection of Ultra High Energy Neutrinos," *Journal of Astroparticle physics,* vol. 26, pp. 243-256, 2006.

[92] L. Liebermann, "Sound propagation in chemically active media," *Physical Review* vol. 76, pp. 1520-1524, 1949.

[93] S. Bevan, "An Investigatation into the Feasibility of a Sea Water and Ice Based Acoustic UHE Neutrino Telscope." vol. PhD thesis: University College London, 2008, p. 232.

[94] J. A. Agulilar, I. A. Samarai, and A. Albert, "AMADEUS-The Acoustic Neutrino Detection Test System of the ANTARES Deep-Sea Neutrino Telescope," *Nuclear Instruments and Methods in Physics Research A (2010), doi:10.1016/j.nima.2010.09.53,arXiv:1009.4179,* 2011.

[95] A. B. Baggeroer, "Acoustic telemetry- an overview," *IEEE Journal of Oceanic Engineering,* vol. OE-9, pp. 229-235, 1984.

[96] M. Stojanovic, "Recent advances in high-speed underwater acoustic communications," *IEEE Journal of Oceanic Engineering,* vol. 21, pp. 125-136, 1996.

[97] J. A. Catipovic, "Performance limitations in underwater acoustic telemetry," *IEEE Journal of Oceanic Engineering,* vol. 15, pp. 205-216, 1990.

[98] D. B. Kilfoyle and A. B. Baggeroer, "The state of the art in underwater acoustic telemetry," *IEEE Journal of Oceanic Engineering,* vol. 25, 2000.

[99] S. E. Cho, H. C. Song, and W. S. Hodgkiss, "Successive interference cancellation for time-varying underwater acoustic channels," in *OCEANS 2010*, La Jolla, CA, USA, 2010, pp. 490-501.

[100] C. Viala, C. Noel, and G. Lapierre, "Simulation of acoustic signal in time-verying multipath underwater channel," in *Underwater acoustics for deep sea application* France, 2002.

[101] D. R. Raichel, *The science and applications of acoustic*. New York: Springer-Verlag New York, Inc, 2000.

[102] B. P. Lathi, *Modern digital and analog communication systems*: Oxford University Press, Inc., 1998.

[103] M. Chitre, "A high-frequency warm shallow water acoustic communications channel model and measurements," *Acoustic Society of America,* vol. 122, pp. 2580-2586, 2007.

[104] T. C. Yang, "A study of spatial processing gain in underwater acoustic communications," *IEEE Journal of Oceanic Engineering,* vol. 32, 2007.

[105] R. S. H. Istepanian and M. Stojanovic, *Underwater acoustic digital signal processing and communication systems*. MA, USA: Kluwer Academic Publishers, 2002.

[106] P. C. Etter, *Underwater acoustic modelling and simulation*, 3 ed. London and New York: Spon Press, 2003.

[107] J. G. Proakis, M. Salehi, and G. Bauch, *Contemporary Communication System using MATLAB*: Thomson Brook/Cole, 2004.

[108] W. Ooppakaew, M. Saldana, and S. Danaher, "Acoustic Array Calibration and Signal Processing for UHE Neutrinos Generation," in *The 8th IEEE International Conference on Mobile Ad-hoc and Sensor Systems (MASS 2011)*, Valencia, Spain, 17-22 October 2011.

[109] R. Lahmann, "Report of measurements with the acoustic array during the sea campaign on 17 September 2011," Erlangen Centre fro Astroparticle Physics (ECAP)2011.

[110] A. V. Oppenheim and R. W. Schafer, *Discrete-time signal processing*. Englewood Cliffs, NJ: Prentice-Hall, 1989.

[111] N. Thrane, J. Wismer, and H. Konstantin-Hansen, "Practical use of the "Hilbert transform"," in *http://www.bksv.com/doc/bo0437.pdf*, Last accessed date: 20 July 2012.

[112] W. Ooppakaew, S. Danaher, R. Lahmann, and K. Graf, "A Linear Array Hydrophone Transmitter for the calibration of acoustic UHE Neutrino Telescopes " in *ARENA 2012- Acoustic and Radio EeV Neutrino Detection Activities*, Erlangen Castle,Germany, 19-22 June 2012.